Decision Support Systems

Can motion measurements during an offshore heavy lift operation on-line help to make a more accurate prediction of the vessel response and decision making operation

Alex Lotgering

MSc. Thesis Report - February 3, 2017

mocean

ADAVANCED OFFSHORE TECHNOLOGY

TU Delft

Decision Support Systems

Can motion measurements during an offshore heavy lift operation on-line help to make a more accurate prediction of the vessel response and decision making operation

by

Alex Lotgering

Master Thesis in partial fulfillment of the requirements for the degree of

Master of Science
in Offshore & Dredging Engineering

at the Delft University of Technology
Faculty Mechanical, Maritime and Materials Engineering.

Graduation date:	February 6, 2017	
Student number:	4321251	
Thesis committee:	prof. dr. ir. R.H.M. Huijsmans,	TU Delft, Graduation professor
	ass. prof. P. Naaijen,	TU Delft, University supervisor
	dr. ir. R. Kamp,	Mocean Offshore b.v., Company supervisor
	dr. ir. A. Vrijdag,	TU Delft, Member

An electronic version of this thesis is available at http://repository.tudelft.nl/

TU Delft

Preface

This document concerns my thesis in order to graduate successful for the Master Offshore & Dredging Engineering at the Technical University of Delft. Mocean Offshore b.v. has given me the opportunity to graduate within their company. The aim of Mocean Offshore b.v. is to develop advanced offshore solutions to matters for a wide variety of customers within the offshore oil & gas and renewable energy industry. Mocean Offshore developed an Decision Support Tool named the Mocean Capability Tool. The aim of this tool is to provide valuable vessel response information during a heavy lift operation in order to support the vessel captain in making decisions about the capability of the vessel. The Mocean Capability Tool features an inertial measurement unit which continuously registers the motions of the vessel. This Tool gave therefore rise to this research with the main question, can motion measurements during a offshore heavy lift operation on-line help to make a more accurate prediction of the response and decision making operation.

I would like to thank Jelte Kymmell for providing this internship and the ability to see the development of this growing company with noteworthy ambitions within this challenging industry. Really cool that I am invited to join the first ski trip to celebrate the achieved success of Mocean Offshore. Than I would like to thank the entire Mocean team for chairing their knowledge and for experiencing your good work spirit. Mark, Willem and Robert I greatly enjoyed the workout sessions in the Amsterdam bos, keep up the spirit. Furthermore I would greatly like to thank my parents for supporting me during my study career. Without you guys I would have never been able to study the way I did and would probably also not come to this stage. Trust me, for now I have studied sufficiently enough. Last but not least a special thank you to my girlfriend, seeking together the puzzle pieces of this research did not come easily nor without grumbling. You supported me by remembering me about the fact that I'm like a diesel engine.

Alex Lotgering
Amsterdam, February 3, 2017

Abstract

Nowadays the costs of specialized offshore crane vessels can roughly vary between €80,000 and €350,000 per day. The impact of those vessel day-rates on the costs of offshore operations is significant. In order to optimise this part of the costs, the deployment of offshore vessels has to be studied an mapped which is referred to as the workability of a vessel. Often workability studies are made for three different phases namely the early stage in an planning, days before the vessel sails towards the jobsite and hours or minutes before the execution of the operation. The latter is the point of no return for which the decision maker would like to have the most accurate information about the capability of the vessel to determine if the operation can be executed safely or not. In order to support the decision maker, so called Decision Support Tools are available. The Mocean Capability Tool is such a tool which moreover features an inertial measurement unit which continuously registers the motions of the vessel. Therefore the question arose whether it is possible to retrieve useful information from these measurements for making a more accurate prediction of the vessel response and decision making operation.

There are numerous methods and techniques available that are able to predict a phenomenon based on the time signal of that phenomenon if it can be described by a stochastic harmonic process. This applies also to predominantly wave induced vessel responses. The capability of the vessel is determined by the significant response at a certain sea state. Thus in order to determine the significant response of the vessel from response measurements at least a measurement period of 20 min is required. The validity of the energy of measured vessel responses, regardless of the correction method, reaches to the duration for which the sea state is stationary Gaussian distributed and for systems without changing dynamics. Thus opportunities for making a more accurate prediction of the vessel response is limited to time-windows of approximately 20-160 minutes and is dependent on the nature of the dynamics.

The operational condition, thus the loading as a result of the present sea state and from the heavy lift operation itself is highly variable during the operation. In order to be able to predict vessel responses for different loading conditions a ship specific deterministic model for ship responses during a heavy lift operation is required. From literature is concluded that the dynamics of ship responses during a heavy lift operation within the applicable domain of safe operations might be approximated linearly. Therefore a spectral sea-keeping simulation model and numerical tool for the coupled motions of a heavy-lift vessel and a freely suspended load is developed. The model considers the motions of the ship in six degrees-of-freedom and the suspended load as a point mass lifted by a single crane. The tool has been verified and the validity of the model and the assumption of linearity is validated by means of an equivalent model in Orcaflex with simulations of heavy lift dynamics in Time Domain.

The wave buoy analogy is a response-based method for the determination of the wave spectrum which can also be applied on other floating objects such as a crane vessel. By making use of response measurements and a deterministic model for ship motions it is thus possible to investigate both the transfer functions as well as the present wave spectrum wherein subsequently corrections can be made. The developed correction method is therefore founded on the concept of the equivalence of energy. The difference between the measured and computed vessel motion response (energy) is the total system error. In on-line motion analysis multiple errors can be made. For the implementation of corrections, it is however not necessary to know where the exact errors originate from and what there exact quantity is. However similar to the dynamics, the nature and consistency of the error is important for extrapolating corrections from one operational condition to another. Based on a sensitivity analysis is concluded that combinations of realistic errors in model-input and hydrodynamic coefficients result in small system errors. Decided is therefore to accept these errors and to apply the correction method for seeking the present sea state. From numerical test cases is concluded that vessel response measurements can help to make a more accurate prediction of the vessel response but not immediately for the decision making operation. It is dependent on the time-window of interest, operational condition and start situation.

Contents

Nomenclature

Abbreviations & Acronyms

App	Aft perpendicular
CoB	Centre of Buoyancy
CoG	Centre of Gravity
DAF	Dynamic Amplification Factor
DMI	Danish Meteorological Institute
DOF	Degrees of Freedom
DP	Dynamic Positioning
DNV	Det Norske Veritas
DST	Decision Support Tool
EOM	Equation Of Motion
FD	Frequency Domain
Fpp	Front perpendicular
FFT	Fast Fourier Transformation
GLND	GL Noble Denton
OWF	Offshore Wind Farm
HDB	Hydrodynamic Data Base
HLO	Heavy Lift Operation
HLV	Heavy lift Vessel
JONSWAP	JOint North Sea WAve observation Project
Ma	Matlab
MPM	Most Probable Maximum
Or	Orcaflex
PM	Pierson–Moskowitzspectrum
PS	Port Side
RAO	Response Amplitude Operator
RMS	Root mean square
SB	Starboard
SD	Standard Deviation
SNAME	Society of Naval Architects and Marine Engineers
TD	Time Domain
var	Variance

Greek

SYMBOL	DESCRIPTION	UNIT
α	Rotational motion suspended load in longitudinal direction	$[rad]$
β	Rotational motion suspended load in transversal direction	$[rad]$
ϵ	Phase shift	$[rad]$
ϵ_r	Error	$[-]$
ϵ_{lr}	Linear rope elastic stretching	$[-]$
∇	Displacement	$[m^3]$
λ	Wave length	$[m]$
γ	Peakedness parameter wave spectrum	$[-]$
μ	Dynamic viscosity	$[Pa \cdot s]$
ν	Kinematic viscosity	$[m^2/s]$
ρ	Sea water density	$[kg/m^3]$

ϕ	Roll	$[rad]$
θ	Pitch	$[rad]$
ψ	Yaw	$[rad]$
η_7	Cargo Surge in the latitudinal x-direction	$[m]$
η_8	Cargo Sway in the lateral y-direction	$[m]$
η_9	Cargo Heave in the vertical z-direction	$[m]$
ω	Wave frequency	$[rad/s]$
ζ	Wave elevation	$[m]$
ζ_a	Wave amplitude	$[m]$
g	Gravitational acceleration	$[m/s^2]$
Φ_{rad}	Radiation potential	$[-]$
Φ_{FK}	Froude-Krylov force	$[-]$
Φ_d	Diffraction potential	$[-]$

Latin

SYMBOL	DESCRIPTION	UNIT
$\mathbf{A}$	Hydrodynamic added mass matrix	$[N/(m/s^2)$ or $Nm/(rad/s^2)]$
$\mathbf{B}$	Hydrodynamic damping matrix	$[Nm/(rad/s^2)$ or $Nm/(rad/s)]$
B_e	Equivalent viscous added roll damping coefficient	$[Nm/(rad/s)]$
$\mathbf{C}$	Stiffness matrix	$[N/m]$
$\mathbf{C_h}$	Hydrostatic stiffness matrix	$[N/m]$
$\mathbf{C_m}$	Mooring restoring matrix	$[N/m]$
$\mathbf{C_c}$	Coupling stiffness matrix	$[N/m]$
$\mathbf{M}$	9-DOF Rigid body Mass and Inertia matrix	$[N/(m/s^2)$ or $Nm/(rad/s^2)]$
$\mathbf{V}$	Mass and inertia matrix of the vessel hull	$[N/(m/s^2)$ or $Nm/(rad/s^2)]$
$\mathbf{L}$	Identity mass matrix of the suspended load	$[N/(m/s^2)]$
$\underline{F_e}$	Vector of the exciting forces and moments	$[N]$
$\overline{AE}$	Axial hoisting rope stiffness	$[Pa \cdot m]$
BM	Metacentric radius	$[m]$
B_{BK}	Bilge keel damping	$[-]$
B_e	Eddy making damping	$[-]$
B_f	Skin friction coefficient	$[-]$
B_L	Lift force damping	$[-]$
B_w	Free surface wave damping	$[-]$
C_B	Block coefficient ship full	$[-]$
D	Hoisting rope diameter	$[m]$
E	Youngs modulus	$[Pa]$
GM	Metacentric height	$[m]$
GZ	Righting stability lever arm	$[m]$
h	Water depth	$[m]$
H	Response amplitude operator	$[-]$
H_0	Half-beam-draft ratio	$[-]$
H_{m0}	Significant wave height	$[m]$
H_{max}	Maximum wave height	$[m]$
I_{xx}	Moment of Inertia around x-axis	$[m^4]$
k	Wave number	$[-]$
k_e	Vertical restoring force due to axial rope stiffness	$[N]$
k_s	Horizontal restoring force due to gravity	$[N]$
k_{xx}	Radii of Gyration around x-axis	$[N]$
l_e	Effective elastic hoisting rope length	$[m]$
l_{eff}	Effective mooring length	$[m]$
l_s	Outstretched hoisting rope length	$[m]$

KB	Distance from keel to CoB	$[m]$
KG	Distance from keel to CoG	$[m]$
m_S	Structural mass vessel	$[kg]$
m_B	Structural mass hoisting cranes	$[kg]$
m_L	Mass suspended load	$[kg]$
m_0	Area under spectral curve	$[m^2]$
OG	Vertical distance from still water level to the roll axes	$[m]$
R_a	Rayleigh distributed	$[-]$
R_e	Reynolds number	$[-]$
S_R	Response Spectrum	$[m^2s/rad]$
S_ζ	Wave Spectrum	$[m^2s/rad]$
T	Vessel draft	$[m]$
T_p	Peak period	$[sec]$
T_{m0}	Mean zero-upcrossing period	$[sec]$
T_n	Natural period	$[s]$
V	Displaced volume	$[m^3]$
WD	Water depth	$[m]$
$WDir$	Wave direction	$[deg]$
$\underline{x}$	Vector of the exciting forces and moments	$[m$ or $rad]$

1 Introduction

1.1. Problem Description

Offshore operations are costly. Nowadays the costs for offshore vessels can roughly vary between €80,000 and €350,000 per day [49]. Specialized offshore vessels such as a offshore heavy lift vessel can have even higher day-rates. The impact of those vessel day-rates on the costs for offshore operations are therefore significant. In order to optimise this part of the costs for offshore operations, the deployment of offshore vessels has to be studied an mapped. This is referred to as the workability of a vessel. The higher the workability the more a vessel can be deployed.

The workability of a offshore vessel is mainly depended on two factors. The capability of the vessel and a certain offshore operation. The capability of the vessel is determined by the response of the vessel such as the response to the loading as a consequence of the operation and environmental factors such as the incoming waves, wind and current. The second factor, the offshore operation itself, determines the boundary within the operation may be performed. For example industry codes from GL Noble Denton[1] which prescribe certain limiting vessel responses in order to be able to execute the operation safely. Larger and more rapid responses of the vessel introduce larger loads which the cranes and hoisting robes have to withstand and visa verse.

Often workability studies for offshore vessels are made for three different operational phases. The distinction between those phases is made according to the time-window of interest. Those time-windows are the early stage in an planning, days before the vessel sails towards the jobsite and hours or minutes before the execution of the operation. If available in the planning phase, the workability of a vessel is calculated according to historical environmental data. From this roughly the workable season of the vessel can be determined. In the second phase the workability is calculated according to the weather forecast for the next days which determines if a vessel can sail to the jobsite or not. The third phase, hours or minutes before execution of the operation, the workability has to be calculated once more in order to determine if the operation can be executed safely or not. This is the point of no return.

Dependent on the sensitivity of the limiting motions according to the operation, the difference between workable or not workable can be relatively small. Therefore especially in the third phase it is of interest to have the most accurate information about the environmental conditions and the capability of the vessel. Since the time window of interest is relatively short, now environmental data cannot only be obtained by a weather forecast but also from wave buoys, wave radars or weather satellites to name a few. However, from an economic point of view and often also because of practical reasons environmental data is frequently only obtained from weather hind and forecasts. Furthermore due to the complexity of ship responses during an heavy lift operation, these are most often computed in an earlier stage with special software for a limited amount of loading conditions. So there are uncertainties in the obtained

[1] The Noble Denton rules and technical guidelines are developed through extensive research and development. The rules and guidelines represent the current state of scientific development and industry practice. Subsidiary company of Det Norske Veritas.

environmental data and uncertainties in the loading conditions for a specific operation. Making a go or no-go decision for executing the operation can therefore be a difficult task.

In order to support the decision maker, most often the captain of a vessel, so called Decision Support Tools are available. The Mocean Capability Tool from Mocean Offshore b.v. is such a Decision Support Tool. The aim of this tool is to provide valuable vessel response information during a certain operation in order to support the vessel captain in making decisions about the capability of the vessel. How does the ship respond under the loading condition and can the operation be executed safely or not? However as discussed there will always be uncertainty in this information as a result that industry codes prescribe a so called alpha factor for the capability of the vessel. This factor increases the safety margin but limits the capability and hence the workability of the vessel. Resulting in costly vessel downtime.

In order to reduce the vessel downtime without a loss in safety margin more accurate information about the capability of the ship and or the to be expected environmental conditions is required. As discussed within this time window of interest this information can be obtained with wave radars and wave buoys but these sensors and tools require investments which can be significant. The Mocean Capability Tool features an inertial measurement unit which continuously registers the motions of the vessel. From Mocean Offshore b.v. therefore the question arose whether it is possible to retrieve information about the capability of the vessel and or the environmental conditions by making use of vessel response measurements.

The concept for retrieving this information is illustrated in the flow chart given below and reads as follows. Within the Mocean Capability Tool the to be expected vessel responses are determined according to precalculated vessel responses for a given metocean input and operational loading condition. The precalculated vessel responses are stored in the hydrodynamic database and the metocean input is obtained from a weather now-cast.[2] By comparing subsequently the measured vessel responses with a number of precalculated vessel responses, errors in the chosen combination for determining the corresponding vessel responses can be mapped. From this information can be learned whereupon possibly corrections can be made for making a more accurate prediction of the vessel response and decision making operation.

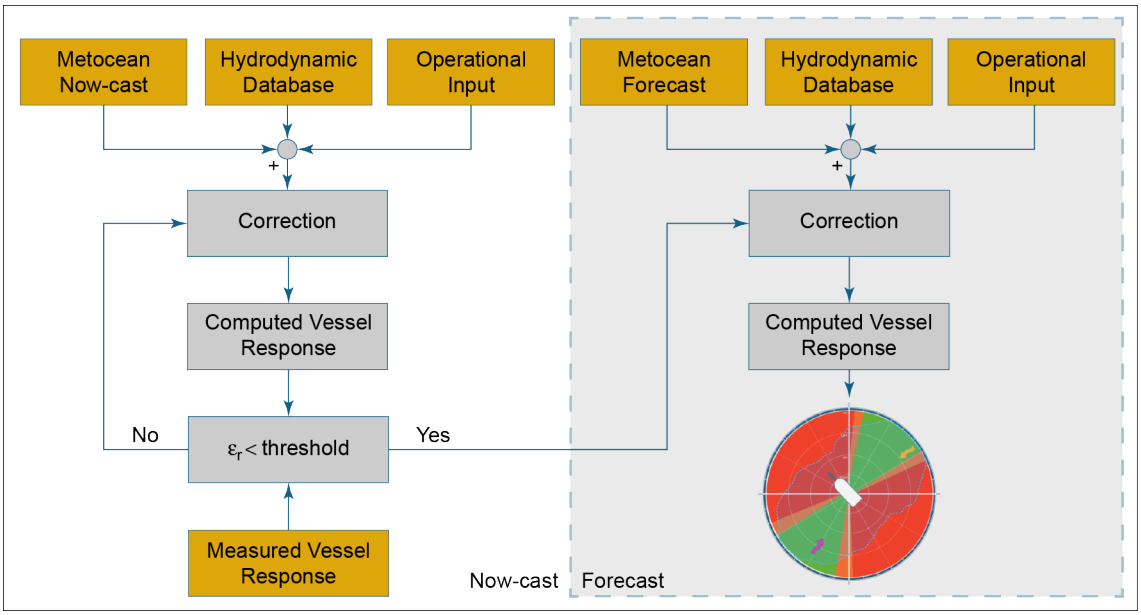

Figure 1.1: Flowchart of the initial correction methodology concept

[2]Nowcasting is a technique for very short-range forecasting that maps the current weather, then uses an estimate of its speed and direction of movement to forecast the weather a short period of 0-6 hours ahead. In this time range it is possible to forecast small features such as individual storms with reasonable accuracy.

1.2. Scope & Relevance

Offshore wind farms (OWFs) are increasingly being installed offshore and this trend continues in the coming years. From an economical and technical point of view especially areas with a relative shallow water depth and sufficient available wind such as the North Sea are highly suitable for OWFs [21]. Roughly an offshore wind farm consists of a large number of wind turbines, at least one transformer substations and kilometres of cable for the export of electricity. Therefore, many offshore operations are involved by OWF installations such as seabed preparation operations, foundation installations, cable lay operations and heavy lift operations to name a few [3].

For the conduction of those operations numerous offshore vessels such as heavy lift vessels, jackups, dredging vessels, barges and tugs are being used [30]. Due to their day-rates the deployment of these vessels make up a large part of the costs of OWF installations as well as of the overall lifetime costs due to maintenance works. In order to make offshore wind energy economically more attractive optimization of the costs is desirable. The most effective cost reduction is an optimization in the deployment of offshore vessels with in particular heavy lift vessels since those have a relatively high vessel day-rate and are used most often looking at offshore work hours [2, 3]. The RAMBIZ 3000, shown in the picture below, is such a vessel. Increasing the workability of this vessel is thus of interest.

Figure 1.2: Aerial photo of the RAMBIZ 3000 during a substation lift operation

Optimization in vessel deployment can be achieved by decreasing the down-time or in other words by increasing the workability of the vessel. The workability is dependent on the physical capability of a vessel and a certain operation for which industry codes describe multiple criteria that limit the capability of the vessel in order to ensure safe operations. The capability of the vessel can possibly be improved with physical changes to the vessel which is accompanied with investments and vessel downtime. Therefore in this research improvements in workabiliy are being examined within the rules of regulations by making use of existing sensors, tools and theoretical approaches to decrease the uncertainty in predicted vessel responses. Due to complexity not all rules and regulations can be taken into account. Therefore only restricting vessel responses are being incorporated in this study since those direct or indirect determine the workability of the vessel.

Lastly only vessel responses within the applicable domain of heavy lift operations are being studied which implies small vessel responses during operations in mild, moderate and medium weather conditions within a time window of roughly 12 hours. Regardless the capability of a offshore vessel the operation will not be executed above wave heights of 2m and vessel roll and pitch motions of 2 degrees for example [13, 14].

Research Scope

- Decision Support Systems,
- Heavy lift operations,
- Limiting vessel responses,
- RAMBIZ 3000,
- Sea states in mild, moderate and medium weather conditions,
- Predictions up to 72 hours in the future,
- North Sea area.

1.3. Research objectives & Research questions

The main objective of this research is to examine the possibilities of on-line vessel response measurements in order to be able to make a more accurate prediction of the vessel response and decision making operation. The proposed correction methodology concept for finding possible corrections by making use of vessel response measurements raises many questions if one takes into account the scope of this research and the existing system (Mocean Capability Tool) for providing operational information. For example between which may be precisely calculated an error taking into account all possible errors in the metocean data input and fitted corresponding precalclulated vessel response. Which system parameters can be corrected based on measured vessel responses and how can vessel motion measurements from the past help to make a more accurate prediction of the vessel response? In order to put a useful first step in the right direction the main question and subsequent questions in this research read as follows:

Main research question

- Can motion measurements during an offshore heavy lift operation on-line help to make a more accurate prediction of the vessel response and decision making operation?

Sub questions

- What kind of model is required for making a more accurate prediction of the vessel response, given on-line vessel response measurements, a certain time window in the future and loading condition to be expected?
- What is the total system error and where do those errors come from?
- Is it possible to correct the total system error by making adjustments or corrections to a certain system parameter without knowing the exact origin of the total system error?
- How can measurements from the past help to improve predictions of the vessel response, in other words how does the correction quality deteriorate over time?

1.4. Assumptions & Limitations

In practice offshore heavy lift vessels are being exposed to many different loadings coming from the operation itself such as the suspended cargo and the mooring system to maintain position but also from environmental factors such as the wind, waves and current. All of these loading factors have their contribution in vessel motion response but their magnitude and combination differ per scenario which is something that has to be determined for proper motion analyses. Due to the amount of imaginable scenarios this involves a significant amount of work. Therefore a number of assumptions are being made which limits the validity and applicability of this research. Furthermore the scope of this study entails limitations as well which together are listed below.

Assumptions

- Waves are the most dominant factor in causing vessel motion responses,
- Sea states in the North Sea can be described sufficiently by parametric spectra such as a JONSWAP or Torsethaugen spectrum,
- The accuracy of inertial measurement units is not studied whereby it is assumed that they are sufficiently accurate for the intended application.

Limitations

- Single crane conducted offshore heavy lift operations,
- Non submerged suspended cargos,
- On-line vessel response measurements,
- Correction method based on short period statistics,
- North Sea area.

1.5. Definition of Motions and Wave Heading

The conversion of the definition of the position and orientation of the ship and cargo are described in nine degrees of freedom according to the SNAME[3] notation. The ship has six-degrees-of-freedom (6-DOF) and the cargo three-degrees-of-freedom (3-DOF) which is illustrated in figure 1.3.

- The three translational motions of the ship at the centre of gravity (G) in the direction of the x-,y- and z-axes:
  - Surge in the latitudinal x-direction, positive forwards,
  - Sway in the lateral y-direction, positive to port side,
  - Heave in the vertical z-direction, positive upwards.
- The three rotational motions of the ship at the centre of gravity about these axis:
  - Roll about x-axis, positive right turning
  - Pitch about y-axis, positive right turning
  - Yaw about z-axis, positive right turning
- The three translational motions of the load at the centre of gravity (Q) in the direction of the η_7-, η_8-, η_9-axes:
  - Cargo Surge in the latitudinal x-direction, positive forwards,
  - Cargo Sway in the lateral y-direction, positive to port side,
  - Cargo Heave in the vertical z-direction, positive upwards.

The definition of wave headings follows the conversion. The waves are defined positive in the direction they are traveling towards. The direction is defined as the angle between the wave and the positive x-axis, measuring anti-clockwise. Thus incoming waves with an angle of zero degrees are referred as stern or following seas and incoming waves from 90 degrees are referred as beam seas.

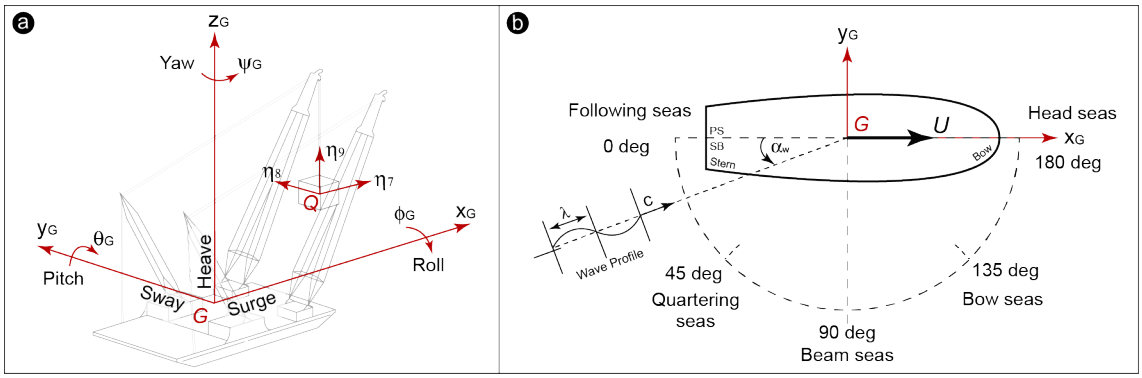

Figure 1.3: a: Definition of Motions. b: Definition of Wave Headings

1.6. Readers Guide

This thesis report is organized in chronological order with respect to the research. Chapter 1 introduced the research subject supported by a problem definition, scope, relevance of scope, the objectives in this study and the assumptions made in advance. In chapter 2 the methodology is given for some of the opportunities regarding a more accurate prediction of the vessel response and decision making operation with the aid of on-line vessel response measurements. Chapter 3 describes the simulation model and developed Matlab tool for ship motions during heavy lift operations and light ship conditions. Model verification and validation is described in chapter 4. The sensitivity of the different parameters of the simulation model has been demonstrated and described in chapter 5. Based on the conclusions of this analysis the correction method is developed of which its functioning is tested and described in chapter D. Finally a persistence study on workable windows is conducted which results are given in chapter 7. All chapters include a brief summary and discussion which is sufficient to study the main findings. The final conclusion and recommendations are described in chapter 8.

[3]The Society of Naval Architects and Marine Engineers (SNAME)

2

Correction Methodology

In this chapter the methodology for making a more accurate prediction of the vessel response and decision making operation by making use of on-line vessel response measurements is described. In order to determine the most suitable correction method, first the available techniques regarding vessel motion measurements and vessel motion predictions within the time window of interest are discussed. Thereafter the most suitable correction method and the associated research steps are described.

2.1. Available Methods

There are numerous methods and techniques available that are able to predict a certain phenomenon based on the time signal of that phenomenon if it can be described by a stochastic harmonic process. In probability theory something is called a stochastic process if the time sequence of the evolution of the system for an phenomenon is an ordered set of random variables. Something is called harmonic simply if it can be represented by a sinusoidal wave or a sum of harmonic waves. For example sea states which are composed of wind generated waves. Even though especially wind waves are highly irregular they can be seen as a super position of many simple, regular wave components, each with its own amplitude, length, period and direction of propagation. The surface elevation ζ of an sea state at one location as a function of time, with duration D, can thus be reproduced as the sum of a large number of harmonic components which as a Fourier series is given by

$$\zeta = \sum_{i=1}^{N} \zeta_{a,i} \cos(2\pi f_i t + \varepsilon_i) \tag{2.1}$$

where, ζ_a and ε is the wave amplitude and phase, respectively of each frequency $f_i = i/D$ for all components $i = 1, 2, 3...$ [24, 29]

With regard to ship motions it is generally assumed that these are mainly induced by wave induced forces. The magnitude of the wave induced force is dependent on the ship hull area and the surface elevation of the incoming waves. The surface elevation of wind-generated waves as a function of time can subsequently be treated as a Gaussian process. Measurements have shown that this is a reasonable approach in the applicable domain of many offshore operations. It has however also theoretical grounds since the surface elevation at any one moment in time can be seen as the sum of the elevations at that time of a large number of harmonic wave components that have been generated by independently of each other, and that have traveled independently of each other across the surface. The central limit theorem which says that the sum of a large number of independent random variables is Gaussian distributed shows that therefore the sea-surface must be Gaussian distributed. It should be mentioned however that this statistical property only applies within the linear approximation of waves (as given by equation 2.1) and that this approximation does not apply to steep waves or high waves in shallow water. Under these circumstances waves interact with each other which consequently makes them no longer independent of each other. Appendix A.1 elaborates more on wave statistics. [24, 29]

Selection method
Scenarios where waves can not be described with the linear approximation are however outside the scope of this study. In other words there are numerous methods and techniques available that can predict a phenomenon, such as vessel motions, based on the time signals of those vessel motions. The most frequently applied and described methods and techniques are summarized and illustrated in figure 2.1. Within the time window of interest for making a more accurate prediction of the vessel response and decision making operation, namely 72 hours, the different methods and techniques are divided in their maximum feasible duration.

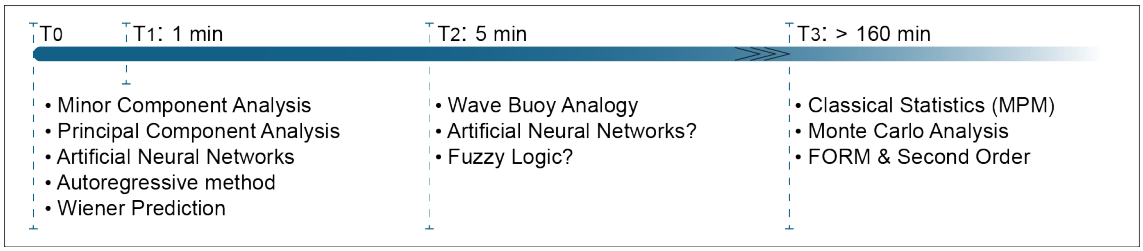

Figure 2.1: Possible methods and techniques for making a (more accurate?) prediction of the vessel response and decision making operation within the time window of interest.

Ultra short term ($T_x < T_2$)
The first category of methods and techniques can predict the motions of the vessel without any deterministic analysis. Thus without any ship specific model for the calculation of wave induced motions. All of the given methods and techniques are in fact algorithms which takes past motion data for training, and predicts the data in the next 10 to 20 seconds based on the recent motion data. The algorithms can update its core from time to time to accommodate the sea state or operational condition. The ability of these algorithms is closely related to the amount of training data, the nature of the signal and the development of computational power. Longer predictions are therefore possible with longer training data or with less accuracy. The required computational power and the nature of the motion signal however, limits the maximum duration for accurate motion predictions well within 5 minutes. Most studies report even a maximum duration of 50 seconds for which accurate motion predictions can be made. These algorithms can therefore be very helpful for example landing and take off of helicopters and aircraft's from ship decks or other floating objects in rough sea conditions. However, given the time window of interest and the duration of the average heave lift operation, these on statistically based algorithms are not suitable. For example even the final phase of the installation of a subplatform, the toutchdown, as has been illustrated in figure 1.2 lastst longer than the maximum feasable duration. In appendix A.6 is given a short and concice explanation about the nature of these algorithms. [31, 61, 62]

Short term ($T_x < T_3$)
Numerical algorithms such as an artificial Neural Networks or an Fuzzy logic are potentially seen two interesting methods. These algorithms are able to form a logic between the input and the output of a system such as a ship specific deterministic model for ship motions. With such a model ship motions can be calculated and predicted for longer periods than 5 minutes because use is made of the statistical nature of the motion signal. This is discussed in more detail later. As discussed the motion of a ship in an open water environment is the result of complex hydrodynamic forces between the ship and the water and sometimes also other random processes. An deterministic analyses involves therefore complex calculations for which a number of theoretical assumptions are required and moreover wherein potentially seen significant errors can be made. This study is focused on these errors in order to be able to make a more accurate prediction of the vessel response and decision making operation. The possibility of errors in deterministic analysis is discussed in more detail later. Regarding the number of possible errors and the unknown relation between those errors, these numerical algorithms can thus be very helpful.

The problem with these algorithms is however that they require a large amount of training data and a type of control that determines which input and output parameters are of importance. The operational

condition, thus the loading as a result of the environmental condition and from the heavy lift operation itself is in fact highly variable. It would therefore be necessary to update the core of the algorithm and to start collecting suitable training data for a specific operational condition. Extrapolating to other operational conditions is thus an excessive challenge. In this stage of the ”mocean prediction” project, in which it is not yet clear how vessel motions during a heavy lift operation should be calculated with regard to on-line corrections, or how motion signals have to be processed and can be interpreted, or which errors in the calculation process are evident and how these at once can be ”corrected”, ensures that these algorithms are at least one step too far. First, these matters should be investigated in order to say something about the possibilities of on-line, automated corrections in a system for a highly variable process. The potential benefits of these relatively new algorithms (with regard to the prediction of vessel motions) do therefore not outweigh the last highlighted concept, namely the wave buoy analogy.

The wave buoy analogy is a response-based method for the determination of the wave spectrum, the most important concept to describe the sea surface as a stochastic process. In general a waveRider buoy is considered to be a reliable device for obtaining a directional wave spectrum of ocean waves, because of the well known dynamic behavior. By means of the equation of motion and response measurements the energy of the wave spectrum can be determined. The relation is given by

$$S_{R_{ij}}(\omega) = \left|H_{ij}(\omega)\right|^2 \cdot S_\zeta(\omega) \tag{2.2}$$

where S_R, is the measured response spectrum for motion $i, j = 1, 2..$ and H_{ij} the transfer function of the energy of the wave spectrum S_ζ. The derivation of the transfer function of a floating object is given in appendix A.4, the most important wave spectrum models for the North Sea are described in appendix A.3. The concept of the wave rider buoy can also be applied on other floating objects such as a vessel. In literature several papers exist [38–40, 52, 55], which deal with the estimation of directional wave spectra from measured ship responses, or the other way around, where transfer functions of ship responses are estimated from measured wave spectra. By making use of vessel motion measurements and a deterministic model for ship motions it is thus possible to investigate both the left and the right-hand side of the relation wherein subsequently corrections can be made for making a more accurate prediction of the vessel response and decision making operation. It is however never been applied, at least not documented, on crane barges during a heavy lift operation. In this study is therefore examined how the dynamics of heavy lift operations can be described and whether this method than holds. [24]

Limitation
The validity of a correction method based on motion measurements from the past is however limited to the statistical nature of the motion signal. In other words the measured motion signals represent the vessel motions as long as the process that is causing this motion is ergodic. If averaging over time gives the same results as averaging over an ensemble of relations, the process is said to be ergodic. Its follows that such a process is stationary which greatly simplifies the description. The surface elevation of random, wind-generated waves is ergodic under the assumption of linear waves (stationary condition). Thus all averages to describe ship motions can be described as time-averages, making it possible to state that the correction is constant and thus valid during the period in which the waves are stationary Gaussian distributed.

Typically, sea states are assumed to be stationary for three hours, but it is recognized that this assumption is not valid during extreme wave growth situations or when the significant wave height is larger than 4 m. Despite the importance there is little to be found in the literature on studies that have investigated the stationarity of sea states. Ewans examined the stationarity (determined from the run test) of 12-months' Directional Waverider data recorded at the US Corp of Army Engineers' Field Research Facility at Duck, North Carolina. He found the vast majority of the records were stationary up to 160 min and that non-stationary records are generally associated with changing wind-sea conditions occurring with local wave growth [**?**]. Statistically seen a time window of up to 160 minutes is thus the limit for which vessel motions can be predicted with the aid of a deterministic model that is corrected on the basis of on-line vessel motions measurements. Without new information, assumptions or agreements, the prediction of vessel motions for one moment longer than this time window is restricted to long period statistical methods and techniques such as the Monte Carlo Analysis or linearized first (FORM and MPM) and second order methods.

As discussed in the introduction, environmental information during the lift operation is being consulted from a weather hind cast. Thus if the total error of the system is corrected by means of an correction in one or more of the forecasted parameters given by the same weather forecast, one might think that the correction can be extended in time. The Health and Safety Executive has researched the trends in the error of weather forecast models over time. The used statistics of offshore wind and wave forecasts of waters around the UK are compiled by the UK Met Office. The conclusion of the study is that the Root Mean Square (RMS) errors in wind speed and wave height forecasts have been found to have a clear seasonal variation. The mean error (bias) also shows some evidence for an annual cycle. However whereas RMS error increases with increasing forecast period, there is no such consistent change of bias with forecast period. RMS errors are larger at higher latitudes (different model grid points) but varies per weather season. There is thus some kind of relation in the error of weather forecasts. [25]

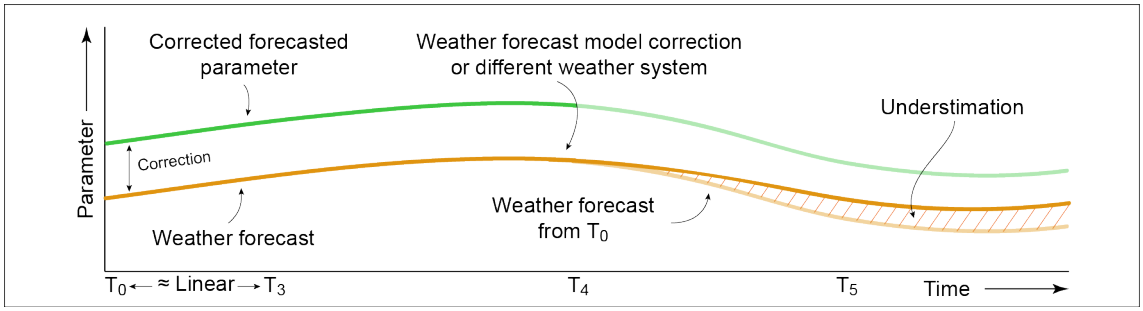

Figure 2.2: Correction in forecasted parameter such as significant wave height or period.

However it should be born in mind that any operational forecasting system is subject to continuous improvements, resulting either from new sources of data or from small- or large-scale improvements in the formulation of the numerical model but also from hand-driven adjustments in the model which on the spot results in an improvement. Findings of this study can therefore not be extrapolated to other weather forecast models without any information of the model or by making assumptions and agreements about the involved risk. The risk of extrapolating is illustrated in figure 2.2. Thus the potential for making corrections in a forecasted parameter falls outside the scope of this research due to the absence of substantiated theoretical proof about the development of weather forecast models.

2.2. Wave Buoy Analogy

The steps required for making corrections in the calculation process of ship motions by means of the wave buoy analogy are illustrated in the flow chart given below.

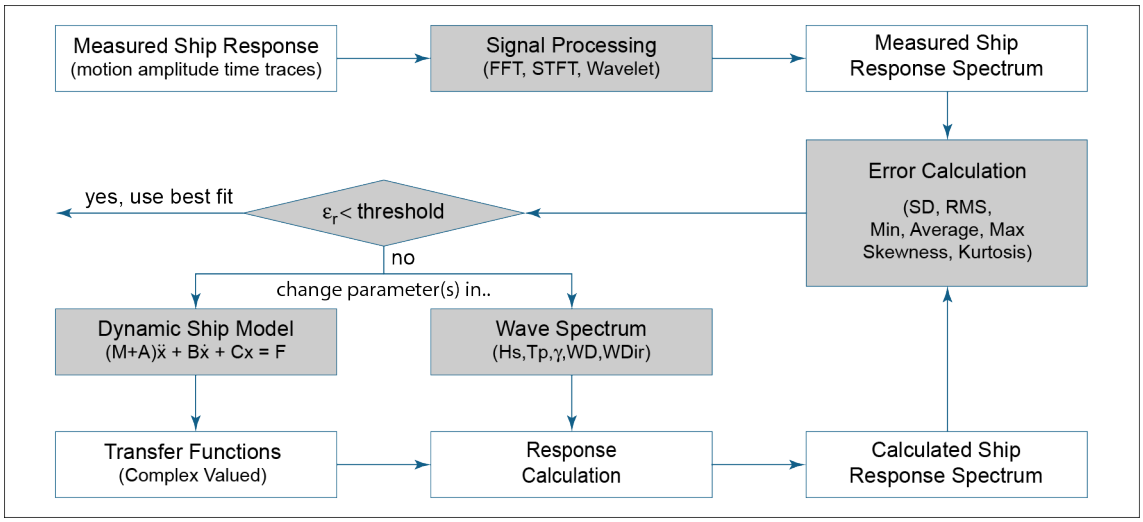

Figure 2.3: Flow chart Correction Methodology by means of the Wave Buoy Analogy.

2.2.1. Signal Processing

The aim of describing ocean waves or vessel motions with a spectrum is not so much to describe in detail one observation of the sea surface or vessel motion amplitude, but rather to describe the phenomenon as a stochastic process. In other words to characterize all possible observations in a time record that could have been made under the conditions of the actual observation. The observation which in this case is the signal of an measured vessel motion is thus formally treated as one realization of a stochastic process. In this way, it is possible to determine all relevant information from measurement signals. Such as for example the significant vessel motion response during a specific operational condition which in the end is the piece of information wherein the crane operator is interested in.

There are numerous techniques available which makes it possible to convert a signal from its original domain, often time or space, to a representation in the frequency domain. The most commonly used and proven algorithm is the Fast Fourier Transform or FFT. The most common output is usually not the amplitude and phase angle as a function of frequency, but the power spectral density per frequency. An example this representation of the energy of a wave record is given in figure 2.4.

In this figure is also illustrated the importance of the duration of the record. The most important wave parameters used in the operation of ship and offshore structures is the significant wave height H_s. The significant wave height is approximately equal to the average of one third of the highest waves of a record of at least 100 wave elevations. Thus $H_s \approx H_{1/3}$. Dependent on the significant wave period T_p, the record or motion measurement should thus have a duration of at least 20 to 30 minutes for sufficient statistical basis. The average significant wave period and thus also measured vessel motion period at the North Sea is 5-9 seconds. Strictly taken the measurement period could thus be shortened. However spectral methods such as the FFT lead to reduction in the data. The calculation work with powers of 2 data points. Thus whit a sampling rate of 2 Hz only 17.07 min of a 20 min measurement period is considered for the analysis (2^{11} data points). Therefore and with regard to the Nyquist frequency (aliasing phenomenon) a minimum sampling rate of 5 Hz is recommended. [5]

By the transform of a single record to a representation in the frequency domain there is only one amplitude per frequency. The error of the amplitude is thus in the order of 100%. In order to obtain statistically reliable estimates of the amplitudes of the vessel motion it is necessary to use multiple time traces or a windowing technique that divides a single record into multiple records. The amplitude per frequency is than taken as the average of the amplitudes per frequency. The latter technique is referred to as the Short-Time Fourier Transform or STFT. However as discussed shortening the signal is at the cost of spectral density whereby the energy at the peak can be missed. The wavelet transform is more subtle. It divides the record in multiple time traces with different lengths dependent on the frequency of the amplitude. In this way more spectral density is obtained. In appendix A.2 a brief and concise explanation of the applied FFT analyzes and windowing techniques is given. [24, 46]

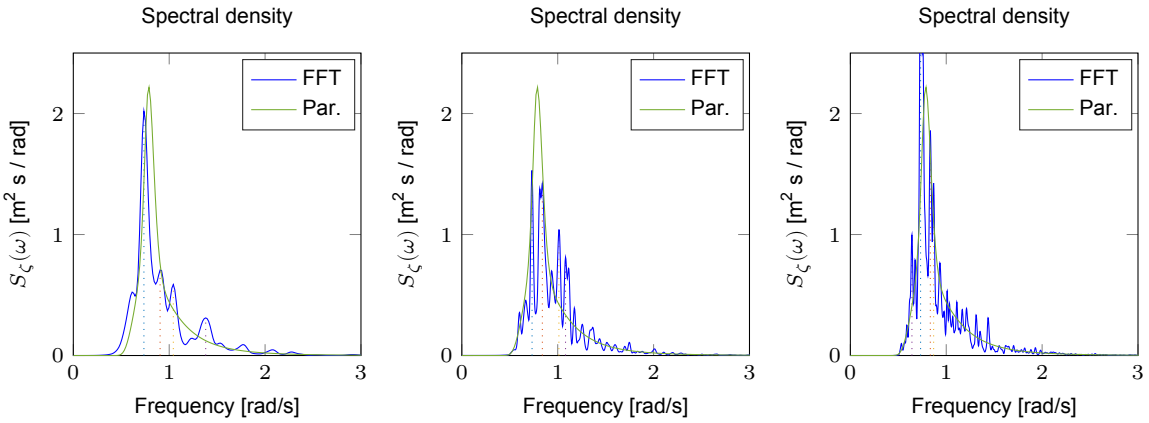

(a) Source length: 100 sec (b) Source length: 8 min (c) Source length: 20 min

Figure 2.4: Transformed surface elevation time trace to the frequency domain (time trace at figure A.1)

2.2.2. Error Calculation

In the calculation process of ship motions multiple errors can be made in virtually all steps of the process illustrated in the flow chart in figure 2.3. The exact quantity of each error and even which errors have been made during this analysis will however never be known exactly. All possible errors in the process can be summarized and divided into five categories given below:

- Vessel response measurements,
- Applied environmental condition,
- Applied operational condition,
- Simulation model,
- Theory.

As discussed in the previous subsection, there are made assumptions for and therefore also errors in the transformation of the motion signal. But there is also an error in the inertial and acceleration measurement sensor itself. It is evident that these errors should be as small as possible. The comparison between the actual vessel response and the computed vessel is response is, after all based on the quality of the transformed motion measurement signal. The quality of the transformation technique is therefore studied but it is assumed that the measuring instruments have no significant error.

The second group of errors is the applied environmental condition for the on-line motion analysis. In case of the Rambiz 3000 on which no special measurement systems are attached for the determination of the relevant parameters of the sea state present, information is consulted from weather now and forecasts. As discussed the error in these weather now and fore-casts is not exactly known. However simply because of the fact that these models are a simplification of the reality and because they are often not modeled for the exact site location (grid-point), it is likely that it contains errors. [25]

The theory used for the determination of the relevant wave parameters is however also be used for the description of wave spectra. Thus the assumptions made such as for example the linear wave approximation and that the waves are narrow banded and stationary Gaussian distributed also apply here. Without this assumption it is for example impossible to derive the H_{m0} and T_{m0} estimators. Strictly taken the significant wave estimator calculated from the wave spectrum $H_s \approx H_{m0} = 4\sqrt{m_0}$ is different from the one obtained directly from a wave record ($H_{1/3}$). The difference between the significant wave height and zero crossing wave period estimators derived directly from a wave record and the ones calculated from a wave spectrum is however small for sea states within the applicable domain of heavy lift operations ($H_s \leqslant$ 2 m) [13]. The wave spectrum to be chosen is also a subject to errors. Depending on the composition of the sea state uni-modal or bi-modal wave spectra with or without wave spreading have to be applied. It is thus of importance that the most applicable wave spectra for the North Sea can be applied in the on-line motion analysis. It is evident that erroneous chosen wave spectra will results in poor estimations of the vessel motion response and thus also in excessive corrections. [6, 34**?**]

Finally also for the simulation model of ship motions during a heavy lift operation assumptions have to be made. In this model only the most relevant dynamics will be included and possibly also linearizations have to be made in order to be able to use time independent complex valued transfer functions. Time independence will be needed for computational speed. Complex valued is needed in order to include phase shifts. The dynamics of floating structures during a heavy lift operation must thus be studied. It is however expected that the suspended load significant influence has on vessel motions. The model to be developed should thus be dynamic such that during the entire operation corrections can be made and more accurate predictions of the vessel response can be given. Setting the model input parameters according to the operational condition is thus also a source for errors.

In figure 2.5 is illustrated an example of a measured motion signal of the Rambiz 3000 during light ship conditions[1]. The computed response spectrum differs from the transformed measured vessel motion while the calculation is based on basic (known?) dynamics and available environmental information.

[1] The vessel is complete and ready for service in every respect, including permanent ballast, spare parts, lubricating oil, and working stores but is without fuel, cargo, drinking or washing water, officers, crew, passengers, their effects, temporary ballast or any other variable load.

2.2.3. Correction

For the implementation of corrections, it is however not of importance to know where the exact errors are coming from and what there exact quantity is. The point is that under the assumption of stationary Gaussian distributed waves and thus also vessel motions, the total system error can be corrected with one ore more wave frequency and possible also wave direction dependent parameter(s). Strictly taken these dependencies are not necessary to change or ”correct” the amplitude of for example the computed energy of the spectrum. However with changing wave period and or direction the vessel is likely to respond differently. In order to be able to develop an ”smart” correction algorithm which only corrects the most urgent motions of the vessel with regard to the workability, these dependencies are necessary.

Transfer functions are wave frequency and wave direction dependent. Thus in order to be able to extrapolate corrections for a specific operational condition (transfer function) towards a different operational condition it is important that the measured error is consistent between transfer functions. Thus in essence it necessary to be able to approximate the dynamics of vessel motions during a heavy lift operation in a linear way.

By analyzing the motion signal in the frequency domain the error can be calculated in other characteristics than for example the mean amplitude of the signal alone. The variance of the signal is the most relevant ”characteristic” of the measured phenomenon. For example, in contrast to the amplitude, the variance of the sum is the sum of the variance which again holds for uncorrelated variables such as individual wave components. The second reason is that one can show that the physical quantity ”energy” of the waves is linked to the variance. This means that a link can be made between statistics and physical properties of the measured phenomenon. The correction method is therefore founded on the concept of the equivalence of energy. The difference between the measured and computed vessel motion response (energy) is the total system error. As long as the energy that is causing the vessel motions is stationary Gaussian distributed, the total error in the calculation process can be corrected such that the difference in calculated and measured energy is minimal. If than subsequently the wave direction (not the energy!) and or operational condition changes during this ”statistical period”, then possibly a more accurate prediction of the vessel response and decision making operation can be given. Vice versa therefore also holds that if both the wave energy as well as the operational condition remains constant, the significant vessel response for this statistical period no longer needs to be calculated by means of a deterministic model. The significant motion amplitude is (practically seen) equivalent to twice the square root of the variance of the measured amplitude of that motion. The correction methodology can be summarized by a single optimization problem which is given by equation 2.3 on the next page.

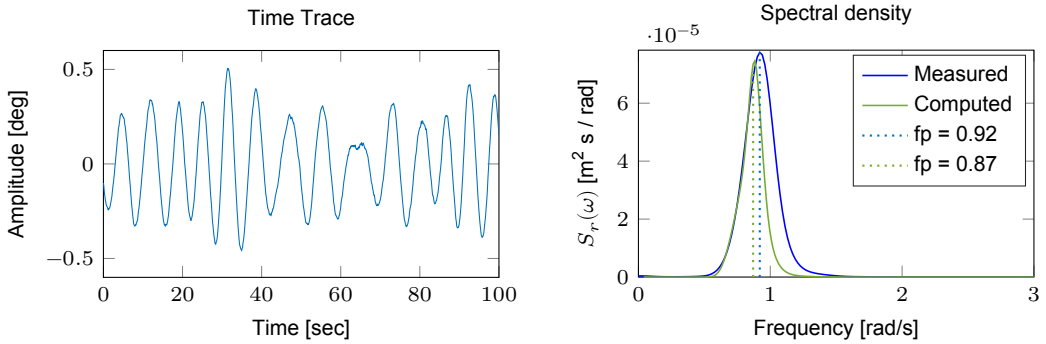

Figure 2.5: Example of a measured time signal of pitch motion amplitudes and the corresponding measured response spectrum. Source length is 20 min with a data density of 25 Hz. Reported sea state: H_s: 0.6 m, T_p: 7.0s, WDir: 30 deg. Computed response spectrum is based on a mean JONSWAP spectrum with these wave parameters. Operational condition: light ship. Calculated response is based on the standard EOM and the rules of thumb for floating objects in 6-DOF.

2.3. Summary

In summary in this study is attempted to make a more accurate prediction of the vessel response and decision making operation by solving an optimization problem between the measured and computed response moment of a specific vessel motion. This method is also referred to as the wave buoy analogy which is widely used and tested on weather buoys and standard ship shaped vessels during light ship conditions, but never, at least not documented, on crane barges during heavy lift operations. There are numerous other methods and techniques available but this method is found to be the most useful regarding, 1) the time window of interest, 2) the variable operational condition, 3) the possibility of on-line corrections and 4) the statistical characteristics of the motion signals itself.

The response moment of an signal is also referred to as the variance of the signal which in this case concerns the time trace of a specific vessel motion. The difference between the measured and computed variances can be optimized by making adjustments or here referred to as corrections in either the transfer function of the vessel motion or the sea state present. The correction methodology can thus be summarized with the optimization problem given by

$$\overbrace{\int \text{FFT(time trace motion}_{ij})d\omega}^{\text{Measured Response Moment}} = \text{var}_{ij} = \overbrace{\int S_{R_{ij}}(\omega)d\omega}^{\text{Calc. Response Moment}} = \overbrace{\int \underbrace{\left|H_{ij}(\omega)\right|^2}_{\text{1: Model}} \cdot \underbrace{S_\zeta(\omega)}_{\text{2: Sea State}} \; d\omega}^{\text{Research}} \tag{2.3}$$

where H_{ij} is the complex valued response amplitude operator for motions $i, j = 1..6$ and, S_ζ, is the spectrum of the sea state present. Since this study towards corrections is limited to the theoretical maximum duration for which a signal is stationary Gaussian distributed, and the average duration of an heavy lift operation is considerably longer than that duration, an simulation model for ship motions during a heavy lift operation have to be developed. In this way, the well-known wave buoy analogy could possible also be applied during the lift operation itself. Such that during the entire time window of interest of 72 hours more accurate predictions of the vessel response and decision making operation can be given. The developed model is described in chapter 3 after which its functioning and validity is covered in chapter 4.

As discussed, it is likely that several errors can be made in the determination of the variances. In order to determine the order of magnitude of the possible errors in either the simulation model or the applied sea state present, an sensitivity study on vessel motions responses have to be performed. Based on this information can subsequently be determined with which parameter(s) the total error can be corrected most effectively. This study is covered in chapter 5.

The optimization problem or correction method, can be drawn between different vessel motion combinations and the problem can be solved in different ways. According to the studied literature regarding the wave buoy analogy and the developed simulation model the most suitable solve method and the most effective motion combination for the optimization model is developed. Chapter D covers the developed correction algorithm.

3

Simulation Model

In this chapter the proposed simulation model for the calculation of ship motions during a heavy lift operation is described. Before elaboration in the coupled equations of motions, the intended purpose of the model and the assumptions made for this model are described. In the next section the kinematics of the model are described in order to clarify the reference systems and its nomenclature. Subsequently the left and right hand side of the coupled equations of motion are described in CH3.3: Kinetics of ship motions. Lastly the developed Matlab Tool in which, among other things, the workability for a specific heavy lift operation can be determined and displayed is covered in CH 3.4: Matlab Tool.

Although the described methodology for ship motions during a heavy lift operation is universally applicable, the proposed model is specifically developed for the Rambiz 3000 owned by the company Scaldiz. This vessel is a special type of a floating sheerleg. This crane barge is a seagoing twin hull lifting vessel originally built in 1996 for the construction of the Vasco di Gama bridge in Portugal. After this job the crane capacity was modified for heavier offshore lift projects. In the table below some general aspects of the vessel geometry and the lifting capacity is given.

Figure 3.1: Rambiz 3000 during the installation of the Rampion jacket

Table 3.1: General aspects Rambiz3000

Main Dimensions Hull:			Main Dimensions Cranes:			Lifting Capacity:		
Length O.A.	85	m	Length Cranes	82	m	Load capacity	3300	ton
Breadth moulded	44	m	Mass SB Crane	226	ton	SB Crane	1600	ton
Depth moulded	5.6	m	Mass PS Crane	215	ton	PS Crane	1700	ton
Displacement	14980	ton	Dis. between	32	m	Mast length	82	m

3.1. Assumptions and Linearization

In order to develop an effective model, the intended applications for developing the model have to be clear. The main objective of this research is to ”Examine the possibility of improved ship motion predictions by making use of ship motion measurements”. This objective is emerged from the work fields of interest. A clear example of these is the installation of offshore wind-farms. During this installation numerous offshore heavy lift operations take place for example sub-platforms or wind turbine installations. Therefore from an safety and an economic point of view ship motions during a heavy lift operation are of great interest and have to be determined with sufficient confidence. Decision Support Tools aim to provide this confidence by providing on-line valuable information about the vessel capability for a specific loading condition. The variable aspect of these loading conditions makes this tool a suitable platform for improvements ship motion calculations. These aspects set roughly the model application and model intentions. In conclusion these are summarized below.

Model Applications & Intentions:

- Ship motions during a heavy lift operation → Multi-body dynamics
- Vessel Capability → Suitable for very long or numerous simulations and statistical results
- Multiple lift cases/ stages → Possibility of on-line model input adjustments
- Possibility of model corrections → Parametric Insight
- Possibility of on-line corrections → Fast vessel response calculations

Domain of Application

Ship motions can basically be computed in frequency domain and time domain. Frequency domain analysis of ship motions are fast, reliable and a proven concept. However, the validity of an model in frequency domain is by definition only guaranteed for linear systems or for systems that behave linear within the domain of application. For this latter group model specific linearizations have to be made. Time domain analysis on the other hand can simulate non-linear behavior by solving the problem of interest per time-step. This concept requires more computational power and is therefore more time consuming. Nowadays the available computational power and the associated costs are more often within the required margins which can make this concept feasible for the intended application. However, in contrast to frequency domain analysis, time domain analysis have limited parametric insight which makes model input corrections for model output improvements more complex and therefore more time consuming as well. The intended model corrections will be based on on-line motion measurements which is why these corrections have to be performed on-line as well. Thus despite the superior precision of time domain analysis in which ship motions can be computed, the time window of interest and the parametric insight of frequency domain analysis makes this the most suitable computational domain for the intended application.

Unfortunately though by definition almost nothing in nature is linear which is especially true for ship motions during heavy lift operations. Therefore within the domain of application the influence of these nonlinearities have to be studied. The domain of heavy lift operations is in fact determined by safe working conditions or in other words the workability of the vessel for a specific operational condition. The workability is dependent on numerous different items prescribed by the rules of regulations from for example DNV. However with regard to vessel motions the structural capability of the vessel or rather those from the hoisting cranes is decisive. Therefore, for example for the vessel a maximum rotational motion of 2 degrees is prescribed. Chapter 7.1.1 elaborates more on the workability. Furthermore the assumption is made that these motions are predominantly induced by wave induced forces. The domain of safe offshore heavy lift operations is thus determined by small excursions within the wave frequency domain.

Linearity

These small allowable motions makes it, by definition, possible to approximate the vessel and suspended cargo motions with the small-angle approximation. Within this domain may, however, occur other phenomena which can have a non-linear behavior. These phenomena are summarized and discussed in the following pages.

Possible factors for non-linear behavior:

- Dynamic hydrostatic force,
- Dynamic moment arm effect,
- Non-linear second order motions,
- Mooring restoring force,
- Non-linear viscous roll damping,
- Axial hoisting rope elasticity,
- Hoisting rope bending and twisting stiffness,
- Elastic boom effects.

From literature It became clear that it is absolutely necessary to perform an ship motion analysis which considers the full coupling between the load motion and the motion of the vessel. Even for rather small load masses, i.e. less than 2% of the displacement of the ship has already a significant impact on the motion behavior of the vessel. This means that the vessel or load response to the sea way can be shifted from a safe into an unsafe region and vice versa. [58, 60]

Furthermore it became clear that the hoisting ropes have to be modeled as springs since the combined horizontal and vertical oscillatory motions of the crane boom tip induce tension variations in the suspended hoisting ropes. This may induce large amplitude, swinging motions of the suspended load and causing nonlinear behavior in the axial hoisting wire stiffness. This kind of lock-in phenomenon occurs due to the excitation of a parametric instability similar in form to that of the Mathieu instability. In general due to parametric excitation, the more severe the sea state, the greater the time-varying stiffness response compared with the time-invariant stiffness response. However, with wave excitation representative of moderate sea states, which is the applicable domain for offshore heavy lift operations, modest behavior is observed since, fortunately, the development of the parametric instability is significantly reduced with the spread of wave excitation frequencies of modest sea states [60].

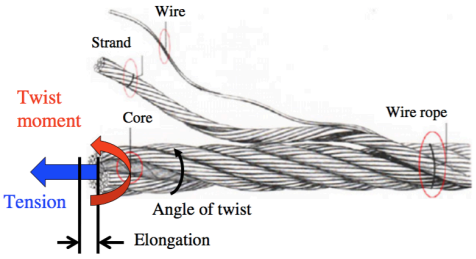

Figure 3.2: The configuration of the wire rope and the tension and torsion acting on the rope [9]

Wire ropes have three properties of stretching, bending and twisting and in practice heavy objects have to be lifted by multiple hoisting ropes clustered in blocks. Although the bending and twisting resistances are relatively small compared to the axial stiffness (tension) these are of importance when considering the cargo to be able to move in 6-degrees-of-freedom. Without additional measures to control the motion of the load these bending and twisting resistances are the only restoring forces present. Servin and Lacoursière introduced these properties modeled by kinematic constraints. By using length constraints, several bodies that were connected by one wire rope could be modeled [22].

From literature it has been found that if rotational motions of the cargo are included in the motion analysis such that the cargo can move in the 6-degrees-of-freedom, the motions of the cargo are larger than those for the 3-degrees-of-freedom motion of the cargo. Especially, the roll motion of the floating crane for the 6-degrees-of-freedom motion of the cargo was almost twice as large as that for the 3-degrees-of-freedom motion of the cargo. From this it is stated that it is important to consider the cargo as a 3-dimensional rigid body that has a 6-degrees-of-freedom of motion in order to estimate the motions of the floating crane and the heavy cargo. Furthermore was found that the twist moment of the wire rope plays the role of restoring the moment to the heavy cargo [9]. However, even though small vessel motions where registered, relative large cargo motions where allowed in this study. For example swinging cargo motions of 5° in pitch motion and a hoisting rope length of 40 m will result in a horizontal displacements of 3.5 m, which is absolutely to abundant for safe installations. Based on this restriction assumed is that rotational motions can be neglected for the intended application of this study. Since the cargo is modeled as a rigid body with only 3-translational-degrees-of-freedom, bending and twisting of the hoisting rope can be neglected as well.

Study shows that at larger motion amplitudes the nonlinear part of the characteristic mooring curve governs the motion characteristics of the vessel. In this scenario 2- and 3-periodic oscillations can occur, causing a substantial increase of loads and motion amplitudes. Based on this result one can state that nonlinear mooring characteristics are indispensable if future heavy lift operations are analyzed. However this study ends with the conclusion that a linear analysis of the dynamic behavior of floating cranes is sufficient and acceptable as long as nonlinear effects of system parameters are negligible and or outside the applicable domain, such as shallow water (with respect to the mooring line length) and small allowable excursions [12]. Therefore decided is to model the mooring system linearly.

Furthermore in studies is shown that slowly varying, low-frequency horizontal motions induced by second-order forces in wave groups generally did not affect the hook load response, and thus appear to be of no crucial influence on crane ship operation [51]. It should be mentioned however, that if the magnitude of the mooring restoring forces have to be determined these second order wave drift forces are the one to be studied since first order wave forces are generally to large for mooring systems to restore.

Taking into account the position and the mass of the hoisting cranes (2 x 220 tonnes at the bow) or in other words the booms it is expected that these will have significant influence on the vessel motions. Therefore the inertia of the booms is included in vessel motion calculations. The crane boom stiffness have influence on ship motions as well, however information about the boom stiffness is not available. Before making estimations on the crane boom stiffness, literature is studied in which the boom was modeled as an elastic body using finite element formulation and floating frame of reference formulation. The equations of motion were derived based on multibody dynamics. The dynamic motions of the floating crane and the barge were simulated by numerically solving the equations of motion. With a regular wave of 0°, simulations showed that vessel motions of the floating crane barge where increased by approximately 20% in all motions. For various cargo masses under the 45° wave, surge, pitch, and heave motions with the elastic boom were slightly larger than those with the rigid boom, while roll and sway motions were slightly larger with the rigid boom. The dynamic factor analysis showed ultimately only a 1.0–4.3% difference between the elastic boom and the rigid boom, according to the wave direction and the cargo mass [47]. Based on this information and the absence of proper information about the boom stiffness the boom is modulated as a rigid body.

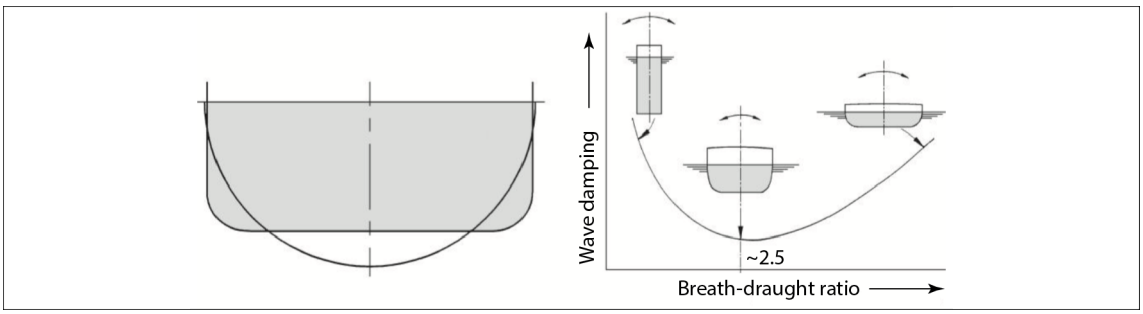

Figure 3.3: Roll Damping as function of shape and B/T ratio [29]

.

Due to the used linear wave theory (Airy wave theory) which for example is used for determining the wave effect diffraction, fluid viscosity is neglected. Airy wave theory uses a potential flow approach to describe the motion of gravity waves on a fluid surface. By assuming the fluid to be – inviscid and irrotational – potential flow in water waves is remarkably successful in describing the motions of the fluid. For many other fluid flows where it is often essential to take viscosity, vorticity, turbulence and/or flow separation into account this approach would fail. The applicability of this approach comes from the fact that for the oscillatory part of the fluid motion, wave-induced vorticity is restricted to some thin oscillatory Stokes boundary layers at the boundaries of the fluid domain. In deep water this effect is diminished at the boundary of the fluid domain. Without fluid viscosity fluid rotations are impossible which is why these can be omitted. However, by assuming the fluid to be inviscid, viscous roll damping

is neglected as well. This damping term can be very significant and is by definition nonlinear. However, taking into account the hull shape of the Rambiz 3000, which is rectangular with respect to the breadth over draft (B/T) ratio, no significant viscous roll damping is expected with regard to skin friction. Only the sharp corners of the hull will cause some viscous damping due to flow separation. The free surface wave induced damping will be dominant for this vessel which is illustrated in figure 3.3. Furthermore because of small vessel motions, the nonlinear term of this effect is expected to be small as well. Therefore it is assumed to be sufficient to include the equivalend linearized viscous roll damping in vessel response calculations. [10, 24, 29]

Last but not least the non-linear effect of hydrostatic force, due to altering surface area and the moment arm in roll/roll and pitch/pitch, can have significant influence on vessel motions. In the studied literature the effect of the non-linear effect is shown by determining the static equilibrium position with the partial derivatives of the hydrostatic force with respect to the immersion, heel and trim before starting the dynamic simulation. This is illustrated in figure 3.4. Dynamic response analysis shows that nonlinear effects of the hydrostatic force increase the dynamic motions. The analysed sea state was mild with H_s is 0.5m, T_p 10sec, WDir is 45° but near the swinging load resonance frequency. When nonlinear hydrostatic effects are taken into account, the motion amplitudes are 0.26m for surge, 0.18m for sway, 1.29m for heave, 0.54 deg for roll, 0.74 deg for pitch and 0.2d eg for yaw. Using linear hydrostatic forces, the corresponding values are 0.23m, 0.16m, 1.16m, 0.48 deg, 0.67 deg and 0.19 deg. The dynamic response of the cargo is thus increased by 11.5% when the nonlinear effect of the hydrostatic forces is considered [33]. Even though the in this article reported vessel motions for this specific loading condition where small, and thus within the applicable domain, the non-linear effect of hydrostatic force still had influence on vessel responses. Therefore by neglecting this nonlinear effect vessel responses are somewhat underestimated. It should be mentioned however that the magnitude of underestimation is dependent on vessel draft, vessel trim and heel and cargo mass.

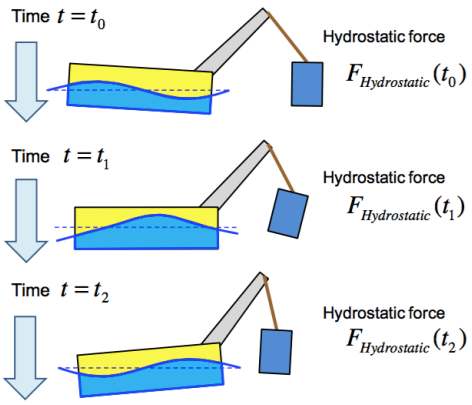

Figure 3.4: Calculation of the nonlinear hydrostatic force at every time step by considering the attitude of the floating crane and the wave elevation [9]

Despite this shortcoming in the applicable domain decided is to model in frequency domain. Parametric insight, the ability of on-line model adjustments (different loading conditions) and the ability of on-line comparisons between measured and computed vessel motion responses have profound implications but are in the first place the most important for this research. In the next chapter the influence of these non-linearities and thus the model validity within the applicable domain is tested and discussed. In summary the model content and the assumptions made are given below.

Model includes

- Fully coupled vessel and cargo motions
- Vessel 6-DOF
- Cargo 3-translational-DOF
- Linear Hydrostatic Force
- Hydrodynamic Force exerted by waves
- Gravity Forces
- Linear axial hoisting rope elasticity
- Linear mooring restoring forces
- Linearized viscous roll damping

Assumptions

- Linear wave theory
- Small vessel and load excursions
- Rigid body dynamics
- First order motions

3.2. Kinematics of Ship Motions

In this section the underlying kinematic model of the sea-keeping analysis for ship and cargo motions during a heavy lift operation is explained. There is a distinction between ship and cargo kinematics. From now the swinging cargo is called the suspended load. Figure 3.5 illustrates the model of the Rambiz3000 and its used nomenclature.

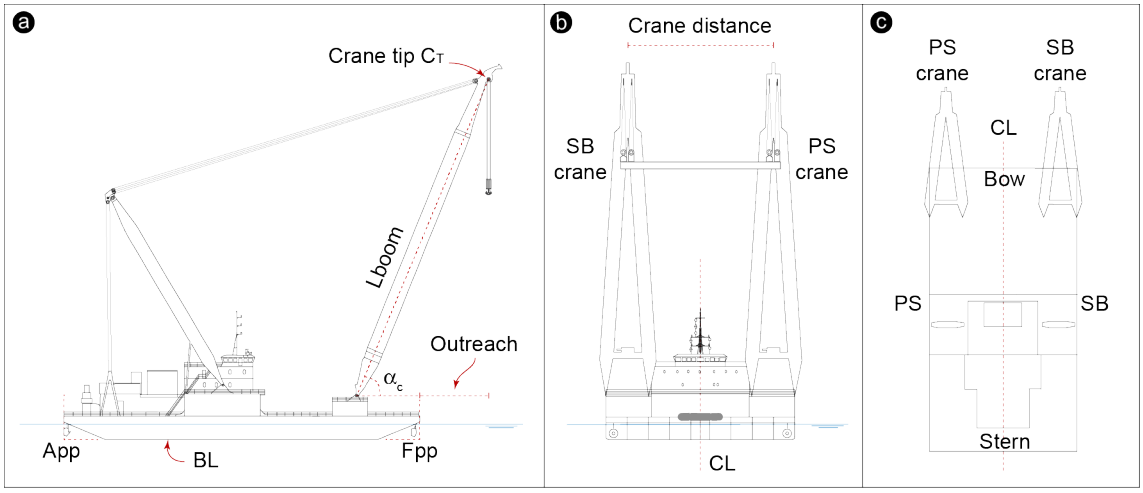

Figure 3.5: Model of the Rambiz 3000 and the used nomenclature.
View points: (a) SB side, (b) Bow, (c) Top.

3.2.1. Ship Kinematics

The motions of the ship are considered in six degrees-of-freedom. The rigid body of the crane barge can have three translatory (surge, sway and heave) and three rotational (roll, pitch and yaw) motions. To describe these motions, two Cartesian frames of reference are used. Namely the earth-fixed frame and the ship-fixed frame. The earth-fixed frame $\{O, x_0, y_0, z_0\}$ lies at the aft-perpendicular (App) of the ship or in other words in the center of the lower aft line of the ship. The second Cartesian frame of reference is fixed to the ship and is denoted by $\{G, x_G, y_G, z_G\}$. For convenience of the calculations the origin of $\{G, x, y, z\}$ is always located in the center of gravity of the ship without loading, so excluding the suspended load in the crane. This loading condition is also know as the Light Ship conditions.

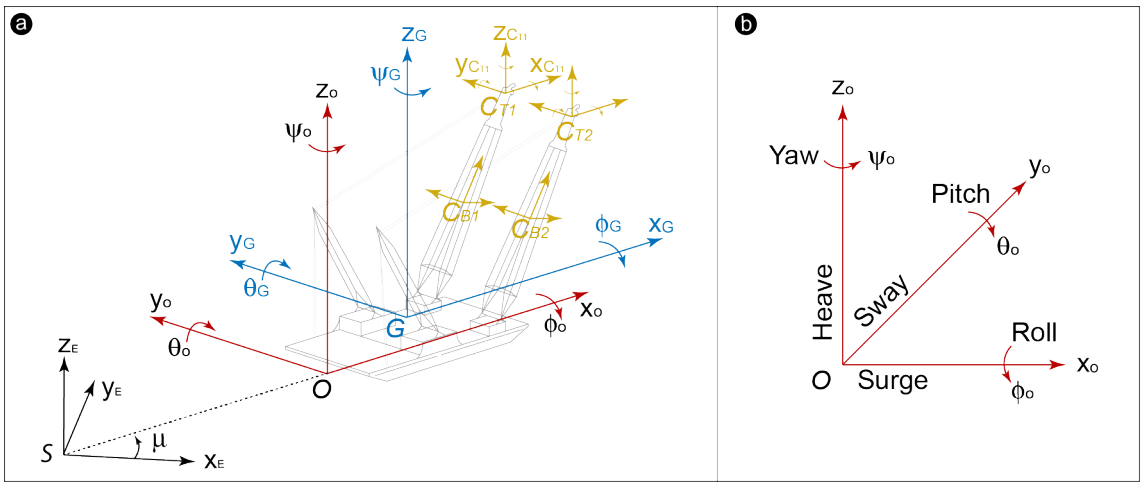

Figure 3.6: (a) Ship reference systems and (b) Ship motions and its nomenclature

As been illustrated in figure 3.6 the magnitudes describing the position and orientation of the ship are described according to the SNAME notation. The position and orientation is expressed in the earth-fixed frame and the coordinates are noted: $[x_o, y_o, z_o]$ and $[\phi_o, \theta_o, \psi_o]$ respectively. On the other hand,

the forces $[X, Y, Z]$, moments $[K, M, N]$, linear velocities $[u, v, w]$ and angular velocities $[p, q, r]$ are expressed in the body-fixed frame [53].

Fully coupled motions between vessel and suspended load are taken into account. Ship induced motions allows swinging of the suspended load and visa verse. Forces due to this swinging load are transferred via the crane tip which makes the position of the crane tip of importance. The position of the crane tip at port side is described in the ship fixed frame $\{C_{T1}, x_{ct1}, y_{ct1}, z_{ct1}\}$ and the position of the crane tip at starboard side is described in the ship fixed frame $\{C_{T2}, x_{ct2}, y_{ct2}, z_{ct2}\}$. The orientation of both reference frames is in line with the orientation of reference frame G.

Lastly the magnitudes describing the position of the hoisting cranes at port- and starboard side are described in the ship fixed frames $\{C_{B1}, x_{B1}, y_{B1}, z_{B1}\}$ and $\{C_{B2}, x_{B2}, y_{B2}, z_{B2}\}$ respectively. For convenience of the calculations the origin of both reference frames are always located at the center of gravity and its orientation in line with the orientation of the hoisting cranes itself. Taking ϕ, θ, ψ as roll, pitch and yaw, the transformation between the B- and G- frame is the result of three consecutive rotations about the principal axes:

$$R_B^G(\Theta_{GB}) \triangleq R_{x,\phi} R_{y,\theta} R_{z,\psi} \tag{3.1}$$

with

$$R_{x,\phi} \triangleq \begin{bmatrix} 1 & 0 & 0 \\ 0 & c\phi & -s\phi \\ 0 & s\phi & c\phi \end{bmatrix} \tag{3.2}$$

$$R_{y,\theta} \triangleq \begin{bmatrix} c\theta & 0 & s\theta \\ 0 & 1 & 0 \\ -s\theta & 0 & c\theta \end{bmatrix} \tag{3.3}$$

$$R_{z,\psi} \triangleq \begin{bmatrix} c\psi & -s\psi & 0 \\ s\psi & c\psi & 0 \\ 0 & 0 & 1 \end{bmatrix} \tag{3.4}$$

in which s ≡ sin(·) and c ≡ cos(·). Finally $R_B^G(\Theta_{GB})$ is given by:

$$R_B^G(\Theta_{GB}) \triangleq \begin{bmatrix} c\psi c\theta & -s\psi c\theta + c\psi s\theta s\phi & s\psi s\phi + c\psi c\phi s\theta \\ s\psi c\theta & c\psi c\phi + s\phi s\theta s\psi & -c\psi s\phi + s\psi c\phi s\theta \\ -s\theta & cs\phi & c\theta c\phi \end{bmatrix} \tag{3.5}$$

Dependent on the mass of the suspended load, crane angles (α_c) between 10.5°and 45°are allowed. Therefore in contrast to ship motion transformations between the G and O frame roll, pitch and yaw angles can not assumed to be small. The hoisting cranes are fixed to the Rambiz3000 such that they can rotate around the y-axis only. Furthermore the y axis of reference frame B is always in line with the y axis of reference frame G which makes this the only principle axes of rotation.

3.2.2. Suspended Load Kinematics

The motions of the suspended load are considerate in 3-degrees-of-freedom and modeled as a swinging pendulum induced by a stochastic process. For this the rotational motions in the horizontal plane of the suspended load are translated to lateral displacements in both the horizontal and vertical plane. This is illustrated in figures 3.7 and 3.8. The load m_L is modeled as a 2-dimensional rigid body and is suspended by a single hoisting rope with length l_s. The position of the suspended load is described in the ship fixed frame $\{Q, x_Q, y_Q, z_Q\}$. For convenience the magnitudes of displacement in the horizontal and vertical plane are described by $[\eta_7, \eta_8]$ and $[\eta_9]$ respectively. Kinematics of the suspended load and the interaction between the moving suspended load and the moving vessel is illustrated in figure 3.7.

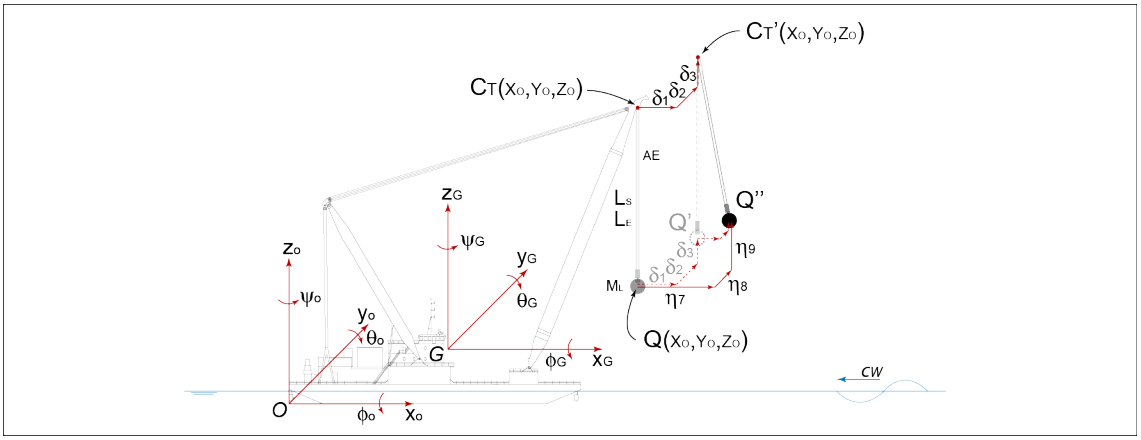

Figure 3.7: Suspended load kinematics and its nomenclature

The position of the crane tip $\{C_t, x_{ct}, y_{ct}, z_{ct}\}$ is given in the coordinate system of the ship by the radii vector $\vec{r}_p = x_{ct}\vec{i} + y_{ct}\vec{j} + z_{ct}\vec{k}$. Note that here for convenience the crane tip nomenclature is taken independent of ship side. The combined lateral displacements of the crane tip in horizontal and vertical direction is defined in vector form by

$$\begin{aligned}\vec{\delta} &= \vec{\eta}_{lin} + \vec{\eta}_{rot} \times \vec{r} \\ &= \delta_1\vec{i} + \delta_2\vec{j} + \delta_3\vec{k} \\ &= x_0\vec{i} + y_0\vec{j} + z_0\vec{k} + \begin{vmatrix} \vec{i} & \vec{j} & \vec{k} \\ \phi & \theta & \psi \\ x_{ct} & y_{ct} & z_{ct} \end{vmatrix}\end{aligned} \tag{3.6}$$

where x, y, z are the three translational motions and ϕ, θ, ψ the rotational motions of the ship. More convenient in matrix notation the displacement vector for the crane tip is defined by

$$\begin{Bmatrix} \delta_1(t) \\ \delta_2(t) \\ \delta_3(t) \end{Bmatrix} = \begin{bmatrix} 1 & 0 & 0 & 0 & z_{ct} & -y_{ct} \\ 0 & 1 & 0 & -z_{ct} & 0 & x_{ct} \\ 0 & 0 & 1 & y_{ct} & -x_{ct} & 0 \end{bmatrix} \begin{Bmatrix} x_o(t) \\ y_o(t) \\ z_o(t) \\ \phi(t) \\ \theta(t) \\ \psi(t) \end{Bmatrix} \tag{3.7}$$

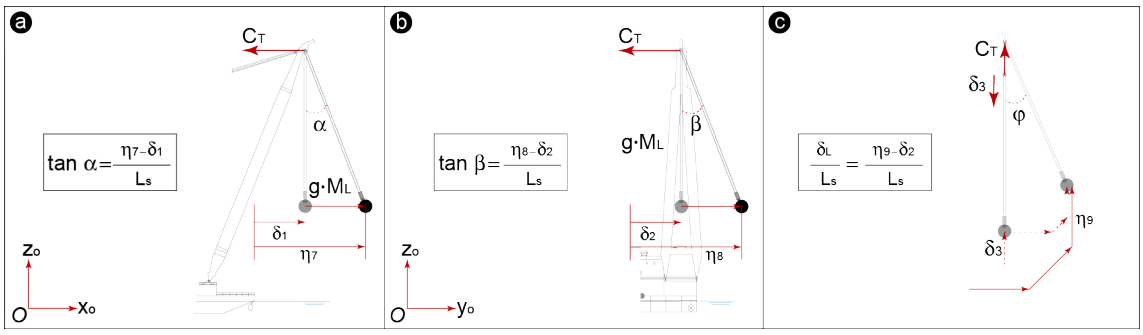

Figure 3.8: Linearized model of the swinging mass

When the displacement vector $\vec{\delta}$ in equation 3.6 is extended by the three rotational displacements α, β, φ of the suspended load, the displacements in longitudinal and transversal vertical planes are defined by

$$\eta_7(t) = l_s sin\alpha(t) \tag{3.8}$$
$$\eta_8(t) = l_s sin\beta(t) \tag{3.9}$$
$$\eta_9(t) = l_s \left(1 - \cos\varphi(t)\right) \tag{3.10}$$

in which l_s is the outstretched rope length of the hoisting rope. Assuming first order small motions in these planes allows the displacement equations to be linearized to simple displacements in tangential directions. For the rotational motions of the suspended load α and β the displacements in longitudinal and transversal vertical planes therefore becomes:

$$\tan\alpha = \frac{\eta_7 - \delta_1}{l_s} = \frac{1}{l_s}\left(\eta_7 - x_o - z_{ct}\theta_o + y_{ct}\psi_o\right) \tag{3.11}$$
$$\tan\beta = \frac{\eta_8 - \delta_2}{l_s} = \frac{1}{l_s}\left(\eta_8 - y_o - y_{ct}\psi_o + z_{ct}\phi_o\right) \tag{3.12}$$

which is illustrated in figure 3.8. Since the gravitational and restoring forces are dominant and the inertial forces of the suspended load are much smaller, the rope elastic stretching ϵ_{lr} and the rope effective stiffness AE must be taken into account. The linear rope elastic stretching is given by:

$$\epsilon_{lr} = \frac{\delta l_s}{l_s} \tag{3.13}$$

Therefore the vertical displacement as a result of the rope elastic stretching can be defined by

$$\frac{\delta l}{l_s} = \frac{\eta_9 - \delta_3}{l_s} = \frac{1}{l_s}\left(\eta_9 - z_o - y_{ct}\phi_o + x_{ct}\theta_o\right) \tag{3.14}$$

3.3. Kinetics of Ship Motions

In this section the proposed coupled equation of motions for describing vessel motion response during a heavy lift operation is given. The linear differential equation of motion is derived with the condition of small vessel and suspended load excursions. In matrix notation the resulting coupled equation of motions (EOM) is given by:

$$(\mathbf{M} + \mathbf{A}) \cdot \underline{\ddot{x}} + \left(\mathbf{B} + B_{eq}\right) \cdot \underline{\dot{x}} + (\mathbf{C_h} + \mathbf{C_m} + \mathbf{C_c}) \cdot \underline{x} = \underline{F_e} \tag{3.15}$$

in which M and A are respectively the system mass and hydrodynamic added mass matrices, B the hydrodynamic damping, B_{eq} the sea state dependent equivalent viscous roll damping, C_h the hydrostatic stiffness matrix, C_m the matrix of mooring restoring forces and C_c the linearized coupled stiffness matrix due to the interaction with the suspended load. Furthermore, $\underline{x}$ yields the vector of the vessel and the suspended load motions for respectively 6DOF and 3DOF given by:

$$\underline{x} = [x_G, y_G, z_G, \phi_G, \theta_G, \psi_G, \eta_7, \eta_8, \eta_9]^T \tag{3.16}$$

and $\underline{F_e}$ yields the vector of the exciting forces and moments ($\vec{F}_{FK} + \vec{F}_{DIF}$) of the incident waves:

$$\underline{F_e} = [X, Y, Z, K, M, N, X_7, Y_8, Z_9]^T \tag{3.17}$$

Note that all vectors and matrices are generalized since the physical quantities have different dimensions. Furthermore forces $[X_7, Y_8, Z_9]$ are equal to zero if the load is suspended above still water level and for example exited forces due to the wind are neglected. In this study only wave exited forces at the vessel body are taken into account.

3.3.1. Structural Mass and Inertia

The generalized rigid-body mass and inertia matrix with respect to reference frame G is given by:

$$\mathbf{M} = \left[\begin{array}{c|c} \mathbf{V}_{6x6} & 0 \\ \hline 0 & \mathbf{L}_{3x3} \end{array}\right] \tag{3.18}$$

in which $\mathbf{V}$ is the generalized mass and inertia matrix of the vessel hull including the fixed booms given by:

$$\mathbf{V} = \begin{bmatrix} m_S + m_B & 0 & 0 & 0 & 0 & 0 \\ 0 & m_S + m_B & 0 & 0 & 0 & 0 \\ 0 & 0 & m_S + m_B & 0 & 0 & 0 \\ 0 & 0 & 0 & I_{xx} + I_{BGxx} & -I_{xy} - I_{BGxy} & -I_{xz} - I_{BGxz} \\ 0 & 0 & 0 & -I_{yx} - I_{BGyx} & I_{yy} + I_{BGyy} & -I_{yz} - I_{BGyz} \\ 0 & 0 & 0 & -I_{zx} - I_{BGzx} & -I_{zy} - I_{BGzy} & I_{zz} + I_{BGzz} \end{bmatrix}$$

and $\mathbf{L}$ is the identity mass matrix of the suspended load given by:

$$\mathbf{L} = \begin{bmatrix} m_L & 0 & 0 \\ 0 & m_L & 0 \\ 0 & 0 & m_L \end{bmatrix}$$

Note that with respect to reference frame G, which is located at the centre of gravity of both the ship hull and the fixed booms together, the mass of the booms can simply be added to the mass of the ship itself. Also coupling terms between surge, pitch and yaw for example can be neglected. Note as well that for convenience of writing the mass and moment of inertia is taken independent of ship side. In the equation of motion both have to be included. The position of frame G is adopted from the stability booklet in which all dominant structural masses and its position have been described. If one for example would like to know vessel motions with respect to reference frame O the mass and inertia matrix $\mathbf{V}$ will become:

$$\mathbf{V} = \begin{bmatrix} mI_{3x3} & -mS(r_g^o) \\ mS(r_g^o) & I_S + I_{B1,2} \end{bmatrix} \tag{3.19}$$

in which m is the mass of the ship hull and booms together, r_g^o the coordinates vector of the center of gravity with respect to frame O and S(·) is the skew-matrix defined as:

$$S(r_g^o) = -S^T(r_g^o) \triangleq \begin{bmatrix} 0 & z_g^o & -y_g^o \\ -z_g^o & 0 & x_g^o \\ y_g^o & -x_g^o & 0 \end{bmatrix} \tag{3.20}$$

In light ship conditions the mass of the ship m_S and booms $m_{B1,2}$ together can be calculated as the product of the water density and the displacement volume ∇ , $(m_S + m_{B1,2}) = \rho\nabla$. During heavy lift simulations this does not apply since the mass of the cargo has to be modeled separately. Furthermore because of the variable ballast during the operation in order to trim the vessel to the desired working position the ”structural” mass of the vessel is not constant. Therefore the vessel hull mass is calculated as $m_S = \nabla/(m_L + m_{B1,2})$. The displaced volume is obtained from 3-D panel methods by making use of the software package ANSYS AQWA v15.[1] For similar reasons the vessel hull moment of inertia have to be approximated by:

$$I_{ij} = \begin{cases} I_{xx} = k_{xx}^2 \cdot m_S \approx (0.34B)^2 \cdot m_S \\ I_{yy} = k_{yy}^2 \cdot m_S \approx (0.25L)^2 \cdot m_S \\ I_{zz} = k_{zz}^2 \cdot m_S \approx (0.26L)^2 \cdot m_S \end{cases} \tag{3.21}$$

in which B and L are the vessel breadth and length. Due to the symmetric vessel hull shape in the xy-plane coupling terms $I_{xy} = I_{yx}$ are equal to zero and $I_{xz} = I_{zx}$ can be neglected since these are very small.

[1] ANSYS Aqwa software is an engineering analysis suite of tools for the investigation of the effects of wave, wind and current on floating and fixed offshore structures

The moment of inertia of the booms can not be neglected. Unfortunately there is no detailed information available about the quantity. Therefore the moment of inertia with respect to its own reference frame CB is simply approximated by:

$$\mathbf{I}_B = \frac{M_B}{12} \begin{bmatrix} (y_b^2 + z_b^2) & 0 & 0 \\ 0 & (x_b^2 + z_b^2) & 0 \\ 0 & 0 & (x_b^2 + y_b^2) \end{bmatrix} \tag{3.22}$$

which is then translated to the position and orientation of reference frame G by making use of the parallel axes theorem and equation 3.3. The translation of the moment of inertia from frame CB to frame G is given by:

$$\mathbf{I}_B^G = M_B \begin{bmatrix} (y_{cb}^2 + z_{cb}^2) & -x_{cb}y_{cb} & -x_{cb}z_{cb} \\ -y_{cb}x_{cb} & (x_{cb}^2 + z_{cb}^2) & -y_{cb}z_{cb} \\ -z_{cb}x_{cb} & -z_{cb}y_{cb} & (x_{cb}^2 + y_{cb}^2) \end{bmatrix} \tag{3.23}$$

Together with the rotation of axes system CB to the orientation of axes system G gives the contributing moment of inertia with respect to frame G:

$$\begin{aligned} \mathbf{I}_{BG} &= R_{y,\theta} \cdot \mathbf{I}_B + \mathbf{I}_B^G \\ &= \begin{bmatrix} \cos\theta & 0 & \sin\theta \\ 0 & 1 & 0 \\ -\sin\theta & 0 & \cos\theta \end{bmatrix} \cdot \frac{M_B}{12} \begin{bmatrix} (y_b^2 + z_b^2) & 0 & 0 \\ 0 & (x_b^2 + z_b^2) & 0 \\ 0 & 0 & (x_b^2 + y_b^2) \end{bmatrix} \\ &+ M_B \begin{bmatrix} (y_{cb}^2 + z_{cb}^2) & -x_{cb}y_{cb} & -x_{cb}z_{cb} \\ -y_{cb}x_{cb} & (x_{cb}^2 + z_{cb}^2) & -y_{cb}z_{cb} \\ -z_{cb}x_{cb} & -z_{cb}y_{cb} & (x_{cb}^2 + y_{cb}^2) \end{bmatrix} \end{aligned} \tag{3.24}$$

Note also here for convenience of writing $\mathbf{I}_{BG}$, M_B and all coordinates are taken independent of ship side. In the equation of motion both booms with respect to their own orientation have to be included.

3.3.2. Hydrostatic force & Hydrodynamic mass and damping

As discussed the displaced volume is obtained with ANSYS AQWA v15. The resultant hydrostatic restoring forces proportional to the vessel translation and rotation are obtained from this software package as well. The hydrostatic stiffness of the system in matrix form is given by:

$$\mathbf{C}_h = \left[\begin{array}{c|c} \mathbf{c}_{ij} & 0 \\ \hline 0 & 0 \end{array}\right] \tag{3.25}$$

where $\mathbf{C}_h$ has dimensions 9 x 9 and $\mathbf{c}$ with $i, j = 1..6$ represents the hydrostatic restoring forces for all six vessel motions. The non zero spring coefficients of c_{ij} are in heave roll and pitch and their non trivial terms are namely:

$$\begin{aligned} c_{33} &= \rho g \iint_{S_b} n_3 dS = \rho g A_{wl} \\ c_{35} &= c_{53} = -\rho g \iint_{S_b} x n_3 dS \\ c_{44} &= \rho g \iint_{S_b} y^2 n_3 dS + \rho g \nabla z_b - m g z_g = \rho g \nabla GM \\ c_{55} &= \rho g \iint_{S_b} x^2 n_3 dS + \rho g \nabla z_b - m g z_g = \rho g \nabla GM_L \end{aligned} \tag{3.26}$$

Note that the centre of rotation (in statics equivalent to the centre of gravity) has to be chosen carefully. Due to the proposed coupled stiffness matrix $\mathbf{C_c}$ representing the coupling between the suspended load and vessel, the centre of gravity from the system excluding the suspended load has to be taken. If the the mass of the suspended load transferred via the crane tip is included in the centre of gravity, coupling between the vessel and suspended load is counted twice in roll/roll and pitch/pitch motions. Obviously

it must be taken into account with regard to the draft and hence the hydrostatic and hydrodynamic forces and moments.

The wave frequency and direction dependent hydrodynamic forces and moments are also obtained with ANSYS AQWA v15. With this software package it is possible to compute numerically the potential flow around a submerged body. The velocity potential is given by:

$$\Phi(x, y, z, t) = \Phi_{rad} + \Phi_{FK} + \Phi_d \tag{3.27}$$

where the right hand side terms represent the the velocity potential components due to radiation, incoming and diffracted waves respectively. The added mass and damping are decomposed from the radiation forces of this potential flow which appear due to change in momentum of the fluid caused by vessel motion. In short these potential coefficient are obtained with ANSYS AQWA which is making use of 3-D diffraction/ panel methods. Based on the Green's integral theorem it is possible to transform the required 3-dimensional linear homogeneous differential equation into a 2-dimensional integral equation. Computationally seen this is more efficient since this surface integral can be solved numerically by dividing the surface in a number of flat panels. The panel size determines the minimum wave length for which the assumption of constant doublets strengths and fluid pressures can be ensured. In the figure bewlow a representation of the Rambiz3000 hull form in 3-D and the applied grid size is given.

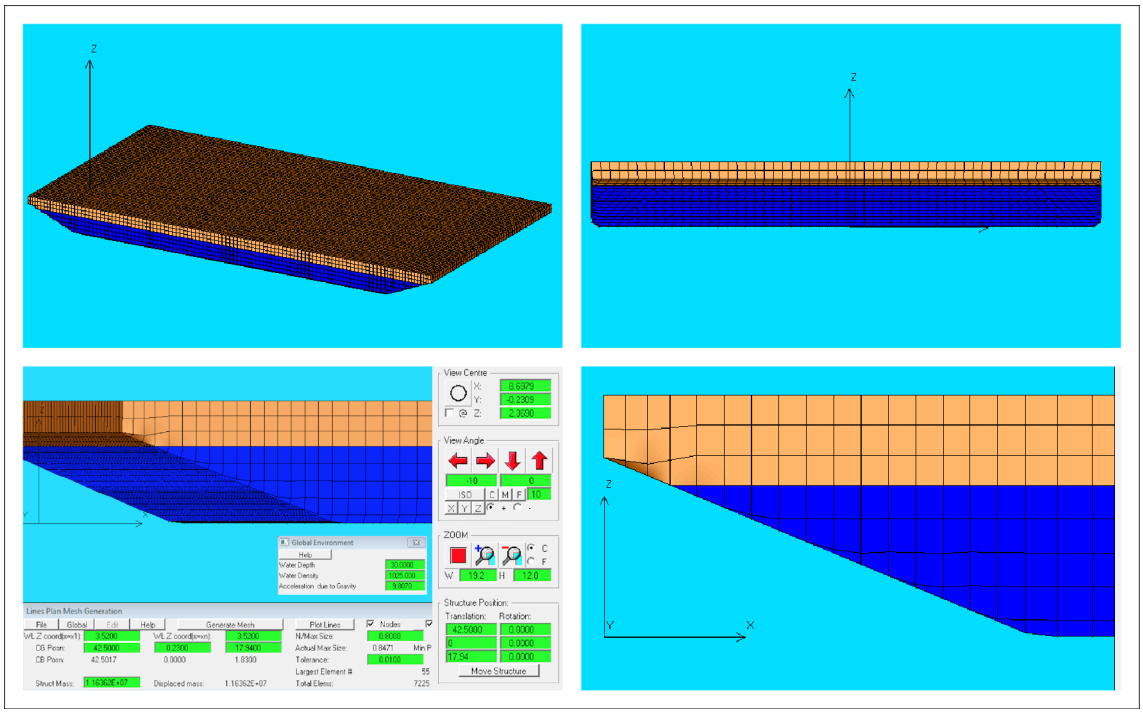

Figure 3.9: AQWA model representing the Rambiz3000 hull form in 3-D and its panel grid-size

In matrix notation the frequency dependent linearized hydrodynamic added mass and damping coefficients for the total system is given by:

$$\mathbf{A} = \left[\begin{array}{c|c} a_{ij} & 0 \\ \hline 0 & 0 \end{array}\right] \quad and \quad \mathbf{B} = \left[\begin{array}{c|c} b_{ij} & 0 \\ \hline 0 & 0 \end{array}\right] \tag{3.28}$$

where $\mathbf{A}$ and $\mathbf{B}$ have dimensions 9 x 9 and a_{ij} and b_{ij} with motions $i, j = 1..6$ represents the vessel added mass and damping given by:

$$a_{ij} = \begin{bmatrix} a_{11} & 0 & a_{13} & 0 & a_{15} & 0 \\ 0 & a_{22} & 0 & a_{24} & 0 & a_{26} \\ a_{31} & 0 & a_{33} & 0 & a_{35} & 0 \\ 0 & a_{42} & 0 & a_{44} & 0 & a_{46} \\ a_{51} & 0 & a_{53} & 0 & a_{55} & 0 \\ 0 & a_{62} & 0 & a_{64} & 0 & a_{66} \end{bmatrix} \quad and \quad b_{ij} = \begin{bmatrix} b_{11} & 0 & b_{13} & 0 & b_{15} & 0 \\ 0 & b_{22} & 0 & b_{24} & 0 & b_{26} \\ b_{31} & 0 & b_{33} & 0 & b_{35} & 0 \\ 0 & b_{42} & 0 & b_{44} & 0 & b_{46} \\ b_{51} & 0 & b_{53} & 0 & b_{55} & 0 \\ 0 & b_{62} & 0 & b_{64} & 0 & b_{66} \end{bmatrix}$$

The terms on the diagonals represent the hydrodynamic mass or damping in one direction to the inertia force or moment in that same direction. Off-diagonal terms represent hydrodynamic mass or damping which is associated with an inertia dependent force or moment in a direction caused by another motion component. Forward speed has influence on the velocity components but is not included in this study since heavy lift installations are conducted at a static position. With zero forward speed matrices a_{ij} and b_{ij} become symmetric.

3.3.3. Viscous Roll Damping

As discussed in chapter 3.1 that the major part of damping is caused by wave damping or in other words potential damping which is obtained from the diffraction analysis in ANSYS AQWA, discussed in the previous section. However especially in roll motion, damping due to viscous effects dissipate energy from the moving vessel as well. Since the magnitude of roll motion is an important limitation in the workability and the roll natural period of the vessel falls within the frequency range of a typical wave energy spectrum, this damping is included. The linearized viscous roll damping, in the EOM denoted by $\mathbf{B_{eq}}$ is determined according to Subarata Chakrabarti, 2001.

The nonlinear equation of motion in roll may be written as:

$$I\ddot{\phi} + B(\dot{\phi})\dot{\phi} + C(\phi, t) = M\cos(\omega t + \varepsilon) \tag{3.29}$$

in which ϕ is the angular roll motion, I the moment of inertia in roll motion, M the wave exciting moment, ω the wave frequency and t is time. Furthermore the damping coefficient B and the restoring coefficient C are shown as nonlinear quantities. The modulus of the roll velocity in the second term on the left hand side of the EOM is needed for the correct sign to its contribution. This damping moment can be linearised by assuming that the amount of energy dissipated by a equivalent linear term B_{eq} is equal to that of the quadratic term. For a certain period T this reads:

$$\frac{1}{T}\int_0^T \left\{B_{eq}\dot{\phi}\right\} \cdot \left\{\dot{\phi}dt\right\} = \frac{1}{T}\int_0^T \left\{B_1\dot{\phi} + B_2\left|\dot{\phi}\right|\dot{\phi} + B_3\dot{\phi}^3\right\}\left\{\dot{\phi}dt\right\} \tag{3.30}$$

which can be written as

$$B(\dot{\phi}) = B_1\dot{\phi} + B_2\left|\dot{\phi}\right|\dot{\phi} + B_3\dot{\phi}^3 \tag{3.31}$$

in which the first term is linear, the second quadratic and the third cubic. By substituting the linear roll velocity $\dot{\phi} = -\omega_a \sin(\omega t + \varepsilon)$, the linearized viscous roll damping becomes

$$B(\dot{\phi}) = B_{eq}\dot{\phi} \tag{3.32}$$

in which

$$B_{eq} = B_1 + \frac{8}{3\pi}B_2(\omega\phi) + \frac{3}{4}B_3(\omega\phi)^2 \tag{3.33}$$

For prediction of viscous roll damping in irregular seas stochastic linearization, originally described by Kaplan (1966), is applied. By assuming both the input and output to be Gaussian with zero mean the error between the linearized and actual system is defined by:

$$B_{eq} = B_1 + \frac{8}{\pi}\sigma_{\dot{\phi}}B_2 \tag{3.34}$$

where the cubic terms is neglected and, $\sigma_{\dot{\phi}}$, is the standard deviation of roll velocity. The standard deviation of a Gaussian process with zero mean is equal to the root mean square, in other words the squire root of the zeroth moment of the response spectrum denoted by m_0. For the roll velocity this becomes thus,

$$\sigma_{\dot{\phi}} = \sqrt{m_0} = \sqrt{\frac{m_2}{m_0}}\sqrt{m_0} = \sigma_{\phi}\frac{2\pi}{T_z} \tag{3.35}$$

which finally gives the equivalent roll damping due to viscosity in irregular seas:

$$B_{eq} = B_1 + \frac{8}{\pi}\sigma_{\phi}\frac{2\pi}{T_z}B_2 \tag{3.36}$$

The equivalent viscous roll damping comprises of the following terms

$$B_{eq} = B_f + B_e + B_w + B_L + B_{BK} \tag{3.37}$$

where,B_f, is the hull skin friction, B_e, the eddy making damping, B_w, the free surface wave damping, B_L, the lift force damping and ,B_{BK}, is the bilge keel damping. Since the Rambiz 3000 does not have a bilge keel and the vessel velocity is practically seen zero during installations, term ,B_{BK}, is equal to zero and term ,B_L, practically zero. Furthermore as discussed the free surface wave damping is obtained with 3-D panels methods.

Skin friction
Friction damping is caused by friction of the water particles on the ships hull when it is in roll motion. This viscous damping coefficient is the smallest contributing coefficient in roll damping which slightly increases with forward speed. For zero forward speed Kato (1965) gives an expression for the friction damping in a laminar flow field:

$$B_{f0} = \frac{4}{3\pi}\rho S r_e^3 \phi \omega C_f \tag{3.38}$$

in which the friction coefficient is dependent on fluid viscosity, bilge radius, wave frequency and of course roll amplitude. The friction coefficient is given by:

$$C_f = 1.328\left[\frac{2\pi\nu}{3.22 r_e^2 \phi\omega}\right]^{1/2} \tag{3.39}$$

in which the effective bilge radius is computed from

$$r_e = \frac{1}{\pi}\left[(0.887 + 0.145C_B)\frac{S}{L} - 2OG\right] \tag{3.40}$$

The wetted surface of the ship S is calculated in the hydrostatics script of the simulation model by making use of simple geometric relations. The block coefficient C_B of the ship hull is defined by

$$C_B = \frac{\nabla}{L_{WL}BT} \tag{3.41}$$

The vertical distance from still water level to the roll axes, OG, can be computed by $OG = T - KG$ which becomes positive when CoG is below the free water surface. The lateral dimension of the ship hull is denoted by L. It should be noted that the proposed skin friction coefficient (C_f) is a function fluid viscosity which results in higher skin friction coefficients in model scale compared to full scale skin friction coefficients. Scaling by making use of Froud's law is not applicable. The proposed skin friction damping coefficient in laminar flow (equation 3.38) is adjusted for turbulent flow which gives the final friction damping coefficient:

$$B_f = 0.787\rho S r_e^2\sqrt{\omega\nu}\left\{1 + 0.00814R_e^{0.386}\right\} \tag{3.42}$$

where R_e is an equivalent Reynolds number defined as $R_e = (r_e\phi)^2\omega/\nu$.

Eddy making damping

In roll motion viscous eddy damping arises by sharp corners in the hull shape. These sharp corners disturbs the fluid flow along the vessel causing flow separation and consequently pressure differences at these corners. The cross sectional shape of the hull of the Rambiz 3000 is almost square which makes this damping coefficient the largest contributing. This component of damping is found to be a square function of the roll frequency as well as the roll amplitude. Numerous methods for determining the eddy making damping coefficients are known, however, Ikeda (1984) proposed a simple formula based on experiments on two dimensional models of rectangular cross sections with different breadth to draft ratios. The proposed eddy-making damping coefficient for zero forward speed is computed from:

$$B_e = \frac{2}{\pi}\rho L T^4 \cdot \left(H_0^2 + 1 - \frac{OG}{T}\right) \cdot \left[H_0^2 + \left(1 - \frac{OG}{T}\right)^2\right] \cdot \phi\omega \tag{3.43}$$

in which H_0 is the half-beam-draft ratio ($H_0 = B/2T$). In the figure below the equivalent linearized viscous roll damping is illustrated, note the difference in magnitude between the skin friction and eddy making damping coefficients.

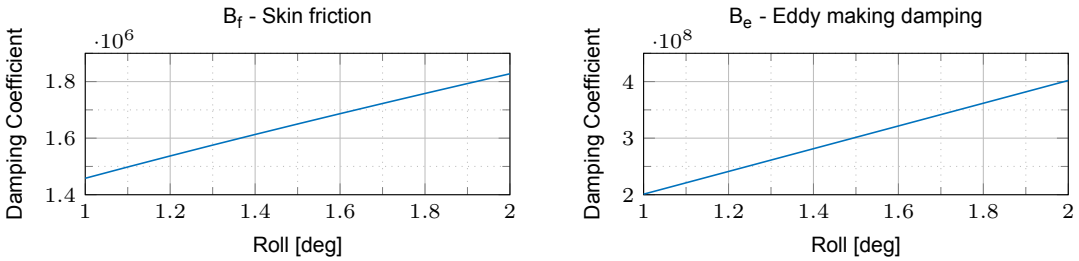

Figure 3.10: Equivalent linearized viscous roll damping

3.3.4. Mooring restoring force

The 9 x 9 mooring restoring stiffness matrix is given by:

$$\mathbf{C}_m = \left[\begin{array}{c|c} \mathbf{C}_{mm} & 0 \\ \hline 0 & 0 \end{array}\right] \tag{3.44}$$

where $\mathbf{C}_{mm}$ is the 6 x 6 mooring stiffness matrix for the crane vessel. The mooring stiffness matrix is symmetric and only horizontal restoring forces are taken into account. Therefore the only non-zero elements are

$$C_{mm11}, \quad C_{mm12}, \quad C_{mm16}, \quad C_{mm22}, \quad C_{mm26}, \quad C_{mm66}$$

If the mooring system is symmetric only the diagonal elements of $\mathbf{C}_{mm}$ are non-zero. The restoring coefficients may be estimated by a mooring analysis program while for simple catenary mooring configurations a static analysis can be done by hand calculations where the restoring forces originate from the gravity of the lifted chain. In the figure below the geometry of a single catenary mooring line with touch down is given [16].

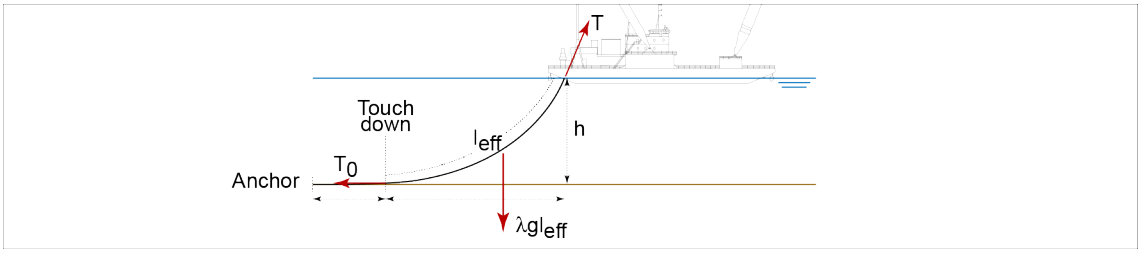

Figure 3.11: Geometry of a simple catenary mooring and its resulting force balance

The restoring force coefficient can be computed with:

$$\begin{aligned} C_x &= \frac{dF}{dx} = \frac{1}{\frac{dL}{dT_0}} = \frac{\lambda g}{\frac{dL}{da}} \\ &= \frac{\lambda g}{\sinh^{-1}\left(\sqrt{\frac{h^2}{a^2}} + 2\frac{h}{a}\right) - (1 + \frac{a}{h+a})\frac{h}{\sqrt{h^2+2ah}}} \end{aligned} \tag{3.45}$$

where λ is the submerged weight of the chain per unit length, h the water depth and a the length that relates the mass of the chain with the horizontal component of the tension. The definition for a is given by:

$$a = \frac{F_x}{\lambda g} \tag{3.46}$$

By making use of this definition and the equation for the effective mooring length, l_{eff}, the horizontal mooring force, F_x, and thus also a can be computed. The effective mooring length is given by:

$$\frac{l_{eff}}{h} = \sqrt{1 + s\frac{a}{h}} \tag{3.47}$$

and lastly the horizontal mooring force is defined by:

$$F_x = \frac{h}{2}\left(\left(\frac{l_{eff}}{h}\right)^2 - 1\right)\lambda g \tag{3.48}$$

Note that if the vessel is not moored but a dynamic positioning (DP) system is used for maintaining position, the DP system may be approximated by a linear spring damper system with a restoring matrix similar to the one given in 3.44.

3.3.5. Coupled Stiffness matrix

Finally based on the accepted assumptions described in chapter 3.1, the relation between the vessel motions and restoring forces as a result of the swinging load suspended by elastic hoisting ropes the symmetric coupled stiffness matrix is given by:

$$\mathbf{C}_c = \left[\begin{array}{cccccc|ccc} k_s & 0 & 0 & 0 & k_s z_{ct} & -k_s y_{ct} & -k_{s1} & 0 & 0 \\ & k_s & 0 & -k_s z_{ct} & 0 & k_s x_{ct} & 0 & -k_s & 0 \\ & & k_e & k_e y_{ct} & -k_e x_{ct} & 0 & 0 & 0 & -k_e \\ & & & C_{c44} & -k_e x_{ct} y_{ct} & -k_s z_{ct} x_{ct} & 0 & k_s z_{ct} & -k_e y_{ct} \\ & & & & C_{c55} & -k_s z_{ct} y_{ct} & -k_s z_{ct} & 0 & k_e x_{ct} \\ & & & & & C_{c66} & k_s y_{ct} & -k_s x_{ct} & 0 \\ \hline sym. & & & & & & k_s & 0 & 0 \\ & & & & & & & k_s & 0 \\ & & & & & & & & k_e \end{array}\right] \tag{3.49}$$

where restoring stiffness terms in roll/roll, pitch/pitch and yaw/yaw are given by:

$$C_{c44} = k_s z_{ct}^2 + k_e y_{ct}^2 \tag{3.50}$$
$$C_{c55} = k_s z_{ct}^2 + k_e x_{ct}^2 \tag{3.51}$$
$$C_{c66} = k_s (x_{ct}^2 + y_{ct}^2) \tag{3.52}$$

The horizontal and vertical restoring forces, respectively due to the gravity and axial stiffness of the hoisting rope are given by:

$$k_s = \frac{m_L \cdot g}{l_s} \tag{3.53}$$

$$k_e = \frac{AE}{l_e} \tag{3.54}$$

in which l_s is the outstretched hoisting rope length and l_e is the effective elastic hoisting rope length which is defined by

$$l_e = \frac{m_L \cdot g \cdot l_s}{AE} \tag{3.55}$$

The length of the outstretched hoisting rope is equivalent to the distance between the crane tip and the centre of gravity of the suspended load. Note that in this case by using equation 3.55 the effective hoisting rope length is overestimated and thus the vertical restoring force k_e is underestimated. The rope area A is simply defined by

$$A = \frac{\pi D^2}{4} \cdot C_f \tag{3.56}$$

where C_f is the filling coefficient of the hoisting ropes which is taken as 0.58. The Youngse modulus is taken as $E = 196 \cdot 10^9$ Pa and the hoisting rope diameter as $D = 51.4 \cdot 10^3$ m. Since the load is suspended by 16 hoisting ropes both the axial rope stiffness and area are multiplied by the same amount. For the sake of clarity the derivation of the horizontal restoring force due to the gravity and the vertical restoring force due to the axial hoisting rope stiffness is given and illustrated in figure 3.12.

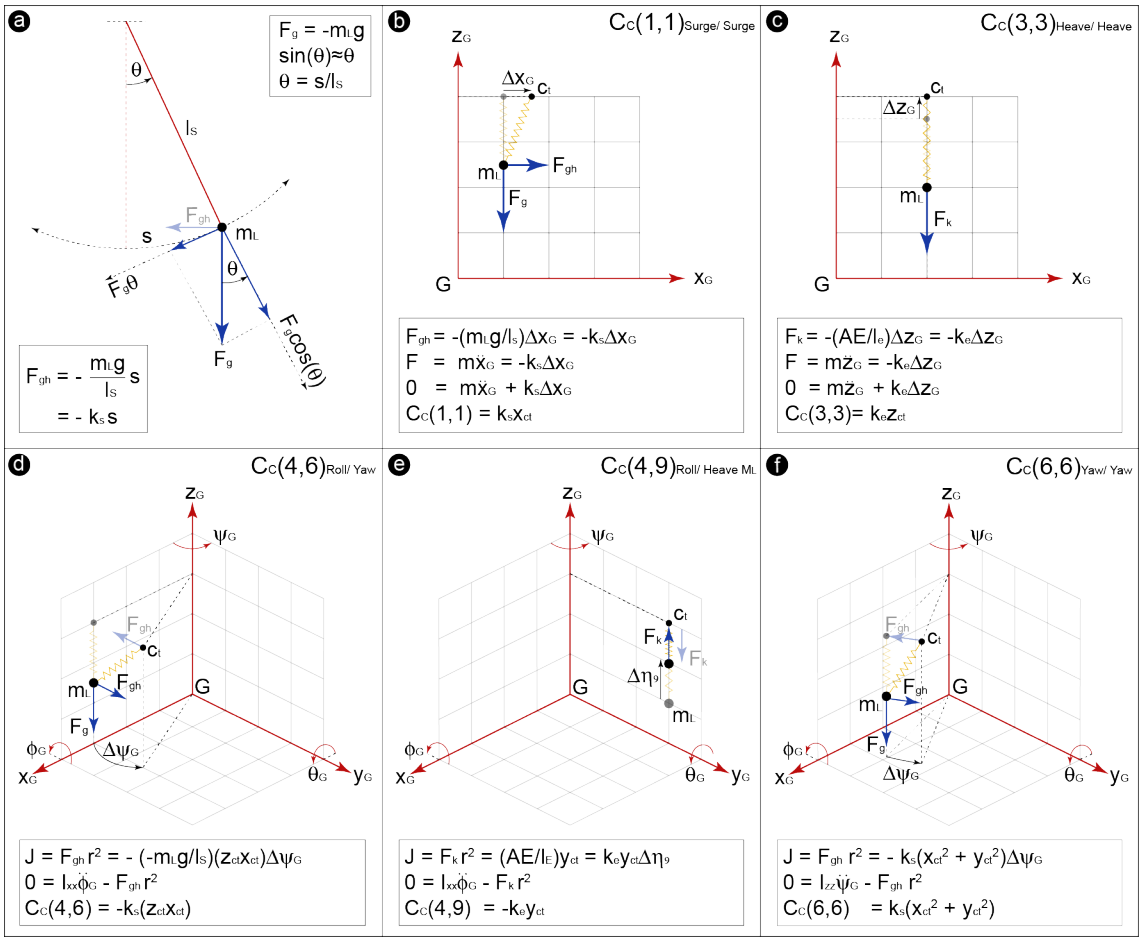

Figure 3.12: Small angle approximation and the derivation of several restoring terms due to gravity or axial hoisting rope stiffness.

3.4. Matlab Tool

To be able to actually study the possibilities concerning improved vessel response predictions by making use of on-line vessel response measurements, a numerical tool has been developed. There are numerous software packages available which support numerical computing of which software packages/ programming languages Python and Matlab are most often used for engineering purposes. Chosen is to program in Matlab because of experience with that language, the available toolboxes and build in features for example matrix operations, interpolation between data points, statistics and data visualizations.

Just as the described simulation model the numerical tool is developed for parametric insight, speed and simplicity bearing in mind that the tool in a later stage could be used on-line for testing. In contrast to the ship kinetics, which is described specifically for the Rambiz 3000, the tool is programmed such that it can easily be used for different crane vessels with different crane configurations. In order to make this possible, the tool is made up of several modules consisting of functions for various applications. The modules are connected with each other in the so called Wrapper. In this Wrapper the desired output, such as point RAOs or the workability for a specific loading condition can be requested simply by giving it the desired input and by turning switches on or off.

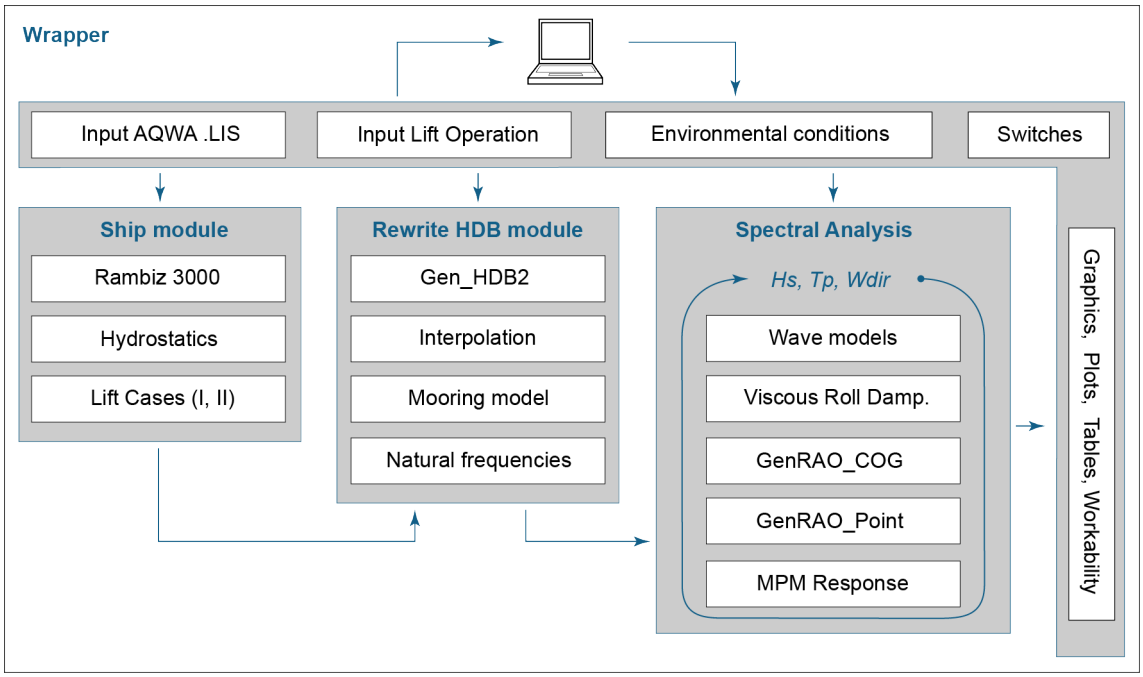

Figure 3.13: Structure of the Matlab Tool for ship motion simulations during a heavy lift operation

As can be seen there are three main modules in the Wrapper and some requested input and desired output. The requested input consist of the following items:

- ANSYS AQWA .LIS file(s)
- Desired wave spectrum:
  - PM, JONSWAP, Torsethaugen
- Wave spectrum parameters:
  - Hs, Tp, γ, Water depth
- Operational condition:
  - Mass & Height suspended load
  - Outreach and Crane configuration
- MPM & Workability Criteria
- Mooring setup

The Ship Module is the only module specifically for the Rambiz 3000, all other scrips and modules could be used for other applications as well. In this module vessel aspects such as the vessel geometry and hoisting rope properties are given and crane positions are computed. Due to the flexibility of different lifting conditions the structural hull mass and moment of inertia together with the hull form coefficients (needed for computing the viscous roll damping) are computed in the Hydrostatics script. The

Rewrite HDB Module is required for a well-organized database in 9 DOF since the original hydrodynamic database is build from one or multiple ANSYS AQWA .LIS file(s) which contains the hydrostatic- and dynamic data in 6 DOF. In this module also the mooring restoring forces and natural frequencies of the ship hull, swinging pendulum and mooring system are computed. Optionally for obtaining the desired density in wave frequencies and wave directions the original hydrodynamic data from ANSYS AQWA can be interpolated with a desired interpolation technique (nearest, linear or spline) and interpolation step. This can be controlled by the switches.

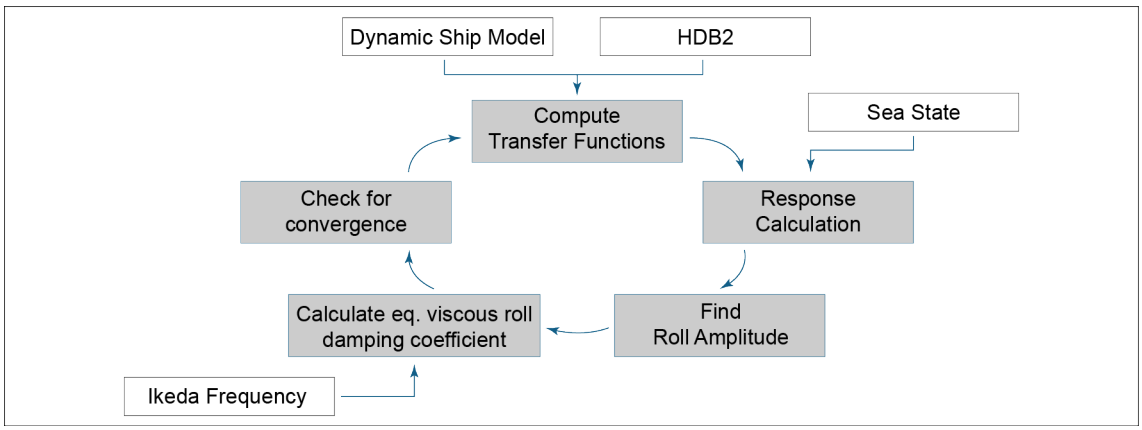

Figure 3.14: Iteration scheme for determining the equivalent viscous roll damping

More interesting is the Spectral Analyses script in which the wave spectra, vessel responses and short term statistics are being computed. Once the desired wave spectrum is computed vessel RAOs with respect to reference frame G are being computed in this module. If desired included in this calculation can be the sea state dependent viscous roll damping. Due to the dependency on roll response the equivalent roll damping has to be determined iterative which is illustrated in figure 3.14. The iteration scheme and script is adopted from Mocean offshore who developed this method in-house. To make it compatible for zero forward speed cases it is however adjusted. Furthermore point RAOs for a predefined point (crane tip or motion measurement sensor) or any other desired point at the ship are calculated from which the RAOs at the crane tip are being used in the MPM script. Here the most probable maximum response according to a desired time window is computed. Last but not least according to some desired criteria such as a maximum DAF, roll response or side lead angle the workability is determined which can be displayed visually as illustrated in the figure below. Chapter 7.1.1 elaborates more on the determination of the MPM side lead angle.

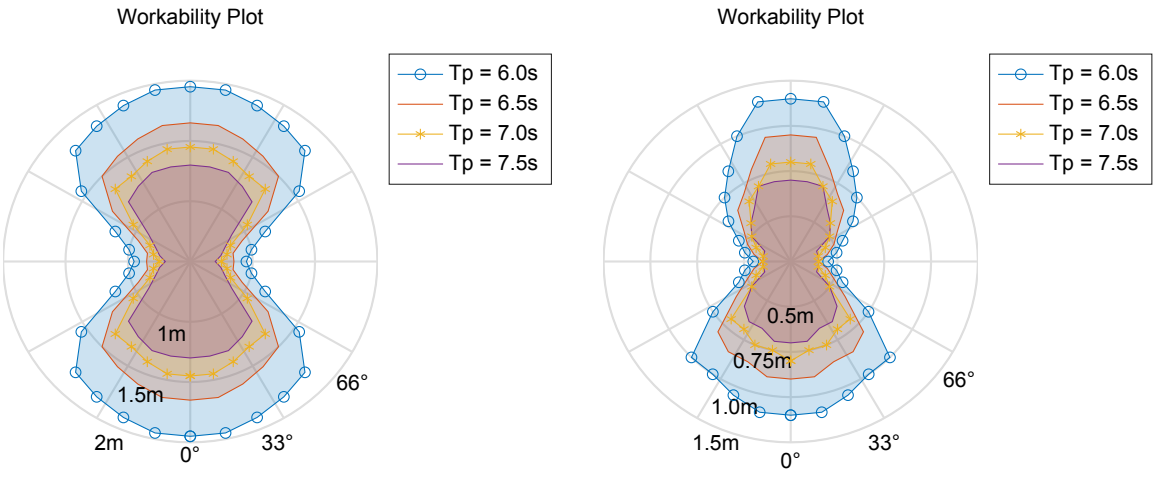

(a) Light Ship (b) Heavy Lift Operation

Figure 3.15: Workability plots for waves that contain the JONSWAP spectrum with $\gamma = 3.3$ and WD = 40m.

The light ship condition mode, or in other words when no heavy lift operation is being conducted, becomes active when zero mass is specified for the suspended load. Then only the crane configuration and its added inertia are being included in the vessel response calculations. The Lift Cases module is no longer active and the Rewrite HDB module does not expand to nine dimensions. In this way, virtually any operational condition can be simulated in the frequency domain. For illustration two more useful data visualizations are given.

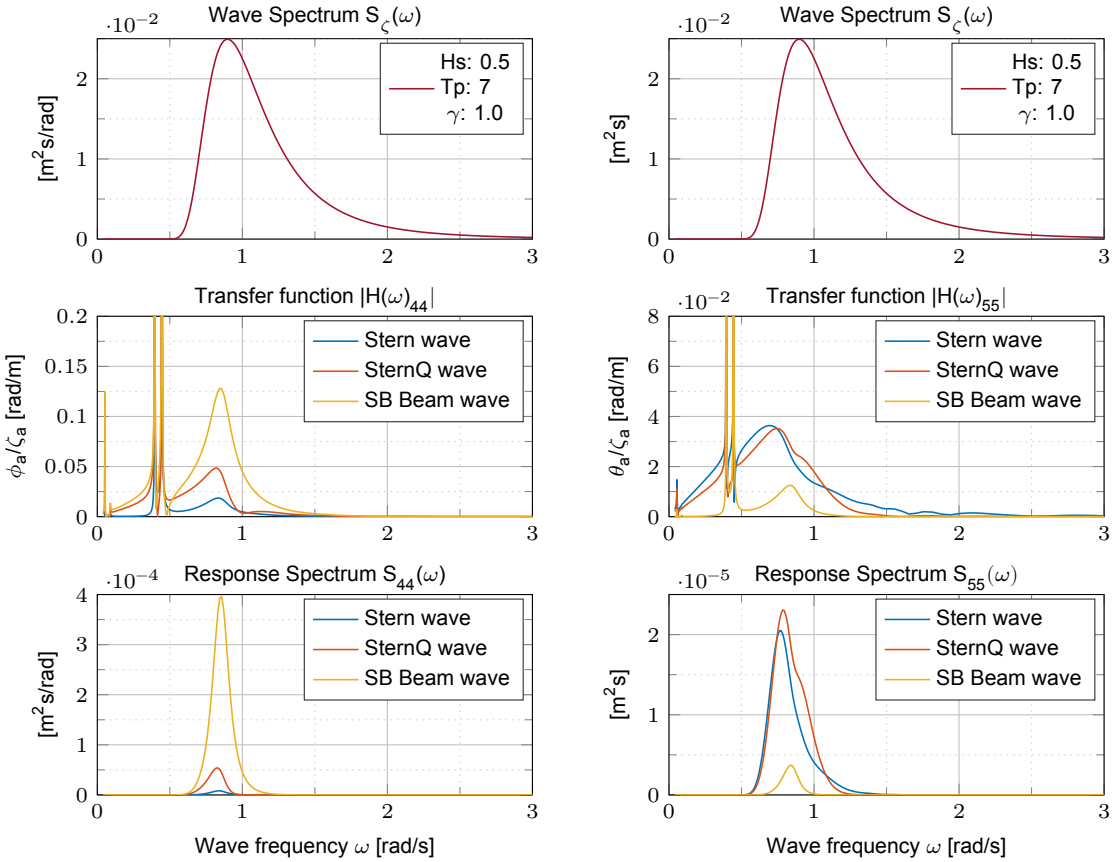

Figure 3.16: Vessel roll and pitch response for incoming waves from 0°, 45° and 90°which contain the JONSWAP spectrum in water depths of 30m water. The calculated gamma is based on the relationship between H_s and T_p.

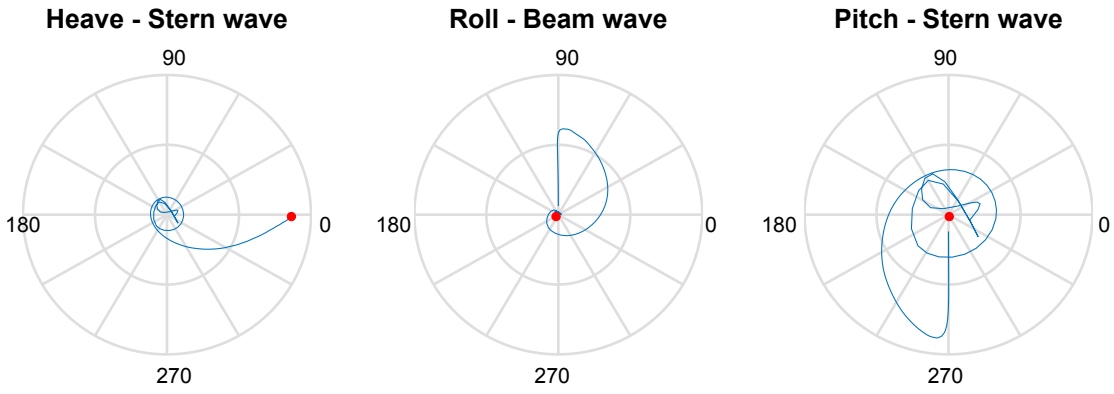

Figure 3.17: Wave Force RAOs for vessel heave, roll and pitch motions. The graph represents Wave Force RAOs as points in polar coordinates (R, ϕ). The purpose of this graph is that the wave forces can be checked for correctness. The curve starts from the short wave response, which amplitude should be zero or very small. This is at the origin. Further, the curve should normally be reasonably smooth and tend towards the expected long wave response limit shown by the solid red circle. Ultimately this polar coordinates way of representing load RAOs provides all information in a single graph.

4

Verification & Validation

The proposed simulation model is developed to calculate ship motions during a specific operational condition for a specific moment in time. These calculations will be conducted on-line in order to compare these with measured ship motions and, if possible, such that the total system error can be corrected for making a more accurate prediction of the vessel response and decision making operation. If use is made of this information individuals such as safety and the workability of the vessel are directly affected on this information. Decision makers should therefore have confidence in the system. This concern is addressed through verification and validation of the simulation model.

4.1. Verification Simulation Model

In the context of computer simulation, verification of a model is the process of confirming that it is correctly implemented with respect to the conceptual model. In other words the model should match the specifications and assumptions deemed acceptable for the given purpose of application. During verification the model is tested to find and fix errors in the implementation of the model. There are many techniques that can be utilized to verify a model. Think about having the model checked by an expert, making logic flow diagrams that include each logically possible action, examining the model output for reasonableness under a variety of model input settings and simply by using an interactive debugger [8].

4.1.1. Basic verification techniques

As described in CH3.4 Matlab Tool, the proposed simulation model is programmed in Matlab language. Despite the fact the model includes a relatively modest number of input parameters and complex numerical operations, the tool is made universally to some extend. Errors in programming, used input parameters, used units, matrix transformations and even simple numerical calculations are easily made. For example the outcome of an matrix transformation such as the transpose of an real valued matrix is different from the transpose of a complex valued matrix. For complex valued matrices not only the row and column indices interchange, also the sign of each imaginary part is switched. For complex valued RAOs this would imply that the response phases are reversed. Incoming waves from starboard suddenly comes from port side and visa verse. To prevent this kind of errors a number of verification techniques are used.

To start with, Matlab has a build in interactive debugger which is constantly used during the development. This debugger warns for programming errors and numerical instability such as singularities in matrix operations. Since the tool is build in layers with a number of functions which communicate between each other, data is transferred from one to another. In order to keep this organized data is stored in unique multidimensional structures. These structures and dimensions are consistent used in calculations and data transfers such that these can be checked visually on correctness. Furthermore the build up of this tool and its communication is explained via a logic flow diagram given in figure 3.13 at CH3.4 Matlab Tool.

4.1.2. Visual verification of RAOs

After the simulation model has passed these basic verifications, the simulation model is being verified by examining the model output for reasonableness under a variety of settings of the input parameters. The most important model outputs are the response amplitudes, phases and on which resonance frequency the maximum response can be expected. The simulation model is based on simple harmonic oscillations of the vessel and the swinging pendulum. Therefore resonance frequencies can be estimated by simple calculations. However, the exact values of the amplitudes and phases are in advance difficult to determine because of the coupling terms in the stiffness matrix C_c as explained in CH3.3.5. Therefore, to begin with, by setting certain input parameters at zero, a visual inspection of the RAOs already provides insight into the functioning of the simulation model during light ship situations.

Response Amplitudes Light Ship

By setting the mooring stiffness C_{mm} at zero and the mass of the suspended load m_L at zero, ship motions are simulated for light ship conditions just as is done during the diffraction analysis in ANSYS AQWA. In contrast with the hydrodynamic model used in ANSYS AQWA, inertia of the cranes is included in the simulation model. Taking into account the geometrical properties of the Rambiz 3000 and the symmetrical hull shape, similar RAOs for surge, sway and heave motions are expected. However, the added inertia does considerably changes the roll and yaw motions of the vessel. The displaced volume of the vessel creates a relative large hydrostatic restoring force in heave and pitch motion but far less in roll motion. Due to the large initial Inertia and this hydrostatic restoring force in pitch motion, only a slightly larger amplitude is expected at the hull natural frequency in pitch motion. The figure below illustrates this verification technique and confirms the expected RAO output during light ship conditions. Note that due to the symmetrical hull shape in ANSYS AQWA, the vessel is responding in yaw direction only for incoming quartering waves. The figure below illustrates this condition.

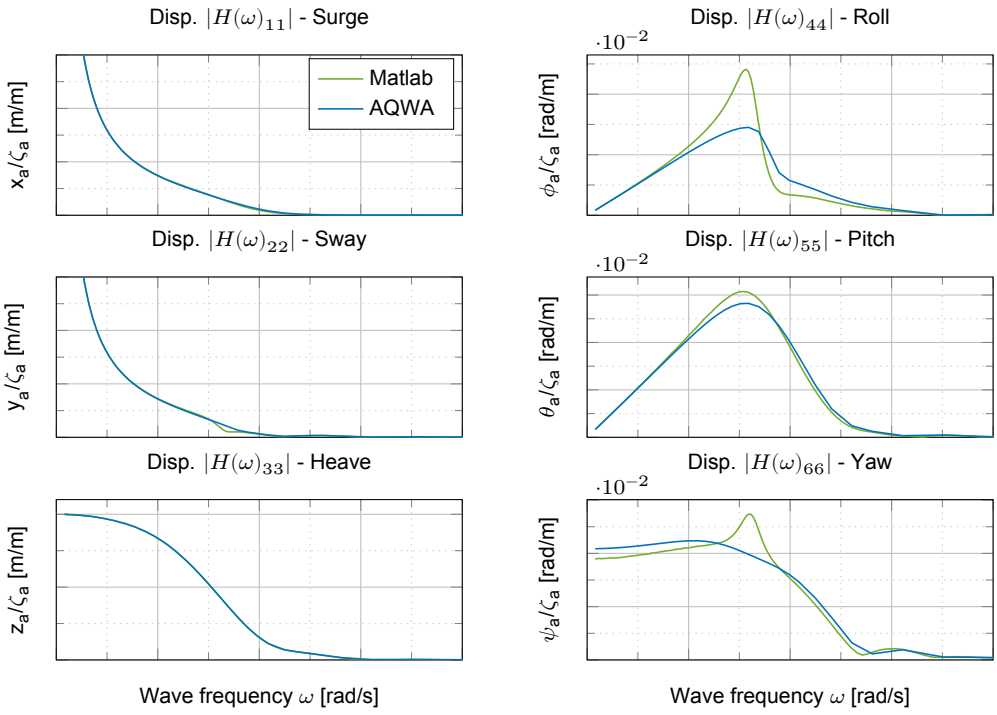

Figure 4.1: Light Ship RAOs, quartering waves

Response Phases Light Ship

An equivalent test can be performed for the phases of the vessel responses. Despite the additional Inertia derived from the hoisting cranes, no significant changes in vessel response phases are to be expected for incoming quartering waves. The direction of the waves is in this case of importance because of motion coupling due to inertia. In contrast to the symmetric hull shape in ANSYS AQWA,

the effect of the inertia coupling terms will for example be reflected in the phases of roll motion for incoming stern waves and a unsymmetrical chosen crane configuration ($x_{ct1} \neq x_{ct2}$). Practically seen however this effect will not be very significant due to the moderate response amplitude in that motion. In the figure below response phases for incoming quartering waves are illustrated.

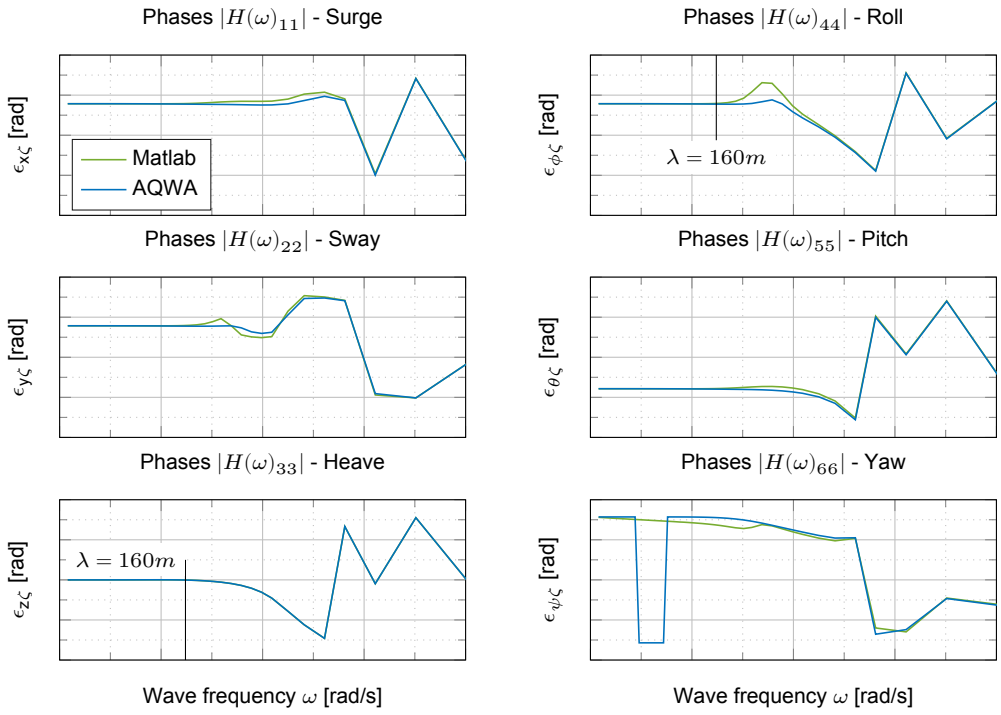

Figure 4.2: Light Ship Response Phases, quartering waves

In this figure can be seen that the simulation model output of vessel response phases are in line with those calculated by ANSYS AQWA. Only small phase differences are seen near the natural hull frequency in which the vessel motions are being affected by the inertia coupling terms. By making use of the dispersion relationship given by a simple check of the vessel heave response phases can be made. The dispersion relation for ocean waves is given by:

$$\omega^2 = kg \cdot \tanh kh \tag{4.1}$$

where k is the wave number which is equivalent to the wave length λ and h is the water depth. By assuming deep water $\tanh kh$ is equal to 1. Allowing to approximate the wave period in which the heave response phase is not equal to zero or in other words from which wave length the vessel is not able to follow the complete wave. The water length in light ship conditions with draft 3.18 m equals 80 m, the breadth 44 m. By making use of the relation $T \approx 0.80\sqrt{\lambda}$, expected is to see a phase shift at wave lengths equal to twice the water length. Although figure 4.2 show response phases for quartering waves, for which a slightly longer water length should be used, indeed phase shifts are seen from 0.62 rad/s in heave motion and 0.83 rad/s in roll motion. The output of the simulation model for light ship conditions is thus in line with the expectations.

Natural Frequencies

More interesting is the simulation model output of ship motions during a specific stage of an heavy lift operation. As mentioned in the previous chapter, due to the coupling terms the exact output for motion amplitudes and motion phases are difficult to approximate in advance. Resonance frequencies or in other words natural frequencies, can on the other hand be estimated in advance. The simulation model of the system is made up of three dominant systems which determine the motion characteristics of the total system. Sorted by contribution these subsystems are respectively the ship hull, the swinging pendulum and the mooring system. All of these subsystems are modeled as simple harmonic oscillations.

Natural frequencies are thus calculated by making use of classical mechanics (undamped mass-spring system $\rightarrow M\ddot{x}(t) = -Cx(t)$, here without hydrodynamic added mass).

Ship Hull
The natural frequency and natural period of the ship hull are thus respectively given by:

$$\omega_{n,ij} = \sqrt{\frac{\mathbf{C}_{ij}}{\mathbf{M}_{ij} + \mathbf{A}_{ij}(\omega_\zeta)}} \quad and \quad T_{n,ij} = 2\pi \cdot \sqrt{\frac{\mathbf{M}_{ij} + \mathbf{A}_{ij}(\omega_\zeta)}{\mathbf{C}_{ij}}} \tag{4.2}$$

in which $i, j = 1, 2, ..6$ are the particular motions of the subsystem, M_{ij} and A_{ij} are respectively the vessel structural mass and inertia and wave frequency depended hydrodynamic added mass of the total system. The hydrostatic stiffness of the total system is denoted by C_{ij}. In this model the suspended load is not submerged. Thus hydrodynamic values of motions $i, j = 7, 8, 9$ are equal to zero. The urgency of applying the frequency-dependent mass is illustrated in figure 4.3. Stiffness due to restoring forces of the mooring system C_{mm} should not be included in the calculation. However for an accurate determination of the hull natural frequencies equation 4.2 has to be solved in 6-DOF (motion coupling). The above equations still apply, but they now have to be interpreted as matrix/vector equations where ω_n remains a scalar, a, x and $\ddot{x}$ become vectors with 6 elements, and M and C become 6×6 matrices.

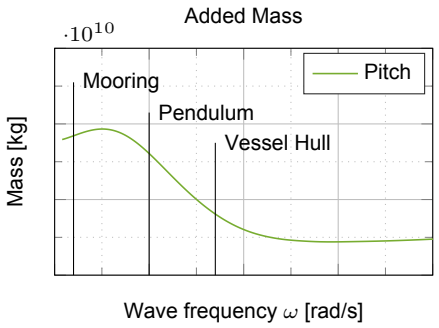

Figure 4.3: Frequency depended added mass

Table 4.1: Natural frequencies ship hull. Case 1: light ship, Case 2: 1217 ton

	Case 1			Case 2 (1-DOF)			Case 2 (6-DOF)		
	Heave	Roll	Pitch	Heave	Roll	Pitch	Heave	Roll	Pitch
ω_n (rad/s)	0.68	0.79	0.82	0.68	0.72	0.80	0.68	0.88	0.71
T_n (sec)	9.65	7.88	7.77	9.65	8.74	7.94	9.65	7.14	8.85

In table 4.1 hull natural frequencies of two different loading conditions are given. The first loading condition concerns light ship, the second loading condition a lift case (PS, 1217 tonnes, outreach 15 m, outstretched robe length 50 m). Given results reflects solutions of equation eq:natural frequency ship hull for a single degree of freedom and for 6 degrees of freedom. Calculated natural hull frequencies for roll and pitch motions for the first loading condition corresponds with the maximum amplitudes given in figure 4.1. Results for the second case in 6-DOF are reflected in figure 4.4. The swinging pendulum reduces the motion amplitude and increases the ship hull natural frequency due to the additional restoring stiffness and strong motion coupling. This effect is reflected in the vessel motion RAOs given below, the model output therefore meets the expectations.

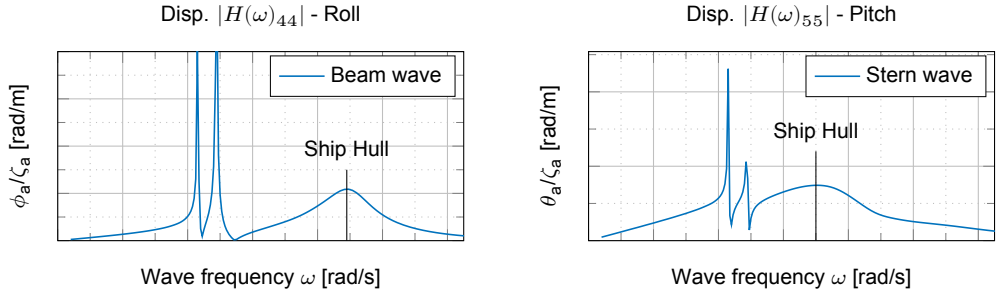

Figure 4.4: Roll and pitch motion RAOs for lift case 2. Verification distorted ship hull natural frequency

Swinging Pendulum
Based on the knowledge gained in CH3.3.5 on may expect to see the coupling terms in the stiffness matrix of the swinging pendulum, C_c, be reflected in the RAOs at least at its own resonance frequency. The translation vectors for the crane tip in longitudinal and traversal directions are given by:

$$\delta_1(t) = x_o(t) + z_{ct}\theta(t) - y_{ct}\psi(t) \tag{4.3}$$
$$\delta_2(t) = y_o(t) - z_{ct}\phi(t) + x_{ct}\psi(t) \tag{4.4}$$

The coupled equation of motion for roll is given by:

$$\begin{aligned} F_4 =&(I_{xx} + A_{44})\ddot{\phi} + B_{44}\dot{\phi} + C_{vh4}\phi \\ &- k_s z_{ct} y_o + k_e y_{ct} z_o + (k_s z_{ct}^2 + k_e y_{ct}^2)\phi - k_e x_{ct} y_{ct}\theta - k_s z_{ct} x_{ct}\psi \\ &+ k_s z_{ct}\eta_8 - k_e y_{ct}\eta_9 \end{aligned} \tag{4.5}$$

and for pitch by:

$$\begin{aligned} F_5 =&(I_{yy} + A_{55})\ddot{\phi} + B_{55}\dot{\phi} + C_{vh5}\phi \\ &+ k_s z_{ct} x_o - k_e x_{ct} z_o - k_e x_{ct} y_{ct}\phi + (k_s z_{ct}^2 + k_e x_{ct}^2)\theta - k_s z_{ct} y_{ct}\psi \\ &- k_s z_{ct}\eta_7 + k_e x_{ct}\eta_9 \end{aligned} \tag{4.6}$$

and for yaw by:

$$\begin{aligned} F_6 =&(I_{zz} + A_{66})\ddot{\phi} + B_{66}\dot{\phi} + C_{vh6}\phi \\ &- k_s y_{ct} x_o + k_s x_{ct} y_o - k_s z_{ct} x_{ct}\phi - k_s z_{ct} y_{ct}\theta + k_s(x_{ct}^2 + y_{ct}^2)\psi \\ &+ k_s y_{ct}\eta_7 - k_s x_{ct}\eta_8 \end{aligned} \tag{4.7}$$

Note for convenience of writing motion coupling of added mass and damping is not written out completely. If the heavy lift operation is conducted with a single crane at the center of the vessel (CE), all coupling terms related to y_{ct} are equal to zero. Thus there is no coupling between roll/yaw and pitch/yaw due to the swinging pendulum. However, if the is conducted at PS all coupling terms are counting causing roll, pitch and yaw motions to be coupled with each other (see equations 4.4). This coupling effect is strong due to the relatively long moment arms x_{ct}, y_{ct} and z_{ct} compared to the vessel geometry. Thus it is expected to see single resonance peaks at the pendulum natural frequency for lifts conducted at CE, and double resonance peaks are to be expected for lifts conducted at PS or SB. Due to motion coupling these resonance peaks are also seen in surge and sway. Because of vessel geometry the initial hydrostatic stiffness in pitch motion is significantly larger than the initial stiffness in roll motion. Thus the vessel is to a lesser extent capable of providing resistance in roll direction than it is in pitch direction resulting in two different natural frequencies for the swinging pendulum. This effect becomes more apparent as the mass of the suspended load increases.

The natural frequency and natural period of a freely swinging pendulum is given by:

$$\omega_n = \sqrt{\frac{g}{l_s}} \quad and \quad T_n = 2\pi \cdot \sqrt{\frac{l_s}{g}} \tag{4.8}$$

in which g is the gravitational speed and l_s the outstretched robe length to the centre of gavrity of the suspended load. Thus for outstretched robe lengths of 40 m and 50 m expected is to see resonance close to 0.49 rad/s and 0.44 rad/s, respectively 12.7 and 14.2 seconds. Figure 4.5 illustrates RAOs for roll an pitch motions for a lifts conducted at CE or PS. These plots verify the expected model output and illustrates the difference in swinging period for roll and pitch and the effect due to the coupling terms. The calculated natural frequencies in longitudinal direction, η_7, are reflected precisely in pitch motion during a single crane lift at the vessel centre line. However, as expected in roll motion a slightly different resonance frequency is reflected. In this motion the vessel responds more rapidly on the swinging suspended load in transverse direction η_8. This makes the period of oscillation in roll motion slightly shorter then it is in pitch motion. To some extend this effect becomes larger with longer pendulum lengths. Thus for single crane lifts performed at PS or SB equation 4.8 only gives an indication of the

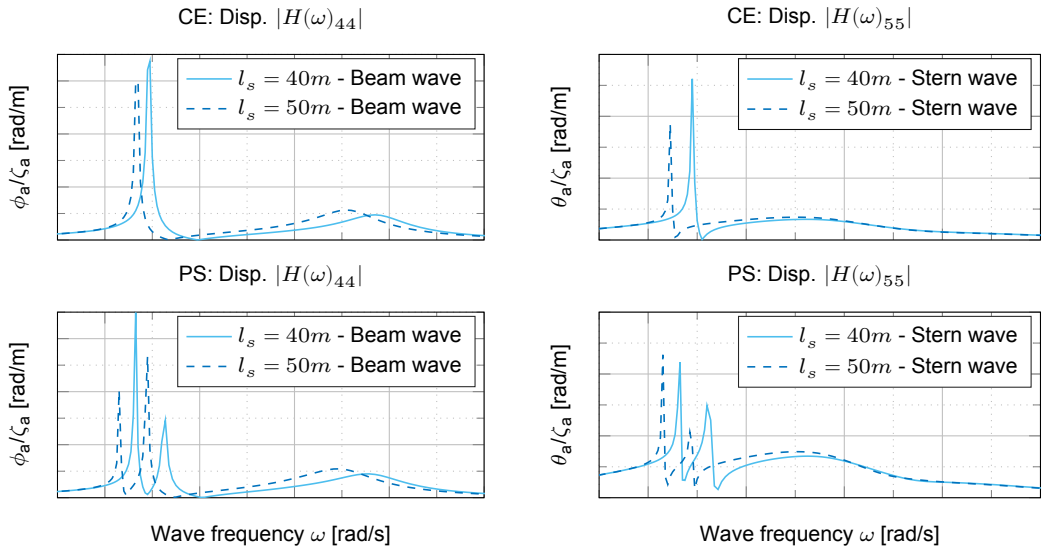

Figure 4.5: Displacement RAOs for different robe lengths and lift cases

resonance frequency. Resonance can be seen close to but not at those calculated for a freely swinging pendulum. For clarification in figure 4.6 roll and pitch RAOs for lifts conducted at CE are illustrated. The pendulum natural frequency in vertical direction is only dependent on axial crane wire stiffness and the mass of the suspended load. The natural frequency is thus simply given by: $\omega_n = \sqrt{EA/m_L}$. The cranes on the Rambiz 3000 are equipped with 16 crane wires of which each has a axial stiffness of $2.36{\cdot}10^8 N$. The pendulum natural frequency in vertical direction with a suspended load of 1217 ton is therefore 0.11 seconds. Although the axial crane wire stiffness causes significant restoring forces in vertical direction (which is important for the determination of vessel motion response), resonance will not be reflected in vessel motion RAOs. The simulation model reflects this expectation.

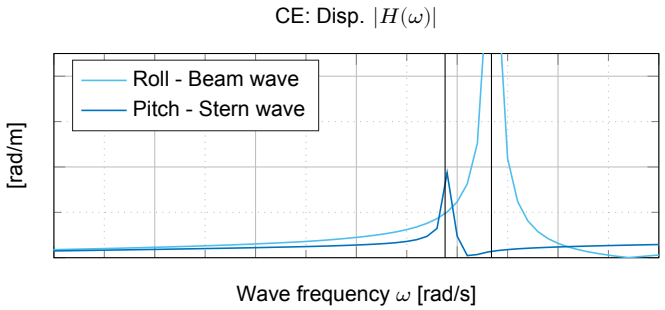

Figure 4.6: Displacement RAOs for Roll and Pitch. CE crane lift, $l_s = 50m$.

Mooring

The last contributing subsystem is the mooring system. The natural frequencies can be found with equation 4.2, in which $i, j = 1, 2, 6$ are the ship motions in the horizontal plane, C the mooring restoring stiffness, M the structural mass of the vessel (including cranes) and A the hydrodynamic added mass of the total system (including load). Soft mooring systems, equivalent systems with a natural period at around 300 seconds are not reflected in vessel motion RAOs. Systems with natural frequencies close to 50 seconds do interfere vessel motions. It is not illustrated here but the model output reflects this expectation as well. In conclusion it can be stated that the Matlab Tool operates properly and the output of the simulation model meets the expectations.

4.2. Validation with Orcaflex

Model validation is usually defined to mean “substantiation that a computerized model within its domain of applicability possesses a satisfactory range of accuracy consistent with the intended application of the model” (Schlesinger et al. 1979) and is the definition used here. An model should therefore be developed for a specific purpose (or application) and its validity determined with respect to that purpose. As mentioned the simulation model is developed in frequency domain for which a number of assumptions have been made. The main reasons for the development in frequency domain instead of an time domain analysis, is its computational speed, parametric insight and thereby the ability of on-line model input corrections by means of the wave buoy analogy and seeking an equivalence of energy between the computed response moments and those measured with motion measurement sensors.

The validity of an model in frequency domain is by definition only guaranteed for linear systems or for situations in which the system behaves linear within the domain of application. The latter is applicable here for which the dynamics of the system are simply linearized by assuming small motions. However, literature indicates a number of possible phenomenons that might cause the system behavior to become non-linear within the domain of application. Whether or not by resonance, whether or not by the nature of the phenomenon itself. Furthermore, it is also of importance to gain insight in the reliability of the calculated amplitudes an phases of the vessel and suspended load motions under stochastic loading.

An comprehensive model validation consists of several elements such as Data Validity, Conceptual Model Validation, Computerized Model Verification and Operational Validity. Data Validity is often not considered to be part of model validation. This because appropriate, accurate, and sufficient data is usually difficult, time consuming, and costly to obtain. Data problems however, are often the reason that attempts to validate a model fail. Conceptual Model Validity is determining that (1) the theories and assumptions underlying the conceptual model are correct and (2) the models representation of the problem entity is “reasonable” for the intended purpose of the model. The theories and assumptions underlying the model should be tested using mathematical analysis and statistical methods on problem entity data. Examples of applicable statistical methods are fitting distributions to data, estimating parameter values from the data, and plotting data to determine if the data is stationary. Operational Validation is determining whether the simulation model output behavior has the accuracy required for the models intended purpose over the domain of the models intended applicability [8].

In order to test the validity of the model output and the assumption of linearity within the domain of application, the latter validation technique have been applied. The operational validity of the simulation model is testes by making use simulation software Orcaflex[1]. This software package allows, among numerous other things, to compute the response of a system such as a floating system in time domain. Thus large motions are allowed and dynamic behavior as a result of incoming waves, current, wind or other forces is included in the response calculations. By comparing time domain analyzes with frequency domain analyzes of equivalent systems one can thus determine possible differences due to assumptions in the modeled dynamics and the applicability of the developed simulation model. This validation method provides thus insight into:

- Motion amplitudes and phases,
- System resonance frequencies,
- Validity assumption linearity,
  - Dynamic moment arm effect in hydrostatic force $\rightarrow$ equations 3.26,
  - Wave memory effect $\rightarrow$ retardation function in the convolution integral.

Although Orcaflex is not able to account for the waterplane area (nonlinear hydrostatic) effects in a nonlinear fashion, it is in contrast to the frequency domain model, able to capture the moment arm effects during a simulation. Under the assumption of an constant volume of displaced water, Orcaflex computes these effects simply by applying the weight and buoyancy forces at the instantaneous position of the centre of gravity and buoyancy respectively. Therefore not only the change in load due to the change in the submerged volume of the vessel as it heaves, rolls and pitches (waterplane area effects),

[1] OrcaFlex is developed by the company Orcina and is the world’s leading software package for dynamic analyzes of offshore marine systems.

but also the change in moment caused by movement of the vessel's centre of gravity and centre of buoyancy as it rolls and pitches (moment arm effects) is included.

The hydrostatic stiffness matrix output by diffraction package ANSYS AQWA account for both of these contributions. However, as stated, the hydrostatic stiffness matrix is only applicable for small changes in the vessels position and orientation. During heavy lift operations only small vessel motions and swinging load angles are allowed thus one would think this linearisation is permissible. Nevertheless, it is valuable to study the influence of the moment arm effect since this effect counts severely in roll motion (small initial hydrostatic stiffness, large moment arm).

To capture the moment arm effect Orcaflex must subtract the linearised approximation to the moment arm effects from the users stiffness matrix, which in this case is obtained with ANSYS AQWA. The buoyancy load arising from waterplane area effects is calculated using the following matrix equation:

$$L = -K' \cdot P \tag{4.9}$$

where $L = [F_{heave}, M_{roll}, M_{pitch}]^T$ is a column 3-vector containing the heave, roll and pitch components of the net weight + buoyancy load that acts on the vessel at the reference origin. K' is the users stiffness matrix K, after the removal of the appropriate moment arm contributions. P is the column 3-vector containing the heave position and roll & pitch angles at the reference origin, relative to the specified vertical datum point, heel and trim of that reference origin. This datum point is similar to the vessel centre of gravity that was used in ANSYS AQWA to calculate the displaced volume, centre of buoyancy and hydrostatic stiffness matrix. So $P[1]$ is the vertical coordinate of reference origin - (mean surface height + vertical datum position relative to surface). $P[2]$ and $P[3]$ are the roll and pitch needed to rotate the vessel from its datum heel and trim orientation to its current orientation.

The moment arm contributions are removed by subtracting a term of the form $(m_d z_b - m z_g)g$ from the roll-roll and pitch-pitch components of K, where m is the structural mass of the vessel, m_d the displaced mass of water and z_b and z_g are the vertical distances of the centre of buoyancy and centre of gravity above the reference origin when the vessel is in its datum position. In addition, OrcaFlex applies a weight force ($F_g = -mg$) at the vessels centre of gravity, and a buoyancy force ($F_b = m_b g$) at the vessels centre of buoyancy. These two forces are applied by OrcaFlex at every time-step of the simulation, which means that the nonlinear effects of the shift in the moment arm between the centres of gravity and buoyancy will be captured precisely [44, 45].

4.2.1. Approach

In order to be sure that both models (Orcaflex and frequency domain) represent the same problem entity, there has been made use of the modal analysis module within Orcaflex. In this way the natural frequencies of the ship hull, swinging pendulum and mooring system as explained in chapter 4.1.2 can be set side by side. If present, the influence of other degrees of freedom, such as the rotational motions of the suspended load can be studied in advance as well.

Data Comparison

If a test determines that a model does not have sufficient accuracy for any one of the sets of experimental conditions, then the model is invalid. However, determining that a model has sufficient accuracy for numerous experimental conditions does not guarantee that a model is valid everywhere in its applicable domain. This is especially true for ship motions during heavy lift operations since there are, at least, three dominant systems which influence these motions at certain frequencies. Since all of these systems directly or indirectly respond on incoming waves, the response of every wave frequency between the applicable domain have to be studied. Decided is to compare vessel RAOs instead of vessel responses due to the efficiency by which this can be done. For convenience a recap of the relation between vessel response and the encountered energy spectrum is given below by:

$$S_{R_{ij}}(\omega) = \left|H_{ij}(\omega)\right|^2 \cdot S_\zeta(\omega) \tag{4.10}$$

From Orcaflex simulations time traces from both the surface elevation and the response amplitudes can be subtracted. Subsequently by making use of the relation given above and a FFT of the time traces, motion RAOs can be obtained.

Truncated White Noise Spectrum
In Orcaflex one has the ability to simulate numerous wave forms including a random wave which covers a truncated white noise spectrum, whereby the energy is spread evenly over a user-specified range of frequencies. A random process (or signal) with a constant power spectral density function is referred to as a white noise process. An example of this spectrum is given in figure 4.7.

In contrast to multiple narrow bounded JONSWAP wave spectra a single truncated white noise spectrum can cover all wave frequencies in the frequency domain of interest. Given the dependency of wave direction of vessel responses a significant reduction in required simulations is achieved. In this research vessel motions at the North Sea is studied. Therefore wave frequencies between 3 rad/s and 0.4 rad/s, respectively 2 and 15 seconds is a typical range of interest. However as explained in the previous section expected is the mooring and the swinging pendulum to have significant influence on vessel motions. Therefore wave frequencies between 0.1 rad/s and 3 rad/s where studied in the first place. However, with regard to the mooring system this gave problems. Due to the large motion amplitudes in surge, sway and yaw at very low, (unrealistic) wave frequencies appropriate vessel position and rotation cannot be achieved with a single mooring system which is soft enough in the wave frequency domain of the North Sea and stiff enough to restore the encountered wave loads. Therefore only wave frequencies between 3 rad/s and 0.3 rad/s where studied.

The total energy of the truncated white noise spectrum is determined by the significant wave height using the standard equation $m_0 = (H_s/4)^2$, where, m_0, is the zeroth spectral moment or in other words the spectral energy. In order to ensure small motions an significant wave height of 0.75 m is maintained. Larger significant wave heights than roughly 1 m with frequencies at the swinging pendulum resonance frequency easily cause large motions. In this situation the swinging pendulum motions predominate the vessel response. This can cause instability when it comes to vessel position, causing an distorted view in wave direction and moreover responses outside the domain of application. Lower wave amplitudes are thus preferable, however the wave amplitude should be high enough for motion amplitudes close to the maximum allowable amplitudes during heavy lift operations.

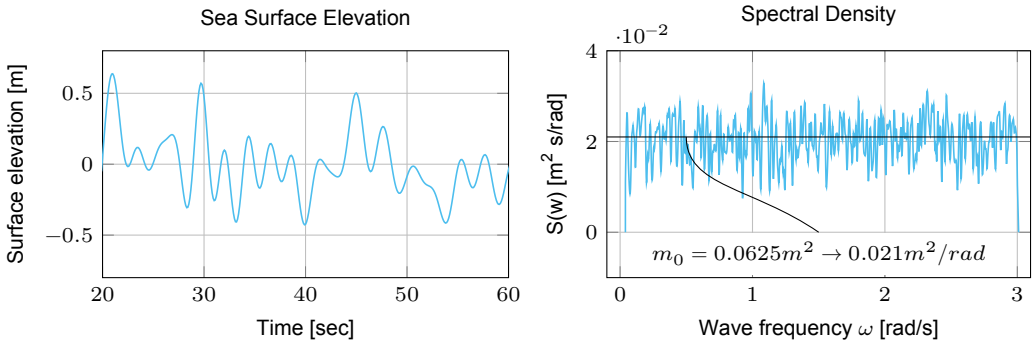

Figure 4.7: Random Wave Elevation and its Truncated White Noise Spectrum

By making use of the Spectral Response Wave, equivalent to a truncated white noise spectrum, Orcaflex can provide vessel RAOs as well. The simulation duration together with the logging interval determine the total numbers of samples available for the FFT. However Orcaflex does not necessarily use all the available samples since the FFT calculation is slow when presented with a time history whose size is a large prime. Further in advance it is difficult to estimate an appropriate logging interval for the desired detail in vessel RAO output due to frequency leakage [42]. Vessel response amplitude time traces are therefore transformed to vessel response spectra in Matlab by making use of the FFT technique and a Dirichlet window or simply a rectangular window. This works best with these kind of signals. For sufficient spectral density a simulation period of 3600 seconds is adhered.

Sinusoidal waves
Due to to frequency leakage and the risk of resonance due to modeling errors in Orcafex also a number of simulations with sinusoidal waves are conducted. By making use of simple sinusoidal waves not only response amplitudes and phases but also the assumption of linearity during small vessel motions can

be studied more straightforward. As long as the vessel response is sinusoidal, the system behaves linear at that specific wave frequency. Vessel motion amplitudes are analyzed in Matlab simply by comparing the wave amplitude from the time trace with half of the significant wave height multiplied by the corresponding frequency dependent RAO. For incoming stern, starboard quartering and starboard beam waves, vessel motions for the following wave periods have been simulated and analyzed:

Table 4.2: Simulated sinusoidal waves coming from stern, sb quartering and sb beam direction

Wave	1	2	3	4	5	6	7	8	9	10	11	12	13
ω	2.09	1.57	1.31	1.21	1.11	0.99	0.90	0.86	0.81	0.71	0.60	0.50	0.40
T_p	3.00	4.00	4.81	5.21	5.69	6.31	7.02	7.33	7.78	8.91	10.43	12.57	15.71

Before the main simulation stage(s) start, there is a build-up stage in Orcaflex. During this stage the wave and vessel motions are smoothly ramped up from zero to their full size. This gives a gentle start to the simulation and helps reduce the transients that are generated by the change from the static position to full dynamic motion. It was been found that a ramp up period of 50 seconds, which is relatively long compared to the shortest waves but normal for the longest waves, gave fastest ”stable” vessel motions. Furthermore in order to reduce transient vessel motions a settling time of 1800 seconds is adhered. From this stage an simulation period of 10800 seconds (3 hours) is maintained. In the figure at the right wave elevation and vessel motions during the ramp up period is shown.

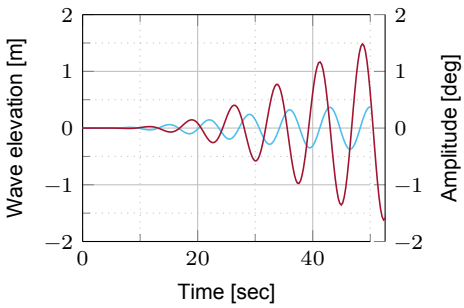

Figure 4.8: Wave elevation and vessel response during build up period

4.2.2. Orcaflex Model

Within Orcaflex numerous options with regard to the calculation method for analysis in statics or dynamics can be consulted which can be a study itself. Chosen is for a implicit time domain solver with a constant time step of 0.1 sec. Reason for this is the speed and stability of this method. It is significantly faster for stiff systems (hoisting wires, mooring system) and it can quite easily achieve stability. The drawback of this method is that it can give inaccurate results for rapidly varying physical phenomena. These are however not expected and the vessel motion response is the primary interest. The model is in essence similarly build with respect to the FD model. It includes a vessel body, hoisting cranes, hoisting ropes and a suspended load.

Vessel

In summary the primary motion of the vessel is calculated in 6-DOF by means of load RAOs. Vessel motions are treated as low and wave frequency depended in order to be able to distinguish possible disturbances for linear behavior (mooring system vs wave frequencies). Only first order wave loads and frequency depended added mass and damping is included. The hydrostatic and dynamic data is similar to the one applied in Matlab. Equivalent viscous roll damping has not been included in bot models.

Hoisting cranes and ropes

The hoisting cranes are fixed to the vessel and modeled as rigid 6-DOF buoys with mass and inertia momentum but without volume since they are not submerged. The hoisting ropes are modeled as tethers (linear in-compressible springs) and the suspended load as a freely moving 6-DOF rigid body, also without volume but with mass and inertia momentum.

Mooring system

Lastly the mooring system is modeled by eight linear spring/ dampers which are evenly distributed at a distance of 30 m from the centre of gravity. The height of the mooring system is equal to the centre of rotation. Damping is set to zero. In the figure above the ”shaded” and ”wired frame” preview of the model is given. The wired frame shows basically all essential model items and their connection.

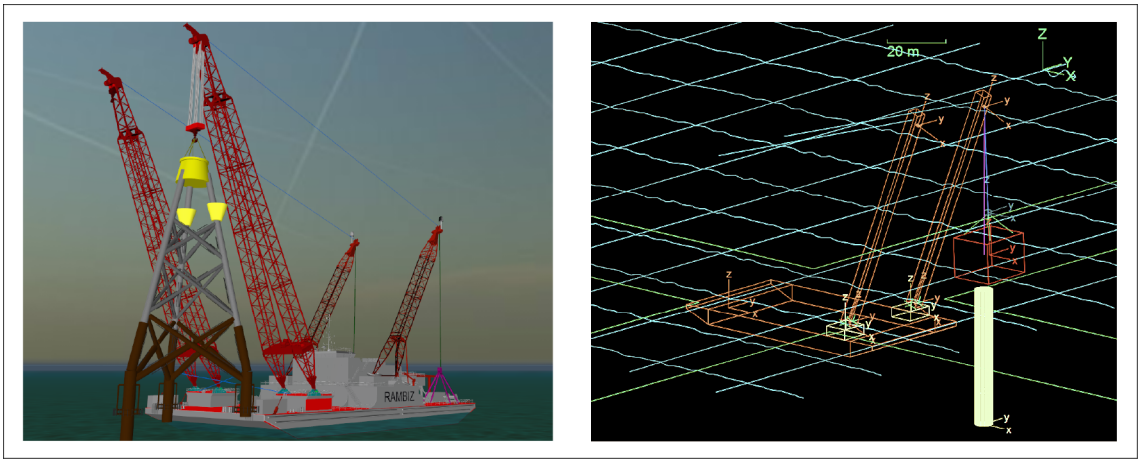

Figure 4.9: Orcaflex model of the Rambiz 3000. Left: Shaded preview, Right: Wired Frame preview

4.3. Operational Validity

The validity of the FD model is measured in several stages wherein the validity of each dominant model element is determined. As discussed these dominant elements are the swinging pendulum, the mooring system and the vessel hull itself. Due to the amount of tests performed in Orcaflex, only a summary and the most urgent figures of the results are given. In appendix B more detailed figures and numbers are bundled. All vessel responses are given at the ship centre of gravity (G).

4.3.1. Light Ship

First the overall quality of the described method of RAO comparisons is verified simply by comparing the RAO output from ANSYS AQWA with those from Orcaflex and Matlab. Note that for this verification the hoisting cranes in Orcaflex and Matlab are modeled as point masses at the centre of gravity of the ship just as is done in ANSYS AQWA. Due to the mooring system larger motion amplitudes in surge, sway and yaw motion at low wave frequencies is expected. The mooring system is modeled such that the resonance frequency ($T_n \approx 150s$) is outside the wave frequency domain.

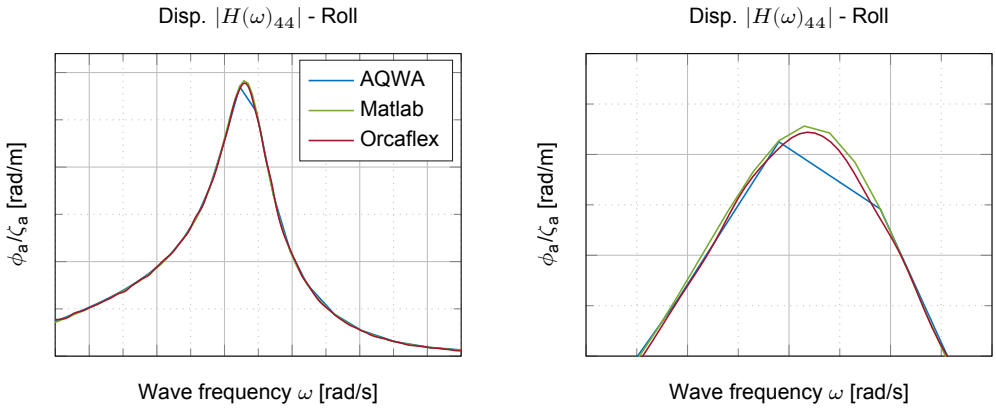

Figure 4.10: Quality RAO comparison method

The quality of the comparison technique is illustrated in the figure above where displacement RAOs for roll motion is depicted. From this is concluded that the wave spectrum and FFT technique appropriately is chosen and applied. The small difference in amplitude at resonance frequency is neglectable. It might come from interpolation or FFT smoothing (windowing). The average error between all models is <1% what is considered to be sufficient for demonstrating the validity of the FD model.

Light ship with hoisting cranes
As described in chapter 3.3.1 expected is to see larger motion amplitudes in roll, pitch and yaw motion near the natural hull frequency since the hoisting cranes are fixed to the vessel at the bow. The dynamics captured in TD reflects this expectation which is illustrated in more detail in appendix B. In the figure at the right displacement RAO for yaw motion is shown. The average error between both models is <1% for all wave directions what is considered to be sufficiently accurate. Thus the mass and inertia matrix and the coupled motions are well derived.

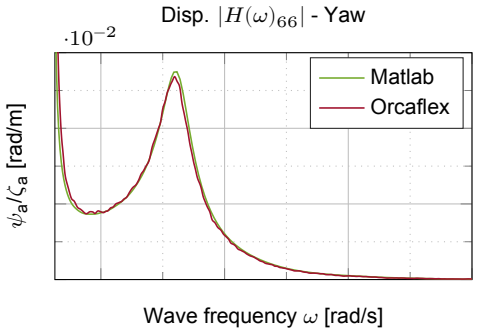

Figure 4.11: Validation mass and inertia matrix

4.3.2. Single Crane Lifts

he validation process is performed in steps in order to be able to distinguish all dynamic phenomena and their interaction. Based on the coupling terms given in matrix, C_c, these steps consists of heavy lifts conducted at Mid Ship, Bow Centre and Bow PS. Lastly the limit in linear response is discussed in order to determine the boundary of applicable sea states, even though the motions are larger than the maximum allowable.

Mid Ship
By modeling the suspended load at the centre and midline of the ship coupling terms in matrix, C_c, containing crane tip coordinates, x_{ct}, and y_{ct}, are equal to zero. Yaw motion coupling between surge and pitch and yaw motion coupling between sway and roll due to the load is therefore not present. For this simulation the hoisting cranes at PS and SB are now in both models (Orcaflex and Matlab) omitted, such that there is only motion coupling between the horizontal and rotational motions due to hydrostatic stiffness. Restoring in rotational motions due to the gravitational force, k_s, is directly coupled with the vertical distance of the crane tip, z_{ct}, with respect to reference frame G. The pendulum length is dependent on the length of the outstretched hoisting rope and thus of the axial hoisting rope stiffness. The suspended load is modeled as a rigid 6-DOF buoy without volume. The rigging module is not modeled thus there are only translational motions of the suspended load. Thus with this test basically the rotational restoring due to gravity and vertical restoring due to the axial crane rope stiffness is validated.

In appendix B.3.1 all displacement RAOs are given. In figure 4.12 a summary of those displacement RAOs is given for all vessel motions and specific wave directions. The suspended mass was 1200 ton and the outstretched hoisting rope length 52 m $\rightarrow \omega_n \approx 0.43$ rad/s. Although dynamics at the pendulum natural frequency is difficult tho capture via FFT (peak), the average error between both models is <2%. The motions of the suspended load are induced by the vessel, thus this error is also observed in the suspended load RAOs (given in appendix B.2).

In appendix B.3.1 sinusoidal wave induced vessel motions are given for all wave directions and vessel motions. In table 4.3 vessel roll motions are given in degrees and abbreviations Or and Ma stand for Orcaflex and Matlab. The difference between Orcaflex and Matlab is denoted by ε_r. These results show the validity of the simulation model. The difference in computed motion amplitudes is between 1% and 5% which is considered to be sufficiently accurate. Modeled horizontal and vertical restoring due to the suspended load and axial hoisting rope stiffness is thus in line with those modeled in Orcaflex.

Table 4.3: Mid Ship: Validation roll motion amplitudes (deg) for incoming sinusoidal waves from sb beam

T_p	3.00	4.00	4.81	5.21	5.69	6.31	7.02	7.33	7.78	8.91	10.43	12.57	15.71
Or	0.00	0.05	0.20	0.38	0.77	1.90	2.06	1.71	1.38	0.96	0.72	0.53	0.14
Ma	0.01	0.07	0.22	0.41	0.84	2.01	1.97	1.65	1.35	0.95	0.71	0.52	0.01
ε_r	0.00	0.01	0.02	0.03	0.07	0.11	-0.09	-0.06	-0.03	-0.01	-0.01	-0.01	-0.12

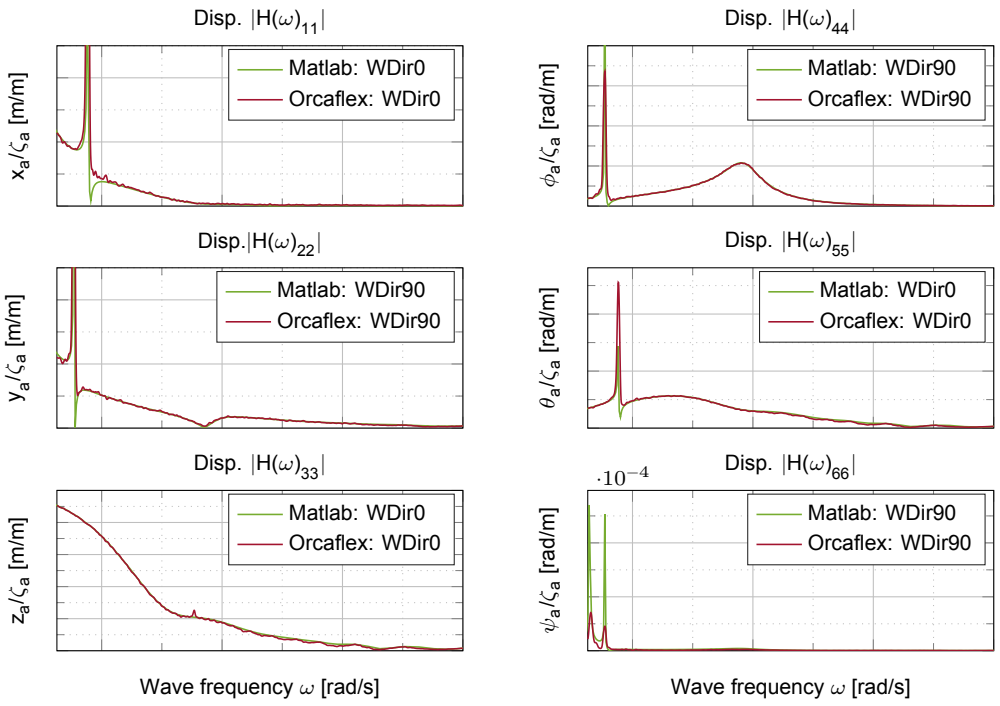

Figure 4.12: Validation restoring force due to gravity

By reviewing TD traces of sinusoidal wave induced responses, concluded is that for all wave frequencies the response was linear as well. Except maybe for wave frequencies near the resonance frequency of the swinging pendulum. Captured vessel motions where small and sinusoidal due to the input, but they included ”second order effects” due to the mooring system. Causing the roll amplitude to become larger in dynamics than can be approximated in FD. In order to maintain appropriate vessel orientation the mooring system had to be modeled such that it is able to restore yaw motions to some extend (wave direction). In order to achieve this the mooring system had to be modeled relatively stiff ($T_n \approx 50$ sec). However this allowed the mooring system to be able to restore vessel motions near the pendulum natural frequency as well (”second order effect”). Concluded is therefore that at least a mooring natural frequency of 150 seconds have to be adhered, especially in yaw motion.

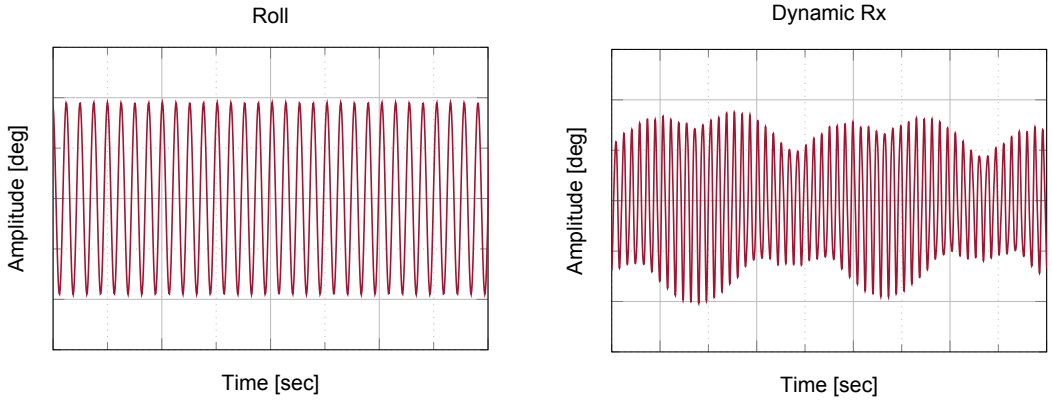

Figure 4.13: Sinusoidal wave induced roll response amplitudes.
Left: Linear response (wave nr. 6). Right: Irregular response (wave nr. 15)

Rigging
By modeling a rigging in Orcaflex to suspended the load is forced to rotate in the vertical plane while it is swinging. Without rigging the suspended load is attached at its centre of gravity, in this case there is no force or moment leading to rotational motions of the suspended load which leads to translational displacements only, even-though the suspended load is modeled in 6-DOF.

It was already indicated in literature but indeed it has been found that vessel roll motion amplitudes are roughly 10% larger if the load is able to rotate while its swinging, even with small excursions/ rotations. The relatively large moment of inertia is causing larger horizontal excursions of the suspended load (η_7, η_8) and thus also larger roll amplitudes of the vessel. This effect is however practically seen only noticeable in vessel roll motion which is illustrated in figure 4.14. It should be noted that due to the moment of inertia the pendulum natural frequency is slightly lower, causing to shift the vessel natural hull frequency as well. The vessel now rolls slightly slower with a larger amplitude. Special rigging modules exist which make use of this phenomena. Dependent on the desired vessel or load response, motions can be counteracted such that the response in vessel roll motion is reduced and thus safety and ultimately also workability can be gained. Load RAOs are given in appendix B.2.

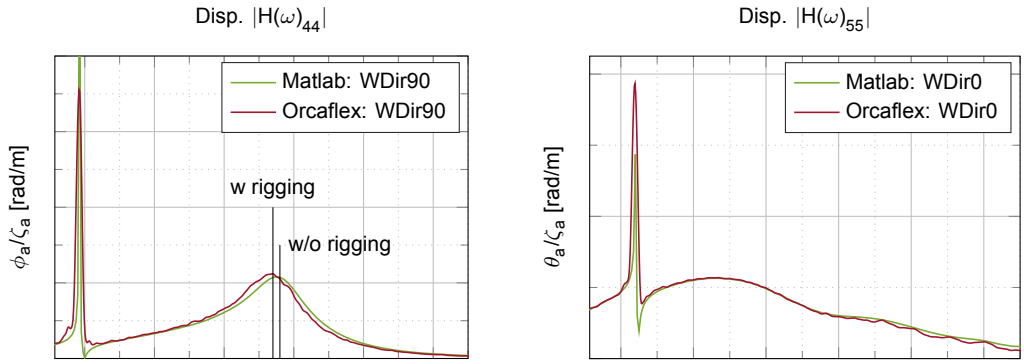

Figure 4.14: FD model validity due to rotational motions of the suspended load

Sinusoidal wave induced vessel responses are given in table 4.4. For convenience also roll response for simulations without rigging is given which is denoted by Or(w/o). The given error is for the difference in computed amplitude between Matlab and Orcalfex with rigging, denoted by Or(w). From this concluded is that roll amplitudes are underestimated when computed in FD with approximately 10% near the hull natural frequency. Fortunate for other wave frequencies and directions and for other vessel motions the effect is almost zero and can therefore be neglected in the analyses for the intended purpose of this study. In appendix B results are given for other wave directions etc.

Table 4.4: Rigging: Validation roll motion amplitudes (deg) for incoming sinusoidal waves from sb beam

T_p	3.00	4.00	4.81	5.21	5.69	6.31	7.02	7.33	7.78	8.91	10.43	12.57	15.71
Or(w/o)	0.00	0.05	0.20	0.38	0.77	1.90	2.06	1.71	1.38	0.96	0.72	0.53	0.14
Or(w)	0.01	0.05	0.19	0.36	0.73	1.84	2.19	1.84	1.45	1.00	0.74	0.55	0.12
Ma	0.01	0.07	0.22	0.41	0.84	2.01	1.97	1.65	1.35	0.95	0.71	0.52	0.01
ε_r	0.00	0.02	0.03	0.05	0.11	0.18	-0.22	-0.19	-0.11	-0.05	-0.03	-0.03	-0.11

Bow Centre
The axial hoisting rope stiffness contributes significant in restoring vessel motions which becomes even more apparent when the crane tip is for example positioned at the bow. Crane tip coordinate, x_{ct}, is not equal to zero any more causing coupled motions between heave and pitch and coupled motions between roll and yaw. The difference in yaw response for uncoupled motions and coupled motions can be seen if one compares figure 4.12 with figure 4.16. For lifts conducted at Mid Ship practically zero yaw motion is observed during incoming sb beam waves which is expected due to the absence of strong coupling. On the other hand for lifts conducted at Bow Centre significant yaw motion

is observed. Unfortunately due to the strong coupling this yaw motion was to large for maintaining appropriate position and orientation. The modeled soft mooring system ($T_n \approx 150s$) was not only allowing larger vessel displacements, it was also causing unstable and unrealistic vessel motions. The strong interaction between the vessel and the load in combination with large allowable yaw motions (soft mooring) became rapidly to large causing the ship to turn around at a given moment (one may laugh).

In order to be able to restore enough vessel yaw motions the mooring had to be modeled such that its natural frequency in surge and sway is 42 seconds and in yaw motion even 30 seconds. Softer mooring systems where not possible due to the strong coupling. Although the Rambiz 3000 does not have a proper DP system, it has some form of propulsion which is in some cases is used for maintaining position. Such a system is however not straightforward modeled within Orcaflex. Especially if it concerns a DP 1 system which is not controlled by an algorithm. Extra damping could be added by adding a constant artificial yaw damping coefficient in the additional damping matrix or by increasing the drag coefficient of the yaw moment due to drag which is defined by

$$M_\psi = 1/2\rho\omega^2 \cdot \underbrace{(C_d T L^4/32)}_{\text{drag factor}} \tag{4.11}$$

where, T, is the draft, L the length between perpendiculars and C_d the drag coefficient. This drag coefficient is taken as 5 which is rather high for a drag coefficient but proposed by Wichers (1979) who found from models tests that with lower values yaw drag is underestimated [43]. However, unfortunately no stable equilibrium was found. Therefore decided was to model the mooring system just stiff enough to maintain position.

In figure 4.15 spectral density plots are given of the tension of a single mooring line. It is clearly visible that for incoming stern waves the vessel only moves in surge direction and energy in no other than its own resonance frequency is captured. However for incoming quartering or sb beam waves coupling between the vessel and load is captured in the mooring tension. The pendulum natural frequency in sway motion, η_8, is 0.55 rad/s and those of the mooring in surge/ sway and yaw respectively 0.15 rad/s and 0.22 rad/s. Note the magnitude of power in the spectral density plot is dependent on FFT window (the energy goes to infinity).

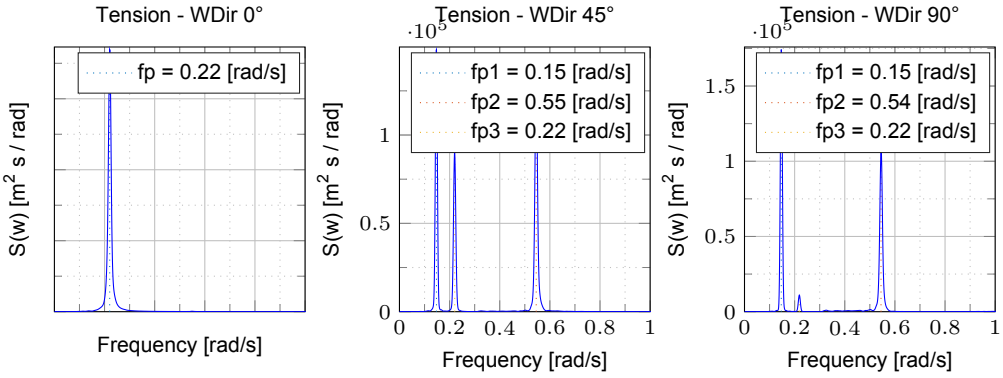

Figure 4.15: Spectral Density of the mooring tension

Despite this drawback satisfactory results were gained by adjusting the mooring stiffness in the FD model with similar quantities as well. Sinusoidal wave induced motion amplitudes for roll and pitch per wave direction are given in appendix B. The rigging module was included in this simulation for which the average error of 10% already was observed. For incoming beam waves the difference in roll amplitude at the natural hull frequency is therefore relatively large. For pitch motion in all wave directions the error is almost zero which together is considered to be sufficiently accurate. Sinusoidal wave induced roll motions for beam and quartering waves are given in the table 4.5.

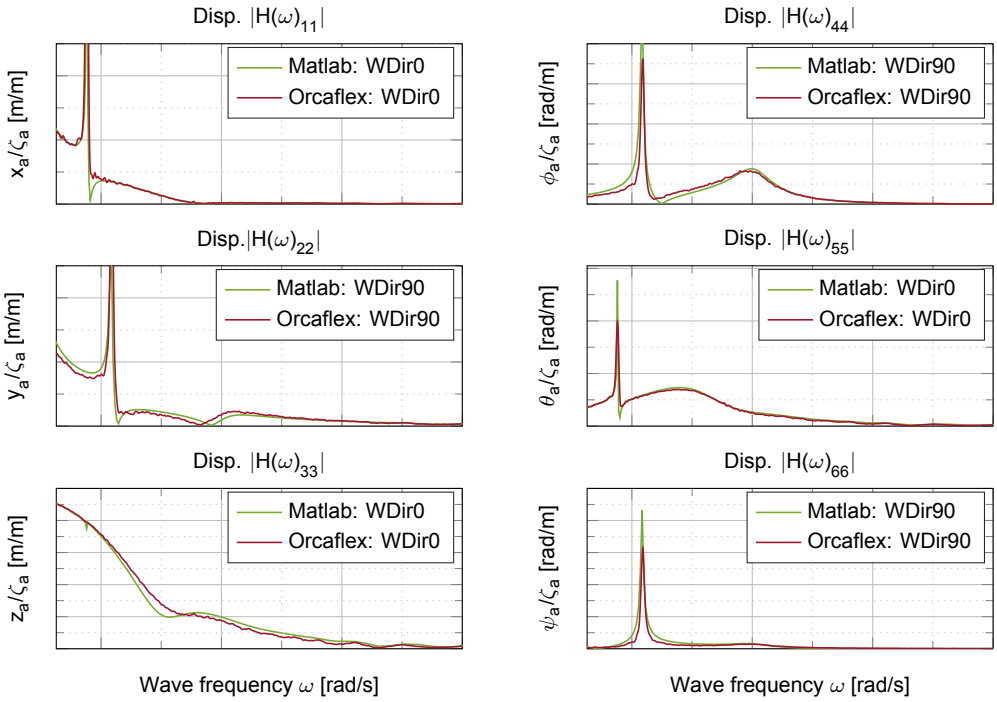

Figure 4.16: Vessel motion RAOs for lifts conducted at the bow centre

Table 4.5: Bow Centre: Validation roll motion amplitudes (deg) for incoming beam and sb quartering sinusoidal waves

T_p	3.00	4.00	4.81	5.21	5.69	6.31	7.02	7.33	7.78	8.91	10.43	12.57	15.71	
Or	0.00	0.07	0.24	0.46	0.94	1.79	1.40	1.20	0.99	0.67	0.22	1.01	2.33	
Ma	0.01	0.07	0.22	0.43	0.89	2.03	1.57	1.32	1.12	0.72	0.16	0.97	0.56	90°
ε_r	0.00	0.00	-0.02	-0.03	-0.05	0.25	0.17	0.12	0.13	0.05	-0.06	-0.05	-1.76	
Or	0.00	0.03	0.12	0.19	0.24	0.10	0.26	0.32	0.37	0.42	0.57	0.75	1.52	
Ma	0.01	0.03	0.11	0.19	0.27	0.21	0.23	0.30	0.36	0.42	0.67	0.68	0.37	45°
ε_r	0.00	0.01	-0.01	0.00	0.03	0.11	-0.04	-0.02	-0.02	-0.01	0.10	-0.07	-1.15	

Bow PS

Lastly the model validity is evaluated for the intended purpose namely lifts conducted at PS or SB. Due to the crane tip position now all coupling terms are contributing as explained in the previous sections. Thus double peaked RAOs near the pendulum frequency are to be expected. The boom moment of inertia is now also included (in both models). Thus a lower natural hull frequency is to be expected. Lastly the rigging module is included (only in Orcaflex), the influence thereof is demonstrated. Results of the validation tests are given in appendix B.2.2. Although these results imply that at least the trend in vessel response coincide in both models, an considerable difference in roll response is observed, see figure 4.17 The double peaks from the pendulum are reflected precisely at the corresponding frequencies. The captured hull natural roll frequency is however apparently lower in dynamics than it is computed in statics.

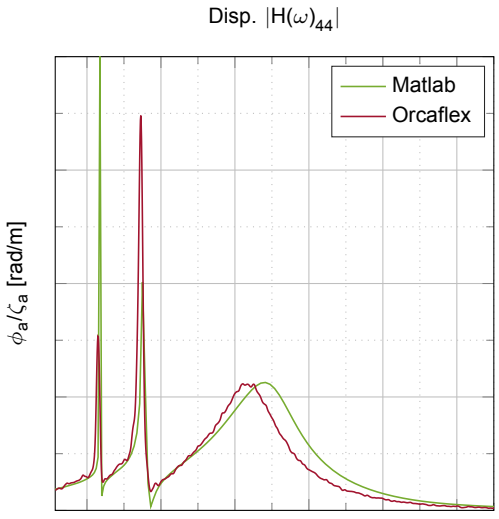

Figure 4.17: Vessel roll RAO for lifts conducted at PS

The modal analysis which have been used for modeling similar systems (at least in statics) is applied during the development of all validation models but has not yet been discussed. For declaring the observed shift in the hull natural roll frequency this method became handy. The modal analysis in Orcaflex was able to find 18 instead of 9 different modes due to the separately modeled ship, rigging module and suspended load (all 6-DOF). If as discussed at page 38 the added mass corresponding with the correct frequency is given, the modal analysis show similar resonance frequencies of the mooring, swinging pendulum and vessel hull, see table 4.6. The validity of the FD model has been demonstrated for light ship conditions (mass matrix) and single crane lifts conducted at bow centre (x_{ct}, z_{ct}) and since the modal analysis show similar systems it is unlikely that the derived coupling due to crane distance y_{ct} is causing this difference. From this is concluded that with regard to the system response in FD, no modeling errors have been made in Orcaflex and Matlab. Thus the shift in the hull natural roll frequency must come from dynamic behavior which could mean that the vessel response in this operational condition can not be approximated linearly with similar accuracy.

Table 4.6: Modal Analysis results for mooring, pendulum and hull DOFs

	Mooring		Pendulum		Ship Hull	
	x/y	ψ	η_7	η_8	ϕ	θ
Or	0.147	0.204	0.431	0.549	0.892	0.719
Ma	0.160	0.200	0.430	0.550	0.880	0.700

As discussed non-linear behavior may be derived from viscous roll damping, large motions or the dynamic moment arm effect in hydrostatic force (also large motions). Damping due to viscosity was however not included and vessel motions where small with roll angles of ≤2.2 deg. Further, the difference in roll resonance frequency may be derived from the wave memory effect which is included in Orcaflex simulations by means of the convolution integral of the hydrodynamic added mass and damping. However most often this effect only becomes noticeable with larger motion amplitudes and in previous simulations this effect was not observed, at least not severe. Thus it is unlikely that this effect suddenly becomes noticeable during PS lifts. The effect must therefore be caused by the dynamic moment arm effect or by an error in the applied length of the arm from the crane tip to "the centre of rotation" (thus lengths x_{ct}, y_{ct}, z_{ct}). Without doubt restoring forces due to gravity and the axial hoisting rope stiffness are derived correctly and without doubt the moment arm effect can not be severe with small motions. However, I am not sure about the way the dynamic moment arm effect in Orcaflex is contributing in vessel motion response. The dynamic moment arm effect is computed by subtracting a term in the from of $(m_b z_b - m z_g)g$ where m is the structural mass of the vessel. Thus including the mass of the cranes and suspended load. In other words, by modeling them separately in Orcaflex, which is needed due to their contribution in Inertia and restoring forces, something goes wrong. The effect can not be disabled, however by setting the mass of the vessel body (here m) at zero and to replace it by another 6-DOF buoy without volume at the vessel centre of gravity, the initial hydrostatic force should than remain untouched. Vessel trim and Inertia remain similar in this manner. Figure 4.18 illustrates this concern. The difference in roll response is clearly visible and that this effect doesn't contribute with small motions as well.

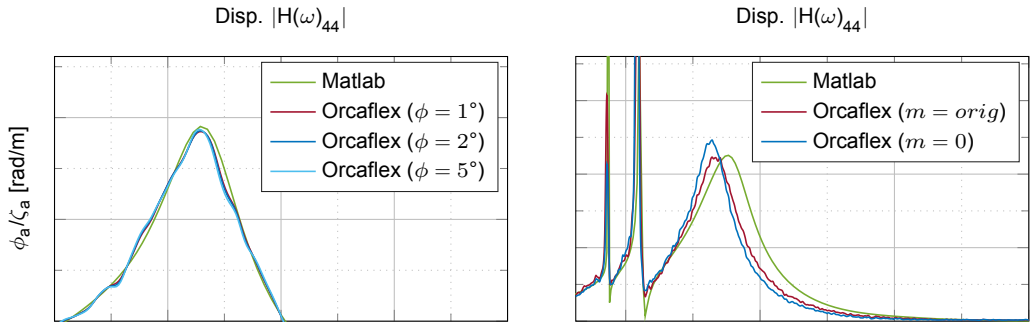

Figure 4.18: Test dynamic moment arm effect. Left, light ship without cranes, Right, Heavy Lift.

Assuming that in Orcaflex this effect is implemented correctly, modeling errors or modeling interpretations have been made for which unfortunately no solution have been found. It must be examined more closely. The difference in roll amplitude is also observed during sinusoidal waves. Results are given in appendix B. In table 4.7 response amplitudes are given for roll and pitch, showing that the computed response in pitch is spot on and that the computed roll response is actually overestimated at these frequencies due to the shift. In conclusion from these tests can be concluded that the difference in roll amplitude is stiffness related and not due to non-linear behavior nor due to resonance with the mooring system.

Table 4.7: PS lift: Validation roll and pitch motion amplitudes (deg) for incoming sinusoidal waves from sb beam (roll) and stern (pitch)

Tp	3.00	4.00	4.81	5.21	5.69	6.31	7.02	7.33	7.78	8.91	10.43	12.57	15.71	
Or	0.01	0.03	0.11	0.20	0.36	0.77	1.76	2.24	2.21	1.21	0.52	0.97	2.05	
Ma	0.00	0.06	0.18	0.31	0.58	1.28	2.39	2.36	1.96	1.16	0.53	0.85	0.60	ϕ
Er	0.00	0.03	0.07	0.11	0.22	0.51	0.63	0.12	-0.25	-0.06	0.01	-0.12	-1.46	
Or	0.02	0.04	0.09	0.13	0.17	0.24	0.37	0.46	0.58	0.87	0.77	0.61	0.61	
Ma	0.03	0.06	0.11	0.16	0.22	0.27	0.36	0.45	0.62	0.83	0.73	0.59	0.57	θ
Er	0.01	0.02	0.02	0.03	0.04	0.03	-0.01	-0.01	0.04	-0.04	-0.04	-0.02	-0.05	

Error Consistency

The magnitude of the error is with regard to the correction method not so important. However the consistency of the error is of importance in order to be able to extrapolate ”the correction” for a specific operational condition, towards another operational condition. In other words is the error of the on-line calculated transfer functions consistent over wave frequency and wave direction for other operational conditions (different crane configurations, hoisting rope length, mass suspended load etc.)? In order to check this, three more simulation in Orcaflex have been performed for which the error between the roll RAOs is calculated and compared to each other ($H_{44}(\omega)_{Matlab} - H_{44}(\omega)_{Orcaflex}$). Base Case: PS lift, 1217 ton, 52 m hoisting rope, outreach 16.7 m. Case 1: PS lift, 1217 ton, 60 m hoisting rope, outreach 16.7 m. Case 2: PS lift, 1217 ton, 52 m hoisting rope, outreach 13 m. Case 3: PS lift, 500 ton, 60 m hoisting rope, outreach 16.7 m. Results are given in the table below. From this is concluded that the error in roll RAO between those computed in FD and TD is roughly in same order of magnitude with regard to wave frequency but not to wave direction. If the mass of the suspended load is smaller, the error in roll RAO decreases. Thus corrections for a specific wave direction is not applicable for another wave direction.

Table 4.8: Error consistency in roll RAO between those computed in FD and TD for different operational conditions. Error is given in rad/m for different wave frequencies.

	ω_ζ					ω_ζ				
Case	0.80	0.85	0.90	0.95	1.00	0.80	0.85	0.9	0.95	1.00
Base	-0.017	-0.005	0.030	0.035	0.024	-0.012	-0.003	0.012	0.011	0.006
1	0.000	0.025	0.028	0.021	0.012	-0.009	0.004	0.005	0.002	-0.002
2	-0.008	0.020	0.029	0.024	0.012	-0.009	0.001	0.006	0.000	-0.005
3	-0.020	0.016	0.016	0.014	0.007	-0.010	0.006	0.004	-0.033	-0.001
	sb beam waves					sb quartering waves				

Linearity

Based on geometry small angles are angles within 0.01 rad or 6 degrees which implies that in theory vessel and swinging suspended load motions can be computed linearly until approximately these excursions. An attempt was made to determine until which motions or until which significant wave height this assumption holds so that is known until when the model is valid. In order to do this sinusoidal wave induced motions have been studied for wave amplitudes between 0.5 and 2.0 m coming from sb beam since this wave direction is most critical for vessel roll response. Unfortunately during this test the mooring configuration which was chosen for appropriate vessel orientation became a problem again. The applied mooring stiffness as was done for the validation tests was sufficient for maintaining

appropriate position with respect to wave direction. However, this was not the case with roll motion amplitudes larger than 1.5 degrees due to the strong motion coupling in yaw direction which was causing the vessel to yaw with 0.5 degrees and more which the mooring system subsequently tried to restore. This effect was building up during the simulation period which can be seen in figure 4.19 where vessel roll motion amplitudes and its spectral density plot is given. Thus sinus in is not sinus out. The results of the tests are given in appendix B.3.4. Although the maximum response per wave frequency is not entirely consistent, the increment in roll response is for all wave frequencies constant until approximately 4 degrees of roll amplitude. Concluded is therefore that within the domain of application vessel motions can be approximated linearly with satisfying results.

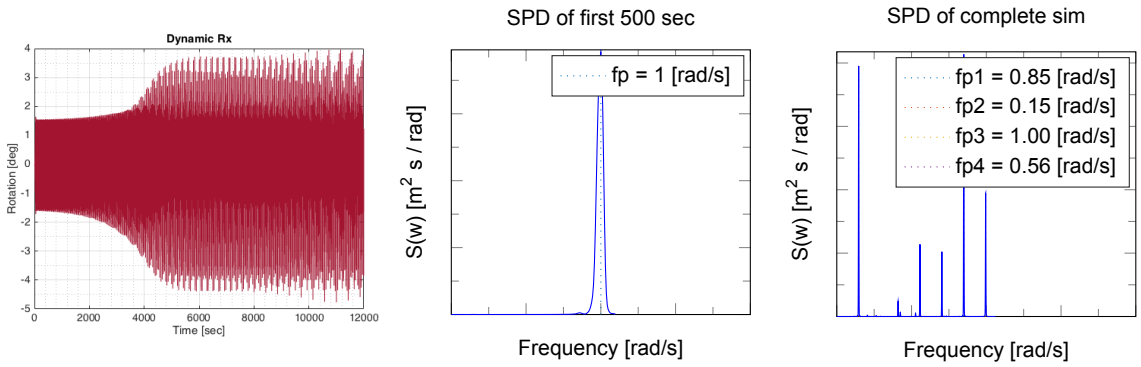

Figure 4.19: Sinusoidal wave induced roll amplitude and its spectral density for specific time windows. PS lift. Wave properties: H_{m0}=1.5m, T_p=6.5sec, Wdir=90°

4.4. Conclusion

- Simulation model output such as resonance frequencies and response phases and amplitudes are in line with those computed in TD by Orcaflex,
- The observed difference in vessel roll motion amplitude between those computed in FD and TD is stiffness related and does not originate from non-linear phenomenons such as viscous roll damping or large motions,
- It is not entirely clear how the correction in hydrostatic force due to the non-linear effect of the dynamic moment arm (for large motions) contributes in vessel response calculations within Orcaflex. However, significant differences in roll response have been observed between different modeling approaches. How heavy lift operations can be simulated most accurate with Orcaflex is for further research,
- By neglecting rotational motions of the cargo, vessel roll motions are underestimated by approximately 10% near the hull natural roll frequency. However, this shortcoming was not observed in other vessel motions and this error is based on sinusoidal waves,
- The mooring system configuration have to be chosen carefully in order to obtain trustworthy calculated vessel motions. Especially during heavy lift operations conducted at PS or SB side where strong motion coupling is present,
- It has been found that for maintaining vessel orientation the mooring system have to be modeled relatively stiff. Therefore and due to strong motion coupling resonance can occur between the swinging pendulum and the mooring system if analyzes are performed in TD (build up effect). For more accurate motion analyzes a softer mooring system is required for which unfortunate no solution have to be found. Suggested is to introduce damping by means of a DP system,
- Although differences in vessel roll amplitudes have been observed between simulations in FD and TD, concluded is that within the applicable domain of heavy lift operations, vessel responses can be approximated linearly with satisfying results,
- By performing analysis in FD the gain in computational time is evident. In comparison, by making use of the developed tool, the workability for a lift operation is computed within roughly 30 sec for 18 different wave directions, 300 wave frequencies and 75 wave heights. With Orcaflex this takes at least 2 min, per environmental condition.

5

Sensitivity Analysis

This chapter describes succinctly the results of the performed sensitivity analysis on the parameters in the frequency domain model. This analysis is performed in order to determine the magnitude of the error which might be present in the model output as a result of an erroneous model input. The result of this analysis tells us what parameters are important for a particular vessel motion response and subsequently on which parameter(s) it might be useful to introduce corrections on.

5.1. Approach

Within the Matlab Tool there are parameters which have to be chose by the user such as the mass and outreach of the suspended load or the wave spectrum for which one would like to know the vessel response. But there are also model input parameters such as the hydrodynamic added mass and damping that are given according to the chosen mass of the suspended load. These so called hydrodynamic model input parameters are obtained with the aid of ANSYS AQWA for a limited amount of suspended loads. Therefore by choosing a certain mass of the suspended load the hydrodynamic data is searched in the database according to the corresponding draft which is computed in the Matlab Tool. Thus, one can approach the influence of the mass of the suspended load from two sides.

In order to obtain an comparable image of the sensitivity between the parameters the analysis is subdivided in three parameters categories: (1) Model Input parameters for the vessel and suspended load composition, (2) Hydrodynamic Input parameters and (3) Wave Input parameters. For the first category a single hydrodynamic database (for a specific draft) is maintained. For the second and third category different hydrodynamic databases are being used to determine for example the influence in trim, draft or water depth. During these tests the model input parameters for the vessel and suspended load composition are being fixed. In this way the sensitivity or influence on vessel motion response as a result of errors in the operational input, the hydrodynamic input or the encountered sea state can be determined.

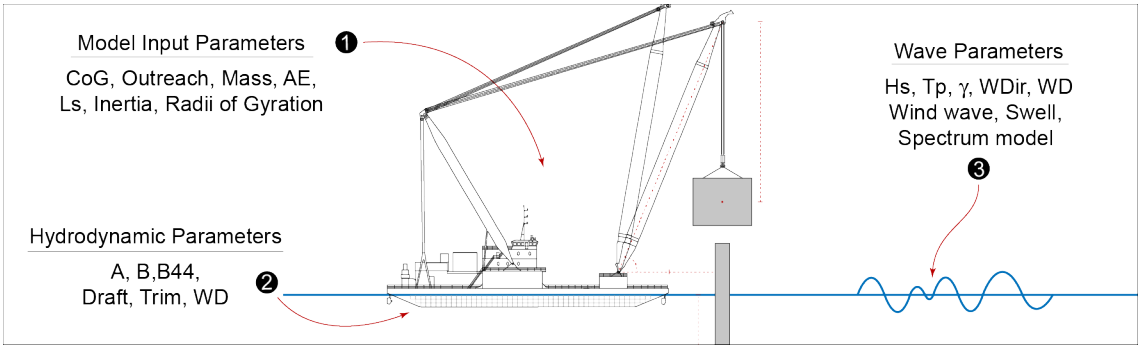

Figure 5.1: Approach sensitivity analysis, classification of parameters

The base case for the sensitivity analysis concerns a heavy lift operation of 1217ton, 32m above still water level. The lift is conducted with the port side crane with an outreach of 16m. For realism the outreach of the starboard crane is 8m. The validation study showed that the wave period and direction is very important for the determination of the vessel response due to the coupling between the suspended load. Since the response is calculated in the frequency domain the significant response or the root mean square of the response is compared for incoming stern, sb quartering and sb beam waves with peak periods of 2, 4, 6, 8 and 10 seconds and a significant wave height of 1m which together contain the mean JONSWAP spectrum ($\gamma = 3.3$). Sensitivity in heave accelerations, roll and pitch rotations of the crane tip have been analyzed.

5.2. Model Input Parameters

As discussed in chapter refch:correction methodolgy only model parameters that are dependent on wave frequency, wave height or wave direction can be directly correlated to measured vessel motion responses. Simply since those are primarily induced by the waves itself. Making on-line corrections on one of these model input parameters is therefore in the first place not very logical. Although it might be possible to make corrections on one of these parameters in a similar way as can be done on wave parameters, (fitting different values of the model input parameters which together with an ”correct” wave spectrum correspond to the measured response spectrum), the concept of making corrections in either the RAO or the wave spectrum is based on the assumption that the error of one of these is within the acceptable limits. Therefore it is of importance to know the sensitivity of the model input parameters in vessel motion response as well. For example if the sensitivity of the length of the hoisting ropes is significantly large in vessel motion response, than corrections in for example the added mass and damping by fitting corresponding magnitudes are nonsensical and moreover not consistent.

A summary of the input parameters for the vessel and load composition that have been tested on sensitivity in vessel motion response are given in table 5.1. Full details are given in appendix C.1. The deviation of the mean value is chosen on a reasonable basis. For example the rules of regulations requires only small deviations of ±2% in the estimated mass of the suspended load before a lift operation may be conducted. This is also the case for the centre of gravity of the load which determines the length of the swinging pendulum (l_s) and therefore the effective restoring force due to gravity and the axial crane rope stiffness. Furthermore it is unlikely that the outreach of the hoisting cranes is misjudged by the crane operators, so in practice only small deviations in these parameters are likely to occur. The centre of gravity of the ship may, however, differ from the predetermined setting as a result of a different trim and heel angle or slightly more or less ballast than was foreseen in the motion analysis. The mass of the ballast is dependent on the mass of the cargo and the outreach of the hoisting cranes. According to the stabilitiy booklet for this specific lift case, 4973 ton of ballast is needed in order to trim and heel the vessel to zero degrees [50]. Furthermore the sensitivity of the radii of gyration, the mooring stiffness and for completeness due to the lack of proper information about the cranes of the Rambiz 3000, also the crane mass and moment of inertia is analyzed as well.

Table 5.1: Sensitivity Analysis on Model Input Parameters

Parameter	Base quantity	Deviation	Parameter	Base quantity	Deviation
Mass Load	1217 ton	±2%		42.50 m	±1.0m
Mass Ballast	4973 ton	±5%	Centre of Gravity Ship	0 m	±0.5m
Mass PS Crane	226 ton	±5%		10 m	±1.0m
Mass SB Crane	215 ton	±5%			
Mooring Stiffness	80.00 kN	±25%		0.34	0.33/0.35
Outreach PS crane	16.00 m	±1.0m	Radii of Gyration Ship	0.25	0.24/0.26
Outreach crane	8.00 m	±1.0m		0.26	0.25/0.27
Centre of Gravity Boom	43.00 m	±2.0m	Inertia Cranes	1395.9 ton*m^2	±5%
Length hoisting rope	52.50 m	±1.0m	Axial wire stiffness	1.98E+09 kN	±5%

Results and Trends

By adjusting model input parameters, one changes in essence the RAO of the vessel motion response. Therefore in advance it is known that an adjustment in for example the mooring stiffness or the pendu-

lum length is changing the RAO the most close to the corresponding natural frequency of that particular subsystem (see chapter 4.1.2 at page 37). Nevertheless due to the coupling between the suspended load and the vessel and the corresponding hydrodynamic data per wave frequency and direction, it is difficult to recognize a particular trend in magnitude of the sensitivity over wave frequency and wave direction. For example the magnitude of the sensitivity of the port side crane outreach or the mass of the suspended load is completely different per motion and wave direction. Drawing conclusion by model input parameter per wave frequency and wave direction is therefore not very effect in order to get a picture of the order of magnitude. Therefore the average difference in vessel roll and pitch response relative to the base case is given in figure 5.2. Detailed results of the sensitivity analysis are given in appendix C.1 at page 137.

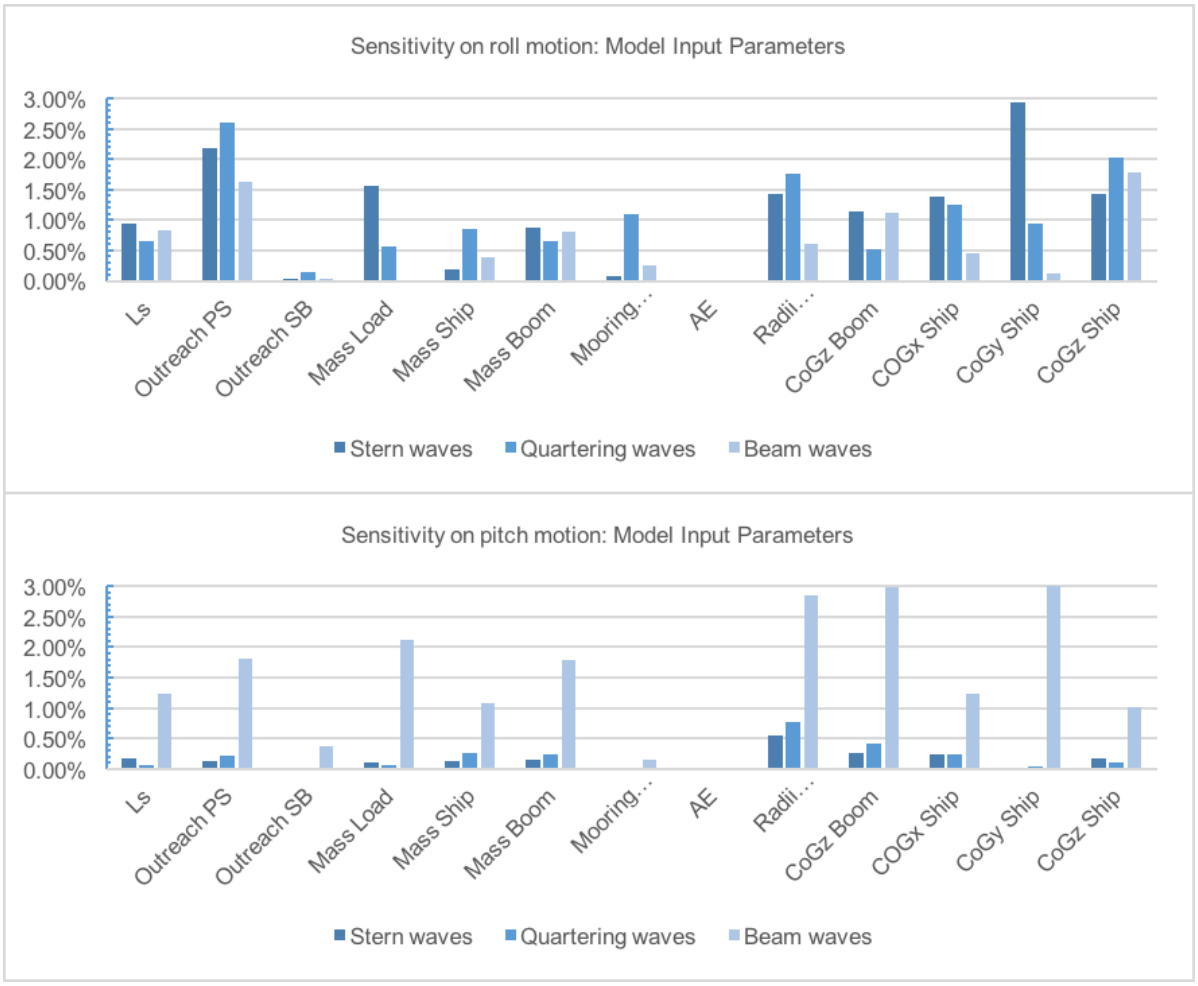

Figure 5.2: Absolute average sensitivity over wave frequency: Model Input Parameters

Although it is very important tho start with conscience parameter inputs for determining accurate vessel motion responses, it is clear that the sensitivity of the model input parameters is very small to almost zero if realistic errors are being made. Obviously the radii of gyration is very important for determining the rotational vessel motion responses and should therefore be properly estimated in advance. Preferably with model tests or finite element methods. It was expected to see an significant sensitivity of the ship centre of gravity and the outreach of the port side crane. However, this is only the case for the centre of gravity in transverse direction. The sensitivity of this parameter on vessel motion response is ≈3-6% at all wave frequencies. This error can occur in the motion analysis if in practice the vessel heels more than initially was estimated for the motion analysis. Shifts in the traverse direction of the centre of gravity should therefore be incorporated in the on-line motion analysis tool for more accuracy in the prediction. The difference in added mass and damping will be elaborated in the next section. For the longitudinal and vertical direction the sensitivity of these parameters is ≈1% at wave periods between

2 and 8 seconds and ≈7% near the pendulum natural frequency. The numbers shown in figure 5.2 are absolute average numbers over wave frequency which in this case does not give an accurate picture of the sensitivity near those wave periods. In appendix C.1 the sensitivity is given per wave direction and wave period.

Worth noticeable is the largest realistically seen possible error or sensitivity in model input parameters. If for example the outreach of the port side crane and the length of the hoisting rope is entered incorrectly with one meter together with a miscalculated mass of the suspended load of 2% and therefore also insufficient ballast for horizontal heel and trim will result in an average error of 5.1% which is still not significant. Near the pendulum natural frequency the error in vessel motions response is larger with 12%. From this it can be concluded that possible errors in the model input parameters cause relatively small errors in vessel motion response analysis. The advantage is that possible correction theories on for example the added mass and damping of the vessel or the spectrum of the incoming waves will not become quickly inconsistent if small errors are made in the model input parameters on vessel motion response.

Note that one has to remember that these quantities are given for the response at a mean JONSWAP wave spectrum. The magnitude of the sensitivity in vessel motion response will differ for example incoming swell. These waves are almost fully developed and can be approximated by a Pierson-Moskowitz Spectrum ($\gamma = 1$) which contains more energy at low frequencies. Model input parameters such as the length of the hoisting rope will therefore become more important since this parameter is dominant in determining the low frequency responses. Section 5.4 elaborates more on the sensitivity of wave parameters.

Examining trends in the magnitude of sensitivity is thus not straightforward but in this case also not very helpful for the intended purpose of making improved predictions in vessel motion responses. However the effect of larger increments in adjustable model input parameters on vessel motion RAOs is useful to know for an first estimate of the vessel motion response. Since the response is linear it can be stated that larger increments in certain input parameters, such the mass of the suspended load cause larger effects in vessel motion RAOs at certain frequencies and vise verse. This is illustrated in figure 5.3 for adjustable input parameters in vessel roll, pitch and yaw motion RAOs for incoming beam waves. Note that the correct hydrodynamic data is used for determining the effect of a larger cargo mass.

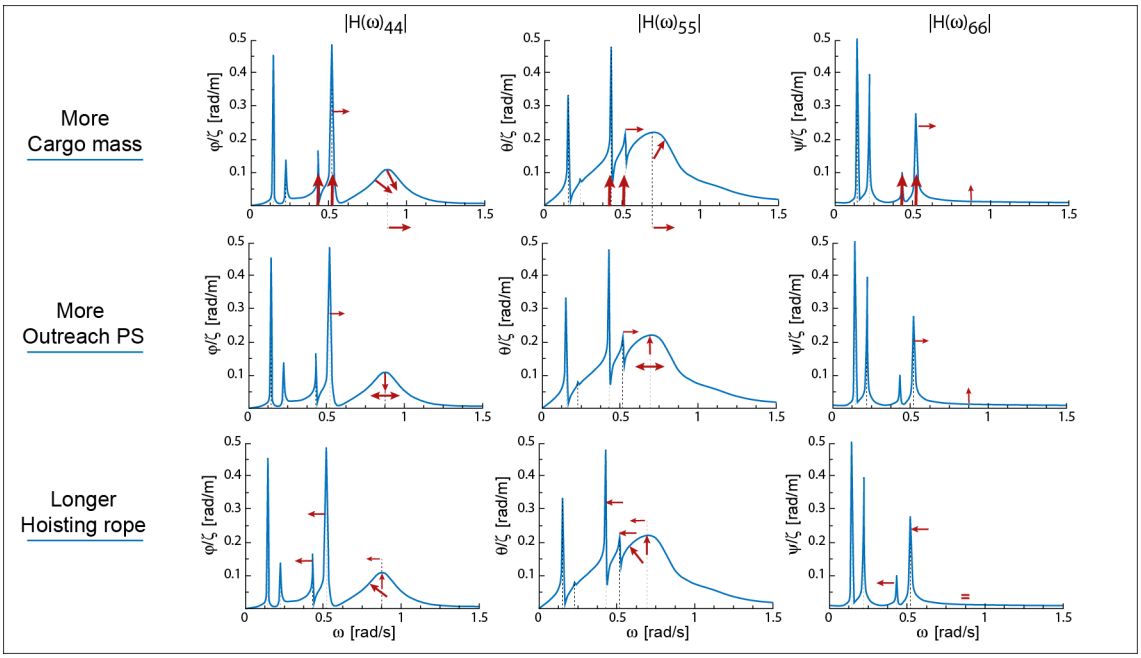

Figure 5.3: Effect of cargo mass, outreach and suspended height on vessel motion RAOs

5.3. Hydrodynamic input

In order to get insight into the order of magnitude of the sensitivity in vessel motion response due to an error in the applied hydrodynamic data in the on-line motion analysis, a sensitivity study was done on the following hydrodynamic input parameters:

- Added mass and damping coefficients,
- Added viscous roll damping coefficient,
- Vertical hydrostatic restoring coefficient,
- Water depth,
- Vessel draft,
- Vessel trim.

Added mass, damping and vertical restoring

The added mass and damping is dependent on wave frequency and can therefore possibly be correlated to measured vessel responses in order to improve the prediction of vessel motion responses. However before a detailed study will be performed on the possible error in the computed added mass and damping it is in the first place useful to approximate the order of magnitude of sensitivity on vessel motion response. The added mass and damping coefficients are determined with the aid of ANSYS AQWA which computes the coefficients with the aid of 3D-panel methods. The geometry of the Rambiz 3000 is fairly straightforward which reduces the probability of errors in for example the computed hull area due to a coarse selected panel size. Furthermore in practice only small vessel motions are allowed. Thus linear potential theory an panel methods for determining the added mass and damping coefficient is proved to be sufficiently accurate. Stated that the 3-D model of the Rambiz 3000 is made properly, it may therefore be assumed that the accuracy of the computed hydrodynamic data is within the acceptable boundaries.

However, the Rambiz 3000 is constructed out of two merged barges with as a consequence that there exist an closed cushion of 50m by 4.5m by 3.7m (L$\times$B$\times$H) at the centre line of the vessel. Unfortunately this hull shape can not be modeled in ANSYS AQWA v15 without causing numerical instability due to irregular wave frequencies [1]. This could potentially be solved by adding an artificial lid in the closed cushion at still waterline with appropriate damping. However this is rather complex and outside the scope of this research. Therefore due to the absence of the closed cushion in the hydrodynamic model it can expected that there are errors in the computed hydrostatic and dynamic coefficients.

Closed cushions provide additional hydrostatic restoring in vertical direction due to the pressure of the trapped air. The additional heave restoring for a wallsided cushion with horizontal area A_c and volume V_c can be approximated by

$$C_{33} = \gamma \frac{p_0 A_c^2}{Vc} \tag{5.1}$$

where $\gamma = 1.4$ is the gas constant of air and p_0 is the atmospheric pressure of ≈101.325 kPa [56]. Assumed that the complete volume is filled with air the additional hydrostatic force is 8.4E+03 kN which together with the corrected hydrostatic force due to the wetted surface area of 3.2E+04 kN is 5% more than the initial computed hydrostatic force of 3.6E+04 kN with the aid of ANSYS AQWA. From the sensitivity analysis it can be concluded that this additional heave restoring decreased heave acceleration and pitch motion response with ≈2% for incoming stern and stern quartering waves and 10% for incoming beam waves (remember coupling between load and vessel). The difference in roll motion is ≈1%. Detailed results are given in appendix C.2.3.

The effect on added mass and damping is however more difficult to determine. Studies have been conducted on this subject, however all of them report effects for large air cushions beneath a floating structure. For these cases it has been found that enclosed cushions have significant influence on vessel heave and pitch response but the magnitude is dependent on wave direction and frequency. Largest effects where registered in vessel heave motion for high wave frequencies ($\omega > 1.0$). In this scenario the heave response is larger with present enclosed cushions. However for low wave frequencies the response in heave and pitch is decreased. In summary it has been found that for large air cushions below a floating offshore structure and higher wave frequencies the added mass and damping in heave, roll and pitch motion is decreased. This would mean that computed vessel motion responses become

larger if enclosed cushions are included in the hydrodynamic model. Closed cushions also changes the mean dirft forces but it has been found that the difference is small [28].

Without dedicated studies on this effect for this specific vessel the effect on added mass and damping is difficult to approximate. Having said this still an estimation of the error in the added mass and damping coefficients is made between -1% until -4% for the absence of the closed cushion in the hydrodynamic model. The ratio between the closed cushion area and the wetted surface area is 225/3260 = 0.07, which is very small. The assumption of small errors due to the enclosed cushion is therefore, in the first place, reasonable for an estimation of the order of magnitude of sensitivity in vessel motions response in comparisons to other parameters. The assumed error in the added mass and damping is applied by hand in heave, roll and pitch motions (and their coupled motions) since those are being affected.

From the analysis can be concluded that the sensitivity of small errors in the added mass and damping is most noticeable in vessel motion responses close to the vessel hull natural frequency. However, the difference in vessel motion response remains relatively small with roughly 2-6% dependent on wave direction and frequency. The average sensitivity of the added mass and damping over wave frequency per wave direction and motion including the additional vertical restoring is summarized in figure 5.6. Detailed results are given in appendix C.17. It should be noted that the difference in vessel motion response due to an error in the added mass and damping does not increase linear with an linear increment in the error due to a shift in the hull natural frequency which is explained in more detail for the sensitivity of water depth. Once again detailed studies are required in order to state if the assumption of small errors in hydrodynamic data due to closed cushions is permissible.

Viscous added roll damping
Added viscous roll damping due to skin friction and eddy making damping decreases vessel roll response as has been discussed in chapter 3.3.3. Due to the coupling between the vessel and the suspended load not only vessel roll bot also vessel pitch motion decreases if waves hit from starboard quartering or starboard beam. However, it is expected that the added damping due to viscosity is limited because of zero forward speed, the hull geometry itself and since only small vessel roll motions are allowed. This expectation is reflected in the sensitivity analysis which show that the impact of viscous added roll damping is negligibly small with maximum 0.8% in vessel roll motion and incoming beam waves. Detailed results are given in appendix C.2.1. It should be noted that this concerns the linearized viscous added roll damping in which the cubic term of the equation is neglected (see eq: 3.31). Thus in practice there is slightly more damping than is estimated linearly.

Water Depth
The average water depth of the North Sea is 30m which gave rise to generate the hydrodynamic database of the tool for this water depth [15]. However the water depth is important for the determination of wave forces and hydrodynamic added mass and damping coefficients which is illustrated in the figure below. With decreasing water depth hydrodynamic added mass, damping and wave forces increases. This is causing a shift in the hull natural frequency which is shown in figure 5.5 and can be easily derived from the equation $\omega = \sqrt{C/(M+A)}$, wherein the mass and stiffness remain constant over water depth. Thus with decreasing water depth the hull natural frequency decreases as well.

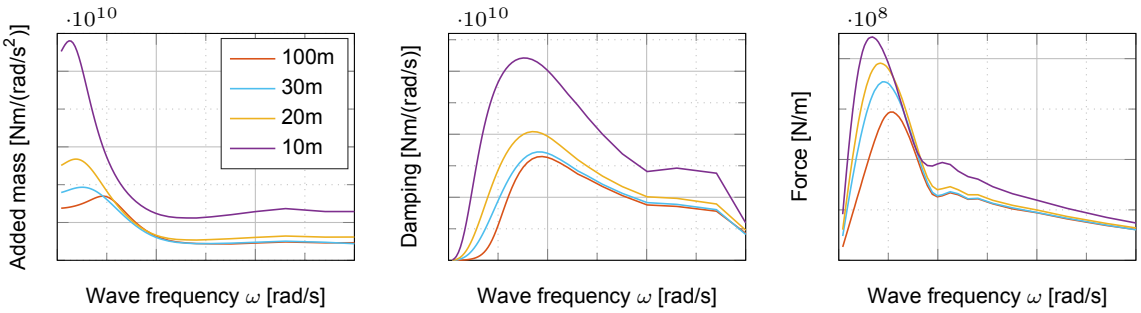

Figure 5.4: Hydrodynamic added mass and damping and wave force for pitch motion and different water depths

The analysis is performed for small and larger increments in water depth and for a water depth dependent and in-dependent wave spectrum. From the analysis can be concluded that the difference in vessel motion response is largest if a water dependent wave spectrum is applied due to a lower peak in the power spectrum which causes a decrease in response. But in order to make a comparison in sensitivity between other parameters, only results for a water depth in-dependent spectrum are given.

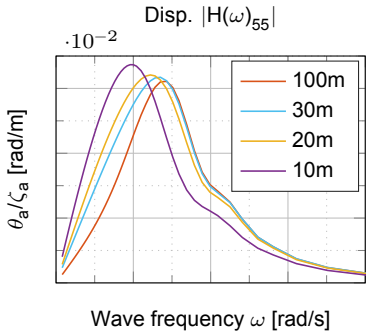

Figure 5.5: Displacement RAO for pitch motion and different water depths

The water depth dependent shift in the hull natural frequency varies per vessel motion which together with the motion coupling due to the interaction between the vessel and suspended load makes it complex to summarize when specific vessel motions responses reduce or increase with a specific magnitude. However it is clear that the difference in vessel motion response between analysis done with 30m and 27.5m and 30m and 25m water depth is not significant. Vessel motion responses decreased with 1% till 5% dependent on the wave frequency and direction. For larger increments in water depth the difference in vessel motion response becomes more evident with a difference of 10% up to 50% predominantly less for all wave periods between 2 and 10 seconds. The difference in vessel motion responses between analysis done with an infinite water depth (100m) and 30m water depth is also significant for roll motions and incoming stern waves and for pitch motions and incoming beam waves. The difference in vessel motion response for wave periods between 6 and 10 seconds varies between +2% and +20%. For higher wave periods the difference is somewhat smaller. From this can be concluded that for more accurate on-line motion analysis hydrodynamic coefficients have to be included for a number of water depths whose urgency increases for water depths between 10m and 20m due to the shift in frequency. Detailed results are given in appendix C.2.4.

Draft and Trim

It is evident that vessel draft is important for the determination of the hydrodynamic coefficients. In order to determine its sensitivity for a small difference in draft and trim due to for example an erroneous estimated mass of the suspended load and ballast, vessel motion responses are analyzed for trim angles of -0.1 until -0.4 degrees and vessel drafts for plus and minus 2% cargo en 5% ballast (±285ton). From the analysis can be concluded that the difference in vessel motion response due to trim is largest for incoming quartering waves. For wave periods between 2 and 8 seconds responses decreased with ≈1-6%. For longer waves periods it increased. For incoming stern waves responses decreased which would be vise verse for positive trim angles. For incoming beam waves vessel pitch response increased while vessel heave and roll decreased. As expected the difference in draft is for wave periods between 2 and 8 seconds neglectable with <1%. For longer wave periods the difference in response is ≈2-5%.

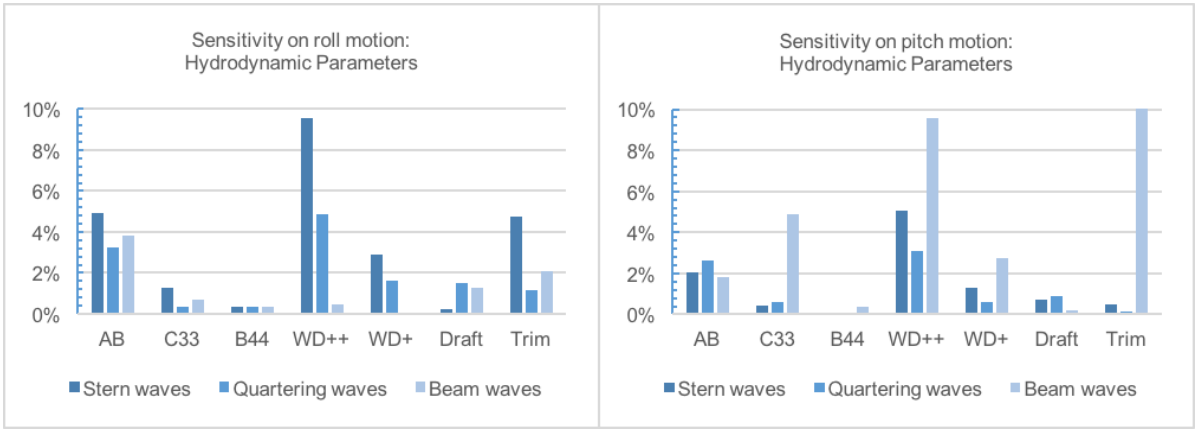

Figure 5.6: Absolute average sensitivity over wave frequency: Hydrodynamic Parameters
Given values for AB correspond to -4% added mass and damping, WD++ values for 30m/20m water depth, WD+ values for 30m/25m water depth and Trim for -0.3 deg trim.

5.4. Wave parameters

The urgency of applying the correct amount of wave energy is evident but in practice very difficult to achieve due to uncertainties in wave direction and wave period(s) for example. In order to get insight into the order of magnitude of the sensitivity in vessel motion response due to an error in the applied wave spectrum in the on-line analysis, a sensitivity study was done on the following ”wave input” parameters:

- Wave height,
- Wave period,
- Spectral peak parameter,
- Bi-modal wave spectrum,
- Water depth,
- Wave direction.

Only hydrodynamic forces are dependent on wave direction. To determine the sensitivity of wave direction, hydrodynamic data is computed per wave angle with increments of one degree in order to diminish errors due to interpolation. Vessel motion responses induced by a sea state which is composed of swell and wind waves have been approximated with the torsethaugen spectrum as explained in appendix A.3.3. This chapter elaborates also on the calculation of a depth dependent wave spectrum. The sensitivity of wave height, period and spectral peak parameter are adjusted by hand in Matlab. The initial wave height of 1 m which is used in the base case is in- and decreased with 0.1m and the wave period with 0.5 s in order to simulate realistic errors in the obtained environmental data from weather hind casts. The initial applied spectral peak parameter of 3.3 is adjusted with small increments of 0.2 in order to simulate a slightly less or more developed wave than the average wave present in the North Sea. The difference in response due to the spectral peak parameter is also analyzed for steps according to the parametric relation between the significant wave height and significant wave period (see A.3.1).

Wave height

Due to the applied linear relation between vessel motion response and wave height it can be stated that vessel motion responses independent of wave direction increases or decreases with the same difference in percentage in wave height.

Wave period

The significant wave period is very important for the determination of the response which is most noticeable at wave periods where the slope and the total area under the transfer function curve is respectively steepest and largest. From the analysis can be concluded that an increase in wave period (which is an decrease in wave frequency) decreases vessel motion response from wave periods between the pendulum and vessel hull natural period which dependent on the operational condition is between 14 and 7 seconds. For longer wave periods vessel motion responses increases with an increase in wave period and vise verse for an decrease in wave period. This principle is illustrated in figure 5.7 where the transfer function for roll, two different wave spectra and their corresponding response areas are given. For wave periods close to the natural hull frequency the difference in roll and pitch response is ±30% until 45%. For longer wave periods the difference in response reduces less rapidly if wave periods become larger with quantities between ±5% until ±20%. If shorter wave periods become longer, responses increase rapidly. Results per wave period are given in appendix C.3.3.

Wave Spectrum and peak parameter

The same principle as is illustrated in figure 5.7 applies to the bi-modal wave spectrum. Sea states composed out of swell and wind waves contain more wave energy at lower wave frequencies and less at higher wave frequencies than wind generated sea states only. The absolute value of the transfer function for vessel motion response between 14 and 7 seconds is however significantly lower. Therefore an decrease of 5-15% in vessel motion response is observed between those periods. Combined spectra with peak frequencies at the natural hull frequency increases only vessel roll response with 10% if waves hit from quartering direction. Otherwise the difference in response is neglecable small.

The sensitivity of small changes in the spectral peak parameter is very small with <1%. Only if the spectral peak is computed by means of the parametric relation, differences in vessel motions response are significant. However the results are not included in figure 5.8 since the chosen combination of wave height and period result in spectral peak parameters of 1 and 5. This represent respectively an fully developed and undeveloped spectrum which explains the big difference in response.

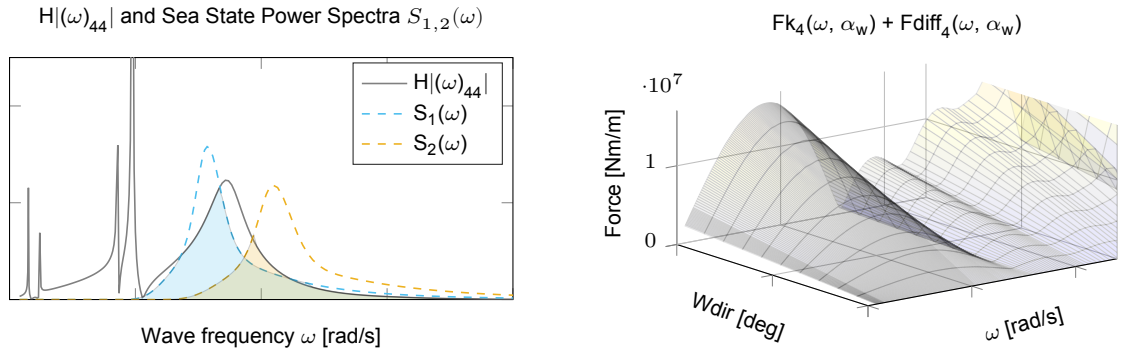

Figure 5.7: Left: Roll transfer function and wave spectra. Right: Wave force over frequency and direction

Water depth

The water depth is just as important for the determination of the wave spectrum as it is for the hydrodynamic coefficients. Less water depth allows for larger wave heights and thus a more narrow bounded wave spectrum. The difference in vessel motion response due to an water in- and water dependent wave spectrum (30m water depth) is -5% for short wave periods and -10% till -20% for longer wave periods. The spectral peak parameters was set on 3.3. Detailed results are given in appendix C.3.5.

Wave Direction

From the analysis can be concluded that the sensitivity of wave direction on vessel pitch motion is largest for wave directions close to 90 degrees. The response increased for wave periods between 2 and 6 seconds and decreased for longer wave periods. For a wave period of 6 seconds the response increased with ≈4.5% per wave degree which result in an increased response of 25%. For incoming stern and quartering waves the difference in vessel pitch response due to a small difference in wave direction is neglectable with <1%.

The difference in vessel roll motion response for incoming beam waves is not significant for small differences in wave direction. For an error of 5 degrees in wave direction the response decreased with 1-7% depending on wave frequency. Largest difference in roll response have been observed for incoming quartering waves with an increase of ≈7-14% dependent on wave frequency. Up to now these results are intuitive. However, for certain wave periods and incoming stern waves vessel roll response decreased as well if waves hit from a slightly wider angle. The difference in response is ≈2-10% less for a wave period of 6s and 10s and ≈3-9% more for a wave period of 4s and 8s. This can not be explained straightforward due to strong motion coupling in combination with the wave direction dependent wave forces which is illustrated figure 5.7.

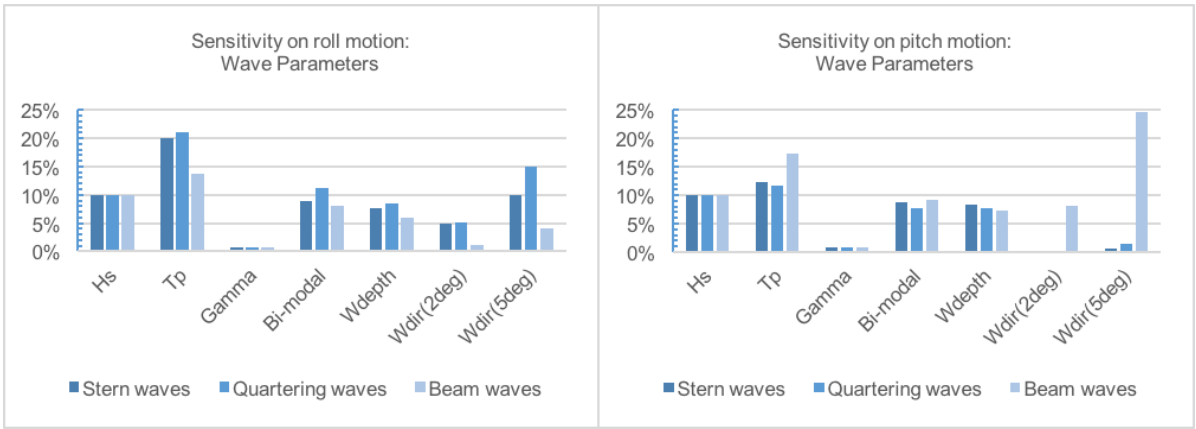

Figure 5.8: Absolute average sensitivity over wave frequency: Wave Parameters

5.5. Summary and Conclusion

With this sensitivity analysis the order of magnitude of errors in computed vessel responses is demonstrated for erroneous applied model input parameters or realistic errors in the applied hydrodynamic data and wave spectrum during on-line motion analysis. The conclusions from this analysis are summarized below:

- It is evident that model input parameters such as the mass and the height of the suspended load are given precisely for accurate motion analyzes. However, realistic small errors in the applied model input parameters cause relatively small errors in vessel motion analyzes. Also combinations of erroneous applied magnitudes cause a small error of ±5-12% in computed responses.
- Largest errors (±10%) in computed vessel responses due to incorrect hydrodynamic coefficient have been observed for a large difference (10m) in the applied water depth in the diffraction analysis. Shallow water provides more added mass and damping which result in a decreased hull natural frequency. For small errors in the applied water depth (5m) the difference in motion responses is however in the order of magnitude of the model input parameters (±5%). Thus for more accurate motion analyzes hydrodynamic coefficients should be included for a number of water depths. Preferably at least for every five meter of water depth.
- Differences in hydrodynamic coefficients due to small differences in vessel trim cause a relative large error in computed pitch motion if waves hit from starboard beam. This is due to strong motion coupling. The response is however very small thus in practice barely perceptible. For other motions and wave directions the difference in response is in the order of magnitude of the model input parameters (±2-5%).
- Due to the present small closed air cushion which is not modeled in the hydrodynamic model of the vessel, it is assumed that small errors in hydrodynamic coefficients can be expected. If this assumption of small errors is correct than can be concluded that this is causing an error of 2-5% in computed vessel responses. The assumption of small errors due to the closed air cushion is based on the small ratio between the wetted surface area and the closed air cushion area. It should be noted however that a significant difference in hydrodynamic coefficients is reported in literature about large closed air cushions. Thus a detailed study into this subject is needed in order to determine the actual difference in hydrodynamic coefficients and thus of the assumption of small errors is permissible.
- Significant wave height, wave peak period and wave direction cause largest errors in computed vessel responses. For small errors in the applied wave parameters such as H_s and T_p the error in vessel responses is already between ±10-20%. Due to the applied linear relationship between wave height and vessel motion response the difference in wave height in percentages is proportional in response. This relationship does not hold for wave period. Certainty in wave period is most important for determining accurate vessel responses. An error of half a second causes an error of roughly 20% in computed vessel responses. An small error of only 2-5 deg in wave direction is most noticeable in vessel roll motion with ±5-15%. Wave spreading is hereby omitted.

Making a more accurate prediction of the vessel response through corrections in model input parameters is not compelling since largest errors originate from erroneous applied wave spectra and its direction with respect to the vessel orientation. Moreover due to the fact that model input parameters are independent of wave frequency nor amplitude it is not straightforward if not impossible to make corrections in vessel response calculations with these parameters. Thus further research with a method such as fuzzy logic that might be able to recognize correlations between model input parameters and measured errors in vessel responses is not worthwhile. Errors in hydrodynamic coefficients can cause noticeable errors, especially if the diffraction analysis is based on an incorrect water depth. However, errors in the applied wave spectrum always veto. Thus largest improvement in vessel response predictions can be achieved if more certainty is gained in the present sea state.

6

Correction Method

Based on the results of the sensitivity analysis the proposed correction methodology has got its shape. Concluded from the sensitivity analysis is that the present wave direction, significant wave height and period are the most dominant parameters in the determination of the vessel response. Furthermore is found that errors in hydrodynamic coefficients, either due to the closed air cushion or an incorrect applied water depth during the diffraction analysis causes a relatively large error in computed responses.

The validation study has shown that the error in computed vessel responses is largest during heavy lift simulations. The error is negligible during light ship condition which basically means that an improved prediction of the vessel response can be given if the forecasted wave parameters do not correspond to the actual energy of the present sea state. The probability that these are incorrect is unknown and moreover variable. However it is evident that a small error can make a big difference. This potential gain is thus quite large and moreover useful for other operational conditions. After all there is not corrected for model errors. During this operational condition is thus sought for the present sea state by fitting different wave parameters.

During heavy lift operations predominantly errors or rather differences in the roll amplitude have been observed. Furthermore became clear that the error in computed roll response, roughly taken, constant is over wave frequency and different crane angles but not over wave direction and not for a different mass of the suspended load. The latter is not important however the hoisting rope length, outreach and wave direction will vary during the operation. Precisely for these situations one would like to have the most reliable and accurate information. Therefore is sought to possible optimizations of predominantly roll motion with the aid of fitting different wave spectra and added mass and damping coefficients. By adjusting the added mass and or damping one basically changes the transfer function between the energy of the sea state and the energy of the vessel motion response. Thus during heavy lift operations initially is sought to both the appropriate transfer functions as well an appropriate energy spectrum.

6.1. Least Squares Problem

The proposed correction method is basically noting more than seeking the minimum difference in energy between the measured and calculated vessel motion response by means of the wave buoy analogy. The problem of finding the minimum difference in energy or point in the solution space is known as the least square problem which for the wave buoy analogy is given by

$$\begin{aligned} \min \chi^2 &\equiv \min \parallel \underbrace{\int S_{Rij}(\omega) d\omega}_{\text{measured}} - \underbrace{\int \left|H_{ij}(\omega)\right|^2 S_\zeta(\omega) d\omega}_{\text{calculated response moment}} \parallel^2 \\ &\equiv \min \parallel \text{var}_m - \text{var}_c \parallel^2 \end{aligned} \tag{6.1}$$

where $i, j = 1..N$ are vessel motions, $S_R(\omega)$ is the measured response spectrum of a particular motion, $H_{ij}(\omega)$ is the complex valued transfer function for the same motion and $S_\zeta(\omega)$ is the sea state spectrum.

The integral of the response spectrum is the response moment which is equivalent to the energy of the motion. The derivation of all spectral moments is elaborated in chapter A. In order to prevent confusion between the spectral moments for a displacement, velocity or acceleration (m_0, m_2, m_4), from now on the resulting measured and computed energy of the motion is respectively denoted by var_m and var_c.

Included Motions
During light ship condition aimed is to retrieve the sea state present. In order to retrieve the wave direction at least three different motions are needed from which at least two motions are asymmetric to each other (starboard, port side asymmetric). Heave and pitch are known as the most reliable responses in a sense that the transfer functions can be calculated with a good accuracy based on strip theory, panel method or experiment. So these motions are popular in the application of wave estimation. The validation study of the FD model confirms indeed that the transfer function of pitch motion is modeled accurately over the total frequency band. This motion is thus usable for the search to equivalence of energy. Unfortunately this can not be said immediately for heave due to its sensitivity of measuring point. The error in the heave transfer function is however constant over wave direction. Thus even though the difference in energy is larger than ideally, the resulting minimum point could still be similar and thus usable in the analysis. The transfer function for the response in vertical motion is relatively flat between the most interesting wave frequencies ($0.8 \geq \omega \leq 1.5$). Differentiate or filtering of narrow bounded energy distributions between different wave frequencies and directions is therefore difficult. The differences in energy are simply very small. However, the accelerations of the vertical motion vary more per wave direction and frequency. The energy of this motion is thus preferred.

Roll and sway motion measurements could be used as asymmetric motions. Most literature recommends to use sway instead of roll since roll motion is lowly damped and thus highly sensitive for resonance. Therefore three different sets of vessel motion responses have been tested:

1. the classical combination of roll, pitch and heave acceleration,
2. the alternative combination of sway, pitch and heave accelerations,
3. all measured motions that contain useful energy surge-sway-roll-pitch-heave acceleration.

Note these motion combinations have not explicitly been used during heavy lift operations for which initially is aimed to optimize predictions in predominantly roll motion.

Equivalence of Energy
From a physical point of view the equivalence of energy between the measured and estimated spectra is important. The least square problem is therefore not only solved for every individual motion but also for the difference between the sum of all measured and estimated spectra. The final least square problem is thus defined by

$$\min \chi^2 \equiv \min \| \sum_{i=1}^{5} \{\alpha_i \cdot \mathrm{var}_i\}_m - \sum_{i=1}^{5} \{\alpha_i \cdot \mathrm{var}_i\}_c \|^2 \tag{6.2}$$

where, i, represents the motion component and, α, is an factor that allows us to control the amount of energy of a particular motion component which should or should not be incorporated in the motion analysis. In this way the outcome can be controlled while the equivalence of energy is guaranteed.

Parametric Method
Literature indicates numerous possible techniques to estimate on-site directional wave spectra that contains energy from swell and wind waves or if desired even from three different wave profiles together. The most studied and tested techniques are the Bayesian and Parametric method. Methods by means of the Kalman filter have also been studied but this method is not yet well developed. Therefore in literature currently no satisfying results for the estimation of directional wave spectra have been reported [48]. Studied results of the Bayesian and Parametric methods are however promising.

The Bayesian technique is based on statistical inference. The key ingredients to a Bayesian analysis are the likelihood function, which reflects information about the parameters contained in the data, (such

as the spectrum parameters), and the prior distribution, which quantifies what is known about the parameters before observing the data. The prior distribution and likelihood can be combined to form the posterior distribution, which represents total knowledge about the parameters after the data have been observed. Summaries of this distribution can be used to isolate quantities of interest and ultimately to draw substantive conclusions. Since prior information about the parameters of interest can be implemented this method is proved to be fast but very sensitive for inaccuracies in the complex valued transfer functions. Furthermore, because of the fact that complex valued transfer functions have to be used, a numerical problem can occur. If the area under the real valued part of the transfer function is positive and the area of the complex valued part is equal but negative, the area will be zero. This will cause problems in solving the least square problem.

The counterpart of this method is the Parametric method which owes its name to the fact that the wave spectrum is parameterized. The most generic method for describing an directional wave spectrum for swell and wind waves is the by Tannuri et al. and Hogben and Cobb suggested 10-parameter bi-modal spectrum [23, 54]. The proposed model is defined by

$$\begin{aligned} S(\omega,\theta) =& \frac{1}{4}\sum_{i=1}^{2} \frac{\left(\frac{4\lambda_i+1}{4}\omega_{p,i}^4\right)^{\lambda_i}}{\Gamma(\lambda_i)} \frac{H_{s,i}^2}{\omega^{4\lambda_i+1}} A(s_i) \\ & \times \cos^{2s_i}\left(\frac{\theta-\theta_{\text{mean,i}}}{2}\right) \exp\left[-\frac{4\lambda_i+1}{4}\left(\frac{\omega_{p,i}^4}{\omega}\right)^4\right] \end{aligned} \tag{6.3}$$

where H_s being the significant wave height, λ is the shape parameter of the spectrum, $\theta_{\text{mean,i}}$ is the mean wave direction, ω_p is the angular peak frequency, s represents the spreading parameter, Γ denotes the gamma function and $A(s)$ is a constant introduced to normalize the area under the cos^{2s}, see appendix **??**. This wave spectrum considers basically a sea component ($i = 1$) and a swell component ($i = 2$), whereby it is possible, in theory, to model most ocean wave spectra.

The Parametric method is in contrast to the Bayesian method less prone to errors in the transfer function and zero valued response areas does not cause problems when solving the least square problem. The downside about the parametric method is however the number of parameters which determines the computational time. [27, 36, 37, 39, 52, 54]

Discretisation
The number of unknown parameters and domain wherein those parameters are searched can however be given in advance. The Matlab Tool is designed for on-line adjustments and includes multiple parametric wave spectra. Thus a discretized solution area for hydrodynamic coefficients and dominant wave parameters can straightforward be included in the least squares problem.

For the sensitivity in added mass and damping the decision is made that errors in the added mass and damping values are most likely in the order of magnitude of ±4%. Decided is not to correct for erroneous applied water depths, since both hydrodynamic coefficients as well as wave forces differ significantly by water depth. Thus the solution area for added mass and damping coefficients lies between the ”original” computed magnitude and this magnitude times a factor of 0.96 until 1.04 with a step size of 1%. The presence of swell, wind waves and the combined sea state parameters such as the 1-D spectral peak parameter and significant wave height is indicated in weather hind-casts. Thus with regard to the North Sea area one should select the Torsethaugen spectrum if swell is present. Otherwise a simple JONSWAP or PM-spectrum has to be selected. These are, of course, simplified wave spectra which in practice does not fit the sea state present exactly. It is however the most accurate method (besides the more generic formulation of Tannuri et al.) available without information from wave scanners, wave buoys or from satellites.

The minimization problem is thus established for a specific wave spectrum, in which only the significant wave height and period is varied. The sensitivity of the spectral peak parameter is small on vessel responses. The solution area of significant wave heights is taken as the hind-casted significant wave

height ±0.5m wave height with a step size of 0.1m. The solution area of the significant wave period is taken as the hind-casted significant wave period ±1.5 second with a step size of 0.1 sec. The spectrum is taken as uni-directional from which its mean direction, θ_{mean}, is varied between the present wave force directions in the hydrodynamic database. In conclusion, the best fitted combination between the wave spectrum and transfer function estimated by the Parametric method is found from the parameters

$$\{\underbrace{H_{m0},\ \omega_p}_{\text{wave spec}}, \underbrace{\theta_{mean},\ A_{ij},\ B_{ij}}_{\text{transfer func.}}\}$$

It should be noted that A_{ij} and B_{ij} is used herein to indicate that the added mass and damping coefficients multiplied by the multiplication factors and not the actual coefficient itself.

Solving Least Squares Problem
The most commonly used method for solving the least square problem and the Parametric method is a genetic optimization algorithm or a gradient search algorithm. The first method is potentially the fastest if a smart algorithm is made. The second method can be fast if the step size, search basin and margin of error is chosen carefully. It is however not straightforward to determine the absolute minimum or best fit solution since probably multiple solutions are optimal.

The algorithm of the developed tool is based on linear algebra and written in Matlab, which is very fast with such calculations. Therefore an different and more straightforward approach is developed for seeking the solution of the least squares problem. Chosen is to compute all possible combinations of the discretized solution area after which the optimal combination between all parameters is retrieved from the cell number of the matrix which contains all solutions of the least squares problem. The sequence of the calculation is known thus the combination of parameters is simply retrieved. If subsequently a finer resolution of certain parameters is sought, a two or thee steps rocket of this approach can be applied which ultimately will find a finer solution without significant additional computational time. Although the solution area to start with is already quit large with $\{17 \times 11 \times 31 \times 9 \times 9\}$ for variations between respectively $\{H_{m0}, \omega_p, \theta_{mean}, A_{ij}, B_{ij}\}$, the computational time of the proposed method is less than one minute (provided an available work space memory of at least 12GB). Making this a practical solution method of the least squares problem for on-line corrections. The operations within the developed tool are summarized in a flow chart given below.

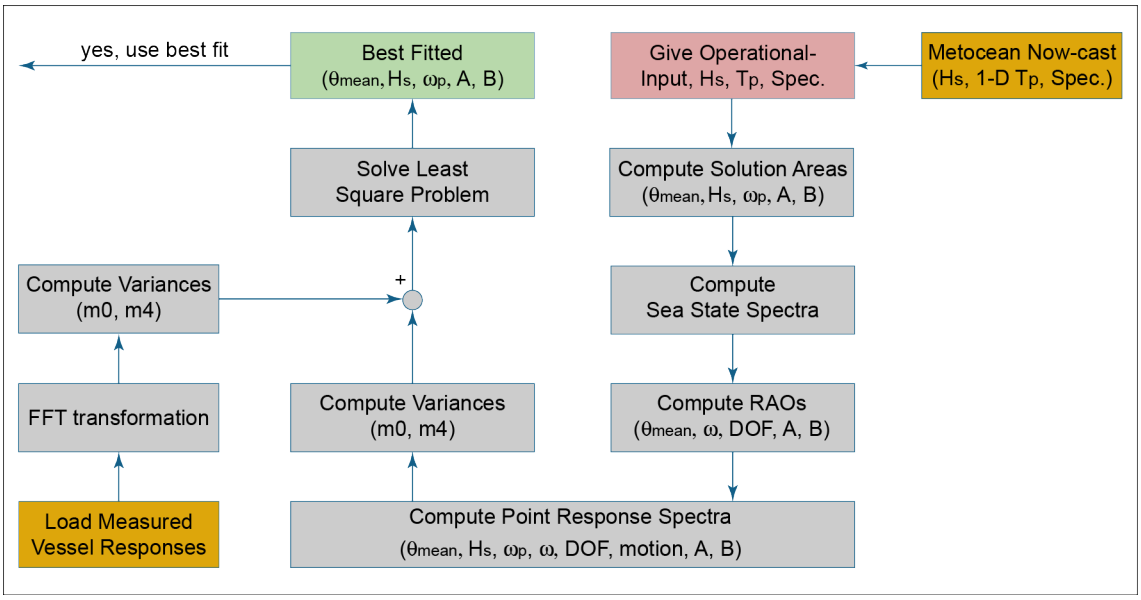

Figure 6.1: Flowchart of the operations of the correction algorithm within the Matlab Tool.

Numerical check
In order to check whether the method and algorithm for solving the least squares problem functions, a simple numeric check is performed. Response moments for an random operational condition and a

random sea state is computed with the tool. The individual energy of all ”measured” motions (motion combination 3) and their total energy is stored. Subsequently response moments for the exact same operational condition but now for multiple sea states within the solution area are being computed after which the correction algorithm solves the least squares problem. Searched is for the combination $\{(H_{m0} = 0.8), (\omega_p = 0.89), (\theta_{mean} = 33.75), (A_{ij} = 1.2), (B_{ij} = 1)\}$. The 10 best fits for the minimum difference between the ”measured” and computed total energy is given in the table below. The fitted or computed values of the variable parameters are here denoted by subscript c.

Table 6.1: Numerical check of the algorithm for solving the least squares problem

Fit	Wdirc	Hsc	Tpc	Ac	Bc	error	error %
1	33.75	0.80	7.00	1.02	0.96	0	0
2	33.75	0.80	7.00	1.02	0.97	0	0
3	33.75	0.80	7.00	1.02	0.98	0	0
4	33.75	0.80	7.00	1.02	0.99	0	0
5	33.75	0.80	7.00	1.02	1.00	0	0
6	33.75	0.80	7.00	1.02	1.01	0	0
7	33.75	0.80	7.00	1.02	1.02	0	0
8	33.75	0.80	7.00	1.02	1.03	0	0
9	33.75	0.80	7.00	1.02	1.04	0	0
10	33.75	0.80	7.00	1.03	0.96	1.67E-05	0.29

From this simple numerical test three things can be concluded. The first conclusion is that a variation of 8% in hydrodynamic damping does not make a difference in the total energy. The error in the total energy is for all combinations, not rounded, zero percent. Hydrodynamic damping variations of 8% are thus not helpful for making corrections and can therefore be left out in the search algorithm. The second and third conclusion is that the search algorithm functions appropriate but that indeed is searched in very small errors. Thus when is aimed to retrieve the present sea state it might be difficult if not impossible to filter between the best fitted results as shown here where the correct solution is fit number 5. To optimize predominantly vessel roll motion simply the best fit has to be apprehended.

6.2. Attempts with Orcaflex simulations

The next step is to retrieve information from motion amplitude time traces. In order to be certain about the applied wave spectrum and the operational condition a similar approach is apprehended as is done for the validation study. An specific operational condition is simulated in Orcaflex, time traces from vessel motions have been extracted, imported in the Matlab Tool, transferred to the frequency domain and analyzed with the correction algorithm. With this approach both the wave spectrum as well as the shortcomings of the transfer functions is known.

Wave Spectrum and Transformation

First, it is checked whether the applied Torsethaugen spectrum in Orcaflex matches with the applied Torsethaugen spectrum in Matlab. The importance of the applied transformation function and windowing technique for the retrieval of the wave spectrum from time traces became immediately clear. It is quite difficult to retrieve the exact wave spectrum from time traces via FFT. Even with an appropriate window shape and length and without data gabs and or measured noise which will be the case with real signals from inertial measurement units. The transfer function and window technique to be applied is thus dependent on the source, the length, the density and the nature of the signal. In this case the signal originates from Orcaflex time domain simulations. The time step was set at 0.1 seconds, the total simulation duration was 3600 seconds for ”stable” motions. Only the last 30 minutes is used for the analysis. Thus in total 18,000 data points where available. For sufficient resolution the window size, with parzen shape, was set on 2000 data points or 200 seconds, representing at least 5 times the length of response periods. Figure 6.2 illustrates the wave elevation time trace extracted from Orcaflex. Next to that figure the transformed spectrum, together with the in Matlab computed spectrum is illustrated. Although the total energy is not exactly equal to each other (due to FFT and duration signal), it can be seen that the applied spectra look very similar. From this is concluded that both the simulation period and applied FFT technique is sufficient for the intended purpose.

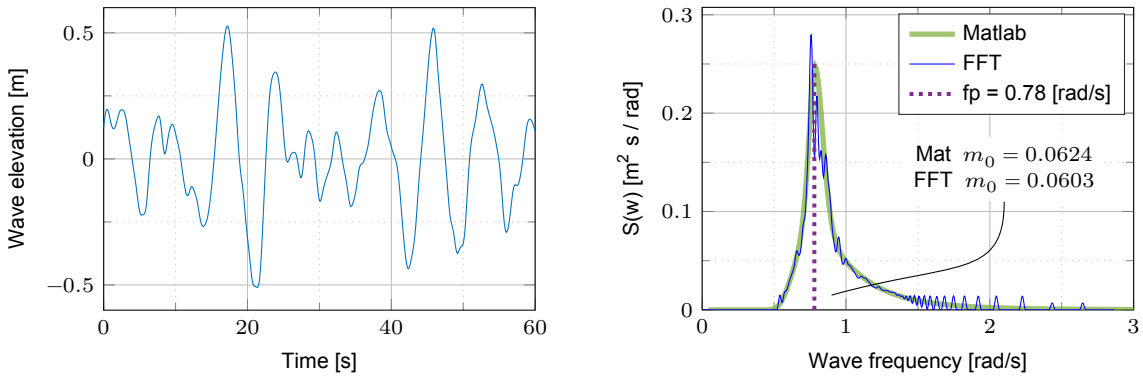

Figure 6.2: Inspection applied wave spectrum in Orcaflex and Matlab. Torsethaugen, Hs: 1.0m, Tp: 8.0 sec

6.2.1. Improve prediction of vessel roll motion

For making a more accurate prediction of the vessel response during heavy lift operations it is necessary to improve the prediction of roll motion. Equivalent to performed validation tests the studied case concerns a PS lift of 1217 ton suspended 16.7m in front of the bow. The load will be lowered thus the hoisting rope length changes from 50m to 60m. Vessel motions have been ”measured” during stern waves with $H_s = 1.2m$, $T_p = 6.3$ and while the hoisting rope length was 50m. In order to improve the prediction of predominantly roll motion different motion combinations have been tested. Due to motion coupling best results have been obtained if only roll and sway motion is included in the algorithm. The solution of the least square problem was given as $\{(H_s = 1.3m), (T_p = 6.5sec), (\theta_{mean} = 0), (A = 0.96)\}$. This causes a difference in total energy of 0.24%. Without corrections in the wave spectrum this was 9%. The shortcoming of the roll transfer function is thus corrected by applying a different energy spectrum whit an equivalent amount of energy.

Assuming a constant wave direction and a stationary Gaussian distributed energy until the next stage of the operation this correction can be apprehended. This indeed gives an improved prediction of roll response, see table 6.2. However due to strong motion coupling, pitch motion for example is approximated worse than before. This can only be prevented by including other motions as well. However this ensures that also a correction is made in wave direction which reflects the findings from the validation study. Note that due to the sensitivity of and the uncertainty in foretasted wave direction it can not be left out of the algorithm. Again this is a significant uncertainty without additional information.

From the persistence study on altering wave direction (elaborated in the next section) became clear that the probability of altering wave direction is significant during a period of 2 hours or more. Concluded is therefore that due to different errors in transfer functions for different wave directions the correction is not helpful for other wave directions and therefore unpractical. Potentially an algorithm can be made to include also model errors due to wave direction. However as indicated model errors are significantly smaller than errors in predicted wave parameters. Decided is therefore to stick with model errors and to study whether it is possible to retrieve the wave spectrum from vessel response time traces.

Table 6.2: Attempt to improve the prediction of vessel roll motion

		Orcaflex		Matlab		
WDir	Stage	roll [deg]	pitch [deg]	Correction	roll [deg]	pitch [deg]
0°	50m	0.673	0.885	no	0.537	0.912
				yes	0.631	1.059
	60m	0.728	0.892	no	0.538	0.920
				yes	0.638	1.072
33.75°	60m	1.036	0.941	no	0.838	1.007
				yes	0.974	1.187

6.2.2. Retrieve present sea state

In total nine different cases are tested in which is investigated how the method and algorithm performs during an heavy lift operation and during light ship conditions. Orcaflex response time traces are treated as the reality which is attempted to retrieve with spectral computations in Matab. The test cases are summarized in the table below. Most interesting results and conclusions of the attempts are summarized in the next paragraphs. Detailed results are given in appendix D.

Table 6.3: Cases for which the present wave spectrum is attempted to retrieve

Wave	Operational Condition	Wave Spectrum	Wdir [deg]	Hs [m]	Tp [sec]	A [-]	B [-]
A	Heavy Lift, PS, 1217ton	Torsethaugen	90.00	0.80	6.30	1.0	1.0
B	Heavy Lift, PS, 1217ton	Torsethaugen	0.00	1.20	6.30	1.0	1.0
C	Heavy Lift, PS, 1217ton	Torsethaugen	45.00	1.20	6.30	1.0	1.0
D	Heavy Lift, PS, 1217ton	Torsethaugen	33.75	1.20	6.30	1.0	1.0
E	Light Ship	Torsethaugen	0.00	0.90	9.00	1.0	1.0
F	Light Ship	Torsethaugen	0.00	1.00	8.00	1.0	1.0
G	Light Ship	Torsethaugen	0.00	0.70	10.0	1.0	1.0
H	Light Ship	Torsethaugen	33.75	1.50	6.80	1.0	1.0
I	Light Ship	Torsethaugen	45.00	1.00	6.50	1.0	1.0

Results Heavy Lift Operation

Taking into account the total time it may take to perform an heavy lift operation and the total time of which the sea state statistically seen might be stationary Gaussian distributed, it is interesting to test the usability of this correction method during the hoisting process. The average duration of a heavy lift operation is 12 to 24 hours from which the hoisting process takes roughly 4 hours if contingency is taken into account (see next chapter). It is thus not inconceivable that the sea state will shift during the operation. Note that variations in hydrodynamic added mass and damping are set to zero.

Despite the largest inaccuracy in RAOs for vessel roll motion and incoming beam waves, best results where observed for test case A with motion combination 1. Both the wave direction and significant wave height can in this operational condition be retrieved with high accuracy. The significant wave period is however estimated poorly. This is due to the inaccuracy of the roll transfer function. The accuracy of the retrieval of the wave frequency is strongly dependent on the distribution of the wave energy over wave frequency, which is determined by means of the RAOs. Small inaccuracies in the distribution lead to large errors in the estimated wave period. This can be seen in figure 6.3 where response spectra are given for motion combination 1 and test case A. The in Matlab computed distribution of wave energy over wave frequency does not correspond well enough with the measured distribution of energy. In table 6.4 the best fitted results are given.

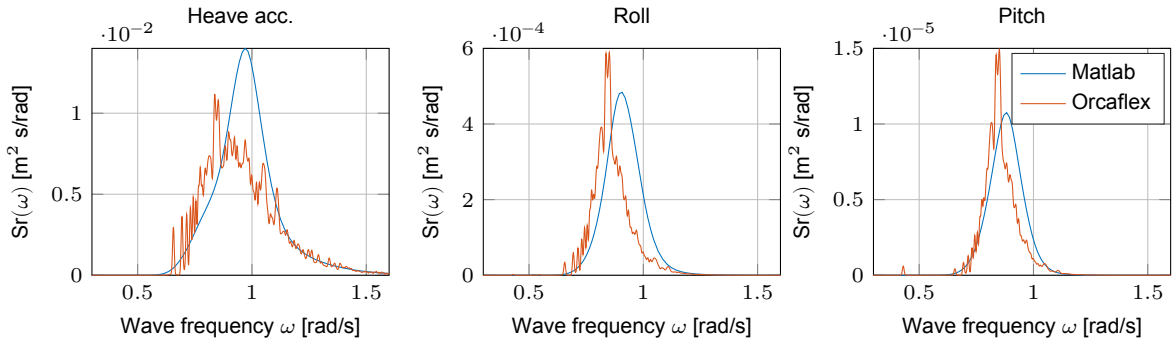

Figure 6.3: Case A: Response spectra from vessel motion time traces and the frequency domain analysis.

The accuracy of the retrieval of the wave direction is less sensitive for RAO inaccuracies but more sensitive for the included motion combination. In other words the distribution of the total energy over the different motions is important. It is found that dependent on the wave direction motion combination

1 and 3 yield the best results. For incoming beam and stern waves motion combination 1 is the best. For other wave directions motion combination 3 is the best. The direction of beam waves are retrieved with accuracy. The direction of stern waves as well but they might also hit the bow. Wave directions around quartering waves are however retrieved with significant lower accuracy. This is due to the strong motion coupling. The wave energy is simply more equally distributed over the vessel motions. Thus the difference in energy between the motions is also smaller with the result that the estimated wave direction can easily deviate a few steps or degrees. These steps are dependent on the included wave directions in the hydrodynamic database. In this case there are 17 wave directions included which is by default the maximum amount of 1 computation cycle in ANSYS AQWA. In other words, if the difference in energy between wave directions of 45 and 33.75 degrees is small, the algorithm fits wave directions between 56 and 22 degrees as well. If more wave directions are included in the hydrodynamic database this issue is addressed (see case D). It should be noted however that the ”exact” wave direction of case D was not found in the best 100 fits. This could be due to the fact that the vessel in Orcaflex was allowed to yaw with 3 degrees (mooring). Thus dependent on the accuracy of the hind-casted mean wave direction and mean vessel orientation during the 30 min measurement period, it might be possible to gain accuracy in the mean wave direction with this approach. However, a deviation of 5 degrees in mean wave direction already result in an error of 15% in the computed vessel motion response (dependent on the wave height).

The accuracy of the retrieved significant wave height is most dependent on the accuracy of the heave acceleration transfer function. Since the location of heave motion measurements is crucial, best results where observed if the motion sensor for heave accelerations is placed at Fpp or App. The transfer function for pitch motion is relatively accurate which makes the comparison between the measured and computed heave accelerations also more accurate. Slightly dependent on the wave direction it is possible to retrieve the significant wave height within an accuracy of 10%.

Table 6.4: Best fitted results for cases A, B and D during a heavy lift operation. Fit number zero is the combination of parameters which have been tried to retrieve. Given errors present the total difference between the measured and computed energy. Errors in percentage are with respect to the total measured energy.

	Fit	Wdirc	Hsc	Tpc	error	error %		Fit	Wdirc	Hsc	Tpc	error	error %
CASE A	0	90	0.8	6.3	0	0	CASE B	0	0	1.2	6.3	0	0
	1	90.00	0.80	6.00	9.79E-05	1.75		1	0.00	1.10	5.50	7.92E-06	0.46
	2	112.50	0.70	7.70	1.05E-04	1.88		2	180.00	1.10	7.20	1.18E-05	0.68
	3	168.75	1.60	6.50	1.06E-04	1.89		3	11.25	1.10	5.70	1.25E-05	0.73
	4	90.00	0.80	5.90	1.23E-04	2.20		4	22.50	1.10	7.00	1.47E-05	0.86
	Fit	Wdirc	Hsc	Tpc	error	error %		Fit	Wdirc	Hsc	Tpc	error	error %
CASE D	0	33.75	1.2	6.3	0	0	CASE D	0	33.75	1.2	6.3	0	0
	1	33.75	0.90	7.80	3.65E-05	1.03		1	35.25	1.30	4.9	1.70E-04	2.57
	2	0.00	1.10	4.80	3.99E-05	1.13		2	36.00	1.30	4.9	1.75E-04	2.65
	3	168.75	1.20	5.40	5.71E-05	1.62		3	37.00	1.30	5.0	1.75E-04	2.66
	4	33.75	1.20	5.60	6.75E-05	1.91		4	34.00	1.30	4.8	1.86E-04	2.82

Results Light Ship Condition

Due to the strong motion coupling between the vessel and the suspended load it is difficult to retrieve the present wave direction if waves come from an angle. The test cases have also illustrated that the significant wave period was estimated poorly. This is an major shortcoming, the sensitivity analysis has demonstrated that this parameter is the most important for accurate vessel response predictions. The Matlab Tool can switch to light ship conditions for which is known that the transfers functions have a higher accuracy with respect to the Orcaflex model.

The effect of a higher accuracy of the transfer functions is clearly reflected in the results of test cases. Moreover the absence of strong motion coupling between the vessel and suspended load makes the vessel to respond more quickly to a different wave direction. The vessel respond also at different wave frequencies with larger motion amplitudes. The amount of energy conserved in a certain vessel motion

is therefore measured more clearly from which the wave parameters can then be filtered more accurate. The difference in measured and computed response spectra for motion combination 1 and test case E is given in figure 6.4. From this can be seen that not all energy is captured or transformed via FFT. For this longer measurements are needed and a better tuned window length as discussed in chapter 2.2.1. More advanced techniques such as the wavelet transformation might therefore give more accurate results. Note that due to the shortcoming in the applied FFT the total error in total energy is therefore also larger during light ship conditions compared to the test cases during heavy lift operations.

The distribution of the energy over wave frequency is however more in line with the measured distribution of energy. Therefore, in some cases, both the significant wave height as well as the wave period are with high accuracy retrieved. With incoming stern waves all dominant wave parameters are retrieved with high accuracy. However for incoming quartering waves or close to this wave direction the fitted results are strongly dependent on the included motion combination. Overall best results where obtained with motion combination 2, but for incoming quartering waves combination 3 gave best results. This is consistent with findings of the heavy lift cases. Thus all measured motions should be included in the analyses if there is motion coupling present.

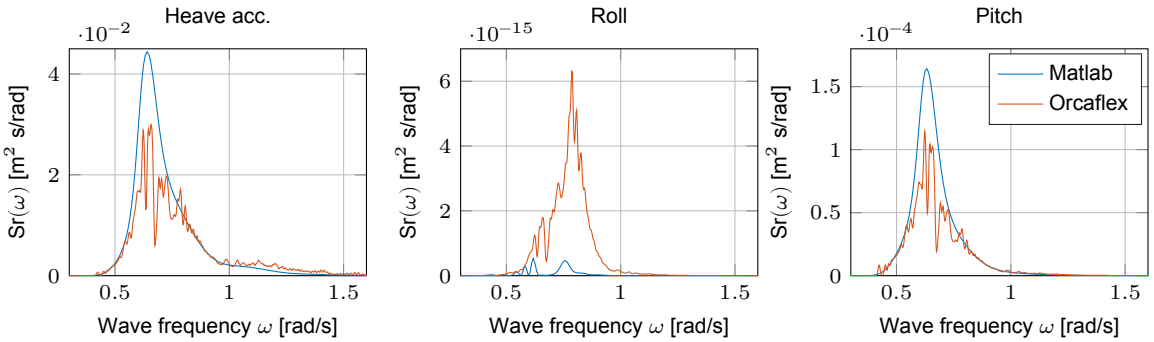

Figure 6.4: Case E: Response spectra from vessel motion time traces and the frequency domain analysis. Note the difference in scale.

The correct combination of the wave parameters for case E and F is included in the top 4 best fits but never placed first. This could be due to the fact that during light ship conditions practically no motion coupling is present. Only the hoisting cranes provide some extra coupling. Thus with pure stern waves there should be almost no roll motion. However in time domain analysis, as well as in realty, the vessel will always rotate somewhat, causing it to roll slightly more than is computed in statics. This can be seen in the figure below and in table 6.5. Although the difference in roll energy is fairly small, it is corrected with a smaller significant wave height. It is therefore not straightforward to filter the ”exact” combination out of the ”best” fits. Furthermore should be remembered that in reality wave spreading is present. Thus in reality the energy will be distributed more evenly over the vessel motions.

Table 6.5: Best fitted results for cases E, F, H and I during light ship conditions.

	Fit	Wdirc	Hsc	Tpc	error	error %		Fit	Wdirc	Hsc	Tpc	error	error %
CASE E	0	0	0.9	9	0	0	CASE F	0	0.0	1.0	8.0	0	0
	1	0	0.90	9.2	4.00E-04	1.55		1	0.0	1.0	8.1	8.91E-04	3.79
	2	0	0.90	9.1	5.79E-04	2.24		2	0.0	1.0	8.0	1.03E-03	4.41
	3	0	0.90	9.3	8.53E-04	3.30		3	0.0	1.0	8.2	1.17E-03	4.99
	4	0	0.90	9.0	1.12E-03	4.33		4	0.0	1.0	7.9	1.47E-03	6.28
	Fit	Wdirc	Hsc	Tpc	error	error %		Fit	Wdirc	Hsc	Tpc	error	error %
CASE H	0	33.75	1.5	6.8	0	0	CASE I	0	45	1.0	6.5	0	0
	1	135.00	1.40	6.50	1.31E-05	0.46		1	45.00	0.80	7.90	5.17E-04	1.54
	2	45.00	1.40	6.50	1.37E-05	0.48		2	45.00	1.30	5.10	7.68E-04	2.29
	3	33.75	1.30	7.60	1.83E-05	0.65		3	67.50	1.10	5.90	7.77E-04	2.32
	4	146.25	1.30	7.60	1.87E-05	0.66		4	45.00	0.80	8.00	9.06E-04	2.70

6.3. Conclusion & Discussion

The validation study has shown that the error in computed vessel responses is largest during heavy lift simulations. Predominantly errors or rather differences in the roll amplitude have been observed. Furthermore became clear that the error in computed roll response, roughly taken, constant is over wave frequency and different crane angles but not over wave direction and not for a different mass of the suspended load. Aimed is therefore to optimize predominantly roll motion with the aid of fitting different wave spectra and added mass and damping coefficients such that a more accurate distribution of energy is found for more accurate predictions of roll motion. It is found that indeed predictions for a single vessel motion can be improved if the method is performed for specific roll and sway motion. However due to strong motion coupling other motions are predicted worse than before. Making this correction with regard to the workability not immediately and improvement at all.

Potentially seen this method could be performed parallel for all vessel motions. As long as the equivalence of energy remains guaranteed than basically every single vessel motion is corrected. Model errors, hydrodynamic coefficient errors etc. and wave parameter errors are then all included in the correction of basically the best fitting magnitude of energy per vessel motion. However this correction will hold cumbersome due to the probability of altering wave direction for which different model errors have been found. Due to this it is not even possible to prove that such an algorithm might work with numerical tests. In practice this remains to be seen since probably more model input errors will be made. Decided is therefore to stick with (small!) model errors and to study whether it is possible to retrieve the wave spectrum from vessel response time traces. After all this remains the biggest uncertainty.

Concluded is that the correction method and algorithm for the retrieval of wave spectrum parameters functions appropriate, however the accuracy of the results is highly dependent on the items summarized by importance below:

- Operational condition,
- Accuracy response transfer functions,
- Included motion measurements,
- Motion signal and its transformation to the spectral domain,

It was already indicated in the studied literature but from the performed test cases it became once more clear that it is evident that the results of this correction method are highly sensitive to the accuracy of the transfer functions. The first two indicated matters are therefore closely related to each other since the method works best during light ship conditions for which the most accurate response transfer functions can be calculated. During this operational condition and incoming stern or beam waves the wave parameters for which was sought where retrieved with high accuracy ($\epsilon \leq 5\%$). Even though there is a noticeable difference between the amount of captured and computed energy, the accuracy of which the energy is distributed over the wave frequencies ensures that even the exact combination of mean wave direction, significant wave height and significant wave period was included in the best 4 fits. However, these promising results are based on Orcaflex simulations. It is therefore interesting to test this method under these operational conditions with real measurement data.

Wave parameters are however with significant lower accuracy retrieved if waves hit from or with angles close to starboard quartering direction. This is due to the motion coupling which ensures that the energy is distributed more evenly over the different vessel motions. With this vessel orientation the method works best if all measured motions are being included in the analysis. With incoming stern or beam waves motion combination 1 performs best (see page 66). This dependence can be incorporated readily into the developed correction algorithm by setting an solution area for the mean wave direction as well. The best combination can then readily be linked to certain wave direction areas.

Motion coupling is especially present during heavy lift operations, even with incoming stern or beam waves without wave spreading. The resulting substantially smaller energy differences between the vessel motions subsequently makes it more difficult to filter between the parameter values given in the discretized solution area. Therefore least accuracy with the method is achieved if the analysis is performed during the lift operation itself. During this condition the mean wave direction and significant

wave height can be retrieved within an accuracy of ±10-15%. The significant wave period, the foremost wave parameter, is estimated even worse with an accuracy of ±20-30%. Unfortunately this is not sufficient regarding the required accuracy in vessel motion response predictions, but also considering the fact that this analysis is based on Orcaflex simulations with full control about the operational condition and thus also about simplifications such as the exclusion of wave spreading or two different mean wave directions for swell and wind waves, which in reality will result in even larger differences. Thus based on these test cases, this correction method and this linearized model for ship motions during heavy lift operations, it is unlikely that more accuracy in the wave spectrum parameters can be gained by making use of response measurements during the lift operation alone.

Taking into account the equivalence of energy the biggest risk of this correction method is the adopted wave spectrum at the beginning of the analysis. If the wave spectrum model is chosen erroneous or if one of the available wave spectrum models does not fit the present sea state at all, the method will fit erroneous wave spectra as well. The biggest shortcoming in for example the Torsethaugen spectrum is the assumption made that both the wind waves as well as the swell originate from one single mean direction. In other words, the total energy is concentrated in a single direction which with respect to the amplitude of a single movement would be the most conservative way to compute ship responses during light ship conditions. During heavy lift operations where strong motion coupling is involved this can not be said immediately. The shortcoming of different wave directions can theoretically seen be complemented with a more advanced description of a combined spectrum such as the discussed wave spectrum model given by equation 6.3. The proposed solution method of the least squares problem is then, however, not practical anymore since the allowance of directional wave spectra would introduce at least two more dimensions for which point response spectra have to be calculated. Unless the amount of wave spreading angles is chosen sparsely, solution methods such as a genetic optimization algorithm or a gradient search algorithm are probably more suitable with respect to computational speed.

Then, at last, a small discussion about the chosen correction method and the discussed results of the test cases. The chosen wave buoy analogy is very sensitive for the accuracy of the response transfer functions and moreover motion coupling. Therefore only test case results from Orcaflex simulations of light ship conditions are encouraging enough for possible further development of the ”correction method”. For highest accuracy vessel response signals have to be measured and processed during this operational condition. The corrected wave spectrum could than subsequently be used for a new motion analyses with another operational condition such as the hoisting stage of the heavy lift operation. After all practically seen there is not corrected for model errors during light ship conditions.

The duration of an average heavy lift operation is however substantially longer than the theoretically substantiated duration of a stationary Gaussian distributed sea state. Furthermore the minimum duration of the measurement period itself is already 30 min in order to capture an useful picture of the conserved wave energy via FFT. With more advanced techniques such as the wavelet transformation this period might be shortened, but the available time left for making reliable predictions remains small. Sea states are always Gaussian distributed, the distribution should however be stationary as well in order to be able to apply linear theory and statistical methods [24, 29]. Thus without making assumptions on the maximum duration of these statistics, the time window for which an prediction can be made with data from the past remains similar as today’s standard. In other words the profit that can be achieved through the corrected sea state parameters is only valid during the period in which the sea state is stationary distributed. And even then there is uncertainty about the maximum duration of this distribution. It might also be only 20 min for example. This method should therefore only be applied for short time predictions for which no different sea states are forecasted. Stated that the dynamics can be approximated linearly, the operational condition and vessel orientation may then alter. Without changes in dynamics there is no need for a deterministic model of ship motions at all.

Taking into account these pros and cons it might therefore be interesting to reverse the problem or to combine techniques. As mentioned in the introduction it is nowadays also possible to measure the present sea state which subsequently can be transformed to a wave spectrum. Either with the aid of a wave buoy or wave scanner, the accuracy at which this can be done is useful. Thus if the present wave spectrum is known with sufficient accuracy one might be able to validate the simulation model

for ship motions. Both the wave spectrum as well as the present ship motions are measured and computed. The acquired information can than be analyzed in the office from which can be learned and possibly more accurate transfer functions or even on-line correction algorithms can be developed. The sensitivity of model input parameters and hydrodynamic parameters as discusses in chapter 5 can than also be analyzed with actual data. Errors due to uncertainty in the present sea state do not automatically override these model errors any more. [55, 59]

7

Workability & Persistence Study

The determination of the workability is not only dependent on the operational condition and the sea state present. The duration of the operation itself also determines whether the operation can be conducted or not. In order to include this criterion in the analysis the persistence of workability windows is studied. First the lift case is described where after the persistence of workable windows for different operational stages is described. The results of the analysis are discussed and given in the last section.

7.1. Lift Case

The case concerns the installation of a substation with a mass of 1200 ton. The platform has to be lifted on top of a jacket with a free surface height of 18 m. The lift has to be conducted at port side with an outreach of 12 m for adequate clearance. The substation serves as a transformer station for the energy generated at the Fécamp offshore wind farm. The farm consists of 83 wind turbines with a diameter of 151 m and a rated power of 6,000 kW. The total nominal power of the farm is 489,000 kW. The geolocation of the site is given in the figure below.

Figure 7.1: Geolocation and water depth profile of Fécamp offshore wind farm [15, 35]

Operational Stages and its duration

The installation of the substation is devided in nine different operations, similarly as has been done in equivalent studies [17]. The duration of each operation is based on internal documents. Each operation is considered to progress from a condition of security to another condition of security. Contingency planning is required by the rules of regulations so that, in the event that an operation cannot be completed in the time and manner intended, an alternative condition of security can be achieved. Foreseeable emergencies such as a mooring failure, fire or personnel accidents can than be recovered within the calculated workable window [13, 57]. For this study an additional operational time of 50% is taken for contingency planning. The transit duration of 5 hours is based on an average speed of 3 kts. Internal

documents show that at least 4 hours is required for the deployment of anchors and that fastening of the rigging takes 2 hours. Disconnecting can be done faster with 1 hour. The time required for hoisting the load is dependent on the maximum pay-in rate. The rate is set on 0.08 m/min, making it possible to hoist the substation in about 3 hours to 20 meters above still water level. The substation installation is determined by the maximum pay-out rate of 0.08 m/min and the minimum clearance of 1.5 m. The different operational stages and its duration are given in table 7.1. The operations are subdivided into 4 stages which is based on the applicable operational criteria. At stage 2 the hoisting rope length is 70 m. To determine the most critical moment at stage 3 the analysis is run for 50 and 60 m hoisting rope.

Table 7.1: Operational stages and its duration. The contingency planning is denoted by Con.

	Operation	Duration	Con	Total	Stage	Total
1	Transit to Fecamp	5.0	50% of the duration	7.5	1	13.5
2	Anchoring at location	4.0		6.0		
3	Connecting rigging	2.0		3.0	2	4.5
4	Ballasting	1.0		1.5		
5	Hoisting	3.0		4.5		
6	Installation	0.2		0.3	3	6.3
7	Disconnet rigging	1.0		1.5		
8	Retrieve anchors	4.0		6.0	4	13.5
9	Transit to harbour	5.0		7.5		
	Total	25.2 hrs	12.6 hrs	37.8 hrs		

Limiting Criteria

In order to ensure safety during a heavy lift operation the rules of regulation prescribe operational limitations such as the maximum allowable significant wave height or the maximum dynamic slack load in the hoisting ropes [13, 57]. The crane vessel it self has also operational limitations due to for example the maximum crane capacity and certain vessel motions for convenience working conditions. In this study the following limiting criteria are taken into account:

- Dynamic Amplification Factor: DAF $\leq$ 1.15 [-]
- Side-lead and In-line angle: $\leq$ 2 deg
- Vessel roll and pitch angle: $\leq$ 2-3 deg

The DAF determines the maximum dynamic load which may be exerted on the hoisting ropes. Factor 1.15 is prescribed for hook loads between 1000-2500 ton. For single hook lifts DAF is expressed as:

$$\text{DAF} = \frac{F_{\text{static}} + F_{\text{dynamic}}}{F_{\text{static}}} \tag{7.1}$$

where the static force is determined by the object weight and the dynamic force by the axial crane rope stiffness (stretching) and the object mass [57]. The maximum side-lead and in-line angles are determined by the maximum crane capacity. The maximum vessel roll and pitch angle between 2 and 3 degrees is specified by the vessel operator in order to ensure convenience working conditions, but also to prevent dangerous moments with slinging objects. In conclusion the applied limiting criteria per operational stage is summarized in the table below.

Table 7.2: Applied limiting criteria per operational stage

Stage	DAF [-]	Side Lead [deg]	In-line [deg]	Roll [deg]	Pitch [deg]	Duration
1	-	-	-	3.0	3.0	13.5 hrs
2	1.15	2.0	2.0	2.0	2.0	4.50 hrs
3	1.15	2.0	2.0	2.0	2.0	6.50 hrs
4	-	-	-	3.0	3.0	13.5 hrs

7.1.1. Workability calculation

Based on the limiting criteria the workability is computed for all operational stages. The dynamic amplification factor and the side-lead and in-line angles are most often the limiting factors during an heavy lift operation. The DAF, side-lead and in-line angles are computed from respectively the vertical and lateral displacements of the vessel crane tip and suspended load. The relation between these motions are given in chapter 3.2.2 by equations 3.12. For convenience the equation of side lead angle is given below

$$\tan(\beta) = \frac{\eta_8 - \delta_2}{l_s} = \frac{1}{l_s}(\eta_8 - y_o - y_{ct}\psi + z_{ct}\phi) \tag{7.2}$$

The transfer function of the effective horizontal displacement ($\eta_8 - \delta_2$) can thus easily be determined by

$$\mathsf{H}_\beta(\omega) = \mathbb{C}\left\{\mathsf{H}_{\eta_8}(\omega) - \mathsf{H}_{y_o}(\omega) - \mathsf{H}_\psi(\omega)y_{ct} + \mathsf{H}_\theta(\omega)z_{ct}\right\} \tag{7.3}$$

where complex valued transfer functions are used such that the phase angles between the motions are incorporated. The most probable maximum side lead angle which should remain under the criteria of 2 degrees can then be determined by

$$\beta = \tan^{-1}\left(\frac{\mathsf{MPM}\left\{\int |\mathsf{H}_\beta(\omega)|^2 S_\zeta(\omega)d\omega\right\}}{l_s}\right) \leqslant 2\,\mathrm{deg} \tag{7.4}$$

in which $S_\zeta(\omega)$ is the wave spectrum and l_s the outstretched crane rope length. In a similar way the in-line angle and vertical displacement for the DAF can be determined. Alpha factors for uncertainty in the environmental condition are not incorporated in the workability analysis. The most probable maximum vessel and supended load motion response is based on three hourly statistics. [41]

7.2. Persistence

The data used for the persistence study on sea states and workable time windows is based on 14 years of hourly modeled surface wind and waves between the year 2000 and 2014. For the persistence of workable windows and occurring sea states only data between March and the end of September (7 months) is used since this is roughly the workable season. Fifteen years of sea state data is given for wind waves and swell separately. However 14 years included data for the combined sea state such as the significant wave height and the 1-D spectral peak period (2006 excluded). For the persistence analysis of workable windows and occurring sea states the combined sea states are used. Thus the persistence analysis is based on 51408 unique hourly sea states.

The combined sea state data is used from which its spectrum is computed on the basis of a Torsethaugen spectrum as explained in chapter A.3.2. This provides a more realistic image on workability since the energy in the low frequency part of the wave spectrum contributes significantly in vessel motion response. It should be noted however that 633 of the 51408 sea states where outside the validity of the spectrum due to the absence of swell. These sea states had significant wave heights below 0.5 m and significant wave periods below 3 sec which is outside the applicable domain of the Torsethaugen spectrum. Sea states with these characteristics are however not exceeding the limiting criteria, regardless of the applied wave spectrum nor wave direction. Thus these scenarios are included in the analysis without any adjustment in the applied wave spectrum model.

The data is provided by the Danish Meteorological Institute (DMI) and consists of rerun data (2000-2004) and operational data (2005-2014). Rerun data is based on the most recent (2014) DMI-WAM set-up. Operational data is based on model status at that particular time. The DMI operational wave forecasting service DMI-WAM uses the 3rd generation spectral wave model WAMCycle4.5 which solves the spectral wave equation. It calculates the wave energy as a function of position, time, wave period and direction. 'Real' wave parameters are calculated as suitable integrals of the wave energy spectrum. The energy source is the surface wind. The sink terms are wave energy dissipation through wave breaking (white capping), wave breaking in shallows, and friction against the sea bed. Depth-induced

wave breaking is only considered in model domains of high spatial resolution, which is the case for the North Sea area. The wave energy is redistributed spatially by wave propagation and depth refraction, and spectrally by non-linear wave-wave interaction. Interaction with sea current and effects due to varying sea level caused by tides or storms are not incorporated in the DMI-WAM set up. [26]

The time series are produced from model fields using nearest model grid point with respect to the site location. The site location is 49° 53' 31.2" North and 0° 13' 37.2" East, decimal degrees: 49.892 North 0.227 East. The relative distance between the nearest model grid point and the site location is between 4.3 and 7.3 km. At this location between this distances the bathymetry, which strongly determines the development of the waves, does not change much. The difference in water depth is less than ±3 m which is illustrated in figure 7.1 [15]. These model grid points are thus close enough for the persistence analysis of workable windows. The sea state data of the workable season contained only one data gab of two hours. The missing values are taken as their predecessor. The data is not interpolated for even greater density. The calculated persistence of workability windows, so the final outcome, is however linear interpolated for half hourly information.

7.2.1. Compute Persistence

Since we are interested in workable windows and not in extreme scenarios we develop a measure of the time during which H_s and or T_p remains below a specific threshold. We define the persistence T as the period during which a particular characteristic H (in terms of either H_s or T_p for example) of the wave field continuously remains below a threshold value H_c. We further define run length, L, which reflects the total amount of time during an extended period (for example the workable season) over which a) the wave field parameter H remains below the threshold H_c and b) the persistence T exceeds a threshold T_c. The run length L is than given by:

$$L\left(H < H_c, T > T_c\right) = \sum_{i=1}^{n} T(i) \tag{7.5}$$

Thus in contrast to extreme value analysis where one is interested in the exceedance of an threshold, here the persistence measures how long the wave field remains below the height threshold, whereas run length is a measure of the total time during which the wave field stays over a certain persistence threshold. Finally, dividing run length L by the total persistence T (thus T_c is set to zero) provides F, the percentage of which reamins below of run length, for a given H_c. Physically, F gives the probability of waves that remain below a given height H_c for different persistence T_c (in hours). [18]

For convenience, an example of this method is given in the figure below for an run length $L(H < 1.25$ m$, T > 20$ hours$)$. The wave height threshold of 1.25 m is in this example not exceeded for 9 periods denoted as T(1,2..9), the total duration of which is 275 hours. Five of these periods persist for longer than the threshold T_c of 20 hours $(T1, T6, T7, T8, T9)$. Thus the run length $L(H < 1.25$ m$, T > 20$ hours$) = \sum_{i=1,6,7,8,9} T(i) = 247$ hours.

The percentage of which remains below of run length is then calculated as $F(H < 1.25, T > 20) = \sum_{i=1,6,7,8,9} T(i) / \sum_{i=1}^{9} T(i) = 247/275 = 89.8\%$. This tells us that if the wave height threshold of 1.25 m is not exceeded the wave field will not exceed the threshold for 20 hours or more, for 89.8% of the time (275 hours).

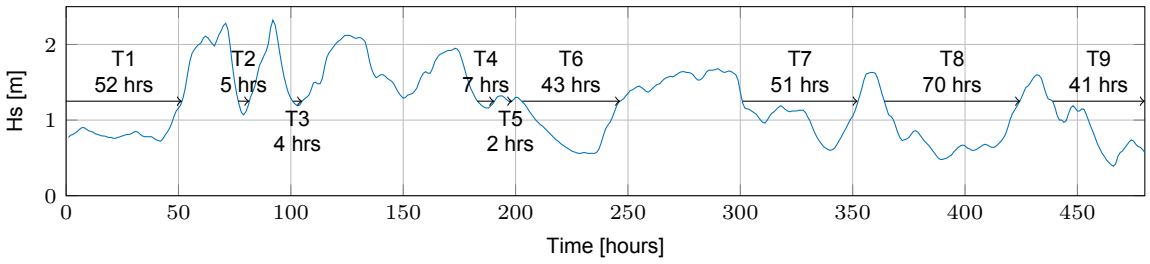

Figure 7.2: Time series of significant wave height in a 480-hour observation period. T represents periods during which the wave height does not exceed the significant wave height threshold of 1.25 m.

7.2.2. Sea State Persistence

The persistence analysis of significant wave height and significant wave period thresholds is run for the complete data set. The result of this analysis for persistence durations of 1 until 24 hours is given in figure 7.3. The color bar indicates the percentage of which the duration of threshold combinations persist. The probability of occurrence of the different sea states is also computed and given in the scatter diagram of significant wave height and period combinations given in figure E.1 which can be found in appendix E at page 175.

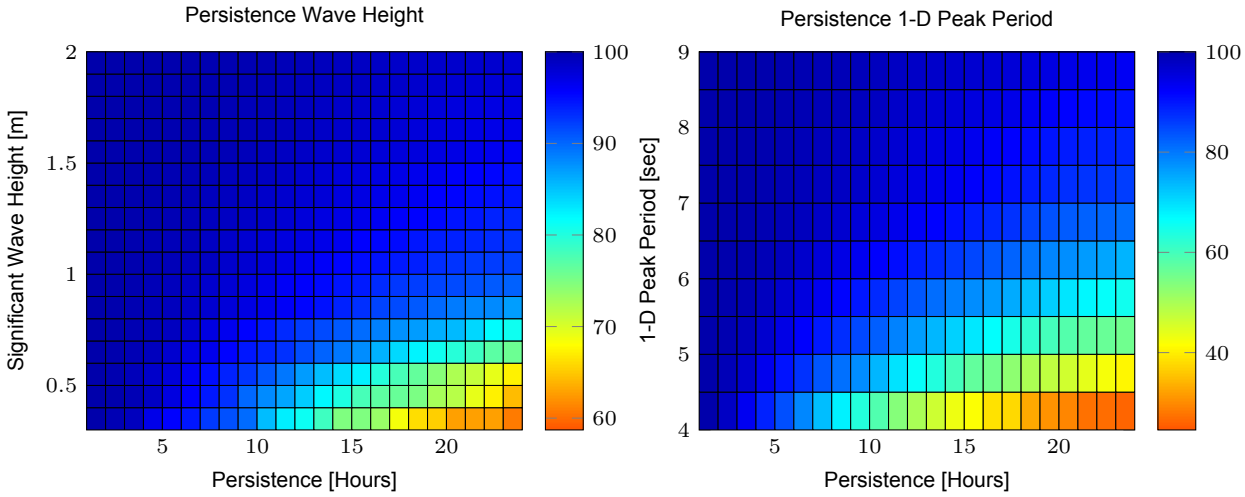

Figure 7.3: Distribution of the average of F, the percentage of which remains below of workable season run length against wave height thresholds (0.4-2.0m) or wave period thresholds (4-9s) and persistence thresholds (0-24 hrs).

7.2.3. Workability Persistence

The persistence analysis on workability windows can be made on basis of the probability of occurrence and the persistence of sea state duration. In order to do this the workability of the operational stage has to be calculated for a predefined step size of significant wave height and significant wave period. Where after on basis of the workability criteria the maximum H_s and T_p combination can be determined. The maximum allowable sea state combinations can than subsequently be used to filter the historical data on workable windows and its duration. This is the standard approach and the fasted with respect to computational time. However the predefined step size omits the actual sea states present in the historical data such that ultimately a coarser distributed image of the workability is obtained. It is therefore more accurate to compute the workability per operational condition for every sea state present in the data. Where after the persistence analysis can be run on workability and its duration.

The advantage of vessel response computations in the frequency domain is that these type of analysis can be made relatively easy and quick. The spectral analysis is thus run fur the full set of sea state data. By making use of the developed tool the computational time required is only roughly 15 minutes on an average computer, per operational stage. Potentially seen one could thus also run this statistical analysis on board of the vessel, a couple of days before the next site job. This could be useful if one is uncertain about the required workability window and its persistence during that specific period. The probability of occurrence of a certain operational duration can than easily be determined with largest accuracy. Specific operational conditions can be given and the analysis can be made for the specific period.

As discussed the workability analysis is based on five criteria. If one of the criteria thresholds is exceeded the operation can not be performed safely. Thus if the operation is conducted up to and including the absolute limit of the criteria, it is too late to stop the operation safely. Thus in order to support the decision maker, most often the captain of a vessel, before this situation arises, the analysis is done for 80% of the limit. The result for the most limiting operational stage is given in figure 7.4. The next section elaborates more on the most limiting stage.

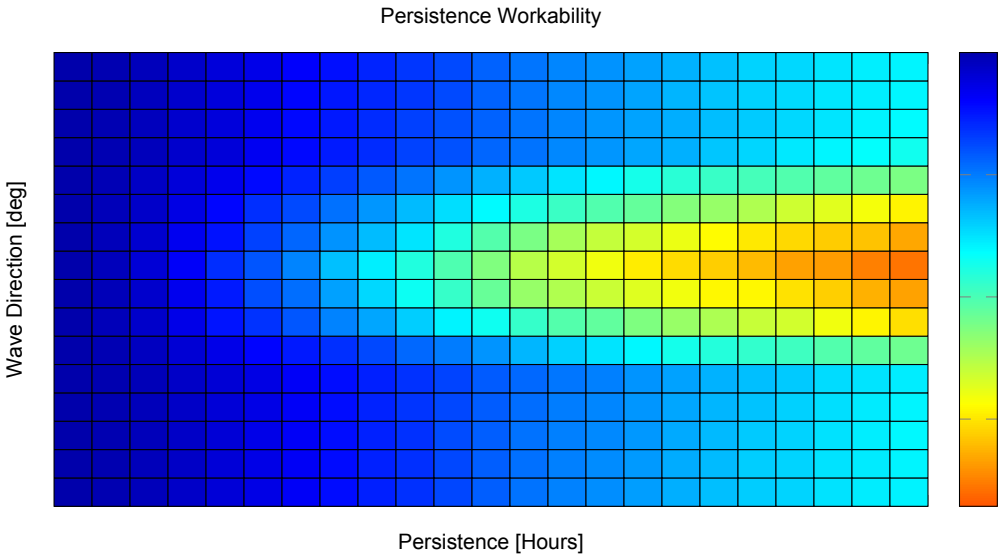

Figure 7.4: Distribution of the average of F, the percentage of which remains below of workable season run length against workability per wave direction (0-180 deg) and persistence thresholds (0-24 hrs). The figure illustrates windows for 80% of the workability limit for a PS lift of 1200 ton with outreach 12 m and a hoisting rope length of 50 m.

As can be seen in figures 7.4 and 7.5 the workability is strongly dependent on the wave direction. During operational stage 2 and 3, after the anchors have been located, the vessel orientation can not be changed any more. The total duration of these periods together is 11 hours. Making it likely that the wave direction can alter during hoisting. In order to determine the probability of altering wave directions, the data is also analyzed by persistence of wave direction altering. The result is given in figure 7.5. In this figure is also given the workability plot for the most limiting stage and most probable wave periods at the Fécamp offshore wind farm. In appendix E.3 an extended version of the persistence of altering wave direction is given.

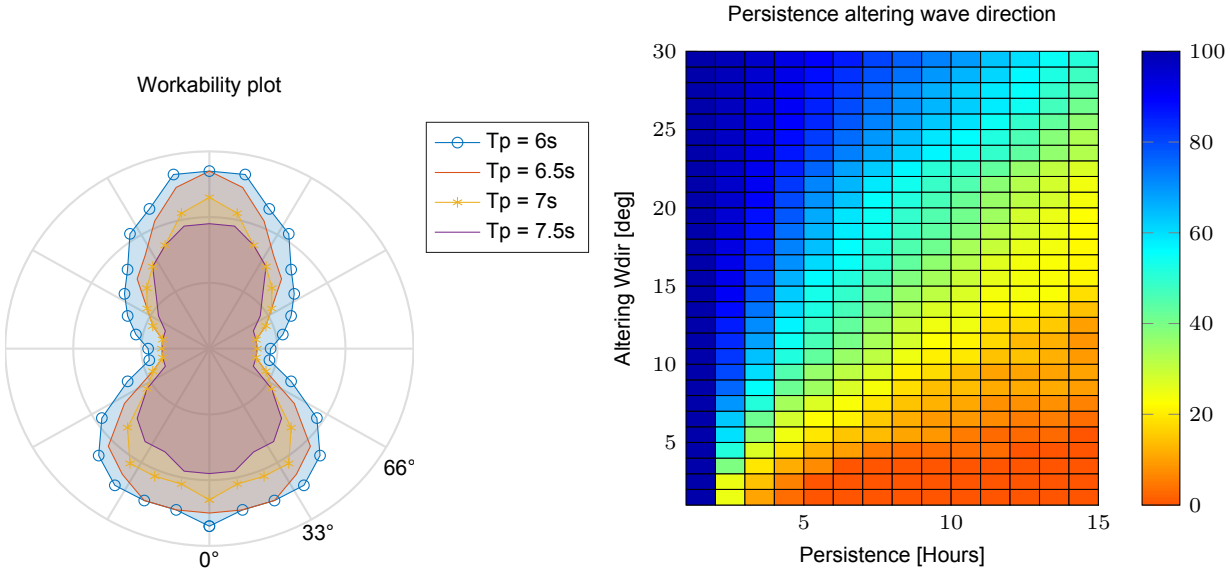

Figure 7.5: Left figure: Workability plot for different sea states, same operational condition as used for figure 7.4. Right figure: Distribution of the average of F, the percentage of which remains below during the workable season run length against wave direction thresholds (1-30 deg) and persistence thresholds (0-15 hrs).

7.3. Persistency based workability

The workability per operational stage is calculated taking into account the duration of each step and that the preceding steps have been performed. Furthermore, the influence of altering wave direction during stage 2 and 3 is taken into account. Such that insight is created into the probability at which the calculated workability for a certain mean wave direction and operational duration can occur.

The workability is calculated as the product of the probability of occurrence of an workable window and the probability of the persistence of the required window duration. The probability at which the computed workability can occur is subsequently determined according to the probability at which the mean wave direction can alter during that required window duration. The operation is planned to be conducted with a vessel orientation of 56.25 degrees with respect to the incoming waves. For this study an altering wave direction of 20 degrees is maintained.

The workability of the total operation is calculated as the product of the workability of all stages. For stage 3 only the most limiting condition is apprehended. This is when the suspended load is hoisted at its highest point. The short pendulum length ensures that the vessel response in the most prevalent wave frequencies appears. Together with the strict operational criteria during heavy lift operations makes this the most critical stage of the operation. The difference in the probability of occurrence of workable windows between the different hoisting rope lengths is substantially. It is therefore useful to perform the workability analyzes per lift stage. The difference in the persistence of workable windows according to the desired operational duration is however modest between a hoisting rope length of 60 m and 50 m. The total workability taking into account the duration of each of these steps is thus almost similar. Therefore only the most limiting condition is apprehended for stage 3. From an operational duration of 5 hours or more it can however be beneficial to subdivide the hoisting stage in multiple stages (hoisting rope lengths).

The persistence of an altering wave direction during stage 2 and 3 is substantially. The total workability can therefore vary between a minimum of X% until a maximum of X% of the workable season between March and the end of September. The probability of occurrence of these scenarios is 35.7%. The probability at which an scenario in between these scenarios arises is then less than 35.7%. It is worth mentioning that there has been no situation in which the wave direction has not altered with 20 degrees or less for the total duration of 37.8 hours. The persistence of altering wave directions should therefore be incorporated in workability studies for a realistic picture of the total workability.

In conclusion, from this analysis it is possible to study the influence of variation of the criteria or the duration of a single step. Workability based on persistency analysis can therefore be seen as the most accurate and reliable approach for calculating the workability of a heavy lift operation. In the table below results of the analysis are given for the 80% workability limit.

Table 7.3: Results persistency based workability analysis wherein the possibility of altering wave directions is taken into account. On the left the probability of occurrence of the required workability window is given for different wave directions and operational stages. On the right the workability is given per operational stage and the possible scenarios with respect to the altering wave direction.

Probability of occurrence						Workability		
		Wave Direction [deg]				Scenarios with altering Wave Direction		
Stage	Condition	33.75	56.25	78.75	90	min (78.75°)	mid (56.25°)	max (33.75°)
1-4	Light Ship	X	X	X	X	X%	X%	X%
2	Ls = 70m	X	X	X	X	X%	X%	X%
3	Ls = 60m	X	X	X	X	X%	X%	X%
	Ls = 50m	X	X	X	X	X%	X	X%
					Total Workability	X%	X%	X%
					Prob.	X%	<X%	X%

8

Conclusions & Recommendations

8.1. Conclusions

The main objective of this research was to examine the possibilities of on-line vessel response measurements in order to be able to make a more accurate prediction of the vessel response and decision making operation. This study specifically refers to possible methods and techniques for making an improved prediction of the vessel response during a single crane conducted heavy lift operation up to 72 hours in the future for sea states corresponding up to medium weather conditions at the North Sea. With regard to this research scope therefore four sub-questions have been examined, namely:

- What kind of model is required for making a more accurate prediction of the vessel response, given on-line vessel response measurements, a certain time window in the future and loading condition to be expected?
- What is the total system error and where do those errors come from?
- Is it possible to correct the total system error by making adjustments or corrections to a certain system parameter without knowing the exact origin of the total system error?
- How can measurements from the past help to improve predictions of the vessel response, in other words how does the correction quality deteriorate over time?

There are numerous methods and techniques available that are able to predict a certain phenomenon based on the time signal of that phenomenon if it can be described by a stochastic harmonic process. Assumed that wave induced forces are sinusoidal in nature and that vessel responses are predominantly wave induced, allows to describe vessel responses by a stochastic harmonic process. Thus multiple methods and techniques can be applied within the time window of interest for making a more accurate prediction of the vessel response and decision making operation. Numerical methods such as Minor Component Analyzes or Autoregressive Methods are able to predict the vessel response without a ship specific deterministic model for ship responses. However these algorithms can only predict vessel responses with sufficient accuracy for time windows of up to one or two minutes and moreover for systems without changing dynamics. The operational condition, thus the loading as a result of the present sea state and from the heavy lift operation itself is in fact highly variable. Therefore, it has been concluded that a ship specific deterministic model for ship responses during a heavy lift operation is required.

The most critical phase of the heavy lift operation is the stage wherein the load is suspended highest above still water level. Dependent on the maximum hoist speed, hoisting height and taking into account contingency planning the time required to achieve this stage is roughly 4 hours. However minutes before the hoisting process is the moment of no return and thus the moment at which the decision maker would like to have the most accurate information about the capability of the vessel for the most critical stage. The capability of the vessel is determined by the significant response at a certain sea state. The significant amplitude of the vessel response is defined as the average of the highest on third of the responses. Thus in order to determine the significant response of the vessel from response measurements at least a measurement period of 20 min is required. However by making use of vessel

response measurements from the past, regardless of the correction method, the validity of this information reaches to the duration for which the sea state is stationary Gaussian distributed. In other words the measured motion signals represent the vessel motions as long as the process that is causing this motion is ergodic. Despite the importance there is little to be found in the literature on studies that have investigated the stationarity of sea states. However most studies have found that for sea states within the linear wave approximation, the vast majority of the records were stationary between 20-160 min.

Numerical algorithms such as artificial Neural Networks or Fuzzy logic are potentially seen two interesting methods. These algorithms are able to form a logic between the input and the output of a system such as a ship specific deterministic model for ship motions. However these algorithms require a large amount of training data and a type of control that determines which input and output parameters are of importance. At the beginning of the research this was entirely unclear and moreover due to changing dynamics during the lift operation it would be necessary to update the core of the algorithm and to start collecting suitable training data again. Therefore concluded is that at this stage of the research the well known wave buoy analogy the most suitable method is for studying possible system errors and therefore also possible improvements for making a more accurate prediction of the vessel response and decision making operation. The actions of this response-based correction method are illustrated in the flow chart given below.

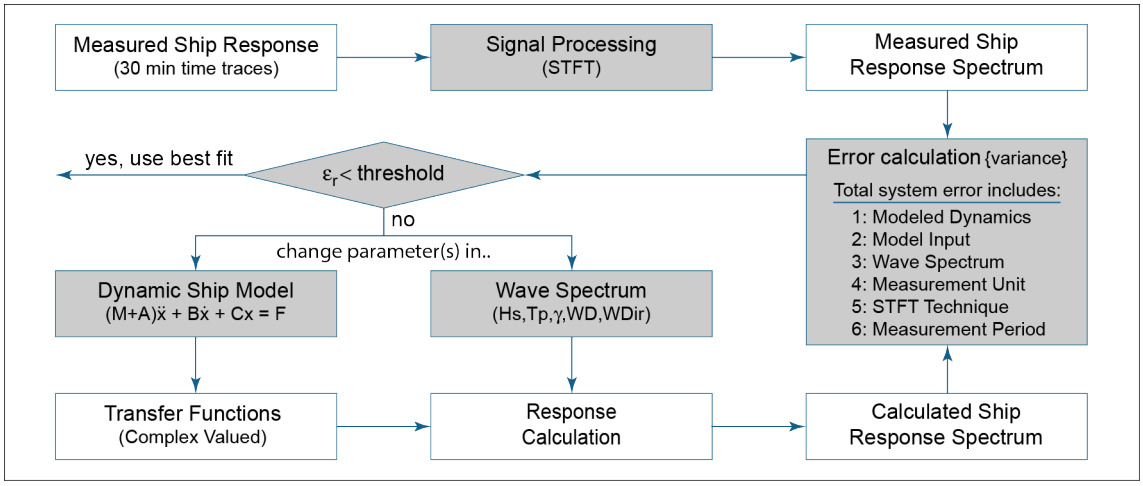

Figure 8.1: Flow chart Correction Methodology by means of the Wave Buoy Analogy.

By making use of a deterministic model, vessel response measurements and the wave buoy analogy both the transfer function for the vessel response at a certain sea state, as well as the sea state itself can be studied and analyzed on potential errors. By analyzing and comparing the measured and calculated vessel responses in frequency domain the total system error for calculating the vessel response can be determined. The variance of the measured response signal and computed response spectrum is the most relevant ”characteristic” of the vessel response. In contrast to the amplitude, the variance of the sum is the sum of the variance whereby the physical quantity ”energy” of the vessel response can be linked to the variance. This means that a link can be made between statistics and physical properties of the measured vessel response. The correction method is therefore founded on the concept of the equivalence of energy.

In the calculation process for ship responses multiple errors can be made in virtually all steps of the process illustrated in figure 8.1. The exact quantity of each error and even which errors have been made during this analysis will however never be known exactly. For the implementation of corrections, it is however not of importance to know where the exact errors are coming from and what there exact quantity is. Under the assumption of stationary Gaussian distributed waves or energy the total system error can be corrected by either an correction in the transfer function or the quantity of energy. However, in order to be able to extrapolate this correction to different operational conditions, thus for different transfer functions, it is required that the calculated errors can be approximated linearly. Therefore without agreements on potential risks it is impossible to translate the total system error in for

example forecasted sea state data for making improved predictions of the vessel response for longer time windows than roughly 3 hours. From literature is concluded that the variance of forecasted sea states have a clear seasonal variation. The mean error (bias) also shows some evidence for an annual cycle. However whereas RMS error increases with increasing forecast period, there is no such consistent change of bias with forecast period. It is dependent on available data and the weather forecast model. Thus statistically seen the correction method may hold up to roughly 3 hours from which its bias is dependent on the possible total system error.

With regard to linearity it is required that the dynamics of vessel responses during heavy lift operations can be approximated linearly. In literature is found that the vessel response during a heavy lift operation might not behave linearly due to for example viscous roll damping, non-linear hydrostatic force and the possibility of large motions. However the rules of regulations prescribe small allowable motions, equivalent ≤2 degrees for the side-lead angle. Thus large motions do not occur with regard to the capability of the vessel in which the decision maker is interest in. Furthermore is found that due to shape of the vessel hull of the Rambiz 3000, strong non-linear behavior due to viscous roll damping does not apply. For on-line motion analyzes it is therefore sufficient to include the linearized equivalent viscous roll damping. Possible, the amplitude of roll motion might be underestimated. However the natural roll frequency of the vessel will not change significantly. Furthermore in studies is shown that slowly varying, low-frequency horizontal motions induced by non-linear second-order forces in wave groups generally did not affect the hook load response, and thus appear to be of no crucial influence on crane ship operations. However, in literature is found that the non-linear effect of hydrostatic force can have significant influence on vessel response calculations. Concluded is therefore that it might be sufficient to approximate the fully coupled vessel response linearly in 9-DOF and to study the validity of the developed model.

The validity of the model in FD is testes by means of an equivalent model in Orcaflex and to simulate the dynamics of a heavy lift operation in TD. Although Orcaflex is not able to account for the waterplane area (nonlinear hydrostatic) effects in a nonlinear fashion, it is in contrast to the frequency domain model, able to capture the moment arm effects during a simulation. Furthermore it is possible to simulate larger motions and thus to study the full dynamics of heavy lift operations. Although differences in vessel roll amplitudes have been observed between simulations in FD and TD, and vessel responses are underestimated with 10% due to the absence of the rotational movements of the suspended load, concluded is that within the applicable domain of heavy lift operations, vessel responses can be approximated linearly with satisfying results.

Strictly taken it is not necessary to know the origin nor the quantity of the error. However in order to make practical corrections it is helpful to know what kind of errors and their order of magnitude can be expected during on-line motion analyzes. Therefore the sensitivity of the model-input, hydrodynamic coefficients and wave parameters have been tested. It is evident that model input parameters such as the mass and the height of the suspended load are given precisely for accurate motion analyzes. However even combinations of small erroneous applied model-input parameters cause a small error of ±5-12% in computed vessel responses. Errors in hydrodynamic coefficients can cause noticeable errors in computed vessel motion responses. Especially if the diffraction analysis is based on an incorrect water depth. However, errors in the applied wave spectrum always veto. Concluded is therefore that if no major errors have been made in the model input parameters and diffraction analysis, largest improvement in computed vessel motion responses can be achieved if more certainty is gained in the present sea state.

Assumed that calculated vessel responses with Orcaflex are correct, predominantly errors in calculated roll amplitudes have been observed. Therefore attempted was to improve the FD ”model error” and the uncertainty in the present wave spectrum predominantly for roll motion. This was done by solving the least square problem for the equivalence of energy for specifically roll and sway motion. It is found that a specific vessel motion can be improved by applying the correction method. However due to strong motion coupling other vessel motions where approximated worse than before. This can only be prevented by including other motions as well. However by doing that the resulting improvement is marginally and moreover not consistent over wave direction and for different operational conditions

for which different errors have been observed during the validation tests. From the persistence study on altering wave direction became clear that the probability of altering wave direction is significant during a period of 2 hours or more. The mean wave direction is thus likely to alter during the heavy lift operation. Based on numerical tests therefore is concluded to stick with these small ”model errors” and to study whether it is possible to retrieve the wave spectrum and its direction with respect to the vessel orientation. The potential gain is relatively large and moreover useful for other operational conditions. After all there is not corrected for model errors.

Based on these results the final correction method has got its shape and is illustrated in figure 8.2. The least square problem of the equivalence of energy can be solved with several techniques for different vessel motion combinations. With regard to the developed Matlab Tool decided is to apply the Parametric method for varying parameters $\{H_s, T_p, \theta_{mean}\}$ and to solve the least squares problem for the entire solution area with the aid of a practical algorithm. For computational speed and realistic solutions the solution area is automatically discretized on the basis of metocean now-cast information. The solution of the least squares problem is by definition the wave spectrum that corresponds best to the applied transfer functions and measured energy. The equivalence of energy remains guaranteed.

Concluded is that the accuracy of this correction method highly sensitive is to the accuracy of the transfer functions. The accuracy of the retrieval of the significant wave height is predominately dependent on the amplitude of the transfer functions. The significant height can therefore be retrieved with an accuracy of 5% during heavy lift and light ship conditions. The significant wave height is the most important parameter for making accurate predictions of the vessel response. The accuracy of the retrieval of the significant wave period is highly dependent on the accuracy of the distribution of the energy by means of the transfer functions. Thus if the calculated natural frequencies of the system do not correspond well enough with reality, the wave period is retrieved poorly. The accuracy of the retrieval of the significant wave period is therefore very low during heavy lift operations. During light ship conditions the accuracy is within 0.3 sec for most cases. For the retrieval of the wave direction it is required to include at least two asymmetrical vessel responses. The accuracy of the retrieval is predominantly dependent on the direction of the incoming waves and the presence of motion coupling. It is therefore found that largest accuracy is obtained if all vessel motions are included in the algorithm. With strong motion coupling the energy is distributed more evenly over wave direction. Making this method during heavy lift operations less accurate as well.

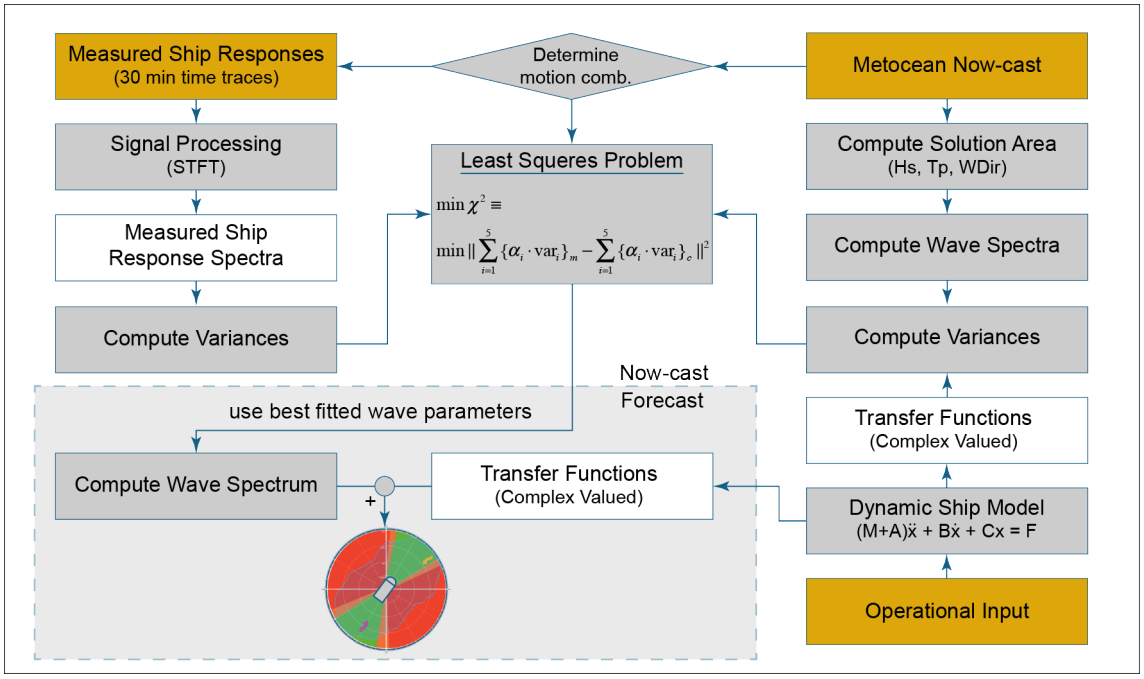

Figure 8.2: Final flow chart Correction Method by means of the Wave Buoy Analogy.

Final Conclusion
Can motion measurements during an offshore heavy lift operation on-line help to make a more accurate prediction of the vessel response and decision making operation? Yes motion measurements can help to make a more accurate prediction of the vessel response, but not immediately for the decision making operation. The quality of the correction is dependent on:

- The time window of interest → up until the duration for which the sea state is stationary Gaussian distributed. Thus statistically seen up to approximately 20 min to 160 min. Due to the amount of possible errors and the possibility of altering sea states it is unknown how large the deterioration of the correction is within this time window. The correction is invalid outside this time window.
- The operational condition → low probability of improvement during heavy lift operations, larger probability of improvement during light ship conditions.
- Start condition → the bias of the improvement is dependent on the accuracy of the metocean now-cast, the applied model-input parameters and hydrodynamic coefficients.

8.2. Recommendations

For accurate on-line motion analysis it is evident that model-input parameters such as the mass and the height of the suspended load are given precisely. It is also important that the hydrodynamic database contains enough variety in for example different water depths and vessel drafts. However based on the results of the validation study and sensitivity analysis I recommend to accept potential model errors since those are very small for realistic errors and moreover since those can alter for different motion analysis. This means that if this error still is considered in the correction algorithm the measured operational condition can be predicted with largest accuracy but that this correction does not hold for different operational conditions. Due to small potential model-input errors I do not recommend to study different methods and techniques such as artificial neural networks for making a more accurate prediction of the vessel response. For systems with changing dynamics a deterministic model and the wave buoy analogy are more suitable. With regard to the Mocean Capability Tool, if necessary and upgrade of the hydrodynamic database of the Mocean Capability Tool can potentially seen already cover model errors which is much more straightforward. However I do recommend to study the possebilites of these methods for ultra short time predictions of any stochastic process. This could for example be very helpful in the final stage of the installation of a sub-platform. The moment at which extreme stability is required is tens of seconds ahead. From literature is found that the described numerical methods are able to make this kind of predictions.

With the aid of the present measurement unit and the Mocean Capability Tool I recommend to validate the output of the tool for increasing the confidence in this DST. This is the biggest improvement that can be achieved. Furthermore I recommend to log uncomfortable and dangerous events and to link those to the operational condition. Such that these unwanted situations are more readily recognized and more over can be prevented during equivalent operations in the future, such that the operation is performed more efficient and safely.

Then finally, by making use of information from metocean now-casts there will always be uncertainty about the present sea state whose effects can be significant. Therefore I recommend to further develop the proposed method for seeking the present sea state during light ship conditions. Recommendations further development are summarized below.

Further Development

- With regard to double crane lifts and the developed simulation model I recommend to extend the degrees of freedom to 10 for yaw motion of the suspended load. It have been found that vessel responses during double crane lifts can be approximated almost like a single crane lift conducted at mid ship. Simply adding yaw stiffness was not sufficient however the result was almost similar to Orcaflex simulations.
- Test results of the correction method are based on uni-directional bi-modal Torsethaugen spectra. Largest shortcoming of this spectrum is the assumption that swell and wind waves originate from the same mean direction. Unfortunately this is often not the case. I recommend to implement

the most generic model for describing an directional wave spectrum for swell and wind waves as suggested by Tannuri et al. and Hogben and Cobb (see page 67). Taking into account the extra parameters I expect the solution area to become much bigger. With regard to computational speed I recommend to optimize the developed solution algorithm by separating the calculation of heave acceleration from the calculation of the displacements. This will decrease the required workspace memory significantly.

- I recommend to incorporate a two or even three step rocket of the developed method for faster convergence and a finer resolution.
- Taking into account the equivalence of energy the biggest risk of this correction method is the adopted wave spectrum and the applied model-input parameters at the beginning of the analysis. If model-input parameters have been set completely wrong the method will still find a solution of the least squares problem. Furthermore if the wave spectrum model is chosen erroneous or if one of the available wave spectrum models does not fit the present sea state at all, the method will fit erroneous wave spectra as well. I recommend to study potential fault detection systems for erroneous applied model-input parameters. See for example [38]. Fitting erroneous wave spectra could potentially seen be avoided by setting a narrower bounded solution area. Especially for the wave direction which will also improve the computational speed. In order to detect still erroneous fitted wave spectra I recommend the develop an lower boundary for the least squares problem.
- I recommend to study the possibilities of Wavelet transformations in order to be able to reduce the required measurement period of roughly 30 min. With regard to the required time for capturing the significant response of the vessel gains can be achieved.

Modelling in Orcaflex

- During the validation study was found that the Rambiz 3000 during heavy lift operations extremely sensitive is for yaw rotations. Especially with single crane conducted operations where strong motion coupling is present. In order to maintain appropriate vessel orientation therefore a stiff mooring system was required. The required stiffness causes resonance in long time simulations, regardless of the applied spectrum or period for sinusoidal waves. Especially mooring systems with pretension causes trouble. More important however, it was found that it was influencing the first order motions as well. For equivalent motion analyzes of heavy lift simulations I recommend to study possible ways for adding damping or even better to include some sort of propulsion force aka DP system.
- During the validation study was found that the way I modeled heavy lift operations, thus the crane barge with separate crane booms and suspended load, produces potential problems for the correction in the moment arm effect of hydrostatic force. I recommend to inform about this feature and to study its effect more closely.
- Although differences in vessel roll amplitudes have been observed between simulations in FD and TD, the final difference in calculated vessel responses for normal wave spectra such as the Torsethaugen spectrum is relatively small. Dependent on the wave direction and the vessel response the difference in vessel roll motion was only 5-10% and even less for other vessel motions. I understand that the latest version of Orcaflex capable is of simulating similar dynamics in FD as well. Therefore, dependent on the desired output of heavy lift simulations, I recommend to run more motion analyzes in FD for quick reviews.

Bibliography

[1] ANSYS AQWA. *Aqwa Theory Manual*. ANSYS, Inc., release 15.0 edition, November 2013.

[2] E Barlow, D Tezcaner Ozturk, AH Day, E Boulougouris, M Revie, and K Akartunali. A support tool for assessing the risks of heavy lift vessel logistics in the installation of offshore wind farms. *Marine Heavy Transport & Lift IV*, 2014.

[3] Euan Barlow, Diclehan Tezcaner Ötzturk, Matthew Revie, Evangelos Boulougouris, Alexander H. Day, and Kerem Akartunali. Exploring the impact of innovative developments to the installation process for an offshore wind farm. *Ocean Engineering*, 109:623 – 634, 2015. ISSN 0029-8018. doi: http://dx.doi.org/10.1016/j.oceaneng.2015.09.047.

[4] Elzbieta M Bitner-Gregersen and Alessandro Toffoli. Uncertainties of wind sea and swell prediction from the torsethaugen spectrum. In *ASME 2009 28th International Conference on Ocean, Offshore and Arctic Engineering*, pages 851 – 858. American Society of Mechanical Engineers, 2009.

[5] Elzbieta M. Bitner-Gregersen, Kevin C. Ewans, and Michael C. Johnson. Some uncertainties associated with wind and wave description and their importance for engineering applications. *Ocean Engineering*, 86:11 – 25, 2014. ISSN 0029-8018. doi: http://dx.doi.org/10.1016/j.oceaneng.2014.05.002.

[6] Elzbieta M. Bitner-Gregersen and Ã¸istein Hagen. Uncertainties in data for the offshore environment. *Structural Safety*, 7(1):11 – 34, 1990. ISSN 0167-4730. doi: http://dx.doi.org/10.1016/0167-4730(90)90010-M.

[7] E Bouws, H Günther, W Rosenthal, and CL Vincent. Similarity of the wind wave spectrum in finite depth water: 1. spectral form. *Journal of Geophysical Research: Oceans*, 90(C1):975–986, 1985.

[8] John S Carson. Model verification and validation. In *Simulation Conference, 2002. Proceedings of the Winter*, volume 1, pages 52 – 58. IEEE, 2002.

[9] Ju-Hwan Cha, Myung-Il Roh, and Kyu-Yeul Lee. Dynamic response simulation of a heavy cargo suspended by a floating crane based on multibody system dynamics. *Ocean Engineering*, 37(14–15):1273 – 1291, 2010. ISSN 0029-8018. doi: http://dx.doi.org/10.1016/j.oceaneng.2010.06.008. URL http://www.sciencedirect.com/science/article/pii/S0029801810001423.

[10] Subrata Chakrabarti. Empirical calculation of roll damping for ships and barges. *Ocean Engineering*, 28(7):915 – 932, 2001.

[11] Young Myung Choi, Young Jun Yang, and Sun Hong Kwon. Validity of ocean wave spectrum using rayleigh probability density function. *International Journal of Ocean System Engineering*, 2 (4):250 – 258, 2012.

[12] GF Clauss, M Vannahme, et al. An experimental study of the nonlinear dynamics of floating cranes. In *The Ninth International Offshore and Polar Engineering Conference*, pages 511 – 518. International Society of Offshore and Polar Engineers, June 1999.

[13] GL Noble Denton. Guidelines for marine lifting and lowering operations. Technical Report 0027/ND, GL Noble Denton, June 2013.

[14] GL Noble Denton. General guidelines for marine projects. Technical Report 0001/ND, GL Noble Denton, December 2015.

[15] EMODnet. Portal for bathymetry, bathymetry viewing and download service. URL http://portal.emodnet-bathymetry.eu/mean-depth-full-coverage.

[16] Odd Faltinsen. *Sea loads on ships and offshore structures*, volume 1. Cambridge university press, 1993.

[17] Henk Feikens, Roel Verwey, Jorrit-Jan Serraris, and René Huijsmans. 'wet handshake': Workability study of an offshore thruster exchange operation. In *ASME 2011 30th International Conference on Ocean, Offshore and Arctic Engineering*, pages 609 – 616. American Society of Mechanical Engineers, 2011.

[18] Xiangbo Feng, MN Tsimplis, GD Quartly, and MJ Yelland. Wave height analysis from 10 years of observations in the norwegian sea. *Continental Shelf Research*, 72:47 – 56, 2014.

[19] WAFO Group et al. Wafo - a matlab toolbox for analysis of random waves and loads: A tutorial. *Mathematical Statistics*, 2015.

[20] WAFO Group et al. Matlab toolbox for analysis of random waves and loads, version 26, 2016.

[21] Andrew H., Ariola M., and Giorgio C. The european offshore wind industry - key trends and statistics 2015, 2016. URL http://www.ewea.org/fileadmin/files/library/publications/statistics/EWEA-European-Offshore-Statistics-2015.pdf. Accessed: 15-03-2016.

[22] Seung-Ho Ham, Myung-Il Roh, Hyewon Lee, and Sol Ha. Multibody dynamic analysis of a heavy load suspended by a floating crane with constraint-based wire rope. *Ocean Engineering*, 109:145 – 160, 2015. ISSN 0029-8018. doi: http://dx.doi.org/10.1016/j.oceaneng.2015.08.050. URL http://www.sciencedirect.com/science/article/pii/S0029801815004485.

[23] N Hogben, FC Cobb, et al. Parametric modelling of directional wave spectra. In *Offshore Technology Conference*. Offshore Technology Conference, 1986.

[24] Leo H Holthuijsen. *Waves in oceanic and coastal waters*. Cambridge University Press, 2010.

[25] J.S. Hopkins. The accuracy of wind and wave forecasts. Offshore Standard OTH 483, Health and Safety Executive - Offshore Technology Report, 1997.

[26] Danish Meteorological Institute. Dmi-wam wave model, December 2016. URL http://ocean.dmi.dk/models/wam.uk.php. Accessed: 23-11-2016.

[27] Toshio Iseki and Kohei Ohtsu. Bayesian estimation of directional wave spectra based on ship motions. *Control Engineering Practice*, 8(2):215 – 219, 2000. ISSN 0967-0661. doi: http://dx.doi.org/10.1016/S0967-0661(99)00156-2.

[28] J.A.Pinkster. The effect of air cushions under floating offshore structures. In J.H.Vugts, editor, *International Conference on the Behaviour of Offshore Structures BOSS '97*, number 1087-P, July 1997.

[29] W.W. Massie J.M.J. Journée and R.H.M.Huijsmans. *Offshore Hydromechanics*. Delft University of Technology, third edition edition, 2015.

[30] Mark J. Kaiser and Brian F. Snyder. Modeling offshore wind installation costs on the u.s. outer continental shelf. *Renewable Energy*, 50:676 – 691, 2013. ISSN 0960-1481. doi: http://dx.doi.org/10.1016/j.renene.2012.07.042.

[31] A Khan, K Marion, and C Bil. The prediction of ship motions and attitudes using artificial neural networks. *Asor Bulletin*, 26(1):2, 2007.

[32] Harald E Krogstad, Stephen F Barstow, et al. Directional distributions in ocean wave spectra. In *The Ninth International Offshore and Polar Engineering Conference*. International Society of Offshore and Polar Engineers, 1999.

[33] Kyu-Yeul Lee, Ju-Hwan Cha, and Kwang-Phil Park. Dynamic response of a floating crane in waves by considering the nonlinear effect of hydrostatic force. *Ship Technology Research*, 57(1): 64 – 73, 2010. doi: 10.1179/str.2010.57.1.006.

[34] Michael S Longuet-Higgins. On the statistical distributions of sea waves. *J. mar. Res.*, 11(3): 245–265, 1952.

[35] Google Maps. Map of fécamp offshore wind farm, 2016. URL https://www.google.com/maps/place/49°53'31.2%22N+0°13'37.2%22E/@49.892,0.2248113,17z/data=!3m1!4b1!4m5!3m4!1s0x0:0x0!8m2!3d49.892!4d0.227. Accessed: 21-12-16.

[36] Najmeh Montazeri, Ulrik Dam Nielsen, and Jörgen Juncher Jensen. Estimation of wind sea and swell using shipboard measurements - a refined parametric modelling approach. *Applied Ocean Research*, 54:73 – 86, 2016. ISSN 0141-1187. doi: http://dx.doi.org/10.1016/j.apor.2015.11.004.

[37] Ulrik D. Nielsen and David C. Stredulinsky. Sea state estimation from an advancing ship - a comparative study using sea trial data. *Applied Ocean Research*, 34:33 – 44, 2012. ISSN 0141-1187. doi: http://dx.doi.org/10.1016/j.apor.2011.11.001.

[38] Ulrik D Nielsen, Zoran Lajic, and Jørgen J Jensen. Towards fault-tolerant decision support systems for ship operator guidance. *Reliability Engineering & System Safety*, 104:1 – 14, 2012.

[39] Ulrik Dam Nielsen. Estimations of on-site directional wave spectra from measured ship responses. *Marine Structures*, 19(1):33 – 69, 2006. ISSN 0951-8339. doi: http://dx.doi.org/10.1016/j.marstruc.2006.06.001.

[40] Ulrik Dam Nielsen and Jörgen Juncher Jensen. A novel approach for navigational guidance of ships using onboard monitoring systems. *Ocean Engineering*, 38:444 – 455, 2011. ISSN 0029-8018.

[41] Michel K Ochi. Principles of extreme value statistics and their application. In *Extreme Loads Response Symposium, SNAME, Arlington, VA*, pages 15 – 30, 1981.

[42] Orcia. Spectral response analysis - truncated white noise spectrum, . URL https://www.orcina.com/SoftwareProducts/OrcaFlex/Documentation/Help/Content/html/SpectralResponseAnalysis.htm. Accessed: 16-01-17.

[43] Orcia. Drag loads due to yaw rate, . URL https://www.orcina.com/SoftwareProducts/OrcaFlex/Documentation/Help/Content/html/VesselTheory,CurrentandWindLoads.htm. Accessed: 11-12-16.

[44] Orcina. Diffraction frame, . URL https://www.orcina.com/SoftwareProducts/OrcaFlex/Documentation/Help/Content/html/VesselTheory,FramesofReference.htm#D. Accessed: 15-01-17.

[45] Orcina. Stiffness load - moment arm effect, . URL https://www.orcina.com/SoftwareProducts/OrcaFlex/Documentation/Help/Content/html/VesselTheory,Stiffness,AddedMassandDamping.htm. Accessed: 08-01-17.

[46] Hewlett Packard. The fundamentals of signal analysis. *HP application note*, 243, 1985.

[47] Kwang-Phil Park, Ju-Hwan Cha, and Kyu-Yeul Lee. Dynamic factor analysis considering elastic boom effects in heavy lifting operations. *Ocean Engineering*, 38(10):1100 – 1113, 2011.

[48] Ricardo Pascoal and C Guedes Soares. Kalman filtering of vessel motions for ocean wave directional spectrum estimation. *Ocean Engineering*, 36(6):477–488, 2009. doi: http://dx.doi.org/10.1016/j.oceaneng.2009.01.013.

[49] IHS Petrodata. Offshore rig day rate trends, 2016. URL https://www.ihs.com/products/oil-gas-drilling-rigs-offshore-day-rates.html. Accessed: 14-11-2016.

[50] Vuyk Engineering Rotterdam. Stability booklet rambiz 3000. Internal document, August 2009.

[51] TE Schellin, T Jiang, and SD Sharma. Crane ship response to wave groups. *Journal of Offshore Mechanics and Arctic Engineering*, 113(3):211–218, 1991.

[52] Alexandre N. Simos, Eduardo A. Tannuri, JoÃ£o V. Sparano, and VinÃcius L.F. Matos. Estimating wave spectra from the motions of moored vessels: Experimental validation. *Applied Ocean Research*, 32(2):191 – 208, 2010. ISSN 0141-1187.

[53] SNAME. Nomenclature for treating the motion of a submerged body through a fluid. *New York: Technical and Research Bulletin*, (1-5):1 – 15, April 1950.

[54] Eduardo A Tannuri, João V Sparano, Alexandre N Simos, and José J Da Cruz. Estimating directional wave spectrum based on stationary ship motion measurements. *Applied Ocean Research*, 25(5):243 – 261, 2003.

[55] Eric Thornhill and Dave Stredulinsky. Real time local sea state measurement using wave radar and ship motions. *Transactions of the Society of Naval Architects and Marine Engineers*, 118: 248, 2010.

[56] D. N. Veritas. Environmental conditions and environmental loads. Technical Report RPC-205, Det Norske Veritas, Oktober 2010.

[57] Det Norske Veritas. Lifting operations. Technical Report DNV-OS-H205, Det Norske Veritas, 2014.

[58] Hendrik Vorhölter, Hannes Hatecke, and Dag-Frederik Feder. Design study of floating crane vessels for lifting operations in the offshore wind industry. In *Proceedings of '15 International Marine Design Conference*, pages 1 – 13, 2015.

[59] A.P. Wijaya, P. Naaijen, Andonowati, and E. van Groesen. Reconstruction and future prediction of the sea surface from radar observations. *Ocean Engineering*, 106:261 – 270, 2015. ISSN 0029-8018. doi: http://dx.doi.org/10.1016/j.oceaneng.2015.07.009.

[60] J.A. Witz. Parametric excitation of crane loads in moderate sea states. *Ocean Engineering*, 22(4): 411 – 420, 1995. ISSN 0029-8018. doi: http://dx.doi.org/10.1016/0029-8018(94)00015-Y.

[61] Wenjun Zhang and Zhengjiang Liu. Real-time ship motion prediction based on time delay wavelet neural network. *Journal of Applied Mathematics*, 2014, 2014.

[62] X Zhao, Roger Xu, and Chiman Kwan. Ship-motion prediction: algorithms and simulation results. In *Acoustics, Speech, and Signal Processing, 2004. Proceedings.(ICASSP'04). IEEE International Conference on*, volume 5, page 5 – 125. IEEE, 2004.

A

Theoretical Background

A.1. Ocean Waves

Ocean waves are wind driven or generated waves and can be classified into two basic categories: sea or simply wind waves and swell. Below a brief and concise explanation is given:

- **Sea**
  Sea or wind waves are local wind driven waves. The waves are short crested and very irregular. High waves are followed unpredictably by low waves and vice versa. Individual wave crests propagate in different directions with tens of degrees deviation from the mean wave direction. The crests are fairly sharp and small waves can be observed on these crests as well. An example of a surface elevation record of a wind driven sea is given in figure A.1. [29]
- **Swell**
  Swell is the wave field that travels from a storm to some distant point in the ocean. They are no longer dependent upon the wind where waves of all frequencies in a broad range of directions are generated. At that point far away the waves are regular and long-crested. Swell is regular because of frequency dispersion (filtering of the frequencies due to longitudinal spreading), the energy of the low frequency waves travels faster then the energy of the higher frequencies. In the storm far away all frequencies are present, but at some point far away the low frequency wave will arrive earlier followed by the higher frequencies. Swell is always long-crested because of direction dispersion (filtering of the direction due to lateral spreading of the waves). [24]

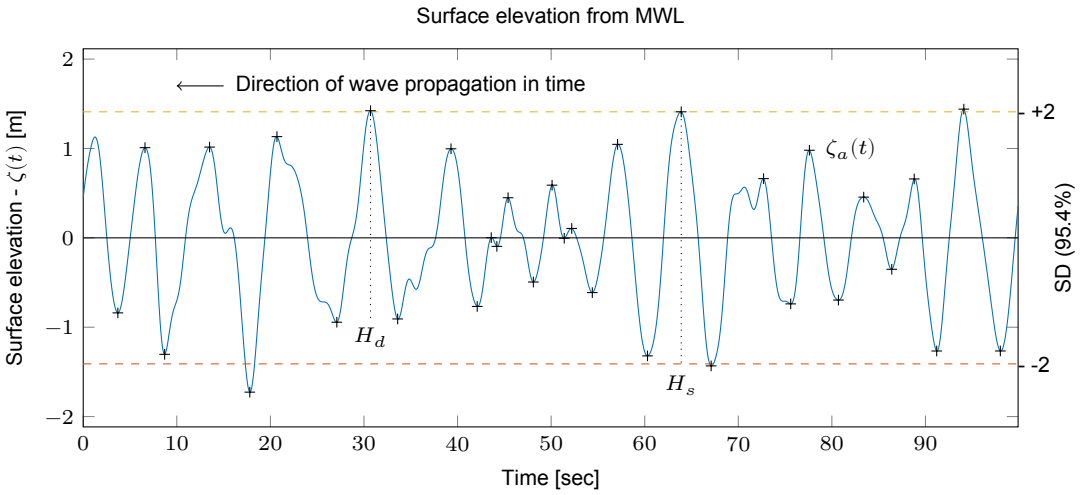

Figure A.1: Time trace of the wave elevation of a sea state that contains the JONSWAP spectrum $H_s = 3.0$ m, $T_p = 8.0$ s, $\gamma = 3.3$

Even though especially wind driven waves are highly irregular, their frequencies are still narrow bounded. Thus the surface elevation of ocean waves can be seen as a superposition of many simple, regular harmonic wave components ($i = 1, 2..$), each with its own amplitude (ζ_a), length (λ), period (T) or frequency (ω) and direction of propagation. For a single direction the surface elevation is than given by

$$\zeta = \sum_{i=1}^{N} \zeta_{a,i} \cos(2\pi f_i t + \varepsilon_i) \tag{A.1}$$

in which the wave frequency (f) is given in Hz .The significant wave height H_s or $H_{1/3}$ is defined as the average centroid of the highest $1/3^{th}$ of the waves in the record. The so-called standard deviation σ of the water level $\zeta(t)$ is given by

$$\sigma = \sqrt{\frac{1}{N-1} \sum_{i=1}^{N} \zeta_i^2} \tag{A.2}$$

This standard deviation is also referred to as Root Mean Square (RMS) value. The significant wave height is related to the RMS by $H_s = 4 \cdot \sigma$. According to measurements it seems to be a reasonable approach that the surface elevation can be seen as a stationary, Gaussian distributed process. The distribution of the surface elevation is than given by

$$f(\zeta_a) = \frac{1}{\sigma\sqrt{2\pi}} \cdot \exp\left\{-\left(\frac{\zeta_a}{\sigma\sqrt{2\pi}}\right)^2\right\} \tag{A.3}$$

According to this distribution the $2 \cdot \sigma$ or 95.4% confidence bound of the surface elevation is illustrated in figure A.1. Since the range frequencies for both sea and swell is narrow banded, the distribution of the surface elevation is given by Rayleigh distribution

$$f(\zeta_a) = \frac{\zeta_a}{\sigma^2} \cdot \exp\left\{-\left(\frac{\zeta_a}{\sigma\sqrt{2}}\right)^2\right\} \tag{A.4}$$

It should be noted however that real waves differ from harmonic waves since in reality, high wave crests are observed slightly more frequently than according to the Gaussian model, and deep troughs slightly less frequently. For steep waves or in shallow water, the discrepancies are large, the waves are ”more” non-linear. The linear approximation of waves does not apply to the latter situations. [24, 29]

A.2. Fourier Transformation

The aim of describing ocean waves or vessel motion signals with a spectrum is not so much to describe in detail one observation of the sea surface or the vessel motion amplitude, but rather to describe the sea surface or vessel motion as a stochastic process. In other words to characterize all possible observations in a time record that could have been made under the conditions of the actual observation. An observation is thus formally treated as one realization of a stochastic process. Time traces of these observations can be transformed with Fourier transformations. For example three sinusoidal waves can be described by a Fourier series by

$$\mathsf{z(t)} = \mathsf{A}_0 + \sum_{q=1}^{end} \left\{ A_q \cos(2\pi f_q t) + B_q \sin(2\pi f_q t) \right\}$$

where A_0 is the mean of the signal, A_q and B_q the Fourier coefficients for components q, f is the frequency and t the time. From Fourier analysis coefficients A_q and B_q are defined as

$$\mathsf{A}_q = \tfrac{2}{T} \int_0^T z(t) \cos(2\pi f_q t) dt \quad \text{and} \quad \mathsf{B}_q = \tfrac{2}{T} \int_0^T z(t) \sin(2\pi f_q t) dt$$

Where the integral can be made discrete with T, the duration of the signal is equal to total number of time steps N times the time step Δt. The frequency is than equal to $q/(N\Delta t)$. The discrete form is thus given by

$$\mathsf{A}_q = \tfrac{2}{N} \sum_{n=1}^{end} z_n \cos \tfrac{2\pi q n}{N} \quad \text{and} \quad \mathsf{B}_q = \tfrac{2}{N} \sum_{n=1}^{end} z_n \sin \tfrac{2\pi q n}{N}$$

The amplitude and phase angle of a signal is than respectively given by

$$a_{FFT(A)} = \frac{\sqrt{(\Re\{FFT(A)\})^2 + (\Im\{FFT(A)\})^2}}{N} \qquad \varepsilon_{FFT(A)} = \arctan\left(\frac{\Im\{FFT(A)\}}{\Re\{FFT(A)\}}\right)$$

The variance density, power or energy spectrum of a single signal is given by

$$S_{AA}(f) = \frac{FFT(A) \cdot FFT^*(A)}{N^2}$$

The cross spectrum of two signals or vessel motions is given by

$$S_{AB}(f) = \frac{FFT(B) \cdot FFT^*(A)}{N^2}$$

where * denotes the complex conjugate. The Parzen window is defined by

$$w(n) = \begin{cases} 1 - 6\left(\frac{n}{N/2}\right)^2 \left(1 - \frac{|n|}{N/2}\right) & \text{for } 0 \leqslant |n| \leqslant \frac{N}{4} \\ 2\left(1 - \frac{|n|}{N/2}\right)^3 & \text{for } \frac{N}{4} < |n| \leqslant \frac{N}{2} \end{cases}$$

and the Hanning window for $0 \leq n \leq N$ is defined by

$$w(n) = 0.5\left(1 - \cos\left(\frac{2\pi}{N-1}\right)\right)$$

[46].

A.3. Standardized Wave Spectra

Short term stationary irregular sea states may be described by a wave spectrum. That is, the power spectral density function of the vertical sea surface displacement [11, 24]. Wave spectra can be given in table form, as measured spectra, or by a parameterized analytic formula as have been used in this study. Knowledge of which kind of spectral density is suitable to describe sea state data are well established from experimental studies. Qualitative considerations of wave measurements indicate that the spectra may be divided into 3 parts:

1. Sea states dominated by wind sea but significantly influenced by swell components,
2. More or less pure wind seas or a swell component located well inside the wind frequency band,
3. Sea states more or less dominated by swell but significantly influenced by wind sea.

The most appropriate wave spectrum depends on the geographical area with local bathymetry, fetch limitations, local currents and the severity of the sea state. In this research, the two most important wave spectra for describing the sea state at the North Sea have been used. These spectra are the JONSWAP and Torsethaugen spectra which respectively describe wind sea dominated sea states (Uni-Modal) and combined sea states which are composed of wind waves and swell (Bi-Modal). The description of these spectra is given in the following subsections. Directional wave spreading and wave spectra transformation to finite water depths is described in respectively subsections A.3.3 and A.3.4.

A.3.1. Uni-Modal

The JONSWAP (JOint North Sea WAve Project) spectrum is a result of a multinational project to characterize standardized wave spectra for the Southeast part of the North Sea. The spectrum is valid for not fully developed sea states. However, it is also used to represent fully developed sea states. It is particularly well suited to characterize wind sea when $3.6\sqrt{H_{m0}} < T_p < 5\sqrt{H_{m0}}$. The JONSWAP spectrum is identical with the two-parameter Pierson-Moskowitz, Bretschneider, ITTC (International Towing Tank Conference) or ISSC (International Ship and Offshore Structures Congress) wave spectrum, given H_{m0} and T_p when γ = 1. The spectrum is given in the form:

$$S^{+}(\omega) = \underbrace{\frac{\alpha g^2}{\omega^M}\exp\left(-\frac{M}{N}\left(\frac{\omega_p}{\omega}\right)^N\right)}_{\text{Pierson - Moskowitz}} \gamma^{\exp\left(\frac{-(\omega/\omega_p-1)^2}{2\sigma^2}\right)} \tag{A.5}$$

where

$$\begin{aligned} \sigma &= \begin{cases} 0.07\omega & \text{for} \quad \omega < \omega_p \\ 0.09\omega & \text{for} \quad \omega \geqslant \omega_p \end{cases} \\ M &= 5, \qquad N = 4, \\ \alpha &\approx 5.061\frac{H_{m0}^2}{T_p^4}\left\{1 - 0.287\ln(\gamma)\right\}. \end{aligned} \tag{A.6}$$

A standard value for the peakedness parameter, γ, is 3.3. However, a more correct approach is to relate γ to H_{m0} and T_p. The relation is given by

$$\gamma = \exp\left\{3.484\left(1 - 0.1975(0.036 - 0.0056T_p/\sqrt{H_{m0}})T_p^4/H_{m0}^2\right)\right\}.$$

Here γ is limited by $1 \leq \gamma \leq 7$. This parameterization is based on qualitative considerations of deep water wave data from the North Sea. Often also an upper limit of γ is 5 is maintained. The relation between the peak period and mean zero-upcrossing period may be approximated by

$$T_{m0} \approx T_p/(1.30301 - 0.01698\gamma + 0.12102/\gamma) \tag{A.7}$$

An example of this spectrum whit γ is 1.0 is illustrated in figure 3.16 at page 34. In figure A.3 at page 102 an example is given for γ is 3.3. [19, 20]

A.3.2. Bi-Modal

Moderate and low sea states in open sea areas are often composed of both wind sea and swell. A two peak spectrum may be used to account for both wind sea and swell. Two commonly used formulations for bi-modal spectra are The Ochi-Hubble spectrum and the Torsethaugen spectrum. The Ochi-Hubble spectrum describe bi-modal spectra by a superposition of two modified Bretschneider (Pierson-Moskovitz) spectra and is given in a somewhat more detailed form in chapter 6.3 at page 67. In this description also wave spreading is included.

For design work the bi-modal Torsethaugen spectrum is probably the only one well established separation procedures for the wave components. This spectrum was developed primarily for one location at the Norwegian Continental Shelf (Statfjord Field) but in qualitative terms is expected to be of much broader validity. It is important to mention that the spectra derived from the Torsethaugen model represent average conditions. Being a design approach, the Torsethaugen spectral description is a good option to be used whenever there is no information available about the nature of two-peaked spectra at a given location. The model is however not been verified systematically for locations outside the Norwegian Continental Shelf. [4]

Torsethaugen proposed to describe bi-modal spectra by

$$S^{+}(\omega) = \sum_{i=1}^{2} S_J^{+}(\ \omega \quad H_{m0,i} \quad \omega_{p,i} \quad \gamma_i \quad N_i \quad M_i \quad \alpha_i\ ) \tag{A.8}$$

where S_J^{+} is the JONSWAP spectrum defined by equation A.5 in the previous section. The parameters $H_{m0,i}$, $\omega_{p,i}$, N_i, M_i, and α_i for i = 1, 2, are the significant wave height, angular peak frequency, spectral shape and normalization parameters for the primary and secondary peak, respectively. These parameters are fitted to 20000 spectra divided into 146 different classes of H_{m0} and T_p obtained at the Statfjord field in the North Sea in the period from 1980 to 1989. The measured significant wave height and period values for the data range from 0.5 to 11 meters and from 3.5 to 19 seconds, respectively. [19, 20]

Given H_{m0} and T_p these parameters are found by the following steps. The borderline between wind dominated and swell dominated sea states is defined by the fully developed sea, for which

$$T_p = T_f = 6.6 H_{m0}^{1/3}, \tag{A.9}$$

while $T_p < T_f$, the local wind sea dominates the spectral peak, and if $T_p > T_f$ the swell peak is dominating. For each of the three types a non-dimensional period scale is introduced by

$$\varepsilon_{lu} = \frac{T_f - T_p}{T_f - T_{lu}}$$

where

$$T_{lu} = \begin{cases} 2\sqrt{H_{m0}} & \text{if } T_p \leqslant T_f \quad \text{(Lower limit)} \\ 25 & \text{if } T_p > T_f \quad \text{(Upper limit)} \end{cases}$$

defines the lower or upper value for T_p. The significant wave height for each peak is given as

$$H_{m0,1} = R_{pp} H_{m0} \qquad H_{m0,2} = \sqrt{1 - R_{pp}^2} H_{m0},$$

where

$$R_{pp} = (1 - A_{10}) \exp\left(-\left(\frac{\varepsilon_{lu}}{A_1} \right)^2 \right) + A_{10},$$

$$A_1 = \begin{cases} 0.5 & \text{if } T_p \leqslant T_f, \\ 0.3 & \text{if } T_p > T_f, \end{cases} \qquad A_{10} = \begin{cases} 0.7 & \text{if } T_p \leqslant T_f, \\ 0.6 & \text{if } T_p > T_f. \end{cases}$$

The primary and secondary peak periods are defined as

$$T_{p,1} = T_p,$$
$$T_{p,2} = \begin{cases} T_f + 2 & \text{if } T_p \leqslant T, \\ \left(\frac{M_2 (N_2/M_2)^{(N_2-1)/M_2} / \Gamma((N_2-1)/M_2)}{1.28(0.4)^{N_2}\{1-\exp(-H_{m0,2}/3)\}} \right) & \text{if } T_p > T_f, \end{cases}$$

where the spectral shape parameters are given as

$$N_1 = N_2 = 0.5\sqrt{H_{m0}} + 3.2,$$
$$M_i = \begin{cases} 4\left(1 - 0.7\exp(-H_{m0}/3)\right) & \text{if } T_p > T_f \text{ and } i = 2, \\ 4 & \text{otherwise.} \end{cases}$$

The peakedness parameters are defined as

$$\gamma_1 = 35\left(1 + 3.5\exp(-H_{m0})\right)\gamma_T, \qquad \gamma_2 = 1,$$

where

$$\gamma_T = \begin{cases} \left(\frac{2\pi H_{M0,1}}{g T_p^2}\right)^{0.857} & \text{if } T_p \leqslant T_f, \\ (1 + 6\varepsilon_{lu})\left(\frac{2\pi H_{M0,1}}{g T_p^2}\right)^{0.857} & \text{if } T_p > T_f, \end{cases}$$

Finally the normalization parameters $\alpha_i (i = 1, 2)$ are found by numerical integration such that

$$\int_0^\infty S_J^+(\ \omega \quad H_{m0,i} \quad \omega_{p,i} \quad \gamma_i \quad N_i \quad M_i \quad \alpha_i\ ) d\omega = H_{m0,i}^2/16.$$

An example of the Torsethaugen spectrum for an severe sea state composed of wind seas and swell is illustrated in in figure A.2a at page 101.

A.3.3. Two-dimensional wave spectra

Actually seen sea waves cannot be depicted by using a single wave spectrum and thus a single mean wave direction alone. Sea waves consist of several different waves (irregularity) and all of them have their own direction. The concept of a directional spectrum is therefore introduced to describe wave fields. A wave spectrum that involves the direction could be expressed as below

$$S(\omega, \theta) = S(\omega) D(\theta, \omega) \tag{A.10}$$

where $S(\omega, \theta)$ is the directional wave spectral density function, or simply the directional wave spectrum, and $D(\theta, \omega)$ is the wave frequency dependent directional spreading function. In addition, the directional spreading function should have no dimension and be normalized, it can readily be proven by

$$\int_0^{2\pi} D(\theta, \omega) d\theta = \int_0^{2\pi} \frac{E(\theta, \omega) d\theta}{E(\omega)} = \frac{\int_0^{2\pi} E(\theta, \omega) d\theta}{E(\omega)} = \frac{E(\omega)}{E(\omega)} = 1.$$

The shape of the distribution $D(\theta)$ is not well known, not even in the idealized situation that is considerate in literature. It is usually speculated that this distribution has a maximum in the wind direction since most of the wave energy travels downwind, and that it falls gradually to the offwind directions. Several expressions with this character have been suggested to describe $D(\theta)$. The best-known and probably most widely used is the $cos^2\theta$ model from Pierson et al. 1952:

$$D(\theta) = \begin{cases} \frac{2}{\pi}\cos^2\theta & \text{for } |\theta| \leqslant 90^\circ \\ 0 & \text{for } |\theta| > 90^\circ \end{cases} \tag{A.11}$$

where the direction θ is taken relative to the mean wave direction ($\theta - \theta_{mean}$). This spreading function is applied for the half plane of $|\theta| > 90^\circ$. However, the wave direction should involve all of the directions and this description of the distribution $D(\theta)$ is still independent of wave frequency. Initiated by Longuet-Higginis et al. (1963), many researchers have therefore adopted the following spreading function for data analysis:

$$D(\theta) = \frac{\Gamma(s+1)}{2\sqrt{\pi}\Gamma(s+1/2)}\cos^{2s}\left(\frac{\theta}{2}\right) \tag{A.12}$$

where the spreading parameter, s, is frequency dependent and Γ is the gamma function which is available in any mathematical reference book for example Abramowitz and Stegun. Mitsuyasu et al. (1975) introduced a spreading function that included the frequency. The introduced directional spreading is the narrowest around the spectral peak frequency and becomes wider as the frequency moves farther from the peak.

$$S = \begin{cases} S_{\max}(\omega/\omega_p)^5 & \text{for } \omega \leqslant \omega_p \\ S_{\max}(\omega/\omega_p)^{-2.5} & \text{for } \omega > \omega_p \end{cases}$$

Mitsuyasu et al. set spreading parameter S_{max} in the range of 5 to 30, with a mean of about 10 for wind generated waves. For engineering purposes Goda and Suzuki (1975) proposed a spreading parameter with fixed values for wind waves and swell.

$$S_{\max} = \begin{cases} 10: & \text{for wind waves} \\ 25: & \text{for swell with short decay distances} \\ 75: & \text{for swell with long decay distances} \end{cases}$$

The directional spreading function has a heavy density near the spectral peak frequency which becomes lower farther from the peak. An example of the Torsethaugen spectrum for an severe sea state composed of wind seas and swell spread over multiple directions is given in the figure below. [11, 20, 24, 32]

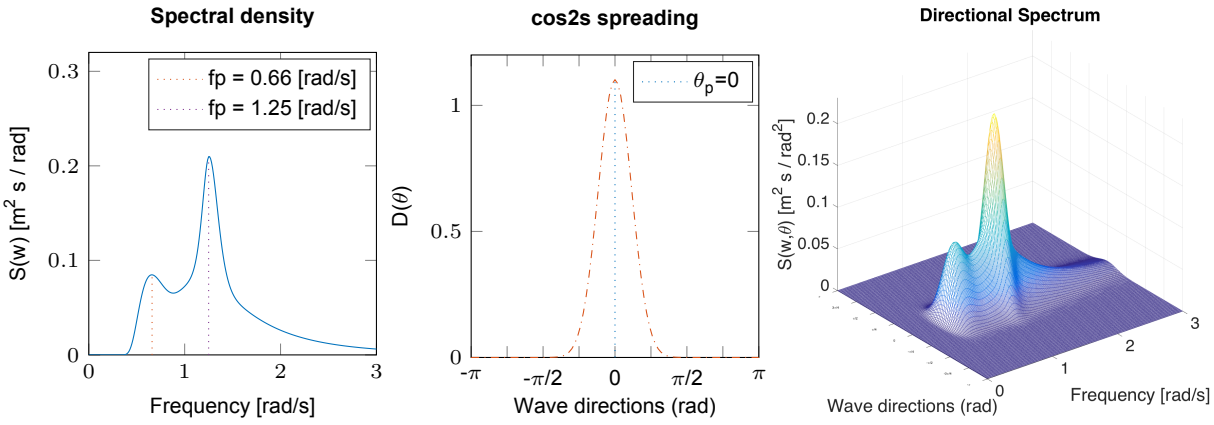

(a) 1-D Power Spectrum (b) Spreading function (c) 2-D Power Spectrum

Figure A.2: Directional bi-modal Torsethaugen wave spectrum. $H_s = 1.5$ m, $T_p = 5.0$ s, $S_{max} = 15$, number of angles is 110.

A.3.4. Finite water depth

In deep water, progress in understanding wave growth resulted from observation that the shape of growing wind wave spectra is, to a reasonable degree regular and can be described by similarity laws. In other words for deep water waves, the sea state can be described by wave spectra such as the JONSWAP and Torsethaugen wave spectra described in the previous sections. These spectra show a characteristic development. With growing energy the sharp peak migrates towards lower frequencies. As described in subsection C.2.3, the high frequency flank can be described by a frequency dependence f^{-m}, with m being measured by various groups between 4 and 5. The low frequency flank is however less known since at these wave frequencies the wave energy decreases very rapidly with decreasing frequency and because the observed wind wave records are often contaminated by swell. Standardized wave spectra has been quantified and the parameters descriptive of spectral shape have been related to growth stage parameters such as duration, fetch and wind speed. [7]

In order to take into account the complicating effects of variable water depth and dissipation of wave energy due to the existence of a bottom boundary layer, Kitaigorodskii et al. (1975) in KKZ, an modified one-dimensional frequency spectrum was proposed. This spectrum is a self-similar spectral shape denoted by TMA. In other words the JONSWAP spectrum for infinite water depths can be used to describe similar sea states in finite water depths if the JONSWAP spectrum is multiplied with the reciprocal KKZ factor $\phi_K(\omega_H)$. The transformation of the JONSWAP spectrum to finite water depths is thus given by

$$S_{TMA}(\omega, H) = S_J^+(\omega) \cdot \phi_K(\omega_H) \tag{A.13}$$

where S_{TMA} is the self-similar JONSWAP spectrum for finite water depth, S_J^+ the JONSWAP spectrum for infinite water depth as described in equation A.5 and ϕ_K the transformation factor given by

$$\phi_K(\omega_H) = \frac{\left[k(\omega, H)^{-3} \frac{\partial k(\omega, H)}{\partial \omega}\right]}{\left[k(\omega, \infty)^{-3} \frac{\partial k(\omega, \infty)}{\partial \omega}\right]}$$

in which, k, is the wave number space and ω_H is the water depth dependent wave frequency given by

$$\omega_H = \frac{\omega_\infty}{2\pi}\sqrt{\frac{H}{g}}$$

Since the scaling factor is best described in the wave number domain, standardized wave spectra have to be translated to this domain as well. This can be done by making use of the dispersion relationship given in equation 4.1 at page 37. The WAFO toolbox which have been used for this transformation uses the Newton Raphson method to find the wave number k. In the figure below for different water depths TMA spectra with JONSWAP parameters are illustrated.

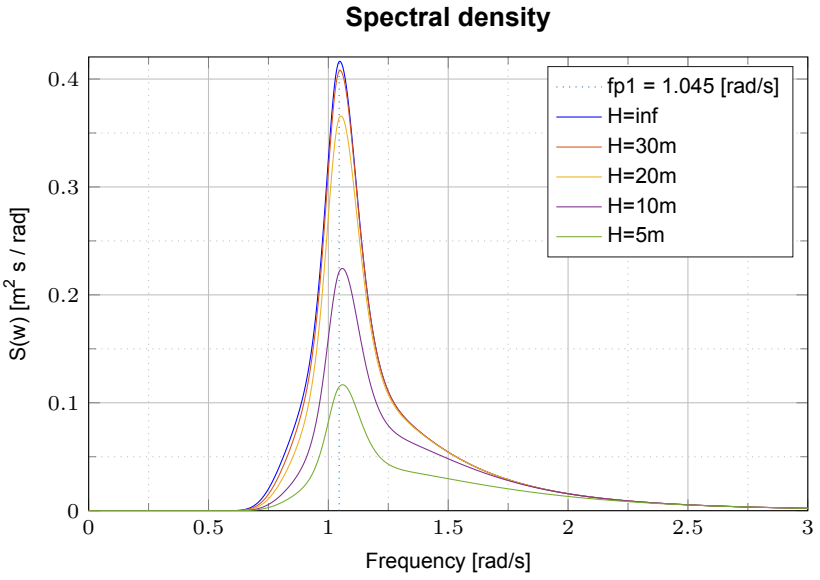

Figure A.3: Self-similar TMA spectra with JONSWAP parameters, $H_s = 1.5$ m, $T_p = 6.0$ sec and $\gamma = 3.3$.

It should be noted that the principal hypothesis used to derive S_{TMA} is that the KKZ scaling is not restricted to the saturation range, it is valid across the entire spectrum. This approach is similar to the applied scaling with f^{-5} as has been done in the JONSWAP and Pierson-Moskowitz spectra. Due to scaling across the entire spectrum the assumption is made that any proposed mechanism, such as breaking, does not dominate the entire spectrum. From the performed validity study, which is based on 2800 different spectra measured at Texel, Marsen and Arsloe, the hypothesis of similarity shape has been confirmed. [7, 20]

A.4. Response Amplitude Operator

According to Journée and Massie, here a brief and concise description of the derivation of the response amplitude operator of vessel motions is given [29]. It is assumed that wave induced forces are sinusoidal in nature and that vessel motions or responses are wave induced only. In complex notations and in time domain the wave force and vessel response in any direction is than given by

$$\begin{aligned}
\vec{F}_w &= \vec{F}_{wa}\cos(\omega t + \vec{\varepsilon}_{F_{w,\zeta}}) = \Re\left\{\vec{F}_{wa}\cdot e^{i\vec{\varepsilon}_{F_{w,\zeta}}}\cdot e^{i\omega t}\right\} \\
\vec{x} &= \vec{x}_a\cos(\omega t + \vec{\varepsilon}) = \Re\left\{\vec{x}_a\cdot e^{i\vec{\varepsilon}}\cdot e^{i\omega t}\right\} \\
\dot{\vec{x}} &= -\omega\cdot\vec{x}_a\sin(\omega t + \vec{\varepsilon}) = \Re\left\{i\omega\cdot\vec{x}_a\cdot e^{i\vec{\varepsilon}}\cdot e^{i\omega t}\right\} \\
\ddot{\vec{x}} &= \omega^2\cdot\vec{x}_a\cos(\omega t + \vec{\varepsilon}) = -\Re\left\{\omega^2\cdot\vec{x}_a\cdot e^{i\vec{\varepsilon}}\cdot e^{i\omega t}\right\}
\end{aligned} \tag{A.14}$$

where $\vec{F}_w$ is the wave force and $\vec{x}$ the vessel response in vector notation, a, is an amplitude, ω, is the wave frequency and $\vec{\varepsilon}$ is an phase shift. The equation of motion for vessel motions in the most general and simple form is given by

$$(M+A)\cdot\ddot{\vec{x}} + B\cdot\dot{\vec{x}} + C\cdot\vec{x} = \vec{F}_w \tag{A.15}$$

where M and A are respectively the structural vessel mass and hydrodynamic added mass, B, the hydrodynamic damping and C, the hydrostatic stiffness. Chapter 3.3 elaborates more on the equation of motion of vessel motions during heavy lift operations. Substitution of equations A.14 into the equation of motion gives

$$\Re\left\{\left(-\omega^2(M+A) + C + i\omega B\right)\frac{\vec{x}_a}{\zeta_a}\cdot e^{i\vec{\varepsilon}}\cdot e^{i\omega t}\right\} = \Re\left\{\vec{F}_{wa}\cdot e^{i\vec{\varepsilon}_{F_{w,\zeta}}}\cdot e^{i\omega t}\right\}$$

which can be simplified to

$$\Re\left\{\left(-\omega^2(M+A) + C + i\omega B\right)\hat{x}_a\cdot e^{i\omega t}\right\} = \Re\left\{\hat{F}_{wa}\cdot e^{i\omega t}\right\}$$

in which

$$\begin{aligned}
\hat{x}_a &= \frac{\vec{x}_a}{\zeta_a}\cdot e^{i\vec{\varepsilon}} \\
\hat{F}_{wa} &= \frac{\vec{F}_{wa}}{\zeta_a}\cdot e^{i\vec{\varepsilon}_{F_{w,\zeta}}}
\end{aligned}$$

If then subsequently the left and right hand side of the equation are being divided by the time dependent term $e^{i\omega t}$ the equation of motion can be solved in the frequency domain and is given by

$$\left(-\omega^2(M+A) + C + i\omega B\right)\hat{x}_a = \hat{F}_{wa}$$

Hence the solution of the equation of motion is given by

$$\hat{x}_a = \frac{\hat{F}_{wa}}{-\omega^2(M+A) + C + i\omega B}$$

The response amplitude operator or RAO and the phase shift of the response is then respectively given by

$$\begin{aligned}
\frac{\vec{x}_a}{\zeta_a} &= \sqrt{\Re\{\hat{x}_a\}^2 + \Im\{\hat{x}_a\}^2} \\
\vec{\varepsilon} &= \arctan\left(\frac{\Im\{\hat{x}_a\}}{\Re\{\hat{x}_a\}}\right)
\end{aligned}$$

Wave induced vessel responses are wave frequency and wave direction dependent. The final solution of the RAO, in this report denoted by H is therefore given by

$$\frac{\hat{x}_a(\omega,\theta)}{\zeta_a} = H(\omega,\theta) = \sqrt{\Re\{\hat{x}_a(\omega,\theta)\}^2 + \Im\{\hat{x}_a(\omega,\theta)\}^2} \tag{A.16}$$

The transfer functions of translations are dimensionless and those of the rotational motions can be made non dimensional by dividing the amplitude of the rotations by the amplitude of the wave slope, $k\zeta_a$ instead of the wave amplitude ζ_a only. The transfer functions for wave induced vessel roll, pitch and yaw motions then becomes

$$\frac{\theta_a}{k\zeta_a}(\omega) \quad \frac{\phi_a}{k\zeta_a}(\omega) \quad \frac{\psi_a}{k\zeta_a}(\omega)$$

A.5. Most Probable Maximum Response

The energy wave spectrum is defined as:

$$S_\zeta(\omega) \cdot d\omega = \frac{1}{2}\zeta_a^2(\omega) \tag{A.17}$$

Analogous to this, the energy spectrum of for example the heave response $z(\omega, t)$ can be defined by:

$$\begin{aligned} S_z(\omega) \cdot d\omega &= \frac{1}{2}z_a^2(\omega) \\ &= \left|\frac{z_a}{\zeta_a}(\omega)\right|^2 \cdot \frac{1}{2}\zeta_a^2(\omega) \\ &= \left|\frac{z_a}{\zeta_a}(\omega)\right|^2 \cdot S_\zeta(\omega) \cdot d\omega \end{aligned} \tag{A.18}$$

In which $\frac{z_a}{\zeta_a}(\omega)$ is thus the transfer function for heave motion. The response spectrum of a motion can be found by using the squared absolute value of the transfer function of the motion H_{ij} and the wave spectrum $S_\zeta(\omega)$:

$$S_{R_{ij}}(\omega) = \left|H_{ij}\right|^2 \cdot S_\zeta(\omega) \tag{A.19}$$

where $i, j = 1..m$ denotes the motion components. The moments of the heave response spectrum are given by:

$$m_{nz} = \int_0^\infty S_z(\omega) \cdot \omega^n \cdot d\omega \tag{A.20}$$

whit $n = 0, 1, 2, ...$ where $n = 0$ provides the area, $n = 1$ the first moment and $n = 2$ the moment of inertia of the spectral curve. For convenience of writing here heave motion ($i = j = 3$) is denoted by z. The velocity and acceleration response spectra are found by a multiplication of the response amplitude operator and the displacement. Since the transfer function is squared to define the response spectra, the spectral moments for heave velocity and acceleration are thus respectively given by

$$m_{0\dot{z}} = m_{2z} \qquad m_{0\ddot{z}} = m_{4z}$$

The extreme value is defined, in general, as the largest value expected to occur in a certain number of observations or in a certain period of time. It can be defined on a short-term basis in which the sea environment is statistically invariant (usually from 30 minutes to several hours) as well as on a long-term basis (usually for many years). In either case, however, the number of observations or a period of time have to be specified in defining the extreme value. Since the assumption is made that vessel responses are being induced by incoming waves only, and that these waves are stationary Gaussian distributed and narrow banded in their frequencies, the response amplitudes are Rayleigh distributed. The short term probability density function of the heave response is then given by

$$f_{ST}(R_a) = \frac{R_a}{m_{0z}} \cdot \exp\left\{-\frac{R_a^2}{2m_{0z}}\right\} \tag{A.21}$$

where R_a is the Rayleigh distributed heave response amplitude. The significant heave amplitude is thus defined as the mean value of the highest one third part of the amplitudes, given by:

$$\bar{z}_{a1/3} = 2 \cdot RMS = 2\sqrt{m_{0z}} \tag{A.22}$$

in which RMS is the Root Mean Square value. The significant heave velocity and acceleration are then respectively given by

$$\dot{\hat{z}}_{a1/3} = 2\sqrt{m_{2z}} \qquad \ddot{\hat{z}}_{a1/3} = 2\sqrt{m_{4z}} \tag{A.23}$$

The most probable maximum response is dependent on the amount of responses, N, during a given period in hours T_{hrs}. The amount of responses, N, is subsequently dependent on the mean duration of the response T_{2r}. The mean duration and the number of heave responses during a given duration in hours is respectively given by

$$T_{2z} = 2\pi\sqrt{\frac{m_{oz}}{m_{2z}}} \qquad N = \frac{T_{hrs}\cdot 3600}{T_{2z}} \tag{A.24}$$

Finally the Most Probable Maximum Response for heave displacement is given by

$$MPM_z = 2\sqrt{m_{0z}}\sqrt{\frac{\ln(N)}{2}} \tag{A.25}$$

which can be done similarly for the velocity and acceleration in heave direction

$$MPM_{\dot{z}} = 2\sqrt{m_{2z}}\sqrt{\frac{\ln(N)}{2}} \qquad MPM_{\ddot{z}} = 2\sqrt{m_{4z}}\sqrt{\frac{\ln(N)}{2}} \tag{A.26}$$

In this manner the most probable maximum response can be determined for any desired period T_{hrs}. In practice however, most often a period 3 hours is taken. Simple because of the assumption that the maximum wave, and thus also response, is included in approximately 1000 waves of which its duration is at least 3 hours. [29, 41]

A.6. Prediction Methods and Techniques

In this appendix a short and concise description of the highlighted prediction methods and techniques is given. ***The information is gathered from various internet sources and is textual to a minimum edited***. This information is therefore only given for convenience of the reader who just as I was not familiar with these methods and techniques.

Principal and Minor Component Analyses

Principal (PCA) and minor (MCA) component flows are matrix differential equations that converge to the eigenvectors associated with the largest and smallest eigenvalues, respectively, of a given symmetric matrix. They are statistical procedure that uses an orthogonal transformation to convert a set of observations of possibly correlated variables into a set of values of linearly uncorrelated variables called principal components. The number of principal components is less than or equal to the number of original variables. This transformation is defined in such a way that the first principal component has the largest possible variance (that is, accounts for as much of the variability in the data as possible), and each succeeding component in turn has the highest variance possible under the constraint that it is orthogonal to the preceding components. The resulting vectors are an uncorrelated orthogonal basis set. PCA is sensitive to the relative scaling of the original variables. MCA has similar mathematics as the Principal Component Analysis, except that MCA utilize the eigenvectors corresponding to the minor components.[1]

Autoregressive methods

In statistics and signal processing, an autoregressive (AR) model is a representation of a type of random process; as such, it is used to describe certain time-varying processes in nature, economics, etc. The autoregressive model specifies that the output variable depends linearly on its own previous values and on a stochastic term (an imperfectly predictable term); thus the model is in the form of a stochastic difference equation. Together with the moving-average (MA) model, it is a special case and key component of the more general Autoregressive–moving-average model or ARMA and Autoregressive integrated moving average or ARIMA models of time series. They have a more complicated stochastic

[1] Source: `https://en.wikipedia.org/wiki/Principal_component_analysis`, Accessed: 15-11-16.

structure, it is also a special case of the vector autoregressive model (VAR), which consists of a system of more than one stochastic difference equation. These kinds of algorithms can therefore be used flexibly. [2]

Wiener Prediction
In signal processing, the Wiener filter is a filter used to produce an estimate of a desired or target random process by linear time-invariant (LTI) filtering of an observed noisy process, assuming known stationary signal and noise spectra, and additive noise. The Wiener filter minimizes the mean square error between the estimated random process and the desired process. The goal of the Wiener filter is to compute a statistical estimate of an unknown signal using a related signal as an input and filtering that known signal to produce the estimate as an output. For example, the known signal might consist of an unknown signal of interest that has been corrupted by additive noise. The Wiener filter can be used to filter out the noise from the corrupted signal to provide an estimate of the underlying signal of interest. The Wiener filter is thus based on a statistical approach and can be applied on any stochastic signal. [3]

Neural Networks
Neural networks (also referred to as connectionist systems) are a computational approach which is based on a large collection of neural units loosely modeling the way a biological brain solves problems with large clusters of biological neurons connected by axons. Each neural unit is connected with many others, and links can be enforcing or inhibitory in their effect on the activation state of connected neural units. Each individual neural unit may have a summation function which combines the values of all its inputs together. There may be a threshold function or limiting function on each connection and on the unit itself such that it must surpass it before it can propagate to other neurons. These systems are self-learning and trained rather than explicitly programmed and excel in areas where the solution or feature detection is difficult to express in a traditional computer program.

Neural networks typically consist of multiple layers or a cube design, and the signal path traverses from front to back. Back propagation is where the forward stimulation is used to reset weights on the ”front” neural units and this is sometimes done in combination with training where the correct result is known. More modern networks are a bit more free flowing in terms of stimulation and inhibition with connections interacting in a much more chaotic and complex fashion. Dynamic neural networks are the most advanced in that they dynamically can, based on rules, form new connections and even new neural units while disabling others.

The goal of the neural network is to solve problems in the same way that the human brain would, although several neural networks are much more abstract. Modern neural network projects typically work with a few thousand to a few million neural units and millions of connections, which is still several orders of magnitude less complex than the human brain and closer to the computing power of a worm.

New brain research often stimulates new patterns in neural networks. One new approach is using connections which span much further and link processing layers rather than always being localized to adjacent neurons. Other research being explored with the different types of signal over time that axons propagate which is more complex than simply on or off. Neural networks are based on real numbers, with the value of the core and of the axon typically being a representation between 0.0 and 1.

An interesting facet of these systems is that they are unpredictable in their success with self learning. After training some become great problem solvers and others don’t perform as well. In order to train them several thousand cycles of interaction typically occur. Like other machine learning methods – systems that learn from data – neural networks have been used to solve a wide variety of tasks, like computer vision and speech recognition, that are hard to solve using ordinary rule-based programming. [4]

[2] Source: `https://en.wikipedia.org/wiki/Autoregressive_model`, Accessed: 15-11-16.
[3] Source: `https://en.wikipedia.org/wiki/Wiener_filter`, Accessed: 15-11-16.
[4] Source: `https://en.wikipedia.org/wiki/Artificial_neural_network`, Accessed: 15-11-16.

Fuzzy Logic

Fuzzy logic has two different meanings. In a narrow sense, fuzzy logic is a logical system, which is an extension of multivalued logic. Something can thus be true and false at the same time, even without a different magnitude. In a wider sense fuzzy logic (FL) is almost synonymous with the theory of fuzzy sets, a theory which relates to classes of objects with unsharp boundaries in which membership is a matter of degree. In this perspective, fuzzy logic in its narrow sense is a branch of FL. Even in its more narrow definition, fuzzy logic differs both in concept and substance from traditional multivalued logical systems. By looking at it this way to complex systems for the determination of vessel responses during heavy lift operations it might be possible to find a semi true logic from which can be learned and possible effective corrections can be made. [5]

[5]Source: https://nl.mathworks.com/help/fuzzy/what-is-fuzzy-logic.html, Accessed: 15-11-16.

B

Results Validation Study

This appendix include detailed results of the validation study of the frequency domain model for vessel motion responses during a heavy lift operation. The results are subdivided in two sections. In the first section vessel and load motion RAOs are given from those computed in frequency domain and time domain (Orcaflex) for comparisons between a static and dynamic motion analysis. In the second section vessel motion responses induced by sinusoidal waves are given which are being compared to vessel motions RAOs obtained from frequency domain analysis.

Furthermore is tested whether the dynamic system behaves linearly over wave amplitude and period simply by studying sinusoidal wave induces vessel responses. For linear systems: single sinusoidal input is single sinusoidal output. The responses are computed for PS lift cases by making use of Orcaflex. Resulting roll motion amplitudes are given per wave period and wave height in the last section.

The validity of the frequency domain model is tested in stages in order to verify and check the influence of the coupling terms and missing elements such as a rigging module or the dynamic effects such as the moment arm effect in hydrostatic force. The stages are divided in lift locations. Those lift locations are Mid Ship, Bow Centre and Bow PS. For the sake of clarity those lift locations are illustrated in the figure below.

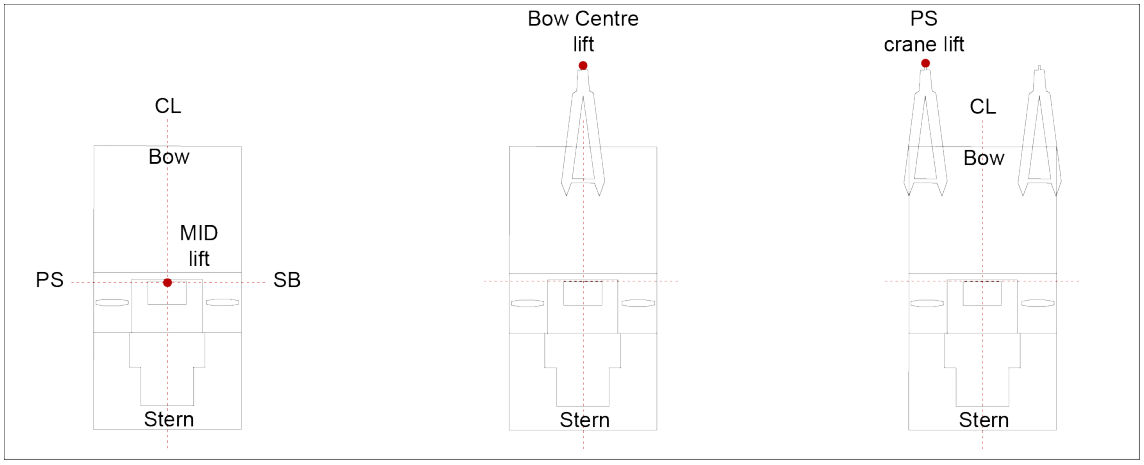

Figure B.1: Different lift locations in order to determine the model validity in frequency domain

B.1. Vessel motion RAOs

B.1.1. Light Ship

Barge with mooring but w/o cranes

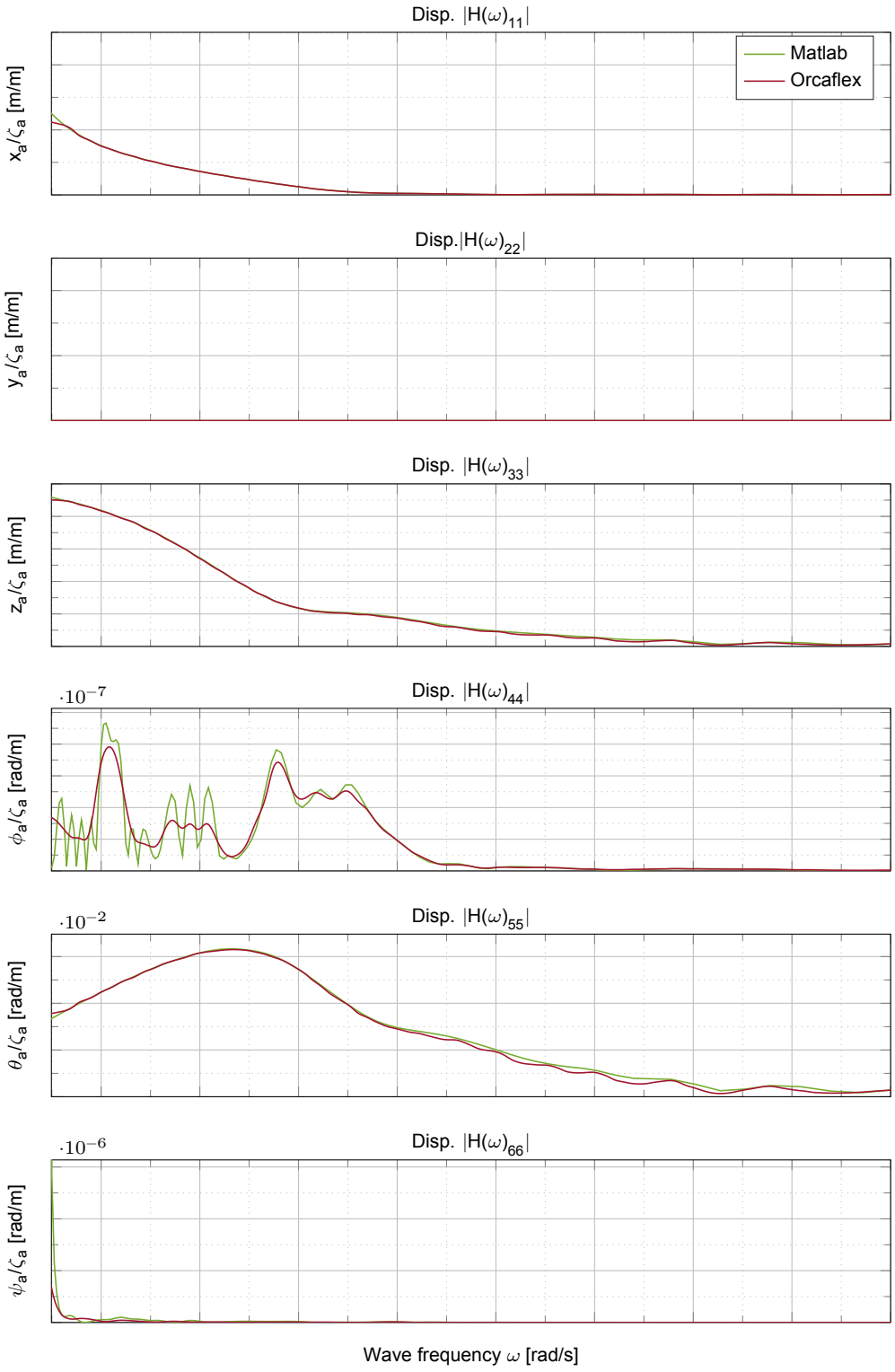

Figure B.2: Displacement RAOs - Stern Waves
Case: Light Ship with mooring

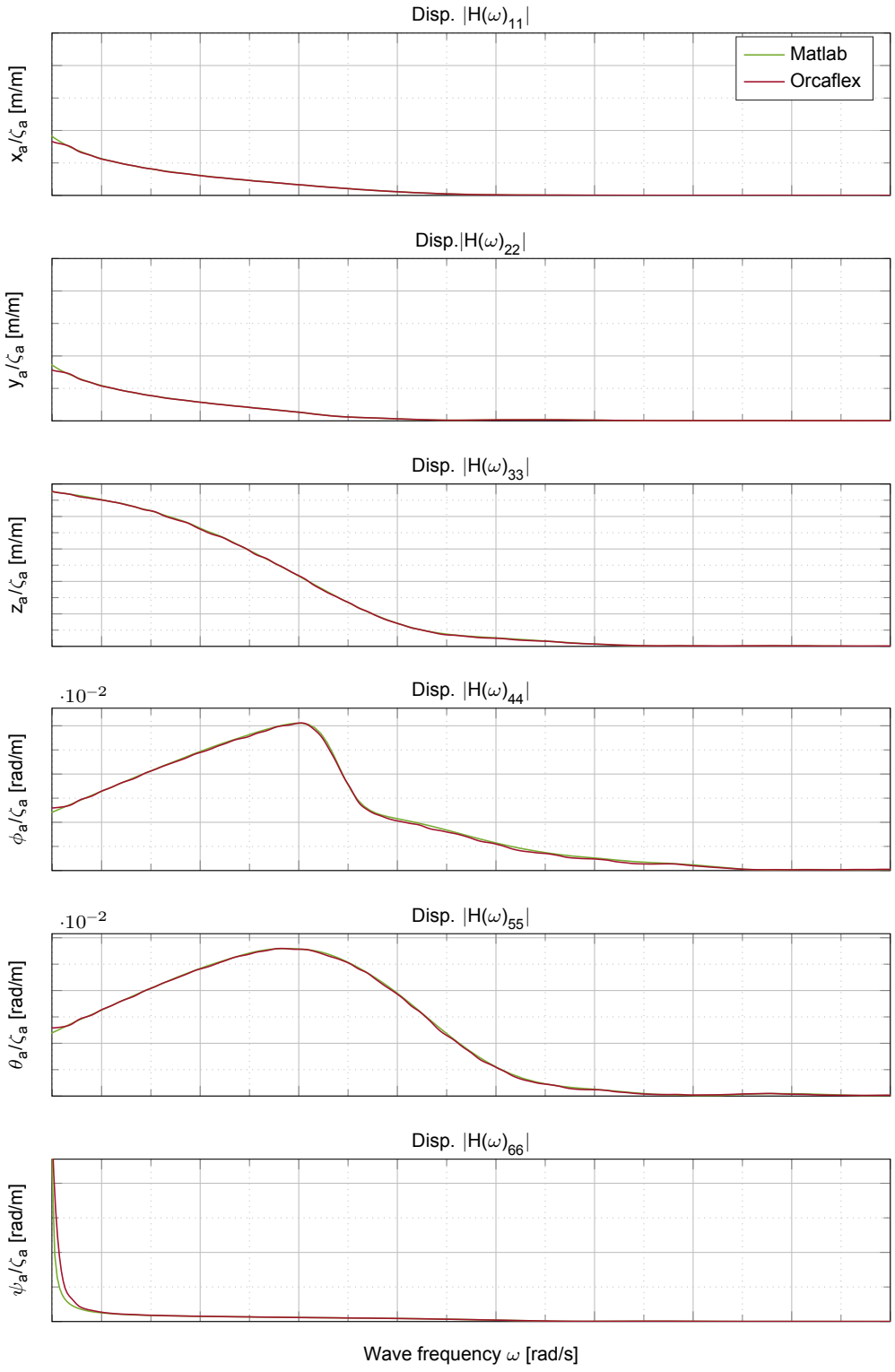

Figure B.3: Displacement RAOs - Starboard Quartering Waves
Case: Light Ship with mooring

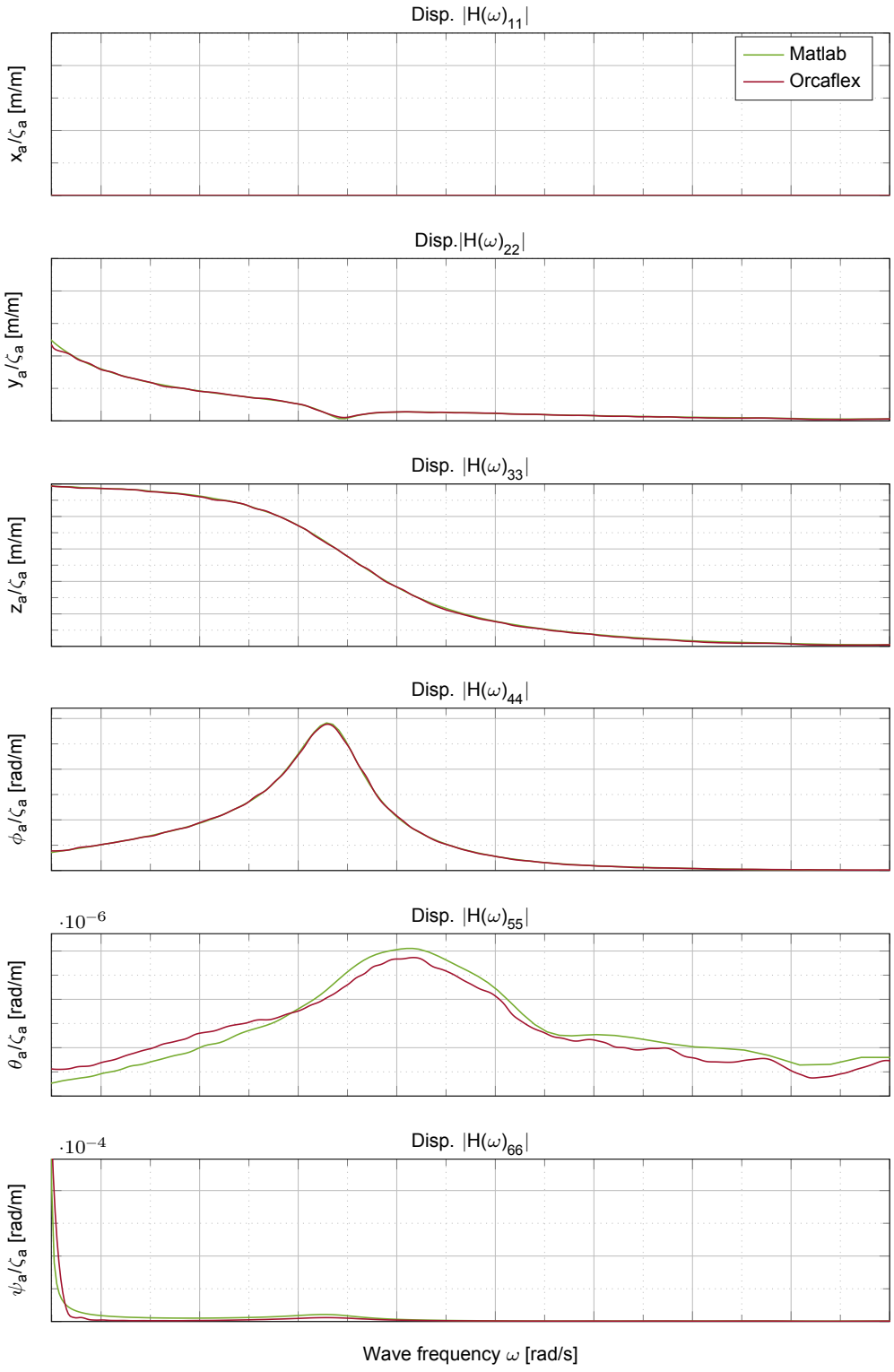

Figure B.4: Displacement RAOs - Starboard Beam Waves
Case: Light Ship with mooring

Barge with mooring and inclined cranes

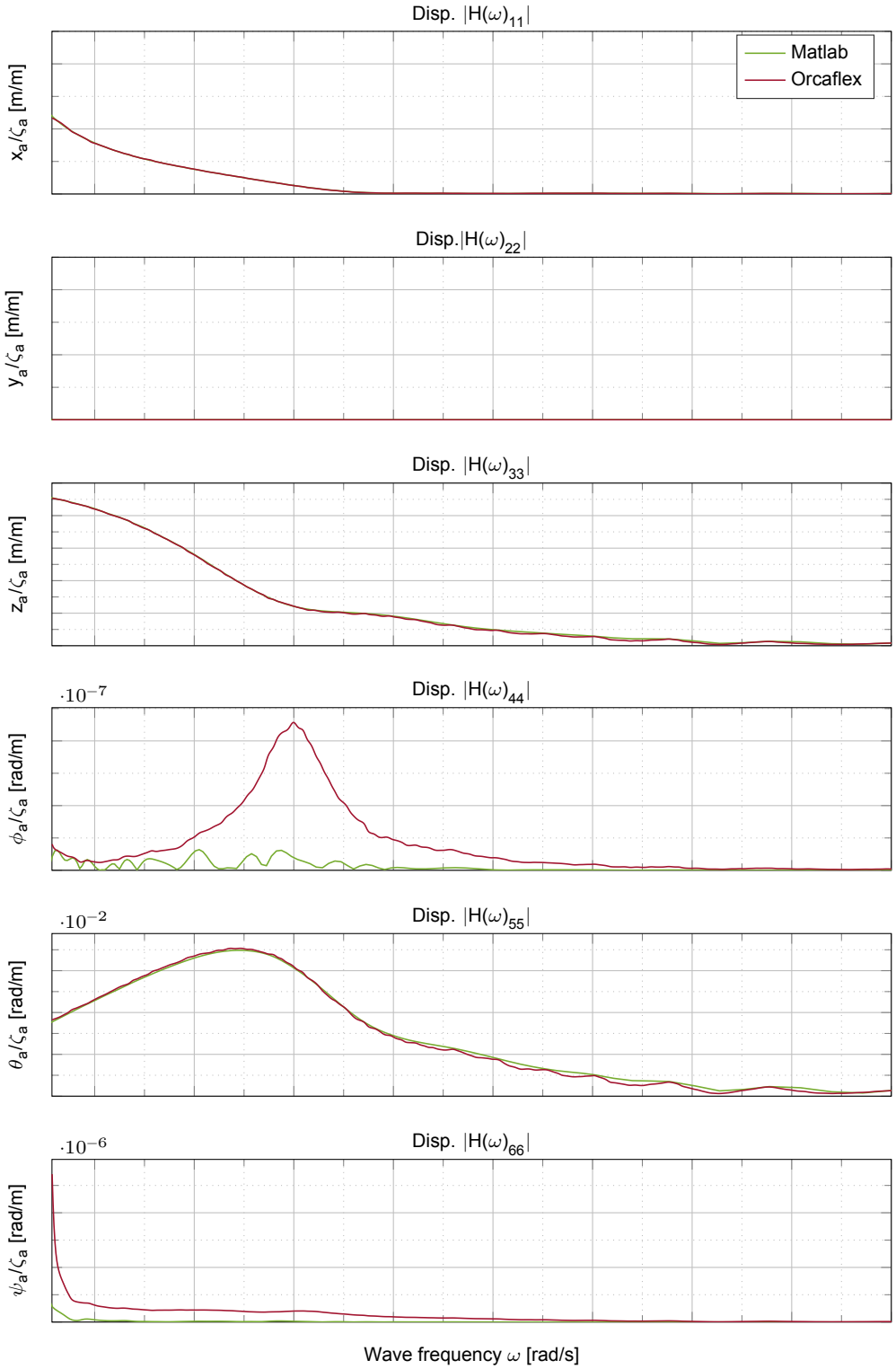

Figure B.5: Displacement RAOs - Stern Waves
Case: Light Ship with mooring and inclined cranes

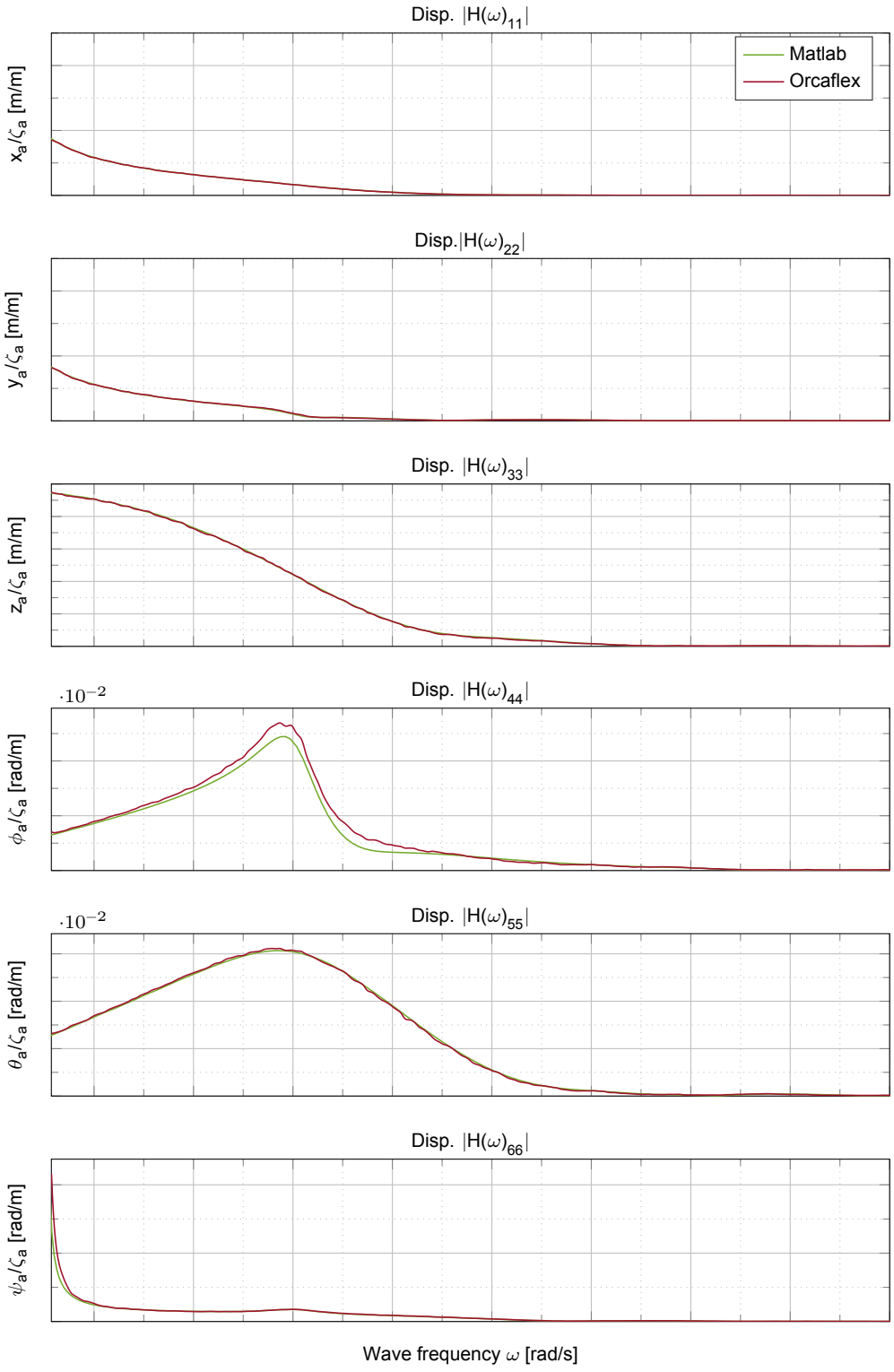

Figure B.6: Displacement RAOs - Starboard Quartering Waves
Case: Light Ship with mooring and inclined cranes

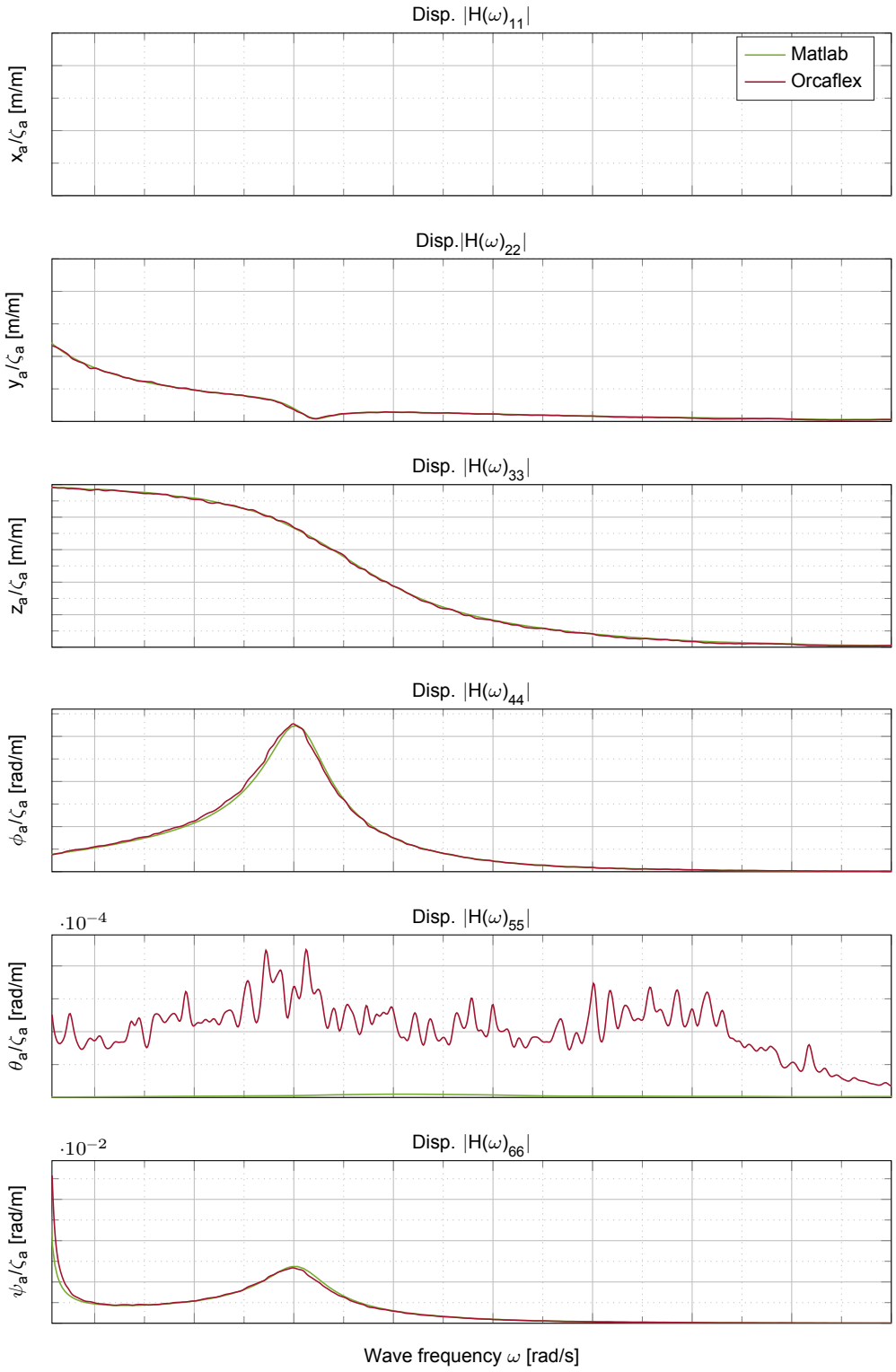

Figure B.7: Displacement RAOs - Starboard Beam Waves
Case: Light Ship with mooring and inclined cranes

B.1.2. Single Crane Lift - MID

Without rigging module in Orcaflex (Cargo has only translational motions)

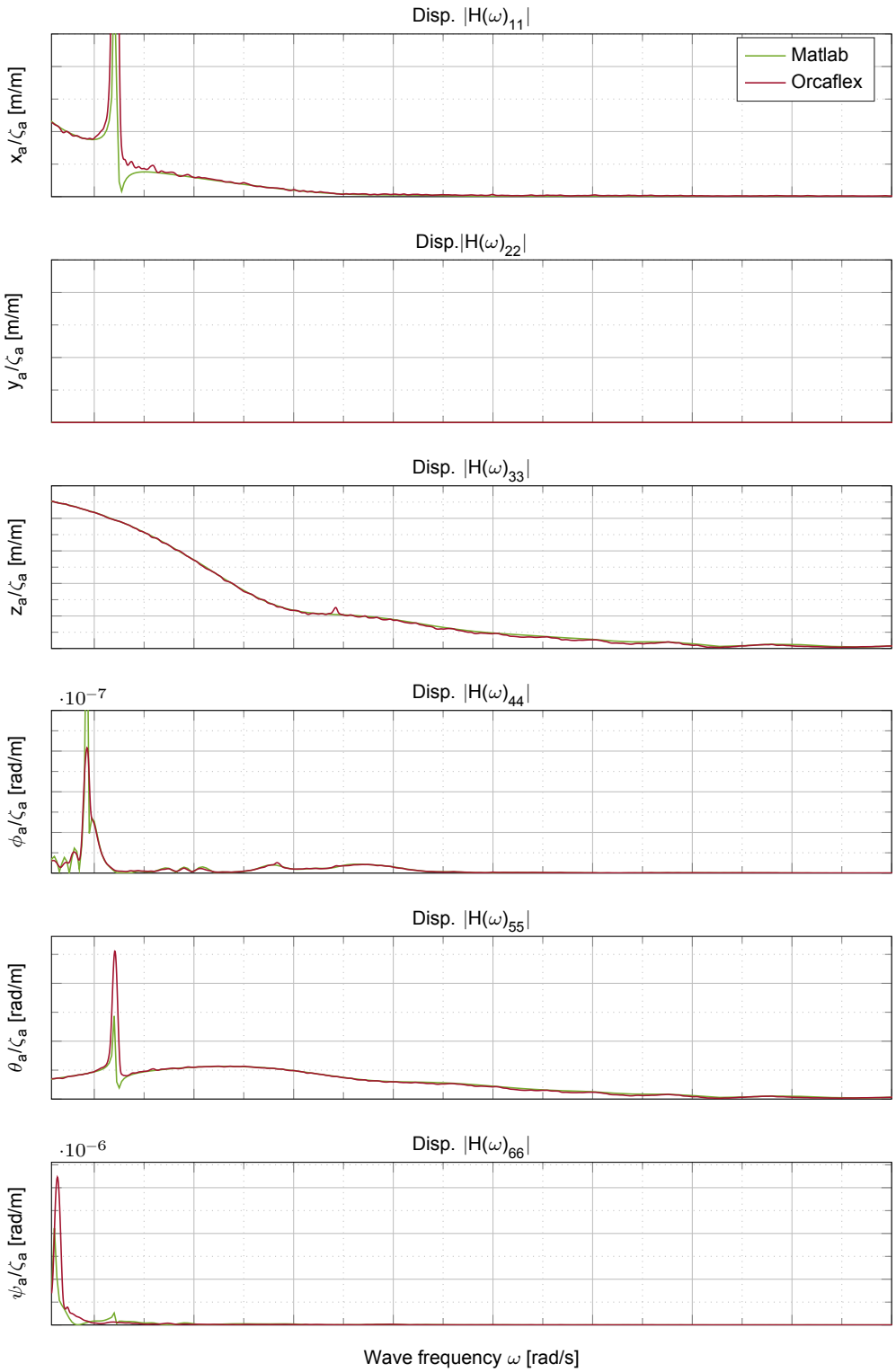

Figure B.8: Displacement RAOs - Stern Waves
Case: MID Lift, without rigging module

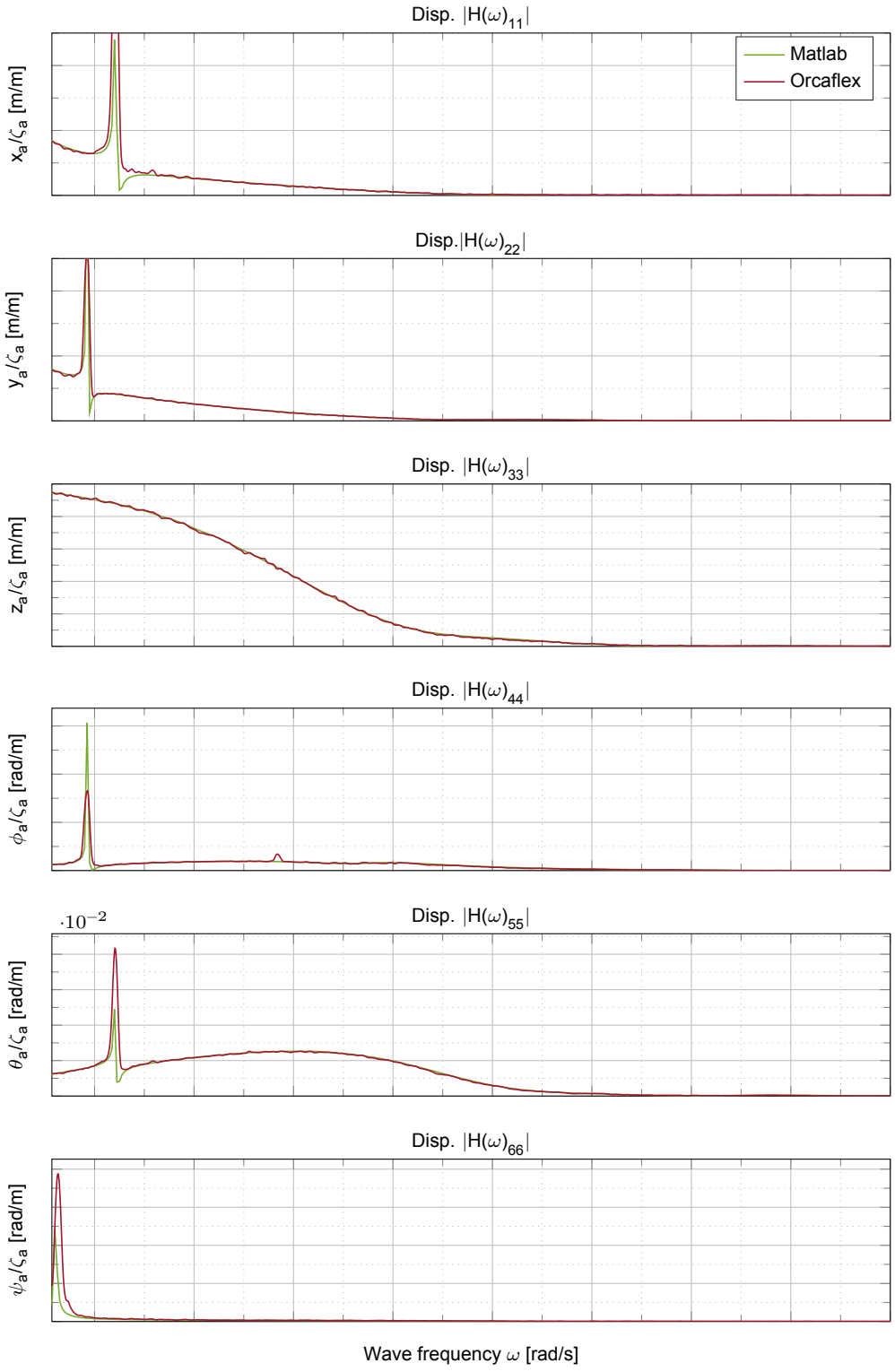

Figure B.9: Displacement RAOs - Starboard Quartering Waves
Case: MID Lift, without rigging module

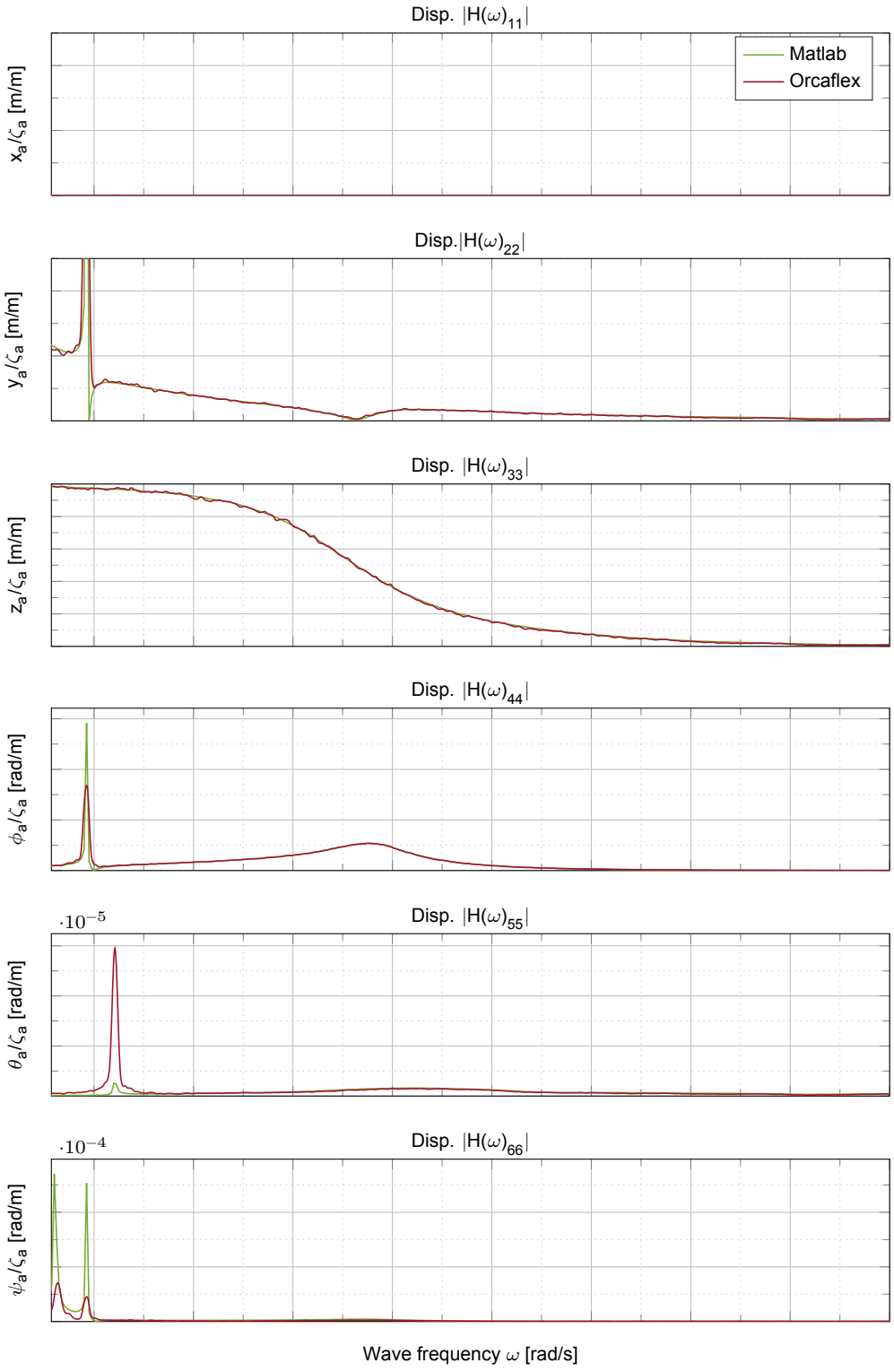

Figure B.10: Displacement RAOs - Starboard Beam Waves
Case: MID Lift, without rigging module

With rigging module in Orcaflex (Cargo can have rotational motions)

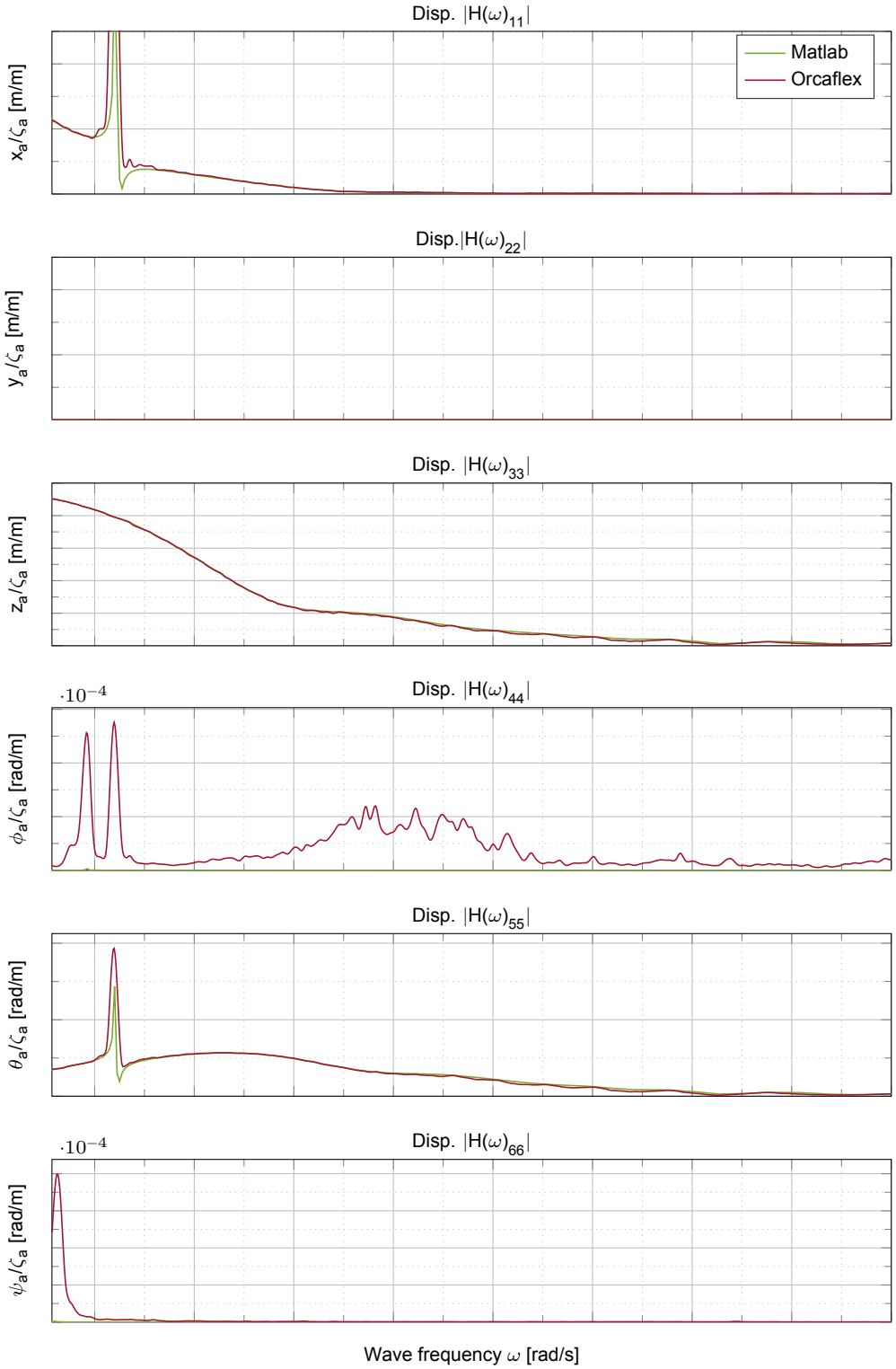

Figure B.11: Displacement RAOs - Stern Waves
Case: MID Lift, with rigging module

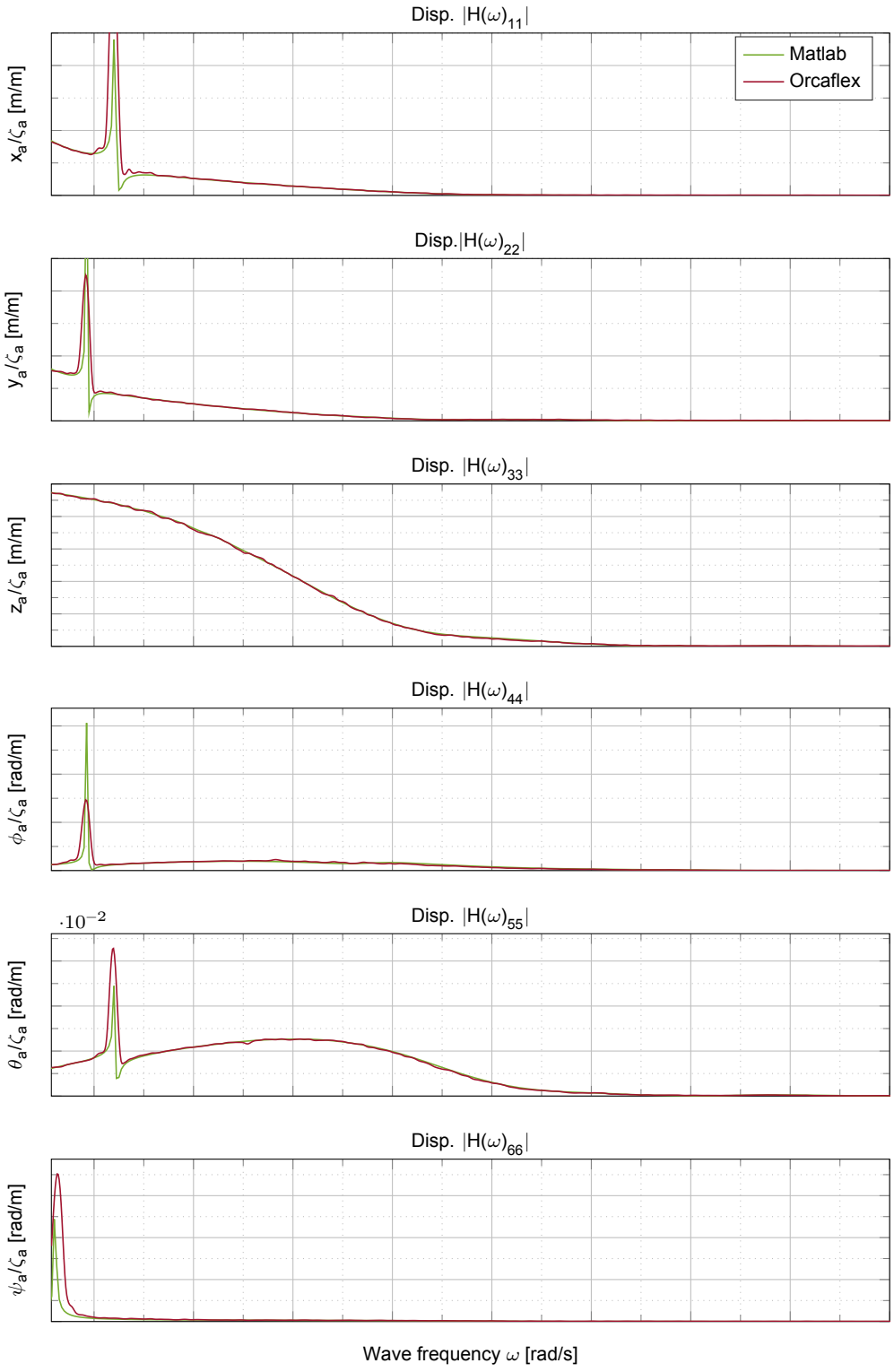

Figure B.12: Displacement RAOs - Starboard Quartering Waves
Case: MID Lift, with rigging module

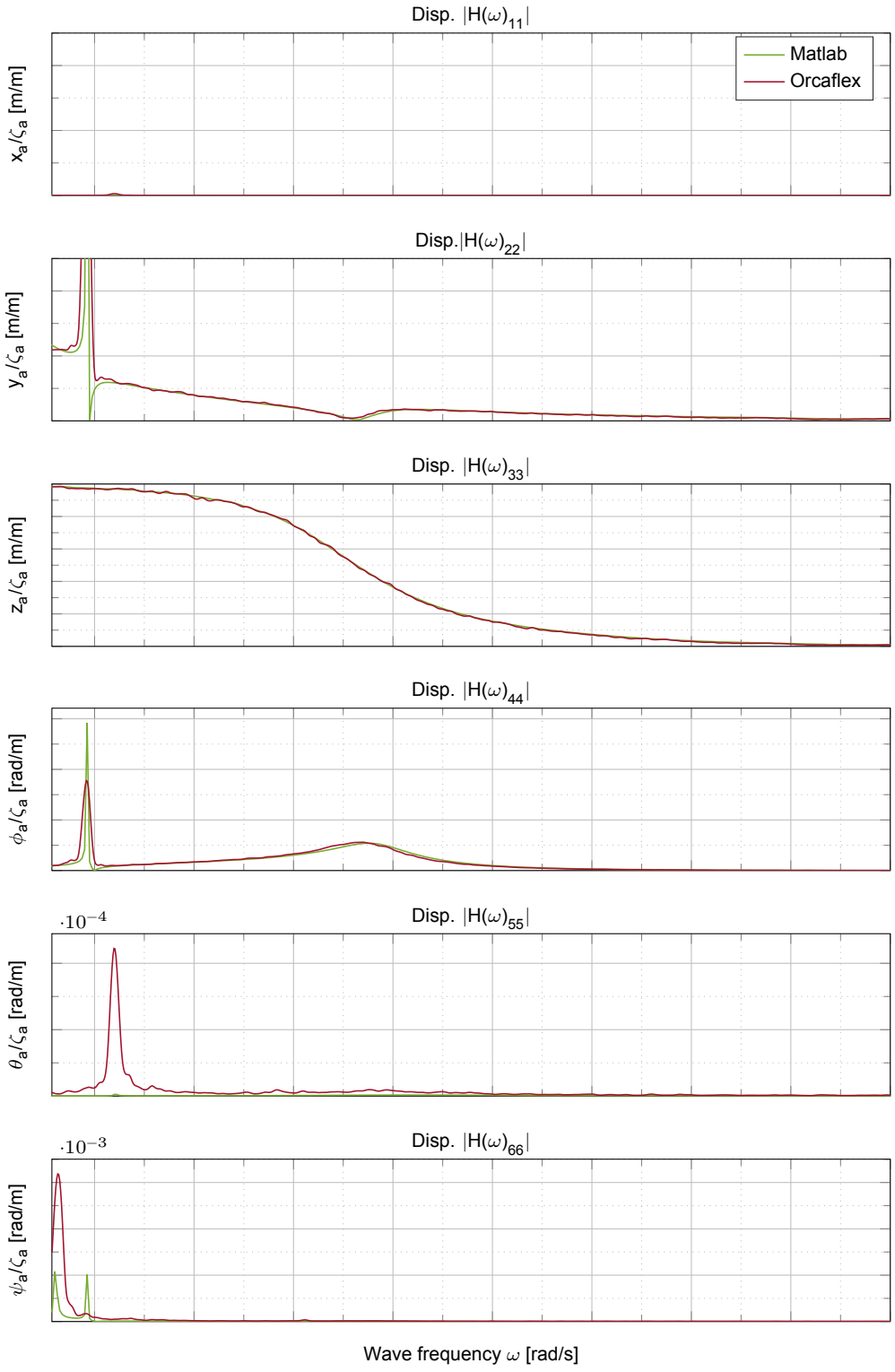

Figure B.13: Displacement RAOs - Starboard Beam Waves
Case: MID Lift, with rigging module

B.1.3. Single Crane Lift - CE

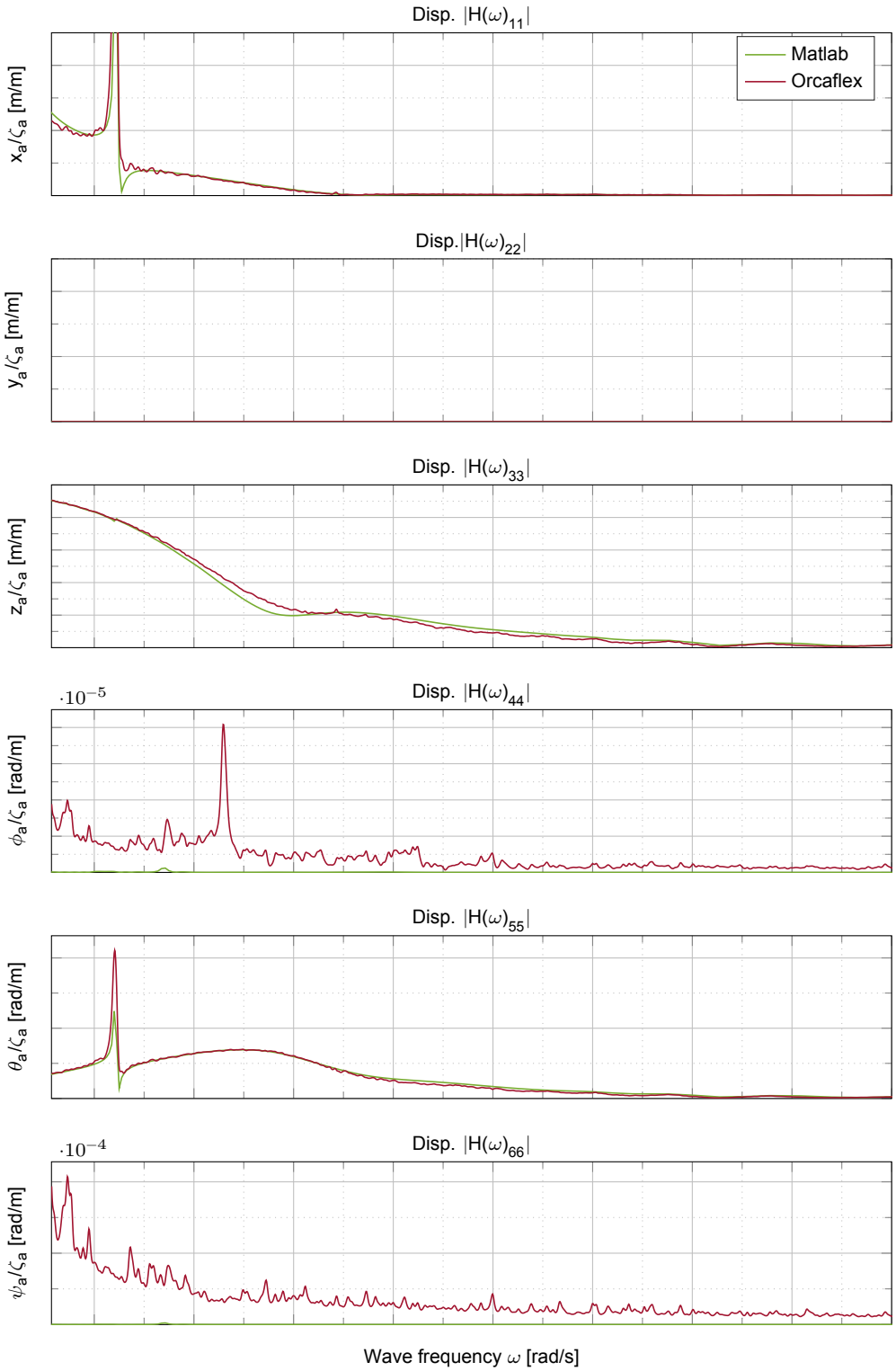

Figure B.14: Displacement RAOs - Stern Waves
Case: CE Lift

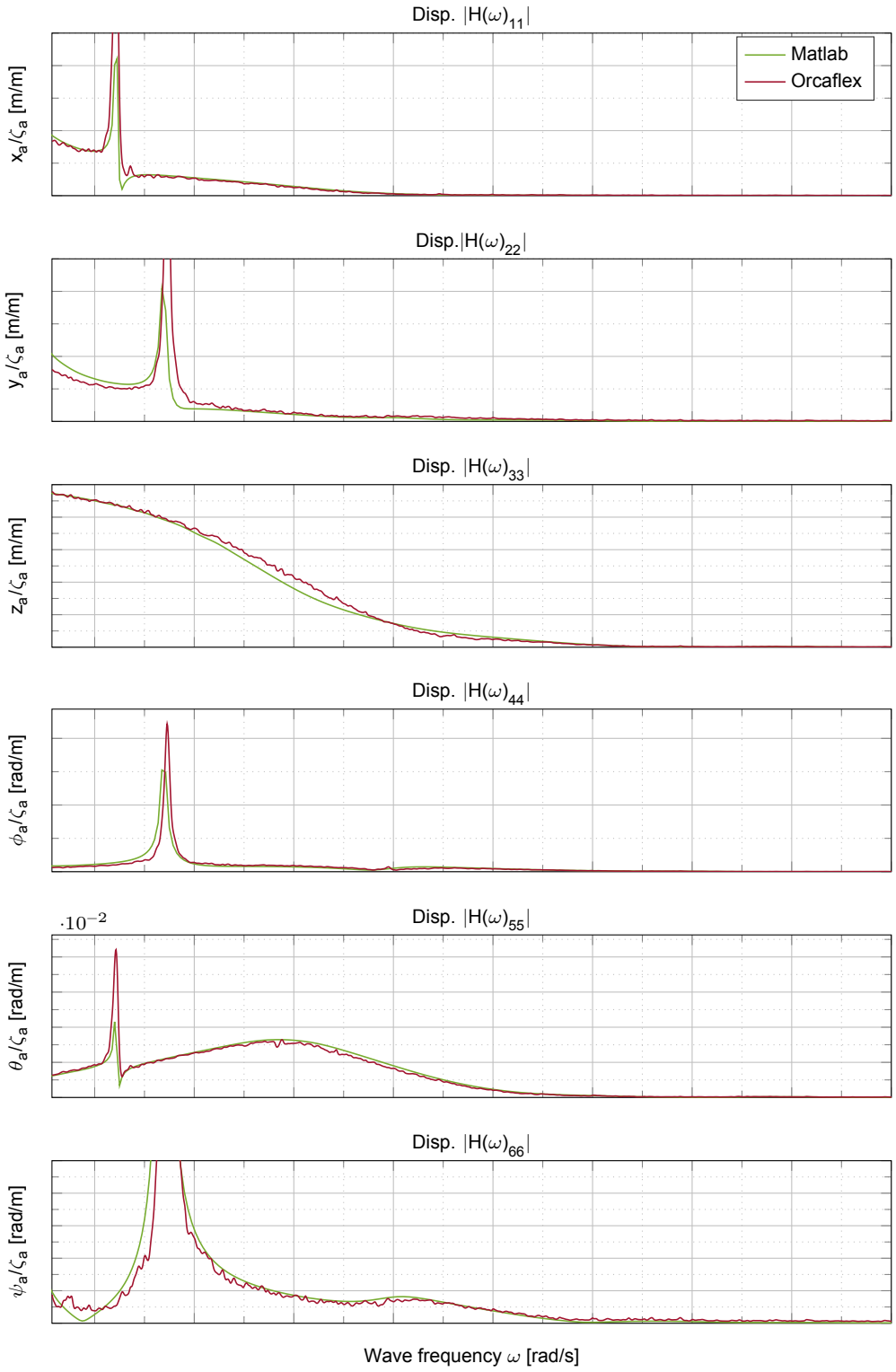

Figure B.15: Displacement RAOs - Starboard Quartering Waves
Case: CE Lift

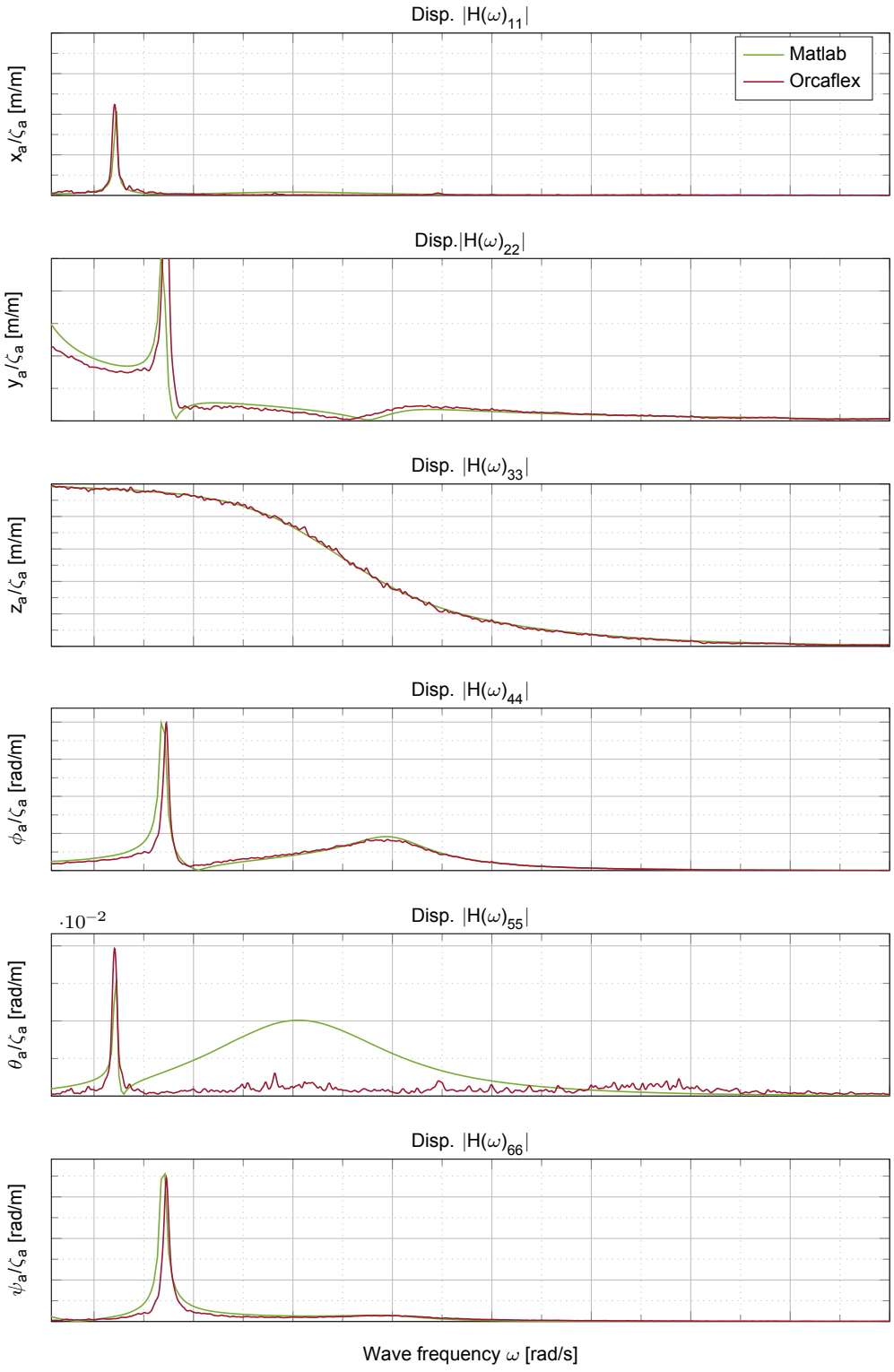

Figure B.16: Displacement RAOs - Starboard Beam Waves
Case: CE Lift

B.1.4. Single Crane Lift - PS

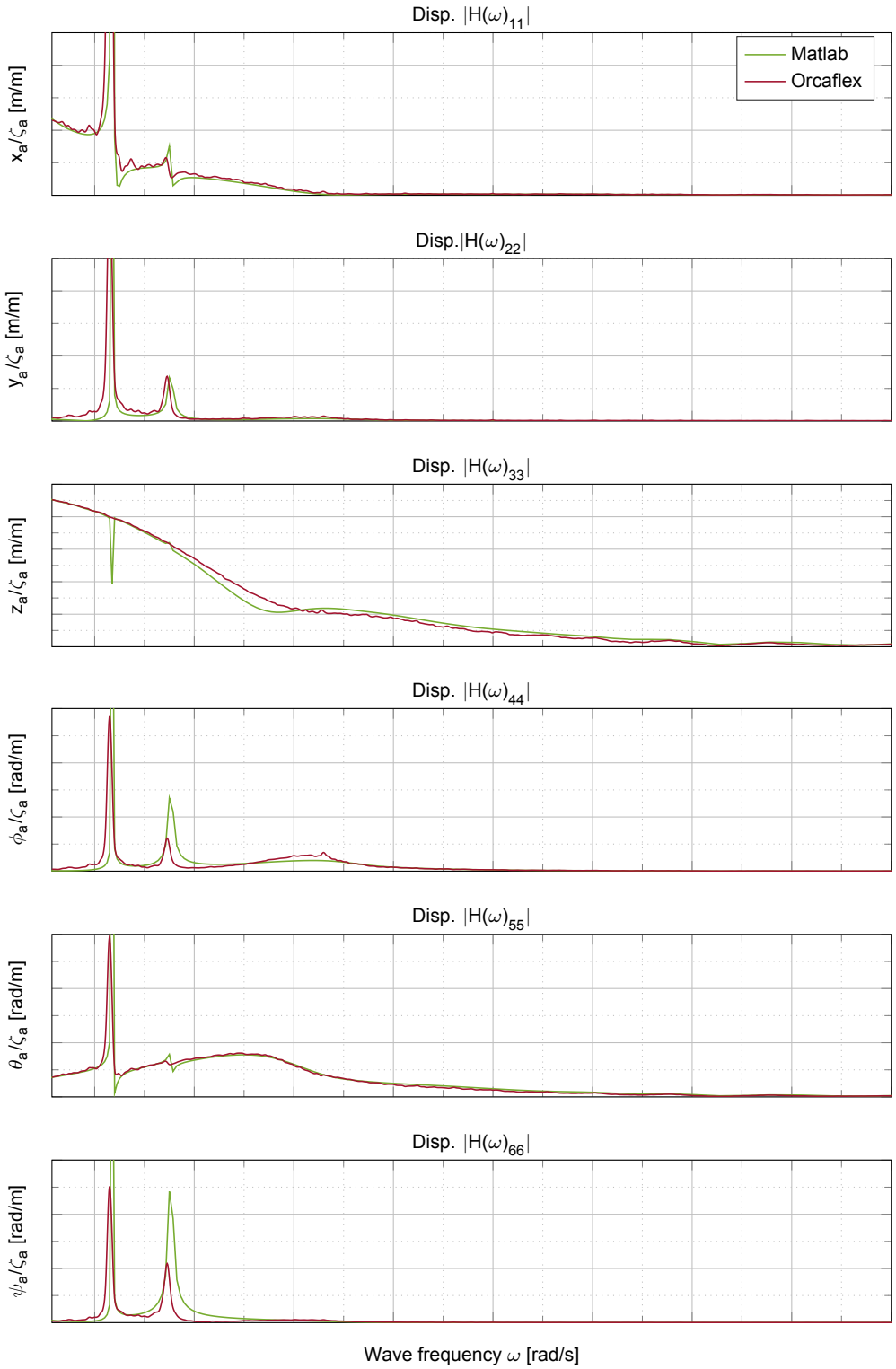

Figure B.17: Displacement RAOs - Stern Waves
Case: PS Lift

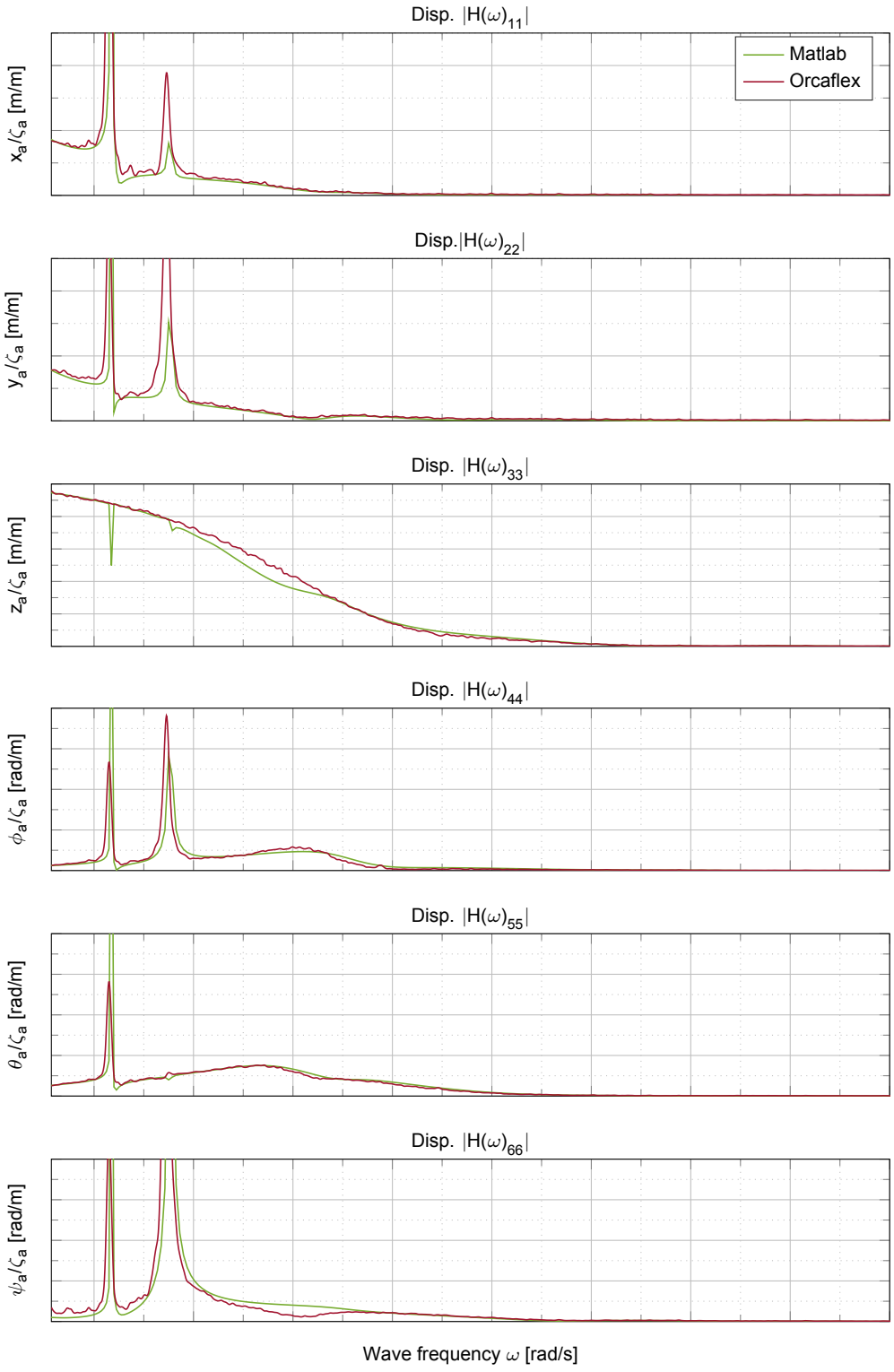

Figure B.18: Displacement RAOs - Starboard Quartering Waves
Case: PS Lift

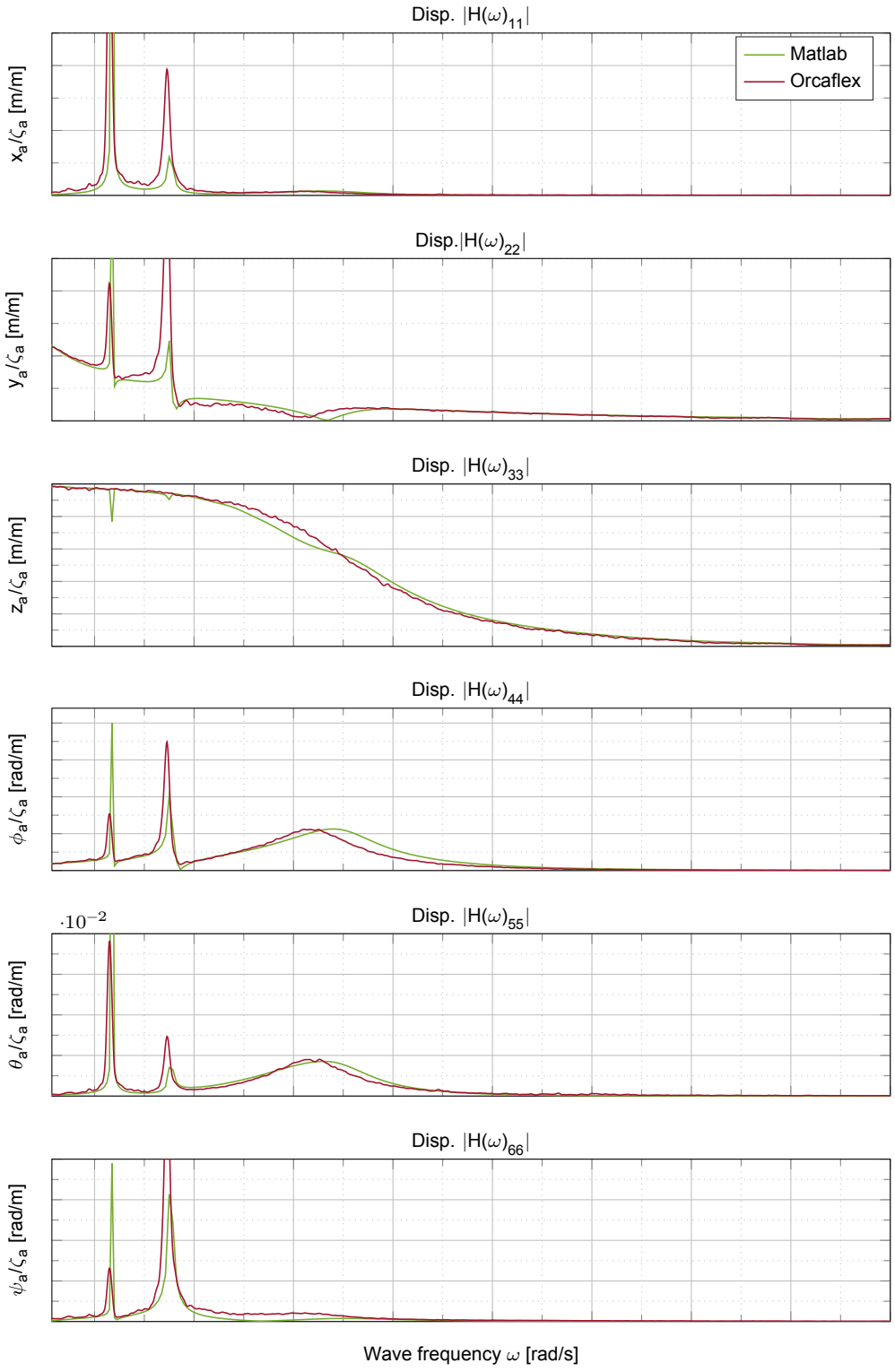

Figure B.19: Displacement RAOs - Starboard Beam Waves
Case: PS Lift

B.2. Cargo motion ROAs

In this section cargo or suspended load motion RAOs are given for motions $\eta_{7,8,9}$ obtained from the static and dynamic motion analysis in order to determine the limitations of a static analysis.

B.2.1. Single Crane Lift - MID

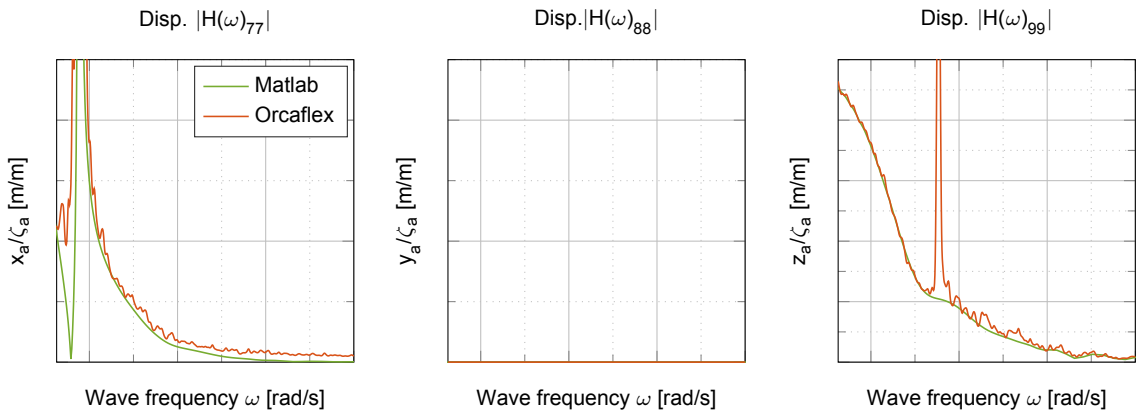

Figure B.20: Displacement RAOs - Stern Waves - Case: MID Lift - wo rigging (3DOF)

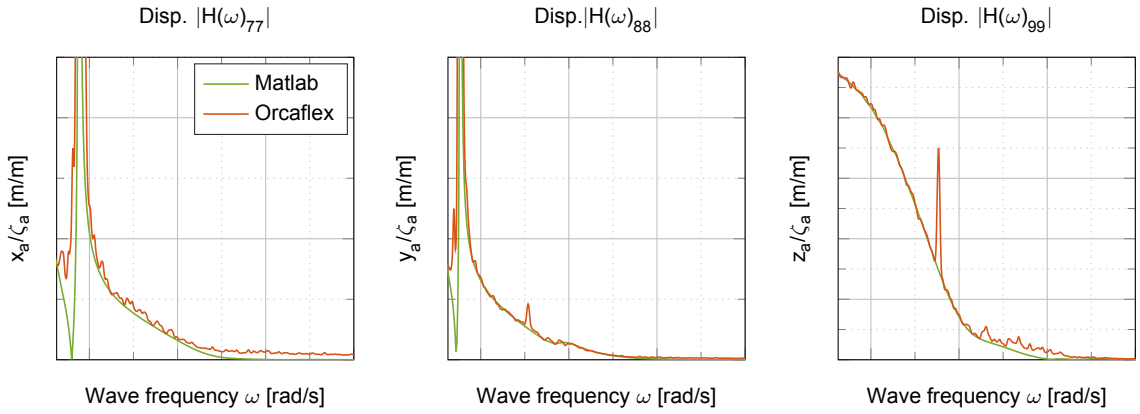

Figure B.21: Displacement RAOs - Stern Q Waves - Case: MID Lift - wo rigging (3DOF)

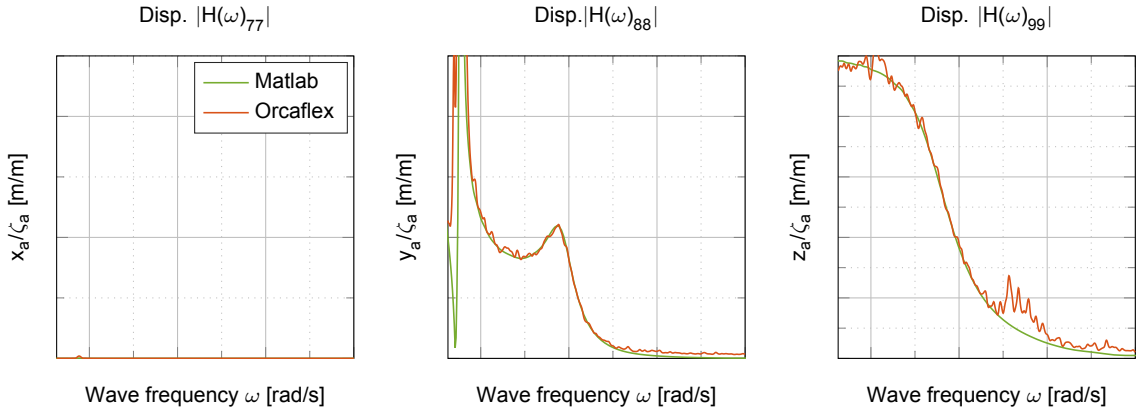

Figure B.22: Displacement RAOs - Beam Waves - Case: MID Lift - wo rigging (3DOF)

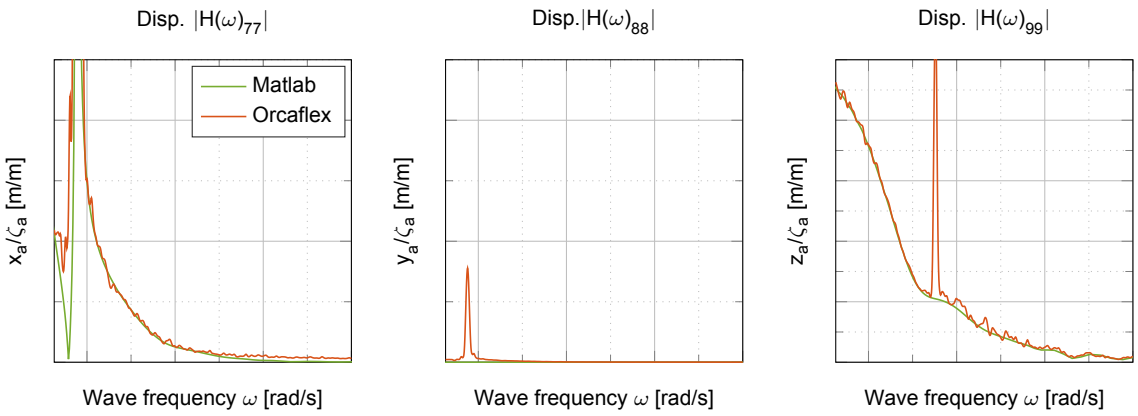

Figure B.23: Displacement RAOs - Stern Waves
Case: MID Lift - w rigging (6DOF)

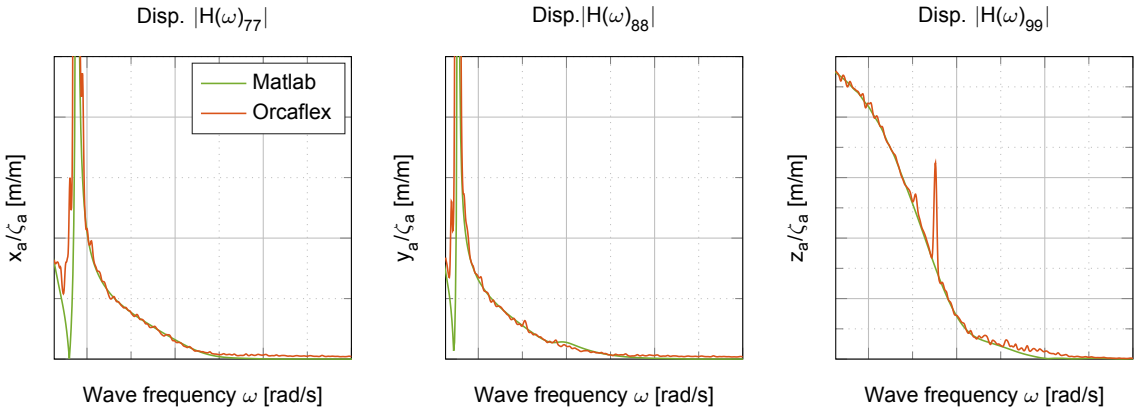

Figure B.24: Displacement RAOs - Stern Q Waves
Case: MID Lift - w rigging (6DOF)

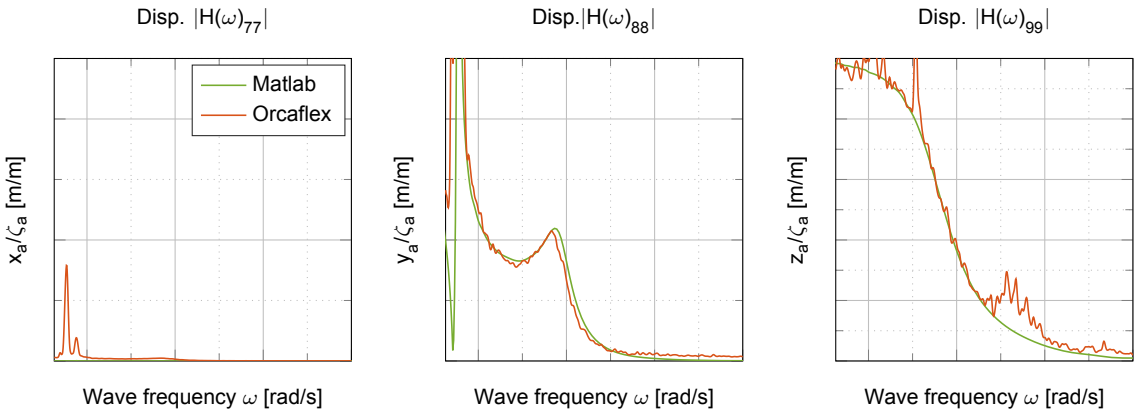

Figure B.25: Displacement RAOs - Beam Waves
Case: MID Lift - w rigging (6DOF)

B.2.2. Single Crane Lift - PS

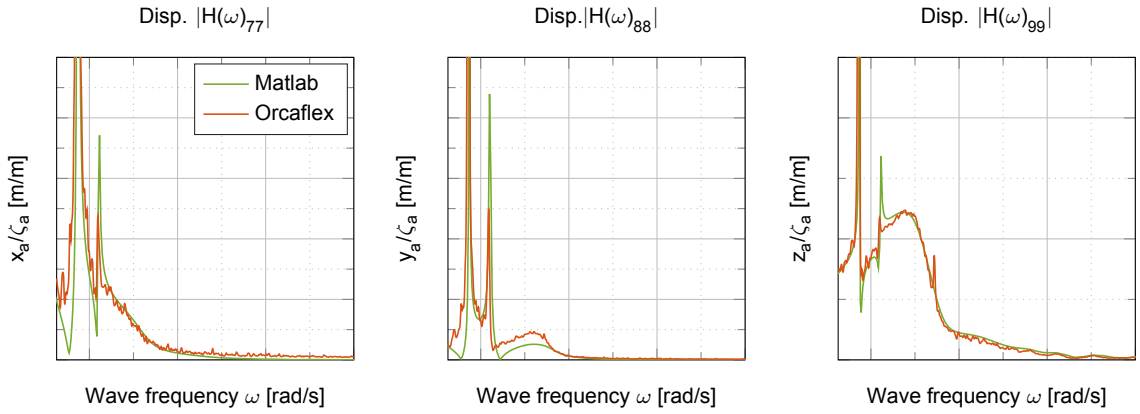

Figure B.26: Displacement RAOs - Stern Waves
Case: PS Lift

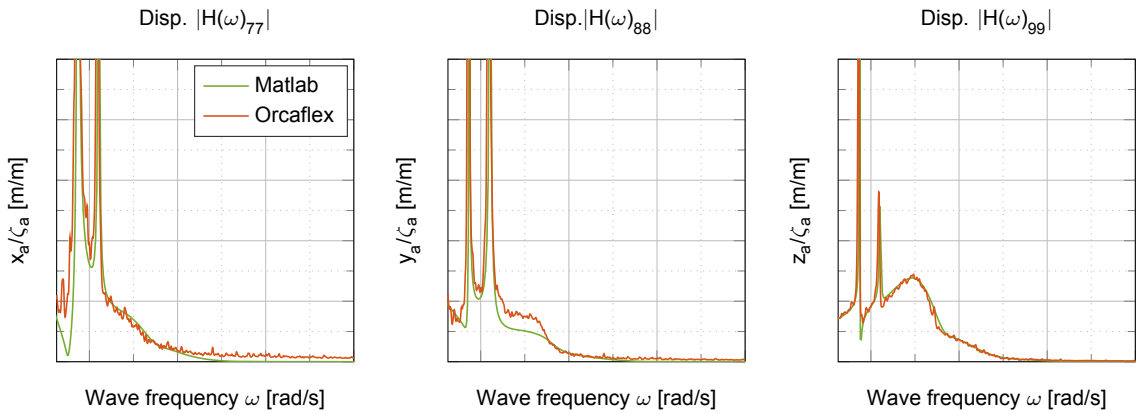

Figure B.27: Displacement RAOs - Stern Q Waves
Case: PS Lift

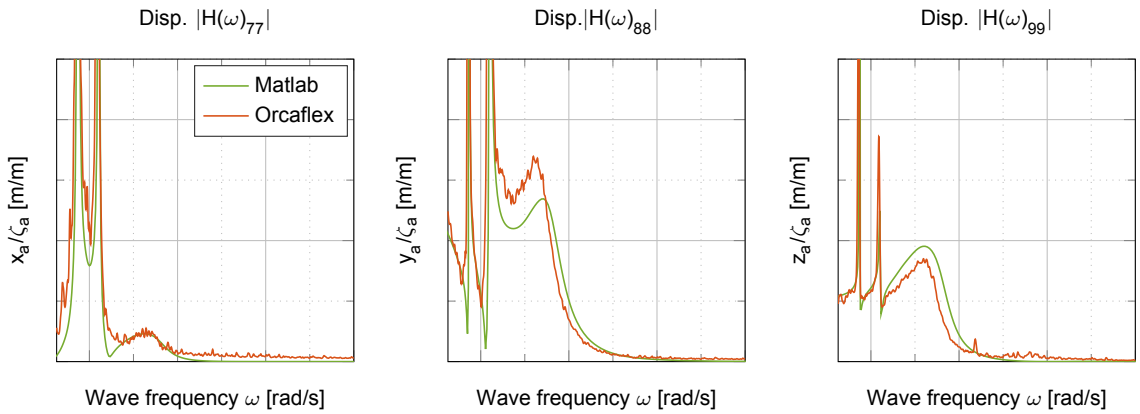

Figure B.28: Displacement RAOs - Beam Waves
Case: PS Lift

B.3. Sinusoidal wave induced response

All results are given in degrees. Wave height was 0.75m. Or = Orcaflex, Ma = Matlab, Er = difference between Matlab and Orcaflex.

B.3.1. Single Crane Lift - MID

Table B.1: Sinusoidal wave induces vessel response. Lift conducted at midship (z_{ct} only) without rigging.

						Without rigging							
Tp	3.00	4.00	4.81	5.21	5.69	6.31	7.02	7.33	7.78	8.91	10.43	12.57	15.71
WDir:0	Roll												
Or	0.00	0.00	0.00	0.00	0.00	0.00	0.00	0.00	0.00	0.00	0.00	0.00	0.00
Ma	0.00	0.00	0.00	0.00	0.00	0.00	0.00	0.00	0.00	0.00	0.00	0.00	0.00
Er	0.00	0.00	0.00	0.00	0.00	0.00	0.00	0.00	0.00	0.00	0.00	0.00	0.00
WDir:45	Roll												
Or	0.00	0.03	0.09	0.15	0.23	0.34	0.33	0.35	0.38	0.42	0.40	0.34	0.12
Ma	0.01	0.04	0.10	0.16	0.26	0.36	0.31	0.34	0.38	0.41	0.39	0.33	0.07
Er	0.00	0.01	0.01	0.01	0.03	0.02	-0.01	-0.01	-0.01	-0.01	-0.01	-0.01	-0.05
WDir:90	Roll												
Or	0.00	0.05	0.20	0.38	0.77	1.90	2.06	1.71	1.38	0.96	0.72	0.53	0.14
Ma	0.01	0.07	0.22	0.41	0.84	2.01	1.97	1.65	1.35	0.95	0.71	0.52	0.01
Er	0.00	0.01	0.02	0.03	0.07	0.11	-0.09	-0.06	-0.03	-0.01	-0.01	-0.01	-0.12
WDir:0	Pitch												
Or	0.02	0.07	0.16	0.22	0.28	0.32	0.41	0.45	0.52	0.60	0.60	0.52	0.54
Ma	0.04	0.09	0.17	0.24	0.30	0.33	0.41	0.46	0.52	0.60	0.59	0.51	0.51
Er	0.02	0.02	0.01	0.01	0.02	0.00	0.00	0.00	0.00	0.00	0.00	-0.01	-0.04
WDir:45	Pitch												
Or	0.00	0.00	0.05	0.12	0.25	0.43	0.52	0.54	0.55	0.53	0.47	0.40	0.39
Ma	0.00	0.01	0.05	0.13	0.27	0.43	0.52	0.54	0.54	0.52	0.47	0.38	0.36
Er	0.00	0.00	0.00	0.01	0.01	0.00	0.00	0.00	0.00	0.00	0.00	-0.01	-0.03
WDir:90	Pitch												
Or	0.00	0.00	0.00	0.00	0.00	0.00	0.00	0.00	0.00	0.00	0.00	0.00	0.00
Ma	0.00	0.00	0.00	0.00	0.00	0.00	0.00	0.00	0.00	0.00	0.00	0.00	0.00
Er	0.00	0.00	0.00	0.00	0.00	0.00	0.00	0.00	0.00	0.00	0.00	0.00	0.00

Table B.2: Sinusoidal wave induces vessel response. Lift conducted at midship (z_{ct} only) with rigging.

						With rigging						
Tp	3.00	4.00	4.81	5.21	5.69	6.31	7.02	7.33	7.78	8.91	10.43	12.57	15.71
WDir:0	Roll												
Or	0.00	0.00	0.00	0.00	0.00	0.00	0.00	0.00	0.00	0.00	0.00	0.00	0.00
Ma	0.00	0.00	0.00	0.00	0.00	0.00	0.00	0.00	0.00	0.00	0.00	0.00	0.00
Er	0.00	0.00	0.00	0.00	0.00	0.00	0.00	0.00	0.00	0.00	0.00	0.00	0.00
WDir:45	Roll												
Or	0.00	0.03	0.09	0.14	0.22	0.33	0.35	0.37	0.40	0.43	0.41	0.35	0.08
Ma	0.01	0.04	0.10	0.16	0.26	0.36	0.31	0.34	0.38	0.41	0.39	0.33	0.07
Er	0.00	0.01	0.01	0.02	0.04	0.03	-0.04	-0.03	-0.03	-0.02	-0.01	-0.02	-0.01
WDir:90	Roll												
Or	0.01	0.05	0.19	0.36	0.73	1.84	2.19	1.84	1.45	1.00	0.74	0.55	0.12
Ma	0.01	0.07	0.22	0.41	0.84	2.01	1.97	1.65	1.35	0.95	0.71	0.52	0.01
Er	0.00	0.02	0.03	0.05	0.11	0.18	-0.22	-0.19	-0.11	-0.04	-0.03	-0.03	-0.11
WDir:0	Pitch												
Or	0.03	0.07	0.16	0.23	0.28	0.33	0.41	0.45	0.52	0.60	0.60	0.53	0.50
Ma	0.04	0.09	0.17	0.24	0.30	0.33	0.41	0.46	0.52	0.60	0.59	0.51	0.51
Er	0.02	0.02	0.00	0.01	0.02	0.00	0.00	0.00	0.00	0.00	-0.01	-0.03	0.00
WDir:45	Pitch												
Or	0.00	0.00	0.05	0.12	0.26	0.43	0.52	0.54	0.55	0.53	0.47	0.40	0.36
Ma	0.00	0.01	0.05	0.13	0.27	0.43	0.52	0.54	0.54	0.52	0.47	0.38	0.36
Er	0.00	0.00	0.00	0.00	0.01	0.00	0.00	0.00	0.00	0.00	-0.01	-0.02	0.00
WDir:90	Pitch												
Or	0.00	0.00	0.00	0.00	0.00	0.00	0.00	0.00	0.00	0.00	0.00	0.00	0.00
Ma	0.00	0.00	0.00	0.00	0.00	0.00	0.00	0.00	0.00	0.00	0.00	0.00	0.00
Er	0.00	0.00	0.00	0.00	0.00	0.00	0.00	0.00	0.00	0.00	0.00	0.00	0.00

B.3.2. Single Crane Lift - Bow Centre

Table B.3: Sinusoidal wave induces vessel response. Lift conducted at Bow Centre (z_{ct} and x_{ct} only) with rigging.

Tp	3.00	4.00	4.81	5.21	5.69	6.31	7.02	7.33	7.78	8.91	10.43	12.57	15.71
WDir:0	Roll												
Or	0.00	0.00	0.00	0.00	0.00	0.00	0.00	0.00	0.00	0.00	0.00	0.00	0.00
Ma	0.00	0.00	0.00	0.00	0.00	0.00	0.00	0.00	0.00	0.00	0.00	0.00	0.00
Er	0.00	0.00	0.00	0.00	0.00	0.00	0.00	0.00	0.00	0.00	0.00	0.00	0.00
WDir:45	Roll												
Or	0.00	0.03	0.12	0.19	0.24	0.10	0.26	0.32	0.37	0.42	0.57	0.75	1.52
Ma	0.01	0.03	0.11	0.19	0.27	0.21	0.23	0.30	0.36	0.42	0.67	0.68	0.37
Er	0.00	0.00	-0.01	0.00	0.03	0.11	-0.04	-0.02	-0.02	-0.01	0.10	-0.07	-1.15
WDir:90	Roll												
Or	0.00	0.07	0.24	0.46	0.94	1.79	1.40	1.20	0.99	0.67	0.22	1.01	2.33
Ma	0.01	0.07	0.22	0.42	0.89	2.03	1.67	1.39	1.12	0.72	0.16	0.97	0.56
Er	0.00	0.00	-0.02	-0.03	-0.05	0.25	0.27	0.20	0.13	0.05	-0.06	-0.05	-1.76
WDir:0	Pitch												
Or	0.02	0.05	0.11	0.16	0.20	0.27	0.43	0.51	0.63	0.75	0.69	0.55	0.57
Ma	0.03	0.07	0.13	0.18	0.24	0.30	0.44	0.51	0.62	0.74	0.69	0.54	0.54
Er	0.01	0.02	0.02	0.02	0.04	0.03	0.01	0.00	-0.01	-0.01	0.00	-0.01	-0.03
WDir:45	Pitch												
Or	0.00	0.00	0.04	0.08	0.18	0.36	0.55	0.61	0.66	0.66	0.55	0.42	0.42
Ma	0.00	0.00	0.04	0.09	0.21	0.40	0.58	0.65	0.70	0.68	0.55	0.41	0.39
Er	0.00	0.00	0.01	0.01	0.03	0.03	0.04	0.04	0.03	0.02	0.00	0.00	-0.03
WDir:90	Pitch												
Or	0.00	0.00	0.00	0.00	0.00	0.01	0.01	0.01	0.01	0.00	0.01	0.00	0.04
Ma	0.00	0.00	0.01	0.02	0.04	0.06	0.09	0.10	0.11	0.09	0.05	0.02	0.02
Er	0.00	0.00	0.01	0.02	0.03	0.06	0.09	0.10	0.10	0.08	0.04	0.02	-0.02

B.3.3. Single Crane Lift - PS

Table B.4: Sinusoidal wave induces vessel response. Lift conducted at Bow PS, full coupling with rigging.

Tp	3.00	4.00	4.81	5.21	5.69	6.31	7.02	7.33	7.78	8.91	10.43	12.57	15.71
WDir:0	Roll												
Or	0.01	0.01	0.03	0.05	0.07	0.14	0.38	0.64	0.61	0.30	0.13	0.11	0.26
Ma	0.00	0.01	0.03	0.05	0.08	0.16	0.37	0.42	0.41	0.31	0.33	0.23	0.07
Er	0.00	0.00	0.00	0.00	0.01	0.02	-0.01	-0.23	-0.20	0.00	0.20	0.11	-0.19
WDir:45	Roll												
Or	0.00	0.02	0.05	0.07	0.08	0.07	0.53	1.63	1.21	0.88	0.65	0.62	1.81
Ma	0.00	0.03	0.08	0.12	0.15	0.20	0.77	0.95	1.00	0.82	0.81	0.49	0.44
Er	0.00	0.01	0.03	0.05	0.07	0.14	0.24	-0.68	-0.21	-0.06	0.16	-0.13	-1.37
WDir:90	Roll												
Or	0.01	0.03	0.11	0.20	0.36	0.77	1.76	2.24	2.21	1.21	0.52	0.97	2.05
Ma	0.00	0.06	0.18	0.31	0.58	1.28	2.39	2.36	1.96	1.16	0.53	0.85	0.60
Er	0.00	0.03	0.07	0.11	0.22	0.51	0.63	0.12	-0.25	-0.06	0.01	-0.12	-1.46
WDir:0	Pitch												
Or	0.02	0.04	0.09	0.13	0.17	0.24	0.37	0.46	0.58	0.87	0.77	0.61	0.61
Ma	0.03	0.06	0.11	0.16	0.22	0.27	0.36	0.45	0.62	0.83	0.73	0.59	0.57
Er	0.01	0.02	0.02	0.03	0.04	0.03	-0.01	-0.01	0.04	-0.04	-0.04	-0.02	-0.05
WDir:45	Pitch												
Or	0.00	0.00	0.03	0.07	0.16	0.32	0.44	0.62	0.61	0.81	0.64	0.44	0.57
Ma	0.00	0.00	0.04	0.09	0.20	0.38	0.45	0.52	0.69	0.79	0.62	0.43	0.43
Er	0.00	0.00	0.01	0.02	0.04	0.06	0.00	-0.09	0.08	-0.02	-0.02	0.00	-0.14
WDir:90	Pitch												
Or	0.00	0.00	0.01	0.02	0.04	0.10	0.26	0.35	0.34	0.15	0.07	0.04	0.18
Ma	0.00	0.00	0.01	0.02	0.05	0.14	0.34	0.37	0.33	0.18	0.09	0.03	0.04
Er	0.00	0.00	0.00	0.00	0.01	0.04	0.08	0.02	-0.02	0.03	0.02	-0.01	-0.13

B.3.4. Linear Response

The red colored values indicate scenarios for which the difference in vessel motion response with respect to the previous increment does not increase with the same magnitude any more. This would imply that the response is not linear any more and thus that vessel motion response during heavy lift operations cannot be computed accurate if these are determined in frequency domain. However the irregular increments in vessel motions response does come from the modeled mooring systems. The system was modeled stiff enough to affect the first order motions. This is a modeling error and not representative for reality.

Table B.5: Sinusoidal wave induces roll response for different wave heights and periods.
Starboard beam waves. PS lift 1250 ton, 14m outreach, 30m high suspended

	T_p												
H_{m0}	3.00	4.00	4.81	5.21	5.69	6.31	7.02	7.33	7.78	8.91	10.43	12.57	15.71
0.50	0.00	0.02	0.07	0.13	0.24	0.51	1.17	1.50	1.51	0.82	0.35	0.64	0.39
0.75	0.01	0.03	0.11	0.20	0.36	0.77	1.76	2.24	2.22	1.21	0.52	0.97	3.90
1.00	0.01	0.04	0.14	0.26	0.48	1.06	2.36	3.51	2.94	1.57	0.69	1.29	5.50
1.25	0.01	0.04	0.18	0.33	0.62	2.94	2.97	4.84	5.61	4.94	0.91	1.89	6.84
1.50	0.01	0.05	0.21	0.39	1.77	3.31	3.45	5.84	6.95	6.93	1.66	6.08	9.85
1.75	0.01	0.06	0.25	0.46	3.01	3.35	6.45	5.68	7.56	7.54	2.04	4.84	11.53
2.00	0.01	0.07	0.28	0.67	2.76	4.45	6.52	8.24	8.65	8.73	2.48	4.99	11.68

Table B.6: Difference in roll amplitude per wave height increment.
It illustrates linear response until the increments in roll amplitude becomes larger than its previous increment

H_{m0}	T_p												
Increment	3.00	4.00	4.81	5.21	5.69	6.31	7.02	7.33	7.78	8.91	10.43	12.57	15.71
0.75-0.50	0.00	0.01	0.04	0.06	0.12	0.26	0.59	0.74	0.70	0.39	0.17	0.32	3.51
1.00-0.75	0.00	0.01	0.04	0.06	0.12	0.29	0.60	1.27	0.72	0.36	0.17	0.33	1.61
1.25-1.00	0.00	0.01	0.04	0.06	0.14	1.88	0.61	1.33	2.67	3.36	0.23	0.60	1.34
1.50-1.25	0.00	0.01	0.03	0.07	1.15	0.37	0.48	0.99	1.34	1.99	0.75	4.19	3.01
1.75-1.50	0.00	0.01	0.03	0.07	1.23	0.04	3.00	-0.16	0.61	0.61	0.38	-1.24	1.68
2.00-1.75	0.00	0.01	0.04	0.20	-0.24	1.10	0.07	2.56	1.09	1.18	0.44	0.15	0.15

C

Results Sensitivity Analysis

C.1. Model Input Parameters

In the table given below is summarized for which model input parameters the sensitivity on vessel motion response is tested. The sensitivity was tested on heave acceleration, roll and pitch motion of the crane tip for incoming stern, starboard quartering and starboard beam waves. The significant wave height was fixed at 1m and results are given for wave periods of 2,4,6,8 and 10 seconds. Responses for the base case are given in degrees and relates to the significant response or in other words the root mean square of the response. The sensitivity of the parameter on this response is given in percentages.

Table C.1: Sensitivity Analysis: Deviation in model input parameters for the vessel and load composition

		Quantity			
Parameter	Symbol	Base	Less	More	Unit
Mass Load	m_L	1217	-2%	2%	ton
Mass Ship	M	9967	-5% ballast	+5% ballast	ton
Mass Booms	M_{B1}	226	-5%	5%	ton
	M_{B2}	215	-5%	5%	ton
Radii of Gyration Ship	kxx	0.34	-0.01	0.01	-
	kyy	0.25	-0.01	0.01	-
	kzz	0.26	-0.01	0.01	-
Inertia Booms	$I_{BG1}(xx)$	139.59E+3	-5%	5%	ton.m^2
	$I_{BG1}(yy)$	139.59E+03	-5%	5%	ton.m^2
	$I_{BG1}(zz)$	602.67	-5%	5%	ton.m^2
	$I_{BG2}(xx)$	132.80E+3	-5%	5%	ton.m^2
	$I_{BG2}(yy)$	13280E+3	-5%	5%	ton.m^2
	$I_{BG2}(zz)$	573.33	-5%	5%	ton.m^2
Centre of gravity ship	Gx	42.50	-1.0	1.0	m
	Gy	0.00	-0.5	0.5	m
	Gz	10.00	-1,0	1.0	m
Centre of gravity Boom	$CB_{1,2}(z)$	43.00	-3	6	m
Mooring Stiffness	C_{cm}	80.00	-25%	25%	kN
Outreach crane	X_{out1}	16.00	-1	1	m
	X_{out2}	8.00	-1	1	m
Length hoisting rope	l_s	52.50	-1	1	m
Axial wire stiffness	AE	1.98E+09	-5%	5%	kN

C.1.1. Mass suspended Load

Table C.2: Sensitivity Analysis: Mass suspended load (m_L)

Stern Waves		Wave period				
Motion	Case	2	4	6	8	10
Heave Acc.	Less	0.47%	0.59%	0.49%	-0.11%	-0.22%
	Base	0.033	0.120	0.244	0.455	0.434
	More	-0.47%	-0.58%	-0.48%	0.10%	0.21%
Roll deg.	Less	-1.56%	-1.82%	-1.25%	-0.62%	-2.63%
	Base	0.001	0.020	0.190	0.381	0.535
	More	1.54%	1.82%	1.22%	0.57%	2.64%
Pitch deg.	Less	0.25%	0.29%	0.25%	-0.08%	-0.13%
	Base	0.006	0.080	0.332	0.745	0.884
	More	-0.25%	-0.29%	-0.25%	0.07%	0.14%

Stern Q Waves		Wave period				
Motion	Case	2	4	6	8	10
Heave Acc.	Less	0.48%	0.69%	0.64%	0.08%	0.01%
	Base	0.003	0.046	0.306	0.578	0.482
	More	-0.47%	-0.68%	-0.63%	-0.08%	-0.01%
Roll deg.	Less	0.11%	-0.60%	-1.01%	0.09%	-1.40%
	Base	0.000	0.041	0.387	0.921	1.261
	More	-0.11%	0.63%	1.01%	-0.11%	1.36%
Pitch deg.	Less	0.30%	0.16%	0.20%	-0.14%	-0.27%
	Base	0.001	0.037	0.381	0.781	0.820
	More	-0.30%	-0.16%	-0.21%	0.14%	0.27%

Beam Waves		Wave period				
Motion	Case	2	4	6	8	10
Heave Acc.	Less	0.57%	-0.59%	-0.03%	0.76%	0.42%
	Base	0.005	0.012	0.216	0.438	0.328
	More	-0.56%	0.61%	0.01%	-0.77%	-0.42%
Roll deg.	Less	0.23%	-0.54%	0.12%	1.40%	-1.17%
	Base	0.001	0.119	1.227	1.901	1.930
	More	-0.22%	0.55%	-0.12%	-1.39%	1.22%
Pitch deg.	Less	-1.37%	-3.11%	-2.06%	-1.42%	-2.66%
	Base	0.000	0.005	0.128	0.269	0.262
	More	1.36%	3.18%	2.05%	1.38%	2.68%

C.1.2. Mass Ship

Table C.3: Sensitivity Analysis: Mass Ship (M)

Stern Waves		Wave period				
Motion	Case	2	4	6	8	10
Heave Acc.	Less	0.38%	0.55%	0.43%	-0.08%	-0.27%
	Base	0.033	0.120	0.244	0.455	0.434
	More	-0.39%	-0.54%	-0.43%	0.07%	0.25%
Roll deg.	Less	1.34%	**2.40%**	0.73%	-0.31%	**5.94%**
	Base	0.001	0.020	0.190	0.381	0.535
	More	-1.32%	**-2.32%**	-0.71%	1.00%	**2.37%**
Pitch deg.	Less	0.45%	0.69%	0.30%	-0.19%	-0.28%
	Base	0.006	0.080	0.332	0.745	0.884
	More	-0.45%	-0.69%	-0.30%	0.21%	0.64%

Stern Q Waves		Wave period				
Motion	Case	2	4	6	8	10
Heave Acc.	Less	0.41%	0.75%	0.44%	-0.06%	0.06%
	Base	0.003	0.046	0.306	0.578	0.482
	More	-0.41%	-0.75%	-0.45%	0.06%	0.43%
Roll deg.	Less	0.90%	1.80%	0.62%	0.48%	**9.69%**
	Base	0.000	0.041	0.387	0.921	1.261
	More	-0.88%	-1.73%	-0.58%	0.39%	-1.50%
Pitch deg.	Less	0.43%	0.92%	0.44%	-0.10%	-0.39%
	Base	0.001	0.037	0.381	0.781	0.820
	More	-0.43%	-0.90%	-0.44%	0.07%	0.39%

Beam Waves		Wave period				
Motion	Case	2	4	6	8	10
Heave Acc.	Less	0.57%	3.11%	1.73%	-0.26%	0.37%
	Base	0.005	0.012	0.216	0.438	0.328
	More	-0.56%	**-2.89%**	-1.70%	0.27%	0.39%
Roll deg.	Less	0.98%	1.92%	0.81%	-0.64%	**7.20%**
	Base	0.001	0.119	1.227	1.901	1.930
	More	-0.96%	-1.86%	-0.81%	1.08%	0.65%
Pitch deg.	Less	1.13%	**4.52%**	1.52%	-0.20%	**4.39%**
	Base	0.000	0.005	0.128	0.269	0.262
	More	-1.11%	**-4.31%**	-1.49%	0.40%	1.11%

C.1.3. Mass Booms

Table C.4: Sensitivity Analysis: Mass Booms ($MB_{1,2}$)

Stern Waves		Wave period				
Motion	Case	2	4	6	8	10
Heave Acc.	Less	0.46%	0.59%	0.49%	-0.03%	-0.20%
	Base	0.033	0.120	0.244	0.455	0.434
	More	-0.46%	-0.59%	-0.49%	0.02%	0.20%
Roll deg.	Less	1.43%	2.58%	0.76%	-1.23%	1.95%
	Base	0.001	0.020	0.190	0.381	0.535
	More	-1.40%	-2.48%	-0.73%	1.35%	-1.09%
Pitch deg.	Less	0.41%	0.58%	0.24%	-0.14%	-0.31%
	Base	0.006	0.080	0.332	0.745	0.884
	More	-0.41%	-0.57%	-0.25%	0.14%	0.33%

Stern Q Waves		Wave period				
Motion	Case	2	4	6	8	10
Heave Acc.	Less	0.46%	0.77%	0.52%	0.03%	-0.12%
	Base	0.003	0.046	0.306	0.578	0.482
	More	-0.45%	-0.76%	-0.52%	-0.04%	0.16%
Roll deg.	Less	0.92%	1.72%	0.01%	-1.14%	2.99%
	Base	0.000	0.041	0.387	0.921	1.261
	More	-0.91%	-1.67%	-0.01%	1.27%	-2.01%
Pitch deg.	Less	0.40%	0.71%	0.33%	0.00%	-0.22%
	Base	0.001	0.037	0.381	0.781	0.820
	More	-0.40%	-0.70%	-0.33%	-0.01%	0.21%

Beam Waves		Wave period				
Motion	Case	2	4	6	8	10
Heave Acc.	Less	0.34%	4.24%	2.28%	-0.14%	0.12%
	Base	0.005	0.012	0.216	0.438	0.328
	More	-0.34%	-3.89%	-2.23%	0.12%	-0.04%
Roll deg.	Less	0.91%	1.97%	0.99%	-1.16%	2.42%
	Base	0.001	0.119	1.227	1.901	1.930
	More	-0.90%	-1.90%	-0.98%	1.22%	-1.45%
Pitch deg.	Less	0.75%	5.61%	2.01%	-0.23%	1.69%
	Base	0.000	0.005	0.128	0.269	0.262
	More	-0.73%	-5.33%	-1.97%	0.24%	-1.13%

C.1.4. Radii of Gyration Ship

Table C.5: Sensitivity Analysis: Radii of Gyration (kxx, kyy, kzz)

Stern Waves		Wave period				
Motion	Case	2	4	6	8	10
Heave Acc.	Less	1.91%	**2.47%**	1.91%	-0.14%	-0.57%
	Base	0.033	0.120	0.244	0.455	0.434
	More	-1.93%	**-2.48%**	-1.97%	0.09%	0.66%
Roll deg.	Less	**4.09%**	**7.01%**	**2.82%**	-1.38%	**2.02%**
	Base	0.001	0.020	0.190	0.381	0.535
	More	**-4.00%**	**-6.60%**	**-2.65%**	**2.17%**	**3.99%**
Pitch deg.	Less	1.56%	2.18%	0.96%	-0.69%	-1.16%
	Base	0.006	0.080	0.332	0.745	0.884
	More	-1.58%	-2.19%	-1.02%	0.69%	1.33%

Stern Q Waves		Wave period				
Motion	Case	2	4	6	8	10
Heave Acc.	Less	1.72%	**2.55%**	1.34%	-0.22%	-0.60%
	Base	0.003	0.046	0.306	0.578	0.482
	More	-1.74%	**-2.59%**	-1.50%	0.14%	0.88%
Roll deg.	Less	**2.01%**	**4.12%**	**2.75%**	0.15%	**7.96%**
	Base	0.000	0.041	0.387	0.921	1.261
	More	**-1.98%**	**-3.82%**	**-2.42%**	**1.02%**	-1.62%
Pitch deg.	Less	1.57%	**2.69%**	1.12%	-0.53%	-1.14%
	Base	0.001	0.037	0.381	0.781	0.820
	More	-1.58%	**-2.66%**	-1.20%	0.47%	1.16%

Beam Waves		Wave period				
Motion	Case	2	4	6	8	10
Heave Acc.	Less	0.54%	**9.31%**	**5.21%**	-0.12%	0.08%
	Base	0.005	0.012	0.216	0.438	0.328
	More	-0.53%	**-7.95%**	**-5.11%**	-0.04%	0.23%
Roll deg.	Less	**2.01%**	**4.08%**	1.86%	**-2.54%**	**3.64%**
	Base	0.001	0.119	1.227	1.901	1.930
	More	**-2.00%**	**-3.91%**	**-1.93%**	**2.93%**	1.84%
Pitch deg.	Less	2.30%	**12.56%**	**4.24%**	-0.75%	0.84%
	Base	0.000	0.005	0.128	0.269	0.262
	More	**-2.28%**	**-11.56%**	**-4.17%**	0.86%	2.85%

C.1.5. Inertia Booms

Table C.6: Sensitivity Analysis: Inertia Booms ($I_{BG1,2}(xx, yy, zz)$)

Stern Waves		Wave period				
Motion	Case	2	4	6	8	10
Heave Acc.	Less	0.07%	0.09%	0.08%	0.00%	-0.03%
	Base	0.033	0.120	0.244	0.455	0.434
	More	-0.07%	-0.09%	-0.08%	0.00%	0.03%
Roll deg.	Less	0.29%	0.50%	0.16%	-0.26%	0.03%
	Base	0.001	0.020	0.190	0.381	0.535
	More	-0.29%	-0.50%	-0.16%	0.26%	-0.03%
Pitch deg.	Less	0.07%	0.09%	0.04%	-0.02%	-0.05%
	Base	0.006	0.080	0.332	0.745	0.884
	More	-0.07%	-0.09%	-0.04%	0.02%	0.05%

Stern Q Waves		Wave period				
Motion	Case	2	4	6	8	10
Heave Acc.	Less	0.08%	0.14%	0.10%	0.02%	-0.01%
	Base	0.003	0.046	0.306	0.578	0.482
	More	-0.08%	-0.14%	-0.10%	-0.02%	0.01%
Roll deg.	Less	0.21%	0.35%	-0.02%	-0.28%	0.06%
	Base	0.000	0.041	0.387	0.921	1.261
	More	-0.21%	-0.35%	0.02%	0.28%	-0.06%
Pitch deg.	Less	0.06%	0.11%	0.05%	0.01%	-0.04%
	Base	0.001	0.037	0.381	0.781	0.820
	More	-0.06%	-0.11%	-0.05%	-0.01%	0.04%

Beam Waves		Wave period				
Motion	Case	2	4	6	8	10
Heave Acc.	Less	0.08%	0.87%	0.48%	0.01%	0.03%
	Base	0.005	0.012	0.216	0.438	0.328
	More	-0.07%	-0.85%	-0.48%	-0.01%	-0.03%
Roll deg.	Less	0.20%	0.41%	0.23%	-0.20%	0.04%
	Base	0.001	0.119	1.227	1.901	1.930
	More	-0.20%	-0.41%	-0.23%	0.20%	-0.03%
Pitch deg.	Less	0.14%	1.12%	0.40%	-0.05%	0.04%
	Base	0.000	0.005	0.128	0.269	0.262
	More	-0.14%	-1.11%	-0.40%	0.05%	-0.04%

C.1.6. Centre of Gravity Ship

Table C.7: Sensitivity Analysis: Centre of Gravity Ship ($G(x)$)

Stern Waves		Wave period				
Motion	Case	2	4	6	8	10
Heave Acc.	Less	1.29%	1.01%	1.17%	**2.01%**	**2.23%**
	Base	0.033	0.120	0.244	0.455	0.434
	More	-1.33%	-1.05%	-1.21%	-2.02%	**-2.23%**
Roll deg.	Less	1.27%	0.87%	0.99%	1.63%	**5.36%**
	Base	0.001	0.020	0.190	0.381	0.535
	More	-1.31%	-0.92%	-1.05%	-1.37%	**-2.25%**
Pitch deg.	Less	-0.71%	-0.96%	-0.56%	0.42%	0.70%
	Base	0.006	0.080	0.332	0.745	0.884
	More	0.71%	0.96%	0.55%	-0.41%	-0.57%

Stern Q Waves		Wave period				
Motion	Case	2	4	6	8	10
Heave Acc.	Less	0.96%	0.30%	0.72%	1.40%	1.80%
	Base	0.003	0.046	0.306	0.578	0.482
	More	-0.99%	-0.33%	-0.75%	-1.40%	-1.59%
Roll deg.	Less	-0.02%	0.45%	0.89%	1.27%	**7.66%**
	Base	0.000	0.041	0.387	0.921	1.261
	More	0.02%	-0.44%	-0.91%	-0.88%	**-4.00%**
Pitch deg.	Less	-0.77%	-0.93%	-0.56%	0.31%	0.58%
	Base	0.001	0.037	0.381	0.781	0.820
	More	0.77%	0.92%	0.55%	-0.33%	-0.67%

Beam Waves		Wave period				
Motion	Case	2	4	6	8	10
Heave Acc.	Less	-0.59%	-0.73%	-0.69%	-0.52%	0.24%
	Base	0.005	0.012	0.216	0.438	0.328
	More	0.59%	0.73%	0.66%	0.51%	0.10%
Roll deg.	Less	0.03%	0.05%	-0.21%	-0.29%	**6.75%**
	Base	0.001	0.119	1.227	1.901	1.930
	More	-0.03%	-0.05%	0.22%	0.53%	**-2.89%**
Pitch deg.	Less	0.86%	0.79%	1.00%	1.40%	**3.99%**
	Base	0.000	0.005	0.128	0.269	0.262
	More	-0.89%	-0.83%	-1.05%	-1.35%	-2.07%

Table C.8: Sensitivity Analysis: Centre of Gravity Ship ($G(y)$)

Stern Waves		Wave period				
Motion	Case	2	4	6	8	10
Heave Acc.	Less	-0.25%	-0.33%	-0.43%	0.38%	0.48%
	Base	0.033	0.120	0.244	0.455	0.434
	More	0.24%	0.32%	0.43%	-0.37%	-0.45%
Roll deg.	Less	**2.67%**	**2.47%**	**2.31%**	**3.30%**	**5.33%**
	Base	0.001	0.020	0.190	0.381	0.535
	More	**-2.70%**	**-2.51%**	**-2.36%**	**-3.18%**	**-3.96%**
Pitch deg.	Less	0.05%	0.10%	-0.11%	-0.12%	0.03%
	Base	0.006	0.080	0.332	0.745	0.884
	More	-0.05%	-0.10%	0.11%	0.12%	0.02%

Stern Q Waves		Wave period				
Motion	Case	2	4	6	8	10
Heave Acc.	Less	-0.01%	0.30%	-0.24%	0.66%	0.78%
	Base	0.003	0.046	0.306	0.578	0.482
	More	0.00%	-0.31%	0.23%	-0.64%	-0.69%
Roll deg.	Less	-0.38%	-0.37%	1.37%	1.84%	**3.34%**
	Base	0.000	0.041	0.387	0.921	1.261
	More	0.38%	0.36%	-1.39%	-1.74%	**-2.27%**
Pitch deg.	Less	0.01%	0.24%	-0.12%	-0.13%	0.17%
	Base	0.001	0.037	0.381	0.781	0.820
	More	-0.01%	-0.24%	0.11%	0.12%	-0.14%

Beam Waves		Wave period				
Motion	Case	2	4	6	8	10
Heave Acc.	Less	1.06%	**4.30%**	**2.69%**	**2.29%**	**2.04%**
	Base	0.005	0.012	0.216	0.438	0.328
	More	-1.07%	**-3.87%**	**-2.73%**	**-2.28%**	-1.91%
Roll deg.	Less	-0.33%	-0.34%	-0.55%	0.20%	**2.63%**
	Base	0.001	0.119	1.227	1.901	1.930
	More	0.32%	0.33%	0.53%	-0.15%	-1.62%
Pitch deg.	Less	1.23%	**6.07%**	**3.34%**	**3.01%**	**4.16%**
	Base	0.000	0.005	0.128	0.269	0.262
	More	-1.23%	**-6.01%**	**-3.39%**	**-2.97%**	**-3.24%**

Table C.9: Sensitivity Analysis: Centre of Gravity Ship ($G(z)$)

Stern Waves		Wave period				
Motion	Case	2	4	6	8	10
Heave Acc.	Less	-0.18%	-0.17%	-0.05%	-0.09%	-0.24%
	Base	0.033	0.120	0.244	0.455	0.434
	More	0.18%	0.16%	0.04%	0.08%	0.25%
Roll deg.	Less	-0.72%	-0.53%	-0.18%	-0.68%	0.07%
	Base	0.001	0.020	0.190	0.381	0.535
	More	0.71%	0.52%	0.18%	1.05%	**4.63%**
Pitch deg.	Less	-0.16%	-0.15%	-0.07%	-0.12%	-0.13%
	Base	0.006	0.080	0.332	0.745	0.884
	More	0.16%	0.14%	0.06%	0.13%	0.31%

Stern Q Waves		Wave period				
Motion	Case	2	4	6	8	10
Heave Acc.	Less	-0.19%	-0.24%	-0.12%	-0.13%	-0.23%
	Base	0.003	0.046	0.306	0.578	0.482
	More	0.18%	0.24%	0.12%	0.14%	0.49%
Roll deg.	Less	-0.52%	-0.29%	0.06%	-1.01%	**-3.35%**
	Base	0.000	0.041	0.387	0.921	1.261
	More	0.51%	0.28%	-0.06%	1.49%	**7.89%**
Pitch deg.	Less	-0.15%	-0.08%	-0.02%	-0.08%	-0.15%
	Base	0.001	0.037	0.381	0.781	0.820
	More	0.15%	0.07%	0.02%	0.07%	0.24%

Beam Waves		Wave period				
Motion	Case	2	4	6	8	10
Heave Acc.	Less	-0.26%	-0.51%	-0.18%	-0.40%	-0.45%
	Base	0.005	0.012	0.216	0.438	0.328
	More	0.25%	0.50%	0.17%	0.42%	0.87%
Roll deg.	Less	-0.61%	-0.35%	-0.29%	-0.94%	**-2.36%**
	Base	0.001	0.119	1.227	1.901	1.930
	More	0.60%	0.34%	0.28%	1.19%	**6.53%**
Pitch deg.	Less	-0.43%	-0.51%	-0.12%	-0.43%	-0.29%
	Base	0.000	0.005	0.128	0.269	0.262
	More	0.43%	0.49%	0.11%	0.54%	**3.46%**

C.1.7. Centre of Gravity Boom

Table C.10: Sensitivity Analysis: Centre of gravity Booms ($CB_{1,2}(z)$)

Stern Waves		Wave period				
Motion	Case	2	4	6	8	10
Heave Acc.	Less	0.73%	0.91%	0.76%	-0.05%	-0.34%
	Base	0.033	0.120	0.244	0.455	0.434
	More	-0.76%	-0.96%	-0.80%	0.01%	0.35%
Roll deg.	Less	2.44%	**4.41%**	1.33%	-2.44%	0.60%
	Base	0.001	0.020	0.190	0.381	0.535
	More	-2.51%	**-4.40%**	-1.31%	2.71%	-0.18%
Pitch deg.	Less	0.63%	0.89%	0.36%	-0.21%	-0.46%
	Base	0.006	0.080	0.332	0.745	0.884
	More	-0.66%	-0.93%	-0.40%	0.21%	0.50%

Stern Q Waves		Wave period				
Motion	Case	2	4	6	8	10
Heave Acc.	Less	0.73%	1.26%	0.88%	0.10%	-0.20%
	Base	0.003	0.046	0.306	0.578	0.482
	More	-0.76%	-1.31%	-0.95%	-0.16%	0.23%
Roll deg.	Less	1.65%	2.96%	-0.22%	-2.48%	1.41%
	Base	0.000	0.041	0.387	0.921	1.261
	More	-1.70%	-2.98%	0.21%	2.77%	-0.95%
Pitch deg.	Less	0.62%	1.08%	0.50%	0.04%	-0.33%
	Base	0.001	0.037	0.381	0.781	0.820
	More	-0.65%	-1.12%	-0.53%	-0.07%	0.34%

Beam Waves		Wave period				
Motion	Case	2	4	6	8	10
Heave Acc.	Less	0.58%	**7.69%**	**4.05%**	-0.13%	0.14%
	Base	0.005	0.012	0.216	0.438	0.328
	More	-0.60%	**-7.04%**	**-4.14%**	0.08%	-0.13%
Roll deg.	Less	1.61%	3.47%	1.81%	-2.00%	1.13%
	Base	0.001	0.119	1.227	1.901	1.930
	More	-1.67%	-3.47%	-1.92%	2.16%	-0.68%
Pitch deg.	Less	1.21%	**9.95%**	3.54%	-0.45%	1.03%
	Base	0.000	0.005	0.128	0.269	0.262
	More	-1.26%	**-9.69%**	-3.63%	0.45%	-0.79%

C.1.8. Mooring Stiffness

Table C.11: Sensitivity Analysis: Mooring Stiffness (C_{cm})

Stern Waves		Wave period				
Motion	Case	2	4	6	8	10
Heave Acc.	Less	0.00%	0.01%	-0.01%	-0.05%	-0.06%
	Base	0.033	0.120	0.244	0.455	0.434
	More	0.00%	-0.01%	0.01%	0.05%	0.07%
Roll deg.	Less	0.00%	-0.04%	-0.03%	0.31%	**8.55%**
	Base	0.001	0.020	0.190	0.381	0.535
	More	0.00%	0.04%	0.02%	0.26%	0.02%
Pitch deg.	Less	0.00%	0.00%	0.00%	-0.01%	0.24%
	Base	0.006	0.080	0.332	0.745	0.884
	More	0.00%	0.00%	0.00%	0.02%	0.10%

Stern Q Waves		Wave period				
Motion	Case	2	4	6	8	10
Heave Acc.	Less	0.00%	0.03%	0.11%	0.10%	0.33%
	Base	0.003	0.046	0.306	0.578	0.482
	More	0.00%	-0.03%	-0.11%	-0.09%	0.07%
Roll deg.	Less	0.00%	-0.16%	-0.50%	-0.37%	**3.40%**
	Base	0.000	0.041	0.387	0.921	1.261
	More	0.00%	0.16%	0.53%	1.01%	**3.76%**
Pitch deg.	Less	0.00%	-0.05%	-0.01%	0.02%	0.18%
	Base	0.001	0.037	0.381	0.781	0.820
	More	0.00%	0.05%	0.01%	-0.04%	-0.10%

Beam Waves		Wave period				
Motion	Case	2	4	6	8	10
Heave Acc.	Less	0.00%	-0.03%	0.09%	0.31%	0.72%
	Base	0.005	0.012	0.216	0.438	0.328
	More	0.00%	0.03%	-0.10%	-0.31%	-0.10%
Roll deg.	Less	0.00%	-0.02%	0.15%	0.57%	**5.32%**
	Base	0.001	0.119	1.227	1.901	1.930
	More	0.00%	0.02%	-0.15%	-0.25%	1.68%
Pitch deg.	Less	0.00%	-0.14%	-0.07%	0.07%	**5.12%**
	Base	0.000	0.005	0.128	0.269	0.262
	More	0.00%	0.14%	0.07%	0.09%	0.48%

C.1.9. Outreach Crane

Table C.12: Sensitivity Analysis: Outreach PS Crane (X_{out1})

Stern Waves		Wave period				
Motion	Case	2	4	6	8	10
Heave Acc.	Less	-1.49%	-1.24%	-1.31%	-2.03%	-2.28%
	Base	0.033	0.120	0.244	0.455	0.434
	More	1.46%	1.20%	1.27%	2.02%	2.27%
Roll deg.	Less	-1.51%	-1.00%	-1.05%	-1.44%	0.75%
	Base	0.001	0.020	0.190	0.381	0.535
	More	1.48%	0.95%	1.00%	1.94%	**5.51%**
Pitch deg.	Less	0.58%	0.81%	0.48%	-0.42%	-0.56%
	Base	0.006	0.080	0.332	0.745	0.884
	More	-0.58%	-0.81%	-0.49%	0.44%	0.83%

Stern Q Waves		Wave period				
Motion	Case	2	4	6	8	10
Heave Acc.	Less	-1.12%	-0.47%	-0.80%	-1.39%	-1.54%
	Base	0.003	0.046	0.306	0.578	0.482
	More	1.10%	0.45%	0.77%	1.39%	1.94%
Roll deg.	Less	-0.02%	-0.35%	-1.03%	-1.21%	-2.79%
	Base	0.000	0.041	0.387	0.921	1.261
	More	0.02%	0.35%	1.01%	1.93%	**9.71%**
Pitch deg.	Less	0.64%	0.79%	0.50%	-0.31%	-0.70%
	Base	0.001	0.037	0.381	0.781	0.820
	More	-0.65%	-0.79%	-0.52%	0.28%	0.56%

Beam Waves		Wave period				
Motion	Case	2	4	6	8	10
Heave Acc.	Less	0.59%	1.14%	0.89%	0.41%	0.17%
	Base	0.005	0.012	0.216	0.438	0.328
	More	-0.59%	-1.16%	-0.91%	-0.41%	0.50%
Roll deg.	Less	-0.11%	0.09%	0.33%	0.33%	-1.31%
	Base	0.001	0.119	1.227	1.901	1.930
	More	0.11%	-0.09%	-0.33%	0.09%	**8.42%**
Pitch deg.	Less	-1.12%	-0.83%	-1.10%	-1.58%	-0.49%
	Base	0.000	0.005	0.128	0.269	0.262
	More	1.10%	0.76%	1.04%	1.70%	4.44%

Table C.13: Sensitivity Analysis: Outreach SB Crane, small increment (X_{out2})

Stern Waves		Wave period				
Motion	Case	2	4	6	8	10
Heave Acc.	Less	0.08%	0.11%	0.08%	-0.03%	-0.03%
	Base	0.033	0.120	0.244	0.455	0.434
	More	-0.04%	-0.06%	-0.04%	0.01%	0.01%
Roll deg.	Less	0.01%	0.03%	-0.04%	-0.02%	0.47%
	Base	0.001	0.020	0.190	0.381	0.535
	More	0.00%	-0.01%	0.02%	0.01%	-0.24%
Pitch deg.	Less	0.06%	0.09%	0.03%	-0.03%	-0.04%
	Base	0.006	0.080	0.332	0.745	0.884
	More	-0.03%	-0.04%	-0.02%	0.02%	0.02%

Stern Q Waves		Wave period				
Motion	Case	2	4	6	8	10
Heave Acc.	Less	0.06%	0.06%	0.03%	-0.06%	-0.05%
	Base	0.003	0.046	0.306	0.578	0.482
	More	-0.06%	-0.06%	-0.03%	0.06%	0.05%
Roll deg.	Less	-0.07%	-0.06%	0.03%	0.05%	0.77%
	Base	0.000	0.041	0.387	0.921	1.261
	More	0.08%	0.08%	-0.04%	-0.07%	-0.77%
Pitch deg.	Less	0.06%	0.11%	0.03%	-0.04%	-0.03%
	Base	0.001	0.037	0.381	0.781	0.820
	More	-0.06%	-0.11%	-0.03%	0.04%	0.03%

Beam Waves		Wave period				
Motion	Case	2	4	6	8	10
Heave Acc.	Less	-0.08%	-0.28%	-0.12%	-0.08%	-0.04%
	Base	0.005	0.012	0.216	0.438	0.328
	More	0.08%	0.33%	0.14%	0.08%	0.04%
Roll deg.	Less	-0.07%	-0.09%	-0.13%	-0.12%	0.65%
	Base	0.001	0.119	1.227	1.901	1.930
	More	0.08%	0.11%	0.14%	0.11%	-0.63%
Pitch deg.	Less	0.16%	0.63%	0.36%	0.26%	0.52%
	Base	0.000	0.005	0.128	0.269	0.262
	More	-0.15%	-0.58%	-0.34%	-0.26%	-0.52%

C.1.10. Hoisting rope length

Table C.14: Sensitivity Analysis: Hoisting rope length (l_s)

Stern Waves		Wave period				
Motion	Case	2	4	6	8	10
Heave Acc.	Less	-0.31%	-0.37%	-0.09%	-0.03%	0.07%
	Base	0.033	0.120	0.244	0.455	0.434
	More	-0.35%	-0.54%	-0.51%	0.22%	0.62%
Roll deg.	Less	0.17%	1.27%	0.41%	-0.51%	**17.49%**
	Base	0.001	0.020	0.190	0.381	0.535
	More	-0.02%	-1.08%	0.03%	**1.72%**	**4.03%**
Pitch deg.	Less	-0.22%	-0.22%	-0.12%	-0.14%	0.39%
	Base	0.006	0.080	0.332	0.745	0.884
	More	-0.26%	-0.46%	-0.16%	0.40%	1.30%

Stern Q Waves		Wave period				
Motion	Case	2	4	6	8	10
Heave Acc.	Less	-0.19%	-0.08%	0.01%	-0.01%	0.22%
	Base	0.003	0.046	0.306	0.578	0.482
	More	-0.24%	-0.34%	-0.19%	0.46%	1.22%
Roll deg.	Less	0.47%	1.47%	-0.05%	-1.41%	**6.95%**
	Base	0.000	0.041	0.387	0.921	1.261
	More	0.32%	-0.58%	-0.31%	**1.73%**	**2.07%**
Pitch deg.	Less	-0.21%	-0.11%	0.00%	0.07%	1.20%
	Base	0.001	0.037	0.381	0.781	0.820
	More	-0.26%	-0.73%	-0.27%	0.24%	1.30%

Beam Waves		Wave period				
Motion	Case	2	4	6	8	10
Heave Acc.	Less	0.29%	**4.45%**	**2.17%**	-0.73%	0.12%
	Base	0.005	0.012	0.216	0.438	0.328
	More	0.43%	-1.01%	-0.69%	1.29%	1.65%
Roll deg.	Less	0.30%	1.72%	0.93%	-1.64%	**5.52%**
	Base	0.001	0.119	1.227	1.901	1.930
	More	0.45%	-0.53%	0.33%	**2.92%**	1.02%
Pitch deg.	Less	-0.67%	**1.97%**	0.24%	-1.37%	**11.34%**
	Base	0.000	0.005	0.128	0.269	0.262
	More	-0.52%	**-5.67%**	**-2.68%**	-0.42%	**3.11%**

C.1.11. Axial Rope Stiffness

Table C.15: Sensitivity Analysis: Axial Rope Stiffness (AE)

Stern Waves		Wave period				
Motion	Case	2	4	6	8	10
Heave Acc.	Less	0.00%	0.00%	0.00%	0.00%	0.00%
	Base	0.033	0.120	0.244	0.455	0.434
	More	0.00%	0.00%	0.00%	0.00%	0.00%
Roll deg.	Less	0.00%	0.00%	0.00%	0.00%	0.00%
	Base	0.001	0.020	0.190	0.381	0.535
	More	0.00%	0.00%	0.00%	0.00%	0.00%
Pitch deg.	Less	0.00%	0.00%	0.00%	0.00%	0.00%
	Base	0.006	0.080	0.332	0.745	0.884
	More	0.00%	0.00%	0.00%	0.00%	0.00%

Stern Q Waves		Wave period				
Motion	Case	2	4	6	8	10
Heave Acc.	Less	0.00%	0.00%	0.00%	0.00%	0.00%
	Base	0.003	0.046	0.306	0.578	0.482
	More	0.00%	0.00%	0.00%	0.00%	0.00%
Roll deg.	Less	0.00%	0.00%	0.00%	0.00%	0.00%
	Base	0.000	0.041	0.387	0.921	1.261
	More	0.00%	0.00%	0.00%	0.00%	0.00%
Pitch deg.	Less	0.00%	0.00%	0.00%	0.00%	0.00%
	Base	0.001	0.037	0.381	0.781	0.820
	More	0.00%	0.00%	0.00%	0.00%	0.00%

Beam Waves		Wave period				
Motion	Case	2	4	6	8	10
Heave Acc.	Less	0.00%	0.00%	0.00%	0.00%	0.00%
	Base	0.005	0.012	0.216	0.438	0.328
	More	0.00%	0.00%	0.00%	0.00%	0.00%
Roll deg.	Less	0.00%	0.00%	0.00%	0.00%	0.00%
	Base	0.001	0.119	1.227	1.901	1.930
	More	0.00%	0.00%	0.00%	0.00%	0.00%
Pitch deg.	Less	0.00%	0.00%	0.00%	0.00%	0.00%
	Base	0.000	0.005	0.128	0.269	0.262
	More	0.00%	0.00%	0.00%	0.00%	0.00%

C.2. Hydrodynamic Input

In this section the sensitivity of the hydrodynamic data on vessel motion response is given. The hydrodynamic data is determined with the aid of ANSYS AQWA. Sensitivity is tested on the parameters given below:

- Viscous added roll damping coefficient (B_{44})
- Added mass and damping coefficients (A, B)
- Hydrostatic restoring coefficient (C_{h33})
- Water Depth
- Draft
- Trim

The added mass and damping coefficients in heave, roll and pitch direction is manually within Matlab multiplied by 0.99 until 0.96 which is respectively 1-4% less added mass and damping than initially was computed with ANSYS AQWA. The linearized viscous added roll damping is not included in the base case of the sensitivity study which is in the table below denoted by wo. The sensitivity in vessel motion response is determined within Matlab and denoted by w. Other parameters such as the water depth and vessel trim are varied in ANSYS AQWA and processed in Matlab.

C.2.1. Viscous Added Roll Damping

Note that the added viscous roll damping counts most at the hull natural roll frequency which is, dependent on the loading condition around 7 seconds or 0.86 rad/s. At this frequency and a significant wave height of 1 m, the vessel roll motion response is 2.058 deg without added viscous roll damping and 2.042 deg which is -0.79%.

Table C.16: Sensitivity Analysis: Added Viscous Roll Damping (B_{44})

Stern Waves		Wave period				
Motion	Case	2	4	6	8	10
Heave Acc.	wo	0.033	0.120	0.244	0.455	0.434
	w	0.00%	0.00%	0.01%	-0.04%	-0.02%
Roll deg.	wo	0.001	0.020	0.190	0.381	0.535
	w	0.00%	-0.07%	-0.39%	-0.37%	-0.83%
Pitch deg.	wo	0.006	0.080	0.332	0.745	0.884
	w	0.00%	0.00%	0.00%	0.00%	0.00%

Stern Q Waves		Wave period				
Motion	Case	2	4	6	8	10
Heave Acc.	wo	0.003	0.046	0.306	0.578	0.482
	w	-0.01%	-0.03%	-0.03%	-0.09%	-0.06%
Roll deg.	wo	0.000	0.041	0.387	0.921	1.261
	w	0.00%	-0.05%	-0.41%	-0.35%	-0.84%
Pitch deg.	wo	0.001	0.037	0.381	0.781	0.820
	w	0.00%	0.00%	0.00%	-0.02%	-0.04%

Beam Waves		Wave period				
Motion	Case	2	4	6	8	10
Heave Acc.	wo	0.005	0.012	0.216	0.438	0.328
	w	0.00%	-0.29%	-0.53%	-0.40%	-0.33%
Roll deg.	wo	0.001	0.119	1.227	1.901	1.930
	w	0.00%	-0.09%	-0.39%	-0.40%	-0.84%
Pitch deg.	wo	0.000	0.005	0.128	0.269	0.262
	w	0.00%	-0.34%	-0.52%	-0.40%	-0.61%

C.2.2. Added Mass and Damping

Table C.17: Sensitivity Analysis: Less Added Mass and Damping (A_{ij}, B_{ij}) for $i, j = 3, 4, 5$

Stern Waves		Wave period				
Motion	Case	2	4	6	8	10
Heave acc	0	0.033	0.120	0.244	0.455	0.434
	-1%	0.40%	-0.10%	-0.99%	-1.14%	-2.74%
	-2%	1.03%	0.85%	0.23%	-0.71%	-2.97%
	-3%	1.67%	1.81%	1.46%	-0.29%	**-3.21%**
	-4%	2.32%	2.80%	2.72%	0.10%	**-3.46%**
Roll deg	0	0.001	0.020	0.190	0.381	0.535
	-1%	0.97%	0.60%	-0.36%	-0.95%	1.12%
	-2%	2.22%	2.99%	1.53%	-0.60%	2.52%
	-3%	3.50%	**5.46%**	**3.46%**	-0.23%	**4.21%**
	-4%	**4.80%**	**8.03%**	**5.46%**	0.15%	**6.13%**
Pitch deg	0	0.006	0.080	0.332	0.745	0.884
	-1%	0.79%	1.49%	0.82%	-0.58%	-1.09%
	-2%	1.55%	2.74%	2.01%	-0.41%	-1.55%
	-3%	**2.31%**	**4.03%**	**3.23%**	-0.25%	-2.00%
	-4%	**3.09%**	**5.35%**	**4.46%**	-0.12%	-2.46%

Stern Q Waves		Wave period				
Motion	Case	2	4	6	8	10
Heave acc	0	0.003	0.046	0.306	0.578	0.482
	-1%	0.49%	-0.03%	-0.90%	-2.63%	**-4.00%**
	-2%	1.13%	1.10%	0.45%	-2.08%	**-4.03%**
	-3%	1.77%	2.26%	1.82%	-1.56%	**-4.06%**
	-4%	2.42%	**3.45%**	**3.21%**	-1.04%	**-4.07%**
Roll deg	0	0.000	0.041	0.387	0.921	1.261
	-1%	0.58%	1.04%	-0.52%	-1.27%	0.93%
	-2%	1.15%	2.05%	0.49%	-1.16%	2.99%
	-3%	1.73%	**3.09%**	1.52%	-1.03%	**5.39%**
	-4%	2.32%	**4.15%**	2.56%	-0.87%	**8.09%**
Pitch deg	0	0.001	0.037	0.381	0.781	0.820
	-1%	0.78%	1.69%	1.08%	-0.57%	-1.34%
	-2%	1.53%	**3.28%**	**2.39%**	-0.18%	-1.64%
	-3%	2.30%	**4.91%**	**3.73%**	0.20%	-1.95%
	-4%	**3.07%**	**6.59%**	**5.08%**	0.56%	-2.26%

Beam Waves		Wave period				
Motion	Case	2	4	6	8	10
Heave acc	0	0.005	0.012	0.216	0.438	0.328
	-1%	1.03%	**-4.32%**	**-4.61%**	**-6.65%**	**-7.90%**
	-2%	1.61%	**-3.01%**	**-3.09%**	-6.09%	**-7.44%**
	-3%	2.19%	-1.65%	-1.54%	**-5.55%**	**-6.96%**
	-4%	2.20%	**5.51%**	**4.49%**	-0.27%	**7.24%**
Roll deg	0	0.001	0.119	1.227	1.901	1.930
	-1%	0.53%	1.59%	1.17%	-0.46%	1.03%
	-2%	1.08%	2.87%	2.26%	-0.41%	2.81%
	-3%	1.64%	**4.17%**	**3.37%**	-0.35%	**4.89%**
	-4%	2.20%	**5.51%**	**4.49%**	-0.27%	**7.24%**
Pitch deg	0	0.000	0.005	0.128	0.269	0.262
	-1%	1.96%	**-4.39%**	**-3.65%**	**-5.79%**	**-3.53%**
	-2%	**3.43%**	-1.45%	-1.71%	**-5.34%**	-2.57%
	-3%	**4.93%**	1.62%	0.27%	**-4.89%**	-1.41%
	-4%	**6.46%**	**4.82%**	2.30%	**-4.46%**	-0.09%

C.2.3. Hydrostatic Restoring

Table C.18: Sensitivity Analysis: Additional vertical restoring (C_{h33})

Stern Waves		Wave period				
Motion	Case	2	4	6	8	10
Heave Acc.	Base	0.033	0.118	0.240	0.446	0.424
	More	1.56%	0.19%	-1.48%	-0.02%	-1.12%
Roll deg.	Base	0.001	0.019	0.188	0.377	0.555
	More	1.19%	-1.48%	-2.09%	-0.56%	-3.46%
Pitch deg.	Base	0.006	0.081	0.333	0.742	0.880
	More	-0.21%	-0.03%	-0.84%	-0.72%	-0.41%

Stern Q Waves		Wave period				
Motion	Case	2	4	6	8	10
Heave Acc.	Base	0.003	0.045	0.303	0.570	0.475
	Less	1.21%	-0.96%	-2.28%	-3.22%	-4.16%
Roll deg.	Base	0.000	0.041	0.382	0.910	1.247
	Less	-0.21%	0.17%	-0.96%	-0.76%	-0.04%
Pitch deg.	Base	0.001	0.037	0.382	0.779	0.814
	Less	-0.30%	-0.12%	-0.65%	-1.21%	-0.80%

Beam Waves		Wave period				
Motion	Case	2	4	6	8	10
Heave Acc.	Base	0.005	0.013	0.219	0.441	0.329
	Less	-0.14%	-9.40%	-10.01%	-11.05%	-12.39%
Roll deg.	Base	0.001	0.119	1.236	1.916	1.940
	Less	-0.14%	0.04%	-0.72%	-1.59%	-1.15%
Pitch deg.	Base	0.000	0.005	0.125	0.263	0.263
	Less	2.56%	-7.59%	-5.88%	-6.87%	-6.57%

C.2.4. Water Depth

Table C.19: Sensitivity Analysis: Water Depth in AQWA, small increments
WD independent wave spectrum in Matlab

Stern Waves		Wave period				
Motion	Case	2	4	6	8	10
Heave acc	30	0.033	0.120	0.244	0.455	0.434
	27.5	0.05%	0.33%	-0.34%	-1.48%	-0.80%
	25	0.15%	0.40%	-1.07%	-3.66%	-2.08%
Roll deg	30	0.001	0.020	0.190	0.381	0.535
	27.5	-0.17%	-0.15%	-1.56%	-2.19%	-1.71%
	25	-0.66%	-0.70%	-4.32%	-5.37%	-3.56%
Pitch deg	30	0.006	0.080	0.332	0.745	0.884
	27.5	-0.12%	-0.06%	-0.72%	-1.23%	-0.08%
	25	-0.67%	-0.37%	-1.89%	-2.94%	-0.47%

Stern Q Waves		Wave period				
Motion	Case	2	4	6	8	10
Heave acc	30	0.003	0.046	0.306	0.578	0.482
	27.5	-0.24%	0.14%	-0.24%	-0.78%	-0.18%
	25	-0.63%	0.59%	-0.49%	-2.11%	-0.59%
Roll deg	30	0.000	0.041	0.387	0.921	1.261
	27.5	-0.22%	-0.11%	-1.34%	-1.07%	-0.61%
	25	-0.52%	-0.09%	-3.58%	-2.72%	-1.08%
Pitch deg	30	0.001	0.037	0.381	0.781	0.820
	27.5	-0.46%	-0.13%	-0.44%	-0.59%	0.34%
	25	-1.11%	-0.05%	-0.97%	-1.60%	0.59%

Beam Waves		Wave period				
Motion	Case	2	4	6	8	10
Heave acc	30	0.005	0.012	0.216	0.438	0.328
	27.5	-0.51%	1.56%	0.85%	-0.07%	-0.25%
	25	-1.77%	4.16%	1.41%	-0.80%	-0.95%
Roll deg	30	0.001	0.119	1.227	1.901	1.930
	27.5	-0.37%	0.54%	0.49%	0.54%	-0.94%
	25	-1.19%	1.31%	0.71%	0.65%	-1.67%
Pitch deg	30	0.000	0.005	0.128	0.269	0.262
	27.5	-0.26%	0.10%	-1.49%	-2.01%	-1.22%
	25	-2.82%	0.41%	-3.93%	-5.00%	-2.48%

Table C.20: Sensitivity Analysis: Water Depth in AQWA, large increments
WD independent wave spectrum in Matlab

Stern Waves		Wave period				
Motion	Case	2	4	6	8	10
Heave acc	30	0.033	0.120	0.244	0.455	0.434
	20	-1.79%	-0.86%	-4.61%	-12.16%	-7.03%
	10	-9.09%	-8.81%	-21.64%	-45.97%	-32.31%
	100	-2.26%	-1.32%	-0.88%	1.21%	0.11%
Roll deg	30	0.001	0.020	0.190	0.381	0.535
	20	-5.44%	-6.64%	-15.06%	-15.12%	-5.64%
	10	-26.37%	-36.83%	-58.21%	-52.69%	-24.02%
	100	-3.01%	-3.35%	1.10%	6.93%	22.60%
Pitch deg	30	0.006	0.080	0.332	0.745	0.884
	20	-3.55%	-2.82%	-6.69%	-9.67%	-2.44%
	10	-14.44%	-17.01%	-29.78%	-39.29%	-20.50%
	100	-1.56%	-0.69%	0.67%	1.49%	-2.05%

Stern Q Waves		Wave period				
Motion	Case	2	4	6	8	10
Heave acc	30	0.003	0.046	0.306	0.578	0.482
	20	-2.89%	-0.65%	-3.49%	-7.26%	-2.48%
	10	-15.24%	-15.53%	-31.68%	-36.66%	-17.29%
	100	-1.81%	-3.01%	-2.04%	-0.02%	-0.89%
Roll deg	30	0.000	0.041	0.387	0.921	1.261
	20	0.80%	-2.47%	-13.06%	-8.16%	-1.49%
	10	-12.46%	-4.66%	-48.72%	-36.86%	-13.08%
	100	2.45%	-2.35%	0.68%	3.08%	11.36%
Pitch deg	30	0.001	0.037	0.381	0.781	0.820
	20	-4.20%	-2.85%	-4.27%	-5.25%	0.96%
	10	-20.48%	-30.72%	-31.66%	-25.99%	-6.08%
	100	-1.66%	-2.53%	-0.76%	0.11%	-3.38%

Beam Waves		Wave period				
Motion	Case	2	4	6	8	10
Heave acc	30	0.005	0.012	0.216	0.438	0.328
	20	-2.10%	7.43%	0.16%	-1.72%	-1.83%
	10	-22.99%	65.95%	-20.95%	-21.89%	-18.27%
	100	1.20%	-7.62%	-5.30%	-0.16%	2.26%
Roll deg	30	0.001	0.119	1.227	1.901	1.930
	20	1.25%	-0.50%	-0.33%	3.70%	-1.93%
	10	-17.40%	2.04%	-20.39%	-1.65%	-14.72%
	100	6.03%	-5.43%	-2.55%	0.81%	16.42%
Pitch deg	30	0.000	0.005	0.128	0.269	0.262
	20	-9.83%	-7.08%	-14.19%	-12.99%	-3.74%
	10	-47.95%	-32.04%	-56.39%	-45.37%	-15.90%
	100	1.22%	-8.19%	0.75%	6.28%	12.56%

C.2.5. Draft

The sensitivity of draft due to a difference of ±5% in ballast than was initially estimated for this specific loading condition is given in the table below.

Table C.21: Sensitivity Analysis: Draft

Stern Waves		Wave period				
Motion	Case	2	4	6	8	10
Heave Acc.	Less	1.70%	0.48%	0.39%	1.55%	1.36%
	Base	0.033	0.118	0.240	0.446	0.424
	More	-0.96%	-0.05%	-0.37%	-1.19%	-1.10%
Roll deg.	Less	1.24%	0.34%	0.86%	1.51%	-0.34%
	Base	0.001	0.019	0.188	0.377	0.555
	More	-1.49%	-0.61%	-0.48%	-0.65%	2.07%
Pitch deg.	Less	1.40%	0.34%	0.49%	1.38%	1.08%
	Base	0.006	0.081	0.333	0.742	0.880
	More	-1.02%	-0.20%	-0.40%	-1.10%	-1.00%

Stern Q Waves		Wave period				
Motion	Case	2	4	6	8	10
Heave Acc.	Less	-1.21%	0.64%	0.48%	0.78%	0.68%
	Base	0.003	0.045	0.303	0.570	0.475
	More	-2.06%	-0.70%	-0.38%	-0.54%	-0.49%
Roll deg.	Less	-3.91%	-0.11%	0.70%	0.37%	-3.88%
	Base	0.000	0.041	0.382	0.910	1.247
	More	1.93%	-0.12%	-0.12%	0.32%	5.48%
Pitch deg.	Less	-1.00%	0.86%	0.29%	0.77%	1.02%
	Base	0.001	0.037	0.382	0.779	0.814
	More	-2.37%	-0.69%	-0.21%	-0.61%	-0.63%

Beam Waves		Wave period				
Motion	Case	2	4	6	8	10
Heave Acc.	Less	-2.82%	0.37%	-0.68%	-0.75%	-0.64%
	Base	0.005	0.013	0.219	0.441	0.329
	More	0.31%	-0.74%	0.75%	1.04%	0.87%
Roll deg.	Less	-4.58%	1.33%	-0.11%	-0.67%	-2.41%
	Base	0.001	0.119	1.236	1.916	1.940
	More	3.34%	-1.65%	0.26%	1.06%	3.48%
Pitch deg.	Less	0.78%	1.37%	0.73%	1.00%	0.19%
	Base	0.000	0.005	0.125	0.263	0.263
	More	1.08%	-2.21%	-0.57%	-0.57%	1.40%

C.2.6. Trim

Table C.22: Sensitivity Analysis: Trim

Stern Waves		Wave period				
Motion	Case	2	4	6	8	10
Heave acc	0	0.033	0.118	0.240	0.446	0.424
	-0.1	0.02%	-1.14%	-0.74%	-0.48%	-0.75%
	-0.2	0.23%	-1.98%	-1.32%	-1.29%	-1.62%
	-0.3	0.38%	-3.04%	-1.96%	-1.93%	-1.67%
	-0.4	0.03%	-4.47%	-2.89%	-2.78%	-3.53%
Roll deg	0	0.001	0.019	0.188	0.377	0.555
	-0.1	-0.23%	-1.17%	-0.60%	-1.11%	3.52%
	-0.2	-0.30%	-1.93%	-1.33%	-2.69%	9.49%
	-0.3	-0.38%	-2.88%	-1.94%	-4.49%	33.56%
	-0.4	-0.85%	-4.28%	-3.07%	-6.71%	16.93%
Pitch deg	0	0.006	0.081	0.333	0.742	0.880
	-0.1	0.57%	-0.57%	-0.09%	0.14%	-0.14%
	-0.2	1.23%	-0.88%	-0.16%	0.03%	-0.10%
	-0.3	2.00%	-1.28%	-0.16%	0.12%	1.79%
	-0.4	2.56%	-1.89%	-0.35%	0.14%	-0.19%

Stern Q Waves		Wave period				
Motion	Case	2	4	6	8	10
Heave acc	0	0.003	0.045	0.303	0.570	0.475
	-0.1	-1.74%	0.13%	-0.25%	-0.46%	-0.62%
	-0.2	-2.07%	0.26%	-0.67%	-1.03%	-1.20%
	-0.3	-3.18%	0.43%	-0.74%	-1.53%	-0.53%
	-0.4	-4.91%	0.33%	-1.17%	-2.25%	-2.55%
Roll deg	0	0.000	0.041	0.382	0.910	1.247
	-0.1	-1.91%	-1.35%	-1.41%	-1.06%	1.55%
	-0.2	-5.37%	-2.61%	-2.92%	-2.28%	4.17%
	-0.3	-6.31%	-3.71%	-4.52%	-3.92%	12.64%
	-0.4	-7.40%	-5.03%	-6.33%	-5.64%	1.29%
Pitch deg	0	0.001	0.037	0.382	0.779	0.814
	-0.1	-1.16%	-0.20%	-0.40%	-0.19%	0.13%
	-0.2	-0.30%	-0.55%	-0.94%	-0.49%	0.31%
	-0.3	-1.16%	-0.58%	-1.16%	-0.66%	4.30%
	-0.4	-2.40%	-1.10%	-1.74%	-1.03%	0.61%

Beam Waves		Wave period				
Motion	Case	2	4	6	8	10
Heave acc	0	0.005	0.013	0.219	0.441	0.329
	-0.1	-1.41%	-2.27%	-0.46%	-0.90%	-0.87%
	-0.2	0.30%	-3.58%	-1.20%	-2.16%	-1.73%
	-0.3	-0.61%	-5.43%	-1.98%	-3.25%	-1.22%
	-0.4	16.29%	-1.56%	-0.24%	-2.85%	-1.18%
Roll deg	0	0.001	0.119	1.236	1.916	1.940
	-0.1	4.46%	-0.43%	0.12%	-0.39%	1.11%
	-0.2	8.10%	-0.69%	-0.06%	-1.34%	3.23%
	-0.3	11.66%	-1.08%	-0.15%	-2.14%	4.16%
	-0.4	16.29%	-1.56%	-0.24%	-2.85%	-1.18%
Pitch deg	0	0.000	0.005	0.125	0.263	0.263
	-0.1	21.58%	2.51%	1.08%	-0.84%	2.30%
	-0.2	28.43%	6.87%	1.91%	-2.20%	6.73%
	-0.3	48.68%	11.42%	2.76%	-3.53%	26.32%
	-0.4	69.46%	17.72%	4.05%	-4.92%	12.08%

C.3. Wave Parameters

In this section the sensitivity of the wave parameters are given. The following parameters are evaluated:

- Wave direction
- Wave height
- Wave period
- Spectral peak parameter
- Water depth dependent wave spectrum
- Bi-Modal spectrum

For checking the sensitivity of wave direction on vessel motion response, hydrodynamic data per wave direction is computed. Wave forces, added mass and damping are therefore not interpolated over wave frequency and direction in Matlab.

C.3.1. Wave Direction

Vessel heave acceleration, roll and pith motions are respectively given in deg/s^2 and degrees. The difference in vessel motion response with respect to the initial wave angle is given in percentages.

Tp = 4 sec	Wave direction (deg)					
Motion	0	1	2	3	4	5
Heave acc	0.120	0.38%	0.76%	0.35%	-0.36%	-0.82%
Roll deg	0.020	-3.97%	-4.84%	-3.07%	1.48%	8.17%
Pitch deg	0.080	-0.05%	-0.04%	-0.53%	-1.14%	-1.65%

Tp = 4 sec	Wave direction (deg)					
Motion	45	46	47	48	49	50
Heave acc	0.046	-0.29%	-0.37%	-0.46%	-0.13%	0.66%
Roll deg	0.041	-2.07%	-4.17%	-6.37%	-8.56%	-10.76%
Pitch deg	0.037	0.32%	0.90%	1.26%	1.95%	2.99%

Tp = 4 sec	Wave direction (deg)					
Motion	90	91	92	93	94	95
Heave acc	0.012	33.17%	91.90%	155.82%	218.01%	275.76%
Roll deg	0.119	-0.89%	-2.06%	-3.64%	-5.51%	-7.63%
Pitch deg	0.005	49.11%	128.97%	214.59%	299.32%	380.13%

Tp = 6 sec	Wave direction (deg)					
Motion	0	1	2	3	4	5
Heave acc	0.244	0.23%	0.43%	0.64%	0.90%	1.11%
Roll deg	0.190	-2.61%	-4.95%	-6.87%	-8.63%	-9.90%
Pitch deg	0.332	0.11%	0.17%	0.34%	0.48%	0.60%

Tp = 6 sec	Wave direction (deg)					
Motion	45	46	47	48	49	50
Heave acc	0.306	1.10%	2.22%	3.05%	4.09%	4.99%
Roll deg	0.387	2.48%	5.10%	8.07%	11.41%	14.91%
Pitch deg	0.381	-0.08%	-0.16%	-0.57%	-0.87%	-1.40%

Tp = 6 sec	Wave direction (deg)					
Motion	90	91	92	93	94	95
Heave acc	0.216	-2.26%	-4.31%	-6.43%	-8.32%	-10.18%
Roll deg	1.227	-0.52%	-1.12%	-2.00%	-2.99%	-4.12%
Pitch deg	0.128	3.62%	8.14%	13.05%	18.67%	24.58%

Tp = 8 sec	Wave direction (deg)					
Motion	0	1	2	3	4	5
Heave acc	0.455	-0.11%	-0.11%	-0.02%	-0.08%	-0.08%
Roll deg	0.381	0.08%	0.51%	1.17%	1.85%	2.81%
Pitch deg	0.745	-0.01%	0.05%	0.18%	0.19%	0.23%

Tp = 8 sec	Wave direction (deg)					
Motion	45	46	47	48	49	50
Heave acc	0.578	0.84%	1.55%	2.18%	2.98%	3.62%
Roll deg	0.921	2.50%	4.94%	7.55%	10.33%	13.12%
Pitch deg	0.781	-0.34%	-0.79%	-1.37%	-1.82%	-2.49%

Tp = 8 sec	Wave direction (deg)					
Motion	90	91	92	93	94	95
Heave acc	0.438	-3.00%	-5.80%	-8.69%	-11.91%	-14.79%
Roll deg	1.901	-0.60%	-1.04%	-1.66%	-2.70%	-3.51%
Pitch deg	0.269	-4.17%	-7.61%	-10.68%	-13.44%	-15.30%

Tp = 10 sec	Wave direction (deg)					
Motion	0	1	2	3	4	5
Heave acc	0.434	0.06%	0.16%	0.24%	0.31%	0.41%
Roll deg	0.535	-1.32%	-2.17%	-2.51%	-2.50%	-2.21%
Pitch deg	0.884	0.03%	0.07%	0.06%	0.06%	0.08%

Tp = 10 sec	Wave direction (deg)					
Motion	45	46	47	48	49	50
Heave acc	0.482	0.20%	0.36%	0.45%	0.67%	0.70%
Roll deg	1.260	1.54%	2.87%	4.28%	5.75%	7.16%
Pitch deg	0.820	-0.71%	-1.47%	-2.33%	-3.06%	-4.08%

Tp = 10 sec	Wave direction (deg)					
Motion	90	91	92	93	94	95
Heave acc	0.328	-2.34%	-4.54%	-6.73%	-9.04%	-11.09%
Roll deg	1.929	-0.07%	0.01%	-0.04%	-0.84%	-0.81%
Pitch deg	0.262	-3.87%	-7.07%	-9.77%	-12.40%	-13.71%

C.3.2. Wave Height

Table C.23: Sensitivity Analysis: Wave Height (H_s)

Stern Waves		Wave period				
Motion	Case	2	4	6	8	10
Heave Acc.	Less	-10.00%	-10.00%	-10.00%	-10.00%	-10.00%
	Base	0.033	0.118	0.240	0.446	0.424
	More	10.00%	10.00%	10.00%	10.00%	10.00%
Roll deg.	Less	-10.00%	-10.00%	-10.00%	-10.00%	-10.00%
	Base	0.001	0.019	0.188	0.377	0.555
	More	10.00%	10.00%	10.00%	10.00%	10.00%
Pitch deg.	Less	-10.00%	-10.00%	-10.00%	-10.00%	-10.00%
	Base	0.006	0.081	0.333	0.742	0.880
	More	10.00%	10.00%	10.00%	10.00%	10.00%

Stern Q Waves		Wave period				
Motion	Case	2	4	6	8	10
Heave Acc.	Less	-10.00%	-10.00%	-10.00%	-10.00%	-10.00%
	Base	0.003	0.045	0.303	0.570	0.475
	More	10.00%	10.00%	10.00%	10.00%	10.00%
Roll deg.	Less	-10.00%	-10.00%	-10.00%	-10.00%	-10.00%
	Base	0.000	0.041	0.382	0.910	1.247
	More	10.00%	10.00%	10.00%	10.00%	10.00%
Pitch deg.	Less	-10.00%	-10.00%	-10.00%	-10.00%	-10.00%
	Base	0.001	0.037	0.382	0.779	0.814
	More	10.00%	10.00%	10.00%	10.00%	10.00%

Beam Waves		Wave period				
Motion	Case	2	4	6	8	10
Heave Acc.	Less	-10.00%	-10.00%	-10.00%	-10.00%	-10.00%
	Base	0.005	0.013	0.219	0.441	0.329
	More	10.00%	10.00%	10.00%	10.00%	10.00%
Roll deg.	Less	-10.00%	-10.00%	-10.00%	-10.00%	-10.00%
	Base	0.001	0.119	1.236	1.916	1.940
	More	10.00%	10.00%	10.00%	10.00%	10.00%
Pitch deg.	Less	-10.00%	-10.00%	-10.00%	-10.00%	-10.00%
	Base	0.000	0.005	0.125	0.263	0.263
	More	10.00%	10.00%	10.00%	10.00%	10.00%

C.3.3. Wave Period

Table C.24: Sensitivity Analysis: Wave Period (T_p)

Stern Waves		Wave period				
Motion	Case	2	4	6	8	10
Heave Acc.	Tp-0.5s	-82.95%	-19.32%	-12.55%	-11.15%	5.07%
	Base	0.032	0.117	0.239	0.459	0.438
	Tp+0.5s	74.71%	27.18%	16.29%	4.59%	-5.22%
Roll deg.	Tp-0.5s	-85.15%	-53.01%	-32.18%	-1.74%	-13.62%
	Base	0.001	0.019	0.187	0.383	0.552
	Tp+0.5s	152.19%	109.91%	39.70%	1.90%	18.73%
Pitch deg.	Tp-0.5s	-84.86%	-40.77%	-23.80%	-15.12%	0.15%
	Base	0.006	0.078	0.328	0.755	0.900
	Tp+0.5s	139.68%	58.97%	26.98%	11.00%	-1.29%

Stern Q Waves		Wave period				
Motion	Case	2	4	6	8	10
Heave Acc.	Tp-0.5s	-86.38%	-47.25%	-27.34%	-7.12%	7.28%
	Base	0.003	0.044	0.302	0.585	0.486
	Tp+0.5s	164.03%	91.18%	24.93%	-0.21%	-6.55%
Roll deg.	Tp-0.5s	-91.03%	-55.84%	-32.43%	-4.58%	-10.98%
	Base	0.000	0.040	0.373	0.913	1.223
	Tp+0.5s	326.75%	94.37%	44.76%	2.40%	15.75%
Pitch deg.	Tp-0.5s	-88.81%	-67.13%	-31.99%	-11.37%	2.20%
	Base	0.000	0.035	0.377	0.792	0.832
	Tp+0.5s	237.63%	135.40%	30.96%	6.54%	-2.41%

Beam Waves		Wave period				
Motion	Case	2	4	6	8	10
Heave Acc.	Tp-0.5s	-84.10%	-38.10%	-34.98%	1.36%	7.21%
	Base	0.005	0.012	0.212	0.441	0.328
	Tp+0.5s	87.50%	179.23%	44.54%	-6.56%	-5.77%
Roll deg.	Tp-0.5s	-84.65%	-61.06%	-31.57%	7.95%	-6.81%
	Base	0.001	0.117	1.232	1.936	1.931
	Tp+0.5s	200.07%	128.15%	36.90%	-7.65%	11.89%
Pitch deg.	Tp-0.5s	-85.85%	-79.38%	-35.77%	0.98%	-5.15%
	Base	0.000	0.005	0.126	0.272	0.266
	Tp+0.5s	127.29%	259.56%	46.61%	-5.03%	10.40%

C.3.4. Spectral Peak Parameter

Table C.25: Sensitivity Analysis: Spectral Peak Parameter - Increments according to DNV (γ)

Stern Waves		Wave period				
Motion	Case	2	4	6	8	10
Heave Acc.	γ =1.0	0.43%	-0.90%	-0.33%	-13.44%	-3.48%
	γ = 3.3	0.033	0.120	0.244	0.455	0.434
	γ = 5.0	-1.81%	0.05%	-0.08%	4.41%	0.89%
Roll deg.	γ =1.0	6.92%	12.29%	5.37%	-10.95%	14.27%
	γ = 3.3	0.001	0.020	0.190	0.381	0.535
	γ = 5.0	-3.87%	-4.96%	-2.66%	3.45%	-6.21%
Pitch deg.	γ =1.0	6.14%	4.34%	-0.58%	-10.71%	-8.21%
	γ = 3.3	0.006	0.080	0.332	0.745	0.884
	γ = 5.0	-3.62%	-1.90%	0.01%	3.43%	2.55%

Stern Waves		Wave period				
Motion	Case	2	4	6	8	10
Heave Acc.	γ =1.0	10.49%	13.98%	-2.74%	-15.43%	1.84%
	γa = 3.3	0.003	0.046	0.306	0.578	0.482
	γ = 5.0	-5.21%	-5.85%	0.85%	5.01%	-1.01%
Roll deg.	γ =1.0	17.12%	11.22%	12.03%	-12.81%	13.09%
	γ = 3.3	0.000	0.041	0.387	0.921	1.261
	γ = 5.0	-6.95%	-4.52%	-5.37%	4.10%	-5.73%
Pitch deg.	γ =1.0	15.18%	21.58%	-2.33%	-12.20%	-5.39%
	γ = 3.3	0.001	0.037	0.381	0.781	0.820
	γ = 5.0	-6.79%	-8.90%	0.55%	3.94%	1.56%

Beam Waves		Wave period				
Motion	Case	2	4	6	8	10
Heave Acc.	γ =1.0	4.33%	21.71%	8.60%	-15.32%	8.15%
	γ = 3.3	0.005	0.012	0.216	0.438	0.328
	γ = 5.0	-2.97%	-8.91%	-4.07%	4.72%	-3.35%
Roll deg.	γ=1.0	6.02%	15.34%	0.65%	-9.40%	17.71%
	γ = 3.3	0.001	0.119	1.227	1.901	1.930
	γ = 5.0	-3.32%	-6.18%	-1.01%	2.67%	-7.61%
Pitch deg.	γ =1.0	9.18%	23.15%	10.24%	-14.62%	12.50%
	γ = 3.3	0.000	0.005	0.128	0.269	0.262
	γ = 5.0	-4.61%	-9.46%	-4.78%	4.53%	-5.33%

Table C.26: Sensitivity Analysis: Spectral Peak Parameter - Small increments (γ)

Stern Waves		Wave period				
Motion	Case	2	4	6	8	10
Heave Acc.	γ = 3.1	0.16%	-0.05%	-0.01%	-0.73%	-0.20%
	γ =3.3	0.032	0.117	0.239	0.456	0.437
	γ = 3.5	-0.17%	0.04%	0.00%	0.68%	0.18%
Roll deg.	γ = 3.1	0.49%	0.69%	0.37%	-0.61%	0.95%
	γ = 3.3	0.001	0.019	0.187	0.381	0.557
	γ = 3.5	-0.48%	-0.66%	-0.36%	0.57%	-0.91%
Pitch deg.	γ = 3.1	0.45%	0.24%	-0.02%	-0.57%	-0.45%
	γ = 3.3	0.006	0.079	0.328	0.751	0.896
	γ = 3.5	-0.44%	-0.23%	0.01%	0.53%	0.41%

Stern Waves		Wave period				
Motion	Case	2	4	6	8	10
Heave Acc.	γ = 3.1	0.69%	0.80%	-0.14%	-0.82%	0.08%
	γ = 3.3	0.003	0.045	0.302	0.580	0.487
	γ = 3.5	-0.67%	-0.77%	0.13%	0.77%	-0.09%
Roll deg.	γ = 3.1	0.98%	0.62%	0.76%	-0.73%	0.84%
	γ = 3.3	0.000	0.041	0.376	0.906	1.233
	γ = 3.5	-0.94%	-0.59%	-0.73%	0.67%	-0.80%
Pitch deg.	γ = 3.1	0.93%	1.26%	-0.10%	-0.66%	-0.29%
	γ = 3.3	0.001	0.036	0.377	0.787	0.830
	γ = 3.5	-0.90%	-1.20%	0.09%	0.61%	0.27%

Beam Waves		Wave period				
Motion	Case	2	4	6	8	10
Heave Acc.	γ = 3.1	0.35%	1.26%	0.55%	-0.79%	0.43%
	γ = 3.3	0.005	0.012	0.213	0.438	0.329
	γ = 3.5	-0.35%	-1.20%	-0.53%	0.73%	-0.41%
Roll deg.	γ = 3.1	0.42%	0.87%	0.10%	-0.50%	1.08%
	γ = 3.3	0.001	0.118	1.233	1.927	1.951
	γ = 3.5	-0.41%	-0.83%	-0.10%	0.45%	-1.03%
Pitch deg.	γ = 3.1	0.60%	1.35%	0.66%	-0.77%	0.80%
	γ = 3.3	0.000	0.005	0.127	0.270	0.269
	γ = 3.5	-0.59%	-1.28%	-0.64%	0.72%	-0.76%

C.3.5. Water Depth

Table C.27: Sensitivity Analysis: Water Depth dependent wave spectrum

Stern Waves		Wave period				
Motion	Case	2	4	6	8	10
Heave Acc.	wo	0.033	0.118	0.240	0.446	0.424
	w	0.00%	-0.04%	-3.14%	-11.03%	-18.30%
Roll deg.	wo	0.001	0.019	0.188	0.377	0.555
	w	0.00%	-0.40%	-4.52%	-10.96%	-30.41%
Pitch deg.	wo	0.006	0.081	0.333	0.742	0.880
	w	0.00%	-0.13%	-4.10%	-12.60%	-21.43%

Stern Q Waves		Wave period				
Motion	Case	2	4	6	8	10
Heave Acc.	wo	0.003	0.045	0.303	0.570	0.475
	w	0.00%	-0.31%	-3.75%	-10.21%	-16.35%
Roll deg.	wo	0.000	0.041	0.382	0.910	1.247
	w	0.00%	-0.26%	-5.65%	-11.28%	-29.08%
Pitch deg.	wo	0.001	0.037	0.382	0.779	0.814
	w	0.00%	-0.64%	-4.05%	-11.53%	-19.84%

Beam Waves		Wave period				
Motion	Case	2	4	6	8	10
Heave Acc.	wo	0.005	0.013	0.219	0.441	0.329
	w	0.00%	-0.91%	-4.97%	-9.05%	-14.25%
Roll deg.	wo	0.001	0.119	1.236	1.916	1.940
	w	0.00%	-0.53%	-3.69%	-8.27%	-24.04%
Pitch deg.	wo	0.000	0.005	0.125	0.263	0.263
	w	0.00%	-1.52%	-5.24%	-9.54%	-23.93%

C.3.6. Bi-Modal Spectrum

Red values are invalid since this wave height and period combination is outside the validity of the Torsethaugen spectrum and moreover outside the computed domain for the hydrodynamic data.

Table C.28: Sensitivity Analysis: Bi-Modal Wave Spectrum (Torsethaugen)

Stern Waves		Wave period				
Motion	Case	2	4	6	8	10
Heave Acc.	wo	0.033	0.118	0.240	0.446	0.424
	w	710.59%	109.58%	0.32%	-8.86%	-12.27%
Roll deg.	wo	0.001	0.019	0.188	0.377	0.555
	w	33142.96%	1191.44%	5.22%	-5.41%	-15.84%
Pitch deg.	wo	0.006	0.081	0.333	0.742	0.880
	w	7419.69%	418.76%	4.25%	-8.53%	-13.52%

Stern Q Waves		Wave period				
Motion	Case	2	4	6	8	10
Heave Acc.	wo	0.003	0.045	0.303	0.570	0.475
	w	11150.35%	523.48%	-1.37%	-9.67%	-12.64%
Roll deg.	wo	0.000	0.041	0.382	0.910	1.247
	w	168684.76%	1311.33%	10.92%	-6.35%	-16.48%
Pitch deg.	wo	0.001	0.037	0.382	0.779	0.814
	w	91891.39%	1031.48%	0.98%	-9.06%	-13.29%

Beam Waves		Wave period				
Motion	Case	2	4	6	8	10
Heave Acc.	wo	0.005	0.013	0.219	0.441	0.329
	w	5007.34%	1584.44%	2.43%	-9.87%	-12.17%
Roll deg.	wo	0.001	0.119	1.236	1.916	1.940
	w	89878.32%	821.18%	-2.30%	-7.76%	-14.38%
Pitch deg.	wo	0.000	0.005	0.125	0.263	0.263
	w	105019.35%	2659.82%	4.77%	-8.66%	-14.32%

D

Correction Method

In this appendix results of the correction method are given. Attempted is to predict the significant wave height, significant wave period and mean wave direction on the basis of measured vessel motion responses and the correction algorithm. Response measurements are taken from Orcaflex simulations in order to have certainty about the present wave spectrum during the ”measurements”. Attempts are made for 9 different scenarios which are referred as case A until Case I, see table 6.3. The first 4 cases are during a heavy lift operation. The rest during light ship conditions. Vessel motion measurement signals originates from Orcaflex simulations. For all test cases 30 min measurement periods have been used. Indicated errors are the absolute difference between the measured and computed response moments of all motions together. The error in percentage is with respect to the total measured response moments.

D.1. Case A - Heavy Lift

Actually present sea state characteristics: Torsethaugen, Wdir: 90 deg, Hs: 0.8m, Tp: 6.3 sec
Applied motion combination: Roll, Pitch, Heave acc.

Table D.1: Case A: Best fits without variation in A and B parameters

Fit	wdirc	hsc	tpc	Ac	Bc	error	error %
1	90.00	0.80	6.00	1	1	9.79E-05	1.75
2	112.50	0.70	7.70	1	1	1.05E-04	1.88
3	168.75	1.60	6.50	1	1	1.06E-04	1.89
4	90.00	0.80	5.90	1	1	1.23E-04	2.20
5	78.75	0.80	6.30	1	1	1.33E-04	2.37
6	11.25	1.60	5.50	1	1	1.45E-04	2.59
7	45.00	1.20	7.60	1	1	1.48E-04	2.63
8	123.75	1.20	6.30	1	1	1.59E-04	2.83
9	45.00	1.40	6.80	1	1	1.60E-04	2.85
10	45.00	1.30	7.40	1	1	1.74E-04	3.11
11	123.75	1.20	6.20	1	1	1.77E-04	3.16
12	168.75	1.60	6.40	1	1	1.79E-04	3.19
13	22.50	1.60	6.40	1	1	1.88E-04	3.35
14	123.75	0.90	7.30	1	1	1.89E-04	3.38
15	56.25	1.00	7.50	1	1	1.99E-04	3.56
16	0.00	1.60	5.20	1	1	2.01E-04	3.58
17	11.25	1.60	5.60	1	1	2.05E-04	3.66
18	33.75	1.40	7.80	1	1	2.06E-04	3.68
19	112.50	0.70	7.80	1	1	2.08E-04	3.71
20	22.50	1.60	6.50	1	1	2.08E-04	3.71

D.2. Case B - Heavy Lift

Actually present sea state characteristics: Torsethaugen, Wdir: 0 deg, Hs: 1.2m, Tp: 6.3 sec
Applied motion combination: Roll, Pitch, Heave acc.

Table D.2: Case B: Best fits without variation in A and B parameters

Fit	Wdirc	Hsc	Tpc	Ac	Bc	error	error %
1	22.50	1.20	5.60	1	1	3.75E-06	0.04
2	180.00	1.20	5.80	1	1	4.48E-06	0.05
3	0.00	1.00	6.60	1	1	6.99E-06	0.08
4	22.50	1.10	6.80	1	1	1.18E-05	0.14
5	0.00	1.00	6.50	1	1	1.35E-05	0.16
6	0.00	1.00	7.40	1	1	1.44E-05	0.17
7	11.25	1.10	5.70	1	1	1.82E-05	0.21
8	168.75	1.20	6.20	1	1	1.90E-05	0.22
9	180.00	1.10	7.00	1	1	1.93E-05	0.22
10	0.00	1.10	5.40	1	1	2.76E-05	0.32
11	45.00	1.20	6.10	1	1	2.76E-05	0.32
12	45.00	1.10	6.50	1	1	2.84E-05	0.33
13	112.50	0.90	5.30	1	1	2.89E-05	0.33
14	0.00	1.00	7.50	1	1	2.98E-05	0.34
15	11.25	1.20	5.00	1	1	3.22E-05	0.37
16	0.00	1.00	6.40	1	1	3.33E-05	0.38
17	22.50	1.30	4.80	1	1	3.35E-05	0.39
18	168.75	1.10	7.10	1	1	3.60E-05	0.41
19	78.75	0.80	5.10	1	1	3.66E-05	0.42
20	33.75	1.30	5.30	1	1	3.84E-05	0.44

D.3. Case C - Heavy Lift

Actually present sea state characteristics: Torsethaugen, Wdir: 45 deg, Hs: 1.2m, Tp: 6.3 sec
Applied motion combination: Surge, Sway, Roll, Pitch, Heave acc.

Table D.3: Case C: Best fits without variation in A and B parameters

Fit	Wdirc	Hsc	Tpc	Ac	Bc	error	error %
1	45.00	1.30	5.10	1	1	8.3E-05	0.96
2	56.25	1.20	4.90	1	1	1.3E-04	1.46
3	33.75	1.40	5.00	1	1	1.3E-04	1.49
4	135.00	1.20	4.90	1	1	1.3E-04	1.56
5	146.25	1.30	5.10	1	1	1.5E-04	1.69
6	157.50	1.40	4.80	1	1	1.7E-04	1.97
7	146.25	1.40	5.70	1	1	2.2E-04	2.59
8	33.75	1.40	4.90	1	1	2.3E-04	2.63
9	146.25	1.30	5.00	1	1	2.7E-04	3.11
10	135.00	1.30	5.60	1	1	2.8E-04	3.24
11	45.00	1.30	5.00	1	1	3.2E-04	3.73
12	135.00	1.30	5.50	1	1	3.3E-04	3.80
13	157.50	1.40	4.90	1	1	3.4E-04	3.91
14	135.00	1.20	5.00	1	1	3.4E-04	3.97
15	56.25	1.20	4.80	1	1	3.7E-04	4.24
16	45.00	1.40	5.70	1	1	3.8E-04	4.36
17	56.25	1.20	5.00	1	1	3.9E-04	4.53
18	33.75	1.40	5.10	1	1	4.1E-04	4.75
19	45.00	1.30	5.20	1	1	4.4E-04	5.12
20	135.00	1.20	4.80	1	1	4.5E-04	5.19

D.4. Case D - Heavy Lift

Actually present sea state characteristics: Torsethaugen, Wdir: 33.75 deg, Hs: 1.2m, Tp: 6.3 sec
Applied motion combination: Surge, Sway, Roll, Pitch, Heave acc.

Table D.4: Case D: Best fits without variation in A and B parameters

Fit	Wdirc	Hsc	Tpc	Ac	Bc	error	error %
1	33.75	0.90	7.80	1	1	3.65E-05	1.03
2	0.00	1.10	4.80	1	1	3.99E-05	1.13
3	168.75	1.20	5.40	1	1	5.71E-05	1.62
4	33.75	1.20	5.60	1	1	6.75E-05	1.91
5	56.25	1.10	5.20	1	1	7.09E-05	2.01
6	146.25	1.20	5.70	1	1	8.01E-05	2.27
7	45.00	1.20	5.70	1	1	9.42E-05	2.67
8	157.50	1.20	5.50	1	1	9.81E-05	2.78
9	22.50	1.00	7.70	1	1	9.87E-05	2.80
10	11.25	1.00	7.80	1	1	0.000129384	3.67
11	157.50	1.20	5.60	1	1	0.000134224	3.81
12	11.25	1.10	4.80	1	1	0.000137565	3.90
13	180.00	1.20	5.40	1	1	0.000138178	3.92
14	0.00	1.10	4.90	1	1	0.000143285	4.06
15	33.75	1.20	5.70	1	1	0.000152926	4.34
16	45.00	1.20	5.80	1	1	0.000155846	4.42
17	0.00	1.00	7.80	1	1	0.000174944	4.96
18	135.00	1.20	5.80	1	1	0.000177344	5.03
19	56.25	1.10	5.30	1	1	0.000182624	5.18
20	22.50	1.20	5.50	1	1	0.00018341	5.20

D.5. Case E - Light Ship

Actually present sea state characteristics: Torsethaugen, Wdir: 0 deg, Hs: 0.9 m, Tp: 9.0 sec
Applied motion combination: Sway, Pitch, Heave acc.

Table D.5: Case E: Best fits without variation in A and B parameters

Fit	Wdirc	Hsc	Tpc	Ac	Bc	error	error %
1	0.00	0.90	9.20	1	1	4.00E-04	1.55
2	0.00	0.90	9.10	1	1	5.79E-04	2.24
3	0.00	0.90	9.30	1	1	8.53E-04	3.30
4	0.00	0.90	9.00	1	1	1.12E-03	4.33
5	180.00	0.80	10.00	1	1	1.22E-03	4.73
6	180.00	0.80	9.90	1	1	1.31E-03	5.08
7	180.00	0.80	10.10	1	1	1.32E-03	5.13
8	0.00	0.90	9.40	1	1	1.43E-03	5.53
9	180.00	0.80	9.80	1	1	1.57E-03	6.08
10	180.00	0.80	10.20	1	1	1.57E-03	6.10
11	0.00	0.90	8.90	1	1	1.70E-03	6.58
12	180.00	0.80	10.30	1	1	1.91E-03	7.38
13	180.00	0.80	9.70	1	1	1.95E-03	7.56
14	0.00	0.90	9.50	1	1	2.02E-03	7.82
15	11.25	0.90	9.10	1	1	2.05E-03	7.95
16	11.25	0.90	9.20	1	1	2.08E-03	8.07
17	168.75	0.80	9.90	1	1	2.12E-03	8.19
18	168.75	0.80	10.00	1	1	2.12E-03	8.22
19	11.25	0.90	9.00	1	1	2.19E-03	8.48
20	168.75	0.80	9.80	1	1	2.22E-03	8.59

D.6. Case F - Light Ship

Actually present sea state characteristics: Torsethaugen, Wdir: 0 deg, Hs: 1.0 m, Tp: 8.0 sec
Applied motion combination: Sway, Pitch, Heave acc.

Table D.6: Case F: Best fits without variation in A and B parameters

Fit	Wdirc	Hsc	Tpc	Ac	Bc	error	error %
1	0.0	1.0	8.1	1	1	8.91E-04	3.79
2	0.0	1.0	8.0	1	1	1.03E-03	4.41
3	0.0	1.0	8.2	1	1	1.17E-03	4.99
4	0.0	1.0	7.9	1	1	1.47E-03	6.28
5	0.0	1.0	8.3	1	1	1.68E-03	7.18
6	0.0	0.9	8.5	1	1	1.82E-03	7.77
7	180.0	0.8	9.1	1	1	1.82E-03	7.77
8	0.0	0.9	8.4	1	1	1.85E-03	7.87
9	180.0	0.8	9.2	1	1	1.88E-03	7.99
10	180.0	0.8	9.0	1	1	1.93E-03	8.24
11	0.0	0.9	8.6	1	1	2.01E-03	8.58
12	0.0	1.0	7.8	1	1	2.02E-03	8.60
13	0.0	0.9	8.3	1	1	2.05E-03	8.74
14	11.3	1.0	8.0	1	1	2.07E-03	8.82
15	180.0	0.8	9.3	1	1	2.08E-03	8.86
16	11.3	1.0	7.9	1	1	2.15E-03	9.14
17	11.3	0.9	8.4	1	1	2.15E-03	9.15
18	180.0	0.8	8.9	1	1	2.18E-03	9.29
19	11.3	1.0	8.1	1	1	2.18E-03	9.29
20	11.3	0.9	8.3	1	1	2.21E-03	9.40

D.7. Case G - Light Ship

Actually present sea state characteristics: Torsethaugen, Wdir: 0 deg, Hs: 0.7 m, Tp: 10.0 sec
Applied motion combination: Sway, Pitch, Heave acc.

Table D.7: Case G: Best fits without variation in A and B parameters

Fit	Wdirc	Hsc	Tpc	Ac	Bc	error	error %
1	180.00	0.60	10.70	1	1	4.01E-04	2.66
2	180.00	0.60	10.80	1	1	4.44E-04	2.94
3	180.00	0.60	10.60	1	1	4.82E-04	3.20
4	0.00	0.70	9.60	1	1	5.68E-04	3.77
5	180.00	0.60	10.90	1	1	5.78E-04	3.84
6	0.00	0.70	9.50	1	1	6.15E-04	4.08
7	180.00	0.60	10.50	1	1	6.44E-04	4.28
8	0.00	0.70	9.70	1	1	7.10E-04	4.71
9	180.00	0.60	11.00	1	1	7.54E-04	5.00
10	0.00	0.70	9.40	1	1	8.22E-04	5.45
11	180.00	0.60	10.40	1	1	8.47E-04	5.62
12	180.00	0.60	11.10	1	1	9.47E-04	6.28
13	0.00	0.70	9.80	1	1	9.59E-04	6.36
14	180.00	0.60	10.30	1	1	1.07E-03	7.10
15	0.00	0.70	9.30	1	1	1.10E-03	7.30
16	180.00	0.60	11.20	1	1	1.15E-03	7.61
17	168.75	0.60	10.70	1	1	1.19E-03	7.90
18	168.75	0.60	10.60	1	1	1.20E-03	7.98
19	168.75	0.60	10.80	1	1	1.22E-03	8.10
20	0.00	0.70	9.90	1	1	1.25E-03	8.29

D.8. Case H - Light Ship

Actually present sea state characteristics: Torsethaugen, Wdir: 33.75 deg, Hs: 1.5 m, Tp: 6.8 sec
Applied motion combination: Sway, Pitch, Heave acc.

Table D.8: Case H: Best fits without variation in A and B parameters

Fit	Wdirc	Hsc	Tpc	Ac	Bc	error	error %
1	135.00	1.40	6.50	1	1	1.31E-05	0.46
2	45.00	1.40	6.50	1	1	1.37E-05	0.48
3	33.75	1.30	7.60	1	1	1.83E-05	0.65
4	146.25	1.30	7.60	1	1	1.87E-05	0.66
5	22.50	1.60	6.00	1	1	2.06E-05	0.73
6	157.50	1.60	6.00	1	1	2.09E-05	0.74
7	157.50	1.40	7.70	1	1	2.28E-05	0.80
8	33.75	1.60	6.30	1	1	2.31E-05	0.82
9	146.25	1.60	6.30	1	1	2.33E-05	0.82
10	22.50	1.40	7.70	1	1	2.36E-05	0.83
11	11.25	1.50	6.60	1	1	2.46E-05	0.87
12	168.75	1.50	6.60	1	1	2.48E-05	0.88
13	45.00	1.30	6.80	1	1	2.49E-05	0.88
14	135.00	1.30	6.80	1	1	2.51E-05	0.89
15	168.75	1.40	8.00	1	1	2.76E-05	0.97
16	33.75	1.60	6.20	1	1	2.78E-05	0.98
17	180.00	1.40	8.00	1	1	2.80E-05	0.99
18	0.00	1.40	8.00	1	1	2.80E-05	0.99
19	146.25	1.60	6.20	1	1	2.80E-05	0.99
20	11.25	1.60	5.30	1	1	2.81E-05	0.99

D.9. Case I - Light Ship

Actually present sea state characteristics: Torsethaugen, Wdir: 45.00 deg, Hs: 1.0 m, Tp: 6.5 sec
Applied motion combination: Sway, Pitch, Heave acc.

Table D.9: Case I: Best fits without variation in A and B parameters

Fit	Wdirc	Hsc	Tpc	Ac	Bc	error	error %
1	45.00	0.80	7.90	1	1	5.17E-04	1.54
2	45.00	1.30	5.10	1	1	7.68E-04	2.29
3	67.50	1.10	5.90	1	1	7.77E-04	2.32
4	45.00	0.80	8.00	1	1	9.06E-04	2.70
5	112.50	0.80	7.40	1	1	9.82E-04	2.93
6	45.00	1.30	5.20	1	1	1.01E-03	3.00
7	56.25	0.80	7.10	1	1	1.07E-03	3.19
8	56.25	0.80	7.20	1	1	1.08E-03	3.23
9	67.50	1.10	5.80	1	1	1.08E-03	3.23
10	67.50	1.10	6.00	1	1	1.17E-03	3.48
11	45.00	1.30	5.00	1	1	1.21E-03	3.62
12	67.50	1.00	6.30	1	1	1.22E-03	3.65
13	45.00	0.80	7.80	1	1	1.23E-03	3.68
14	112.50	0.80	7.30	1	1	1.44E-03	4.30
15	67.50	1.10	5.70	1	1	1.58E-03	4.72
16	45.00	1.30	5.30	1	1	1.69E-03	5.04
17	101.25	1.10	6.20	1	1	1.70E-03	5.08
18	67.50	1.00	6.40	1	1	1.74E-03	5.20
19	101.25	1.10	6.10	1	1	1.77E-03	5.27
20	56.25	0.90	6.90	1	1	2.05E-03	6.12

E

Workability and Persistence

E.1. Scatter Diagram

Total %	0.0	1.3	9.0	18.7	19.6	13.7	5.9	6.1	7.8	6.9	5.3	3.0	1.5	0.8	0.2	0.2	0.1	0.0	0.0	100%
7.00											0.00									0.0
6.75																				0.0
6.50											0.00									0.0
6.25										0.00										0.0
6.00											0.00									0.0
5.75										0.01	0.00									0.0
5.50									0.01		0.00									0.0
5.25									0.01	0.03										0.0
5.00									0.01	0.02										0.0
4.75								0.01	0.00	0.02										0.0
4.50								0.00	0.03	0.01										0.0
4.25							0.00	0.02	0.04	0.00										0.1
4.00							0.02	0.03	0.06	0.00										0.1
3.75						0.00	0.03	0.07	0.06	0.00										0.2
3.50						0.01	0.07	0.12	0.03											0.2
3.25						0.02	0.16	0.16	0.01											0.4
3.00						0.11	0.35	0.13	0.01											0.6
2.75					0.00	0.39	0.58	0.13	0.00											1.1
2.50					0.02	0.89	0.72	0.07	0.00	0.00				0.00						1.7
2.25					0.22	1.83	0.50	0.03	0.00	0.00				0.00						2.6
2.00				0.01	0.85	2.49	0.30	0.02	0.01	0.00	0.00	0.00	0.00	0.01	0.00					3.7
1.75				0.12	2.55	2.35	0.29	0.01	0.02	0.03	0.01	0.02	0.03	0.06	0.01	0.00	0.03	0.03	0.01	5.6
1.50			0.01	0.73	4.63	1.64	0.23	0.07	0.05	0.04	0.13	0.15	0.08	0.04	0.03	0.05		0.02		7.9
1.25			0.17	3.55	5.08	1.28	0.20	0.15	0.18	0.16	0.32	0.35	0.17	0.15	0.01	0.04	0.00			11.8
1.00		0.01	1.66	6.48	3.75	0.94	0.14	0.50	0.70	1.09	0.88	0.73	0.37	0.25	0.04	0.03				17.6
0.75		0.38	4.13	5.77	2.02	0.48	0.64	1.64	2.71	2.85	2.38	1.15	0.54	0.13	0.01	0.02	0.05		0.01	24.9
0.50	0.01	0.78	2.79	2.00	0.45	1.18	1.59	2.62	3.46	2.32	1.38	0.50	0.30	0.12	0.02	0.01				19.6
0.25	0.00	0.08	0.22	0.02	0.06	0.07	0.05	0.31	0.41	0.26	0.16	0.12	0.03	0.02	0.01					1.8
	1	2	3	4	5	6	7	8	9	10	11	12	13	14	15	16	17	18	19	Total %

Significant Wave Height [m]

Significant Wave Period (1-D Spectrum) [sec]

Figure E.1: Scatter diagram of significant wave height an wave period combinations from 14 year historical data. Only data of the workable season between March and September is used to reconstruct this scatter diagram.

E.2. Probability of Occurrence

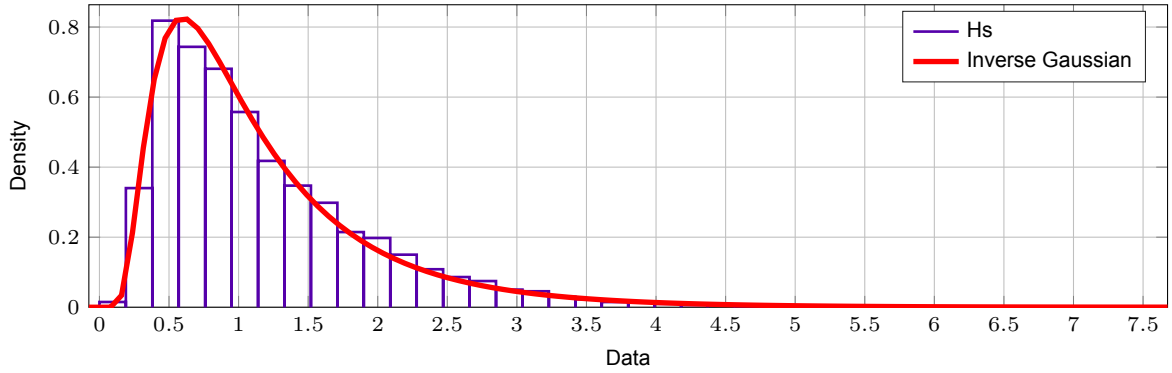

Figure E.2: Probability density function of significant wave height

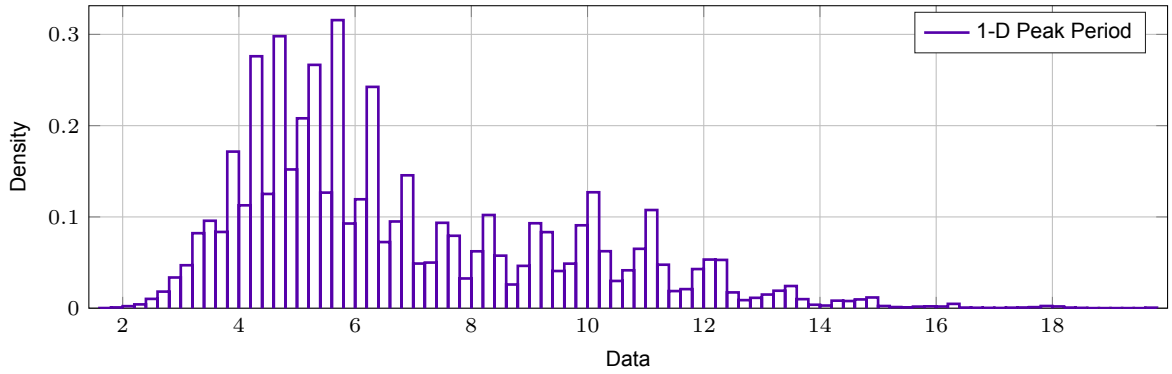

Figure E.3: Probability density function of significant wave period

E.3. Persistence Wave Direction

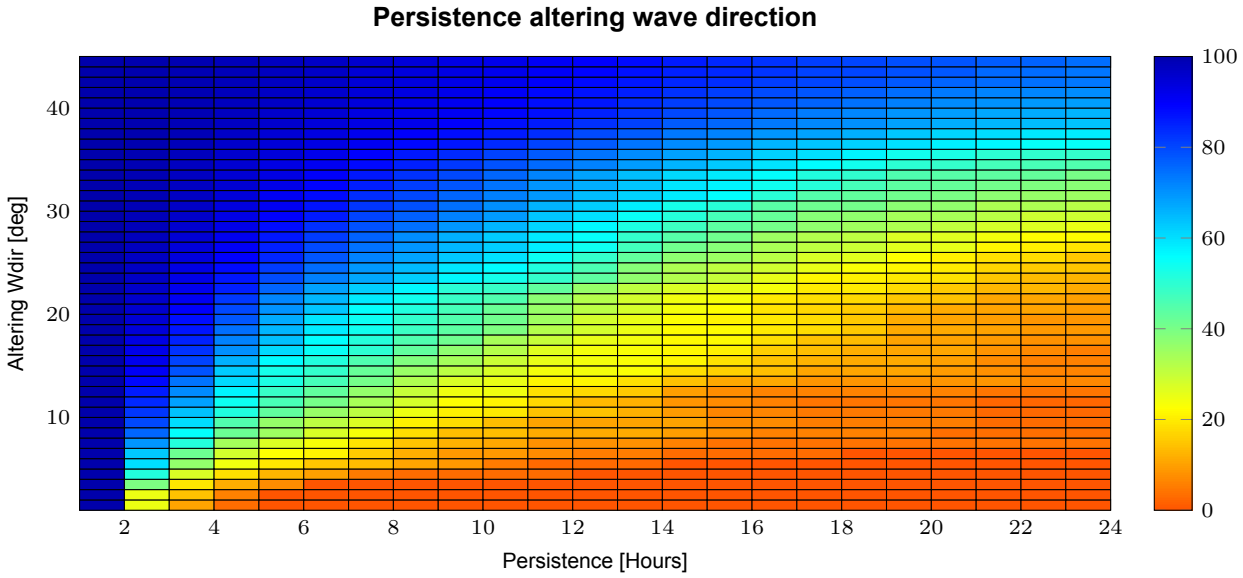

Figure E.4: Distribution of the average of F, the percentage of which remains below during the workable season run length against wave direction thresholds (1-40 deg) and persistence thresholds (0-24 hrs).

E.4. Persistence Wave Height

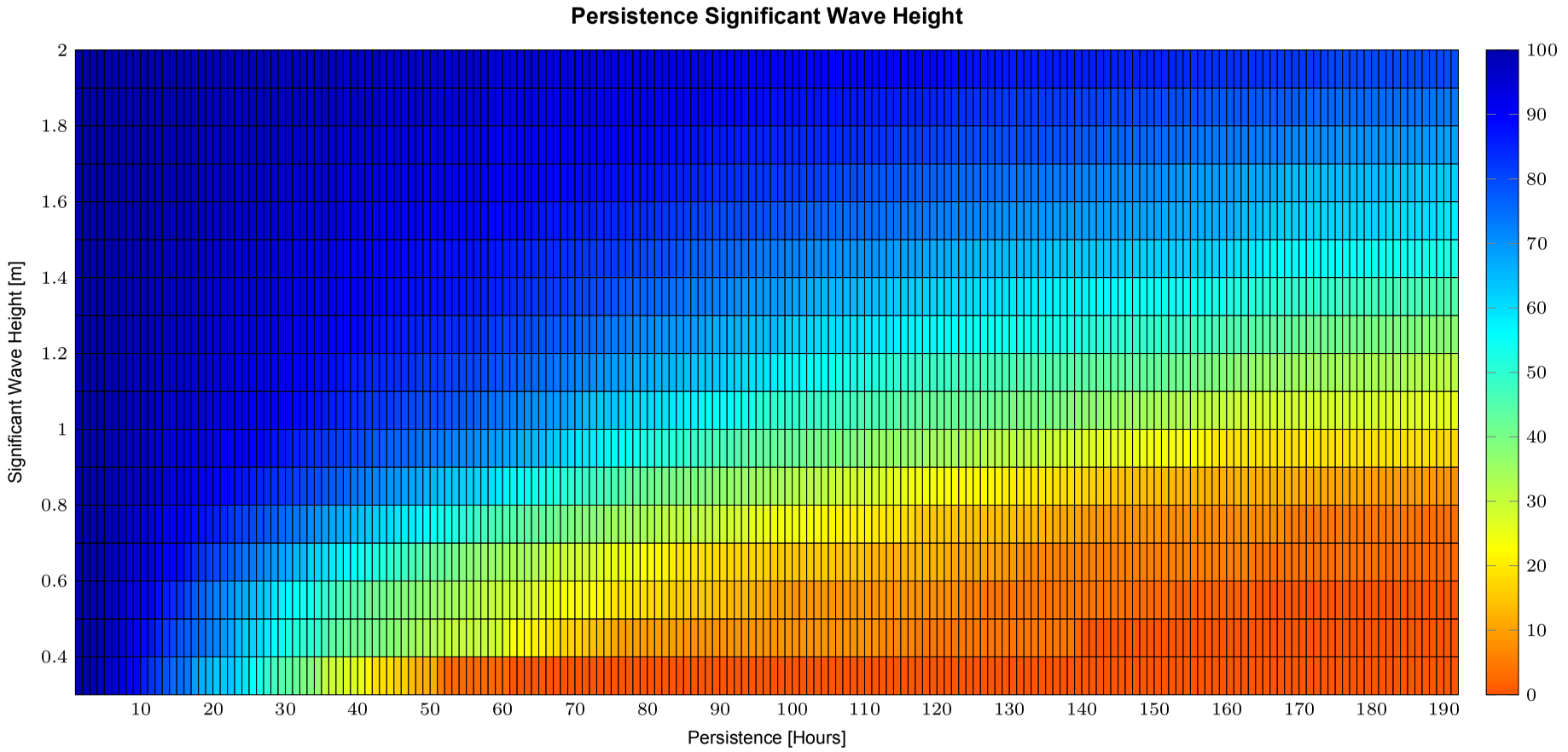

Figure E.5: Distribution of the average of F, the percentage of which remains below during the workable season run length against significant wave height thresholds (0.4-2.0m) and persistence thresholds (0-192 hrs).

E.5. Persistence Wave Period

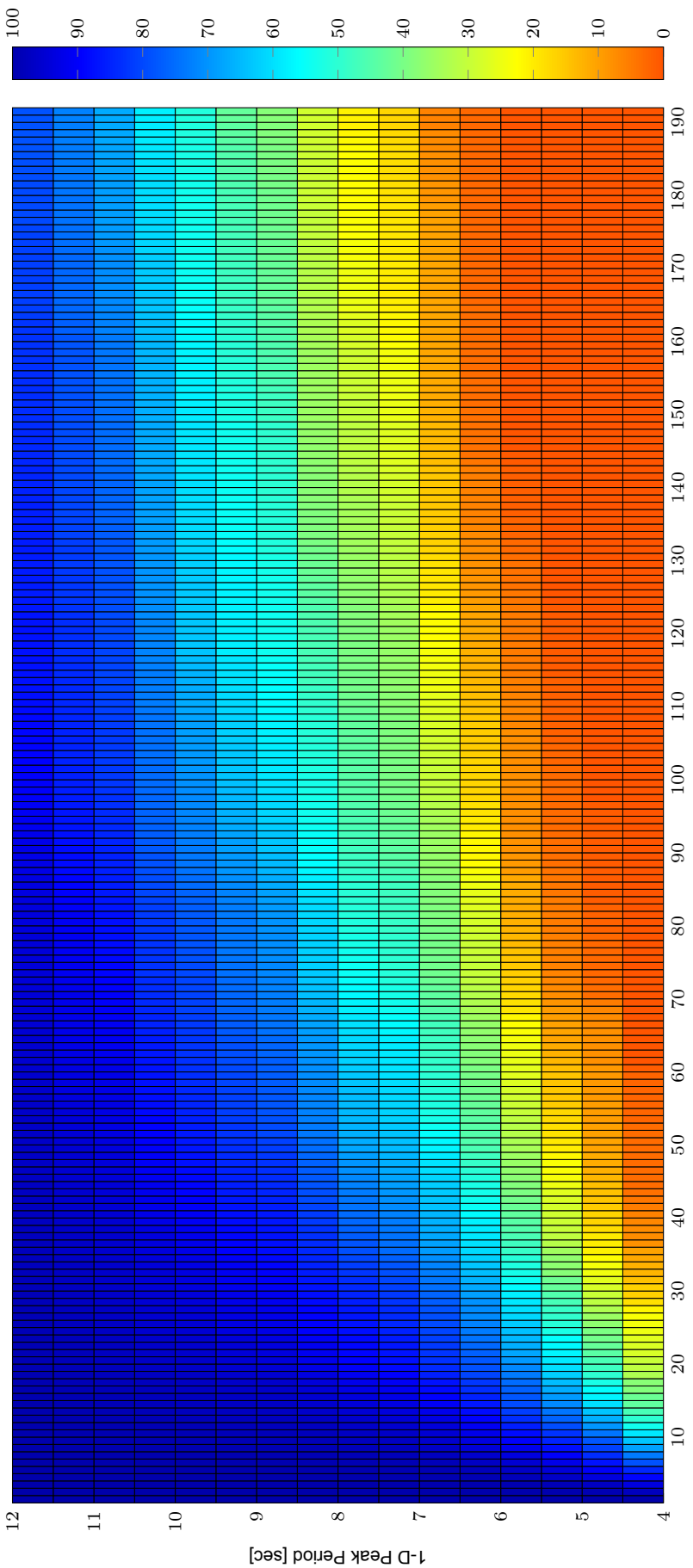

Figure E.6: Distribution of the average of F, the percentage of which remains below during the workable season run length against significant wave period thresholds (5-12s) and persistence thresholds (0-192 hrs).

E.6. Persistence Workability

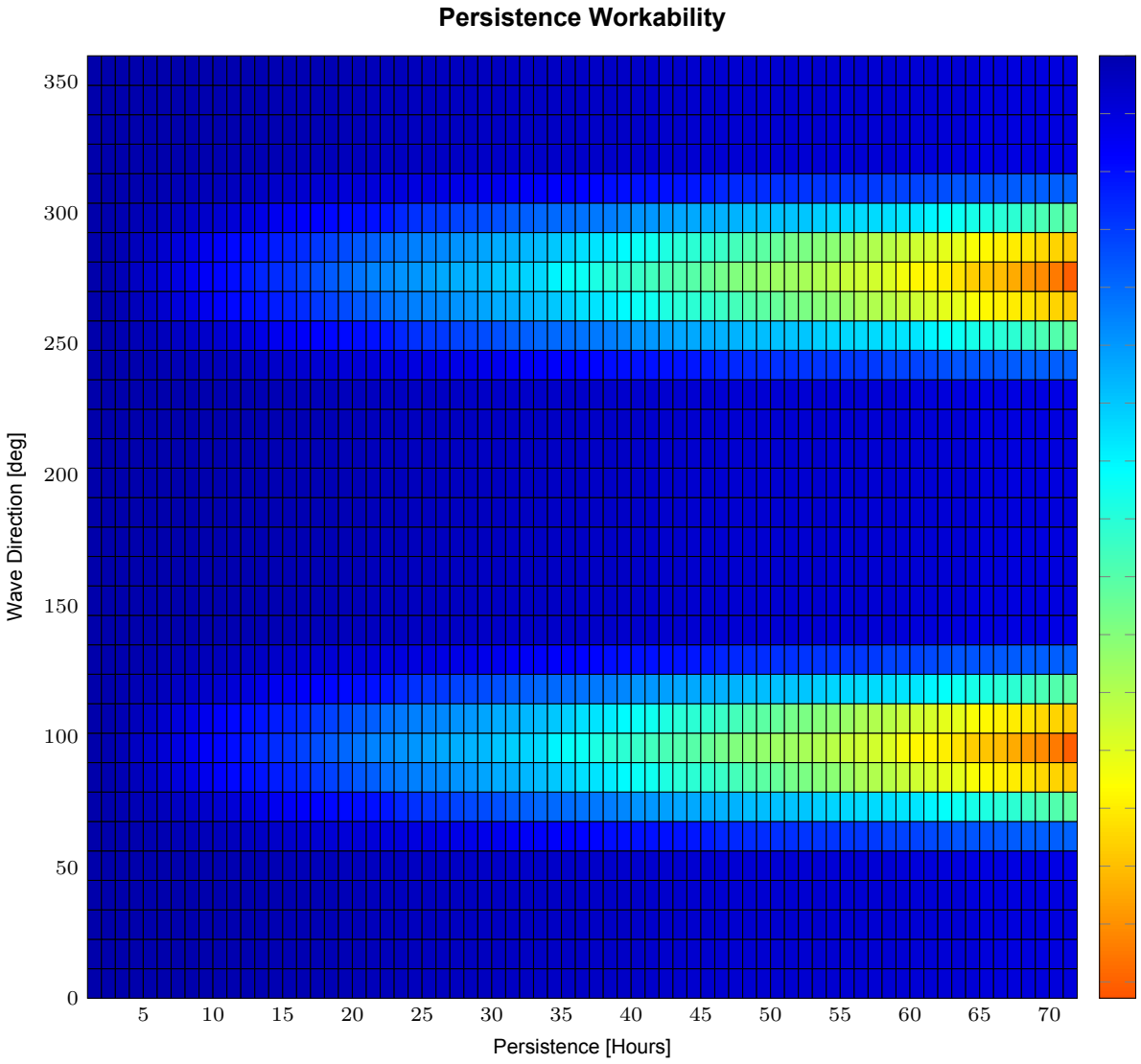

Figure E.7: Distribution of the average of F, the percentage of which the sea state is workable for different wave directions (0-360 deg) and persistence thresholds (0-72 hrs). Operational condition: Light Ship.

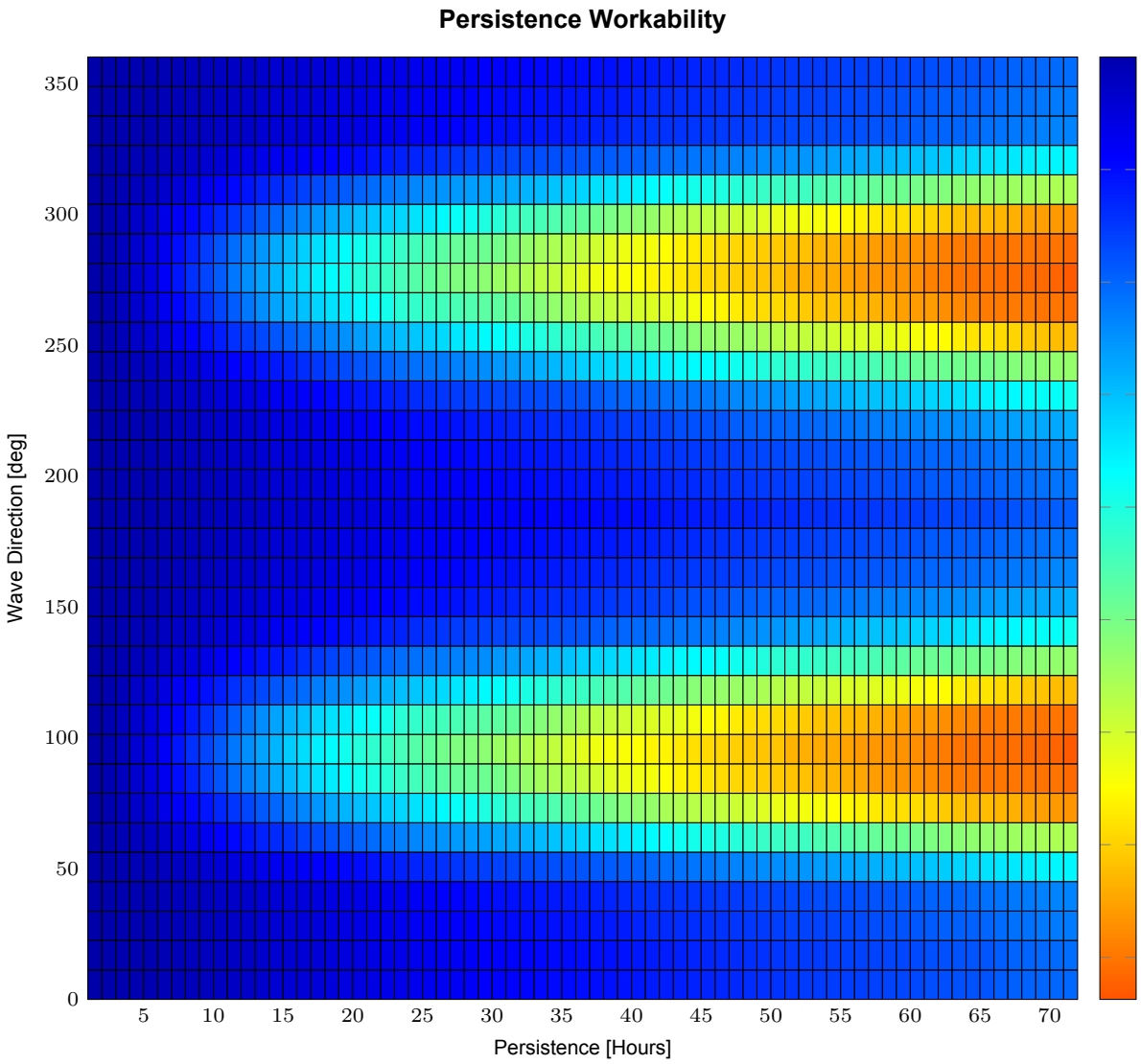

Figure E.8: Distribution of the average of F, the percentage of which the sea state is workable for different wave directions (0-360 deg) and persistence thresholds (0-72 hrs). Operational condition: Heavy lift, PS lift, 1200 ton, Outreach 12m, Ls 70m.

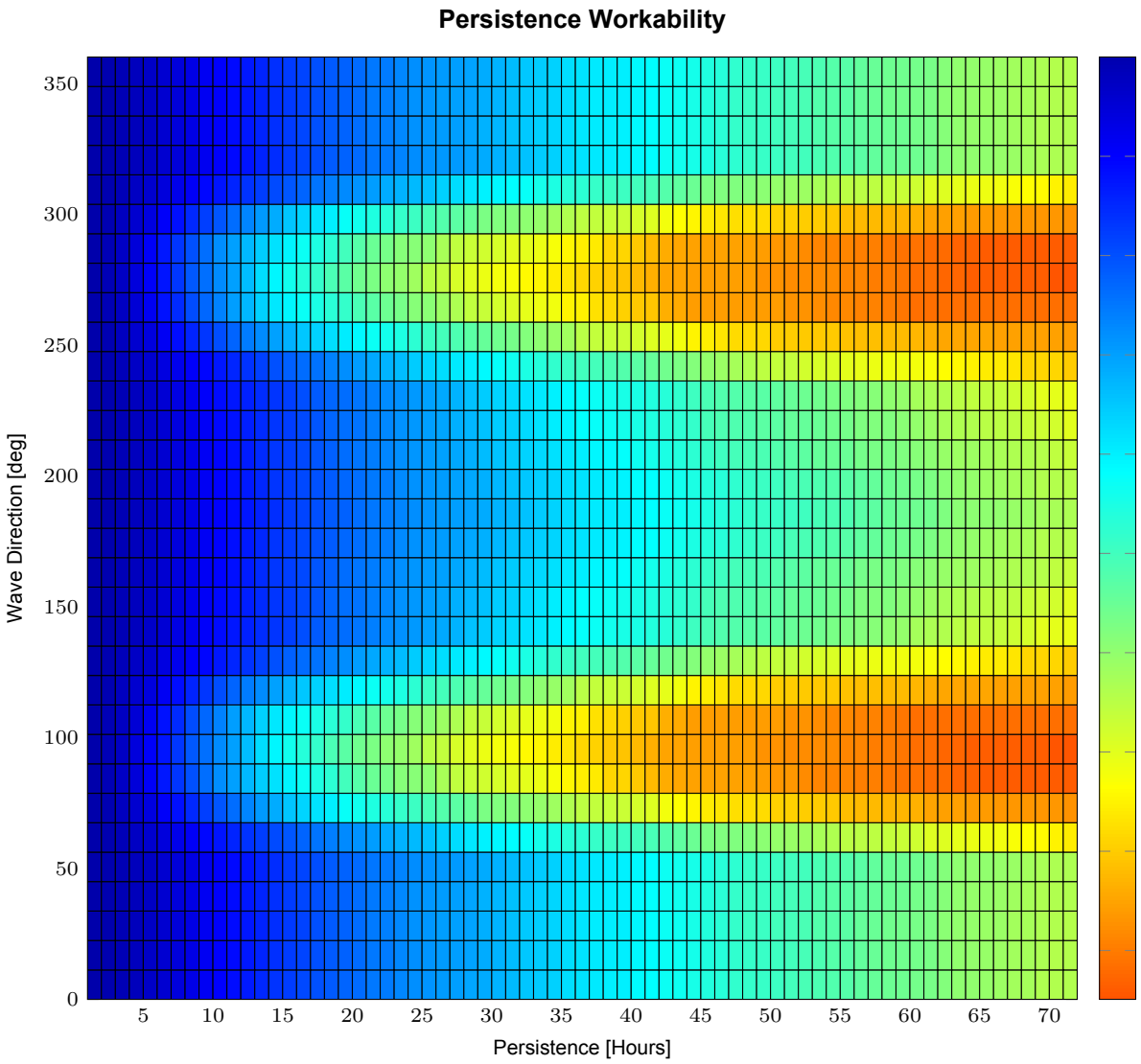

Figure E.9: Distribution of the average of F, the percentage of which the sea state is workable for different wave directions (0-360 deg) and persistence thresholds (0-72 hrs). Operational condition: Heavy lift, PS lift, 1200 ton, Outreach 12m, Ls 50m.